University of Almeria

Evaluation of electrochemical processes assisted by solar energy for water depuration

Irene Salmerón García

PhD Thesis

Almeria, 2020

Universidad de Almería

Departamento de Ingeniería Química

Doctorado en Biotecnología y Bioprocesos Industriales aplicados a la Agroalimentación y Medioambiente

Evaluation of electrochemical processes assisted by solar energy for water depuration

---

Evaluación de procesos electroquímicos asistidos por energía solar para la depuración de aguas

Memory presented for the title of Doctor:

Ms. Irene Salmerón García

Almeria, September 2020

Thesis supervisor:

Dr. Ms. Isabel Oller Alberola

Research Fellow OPI

CIEMAT-PSA

This PhD Thesis has been realized within the finantial support of CIEMAT, Centro de Investigaciones Energéticas, Medioambientales y Tecnológicas, public research institution dependent of the Spanish Ministry of Science and Innovation, through the doctoral felowship published in the call 15/PREEE0/15, developing the research work at Plataforma Solar de Almería.

Index

Abstract

Nowadays society's lifestyle encourages a high rate of consumption of natural resources; many of them are non-renewable, meaning that an inadequate management will lead to a certain degree of scarcity in the medium to long term. The most illustrative example is water, used in almost any human activity, for human consumption, cleaning and domestic use or in industrial processes (even in energy production), either as cooling medium or directly intervening in the productive process, water is present. It was up to the 2000s that the Legislative Authorities were considering water no more than a commercial asset being the implementation of the Water Framework Directive (2000/60/CE) the inception to a mentality change towards water, considering it now more an heritage deserving protection and laying the foundations for the development of specific regulations that will establish minimum quality limits to be achieved prior to the discharge of the effluents into the environment.

Specifically, chemical industry undergone a strong development owed to a growing demand for new products to satisfy the needs of the consumers. The manufacture of drugs, personal care products, or pesticides and fertilizers to improve agricultural production has led to the appearance, development and deployment of new organic substances. These are usually toxic, non-biodegradable and highly recalcitrant, thus they are difficult to assimilate for microorganisms, being active in the environment for long periods of time and with unknown effects on the discharge ecosystems.

That situation motivates arisen, development and application of new highly oxidizing technologies, aiming the degradation of these emerging compounds and even, depending to their complexity, enhancing the biodegradability of the whole effluent. For this reason, electrochemical processes pose a versatile, useful and powerful tool since only by applying an electric current or potential on the electrodes it is able to generate oxidizing species that interacts with a broad spectra of contaminants, facilitating their removal.

Some electrochemical processes have been widely used at industrial scale. For example, electrocoagulation implies an advantage over the conventional coagulation-flocculation physicochemical process, since avoids the addition of chemical reagents by the use of sacrificial electrodes, generating a lower amount of sludge, and presenting higher efficiency in the colloids removal. On the other hand, electrodialysis, an electrically assisted membrane process, is able to separate the ions from an influent, yielding a high-quality effluent of low ionic charge, being mainly applied in desalination processes aimed to produce drinking water.

In spite of involving great advantages such as an easy control of the process and therefore easy automatization, as well as the absence of external reagents, some electro-oxidative processes have not been evaluated further than at laboratory scale. In fact, most of the studies reported in the literature are focused in the development of new materials for electrodes manufacturing, to improve effectiveness and reduce costs associated to this technology. However, it must be highlighted that electrochlorination has been implemented on a larger scale due to the low cost of the electrodes.

The scarcity of studies facing these technologies under a realistic approach and for the purification of complex water matrices, has limited the possibilities of electro-oxidative systems from a commercial standpoint. It is important to note that from the ions species naturally contained in certain waters, a large amount and variety of oxidizing species can be generated, which entails an intrinsic improvement over the basic studies using a supporting electrolyte whose only function is to allow the transition of electrons. Furthermore, many of these electrogenerated species are photoactive, which means that just by irradiating the solution with ultraviolet light the generation of even more oxidizing species could be promoted, which results in an increase of the contaminants degradation rate. This has meant that the development, implementation, start-up and evaluation of these systems on a larger scale have not been also addressed in depth, hindering the scale-up of the electro-oxidative process.

In this context, the opportunity of this PhD Thesis arises bringing the study of electrochemical technology to a new level closer to reality. The application of electro-oxidative processes at pilot plant scale in actual wastewaters is addressed, assessing the operating conditions seeking to improve contaminants removal and water depuration. Combination of electro-oxidative systems with a natural and renewable energy source such as sunlight is also tackled.

The first objective addressed was characterization, start-up and optimization of the main operational parameters of a solar photoelectro-Fenton (SPEF) pilot plant able to treat up to 100 L of water developed and installed at Plataforma solar de Almería (PSA) (CIEMAT). The system consists of four electro-cells equipped with a niobium-supported boron doped diamond anode (Nb-BDD) and a carbon-polytetrafluoroethylene (carbon-PTFE) gas diffusion cathode (GDE) (Electro MP-Cells from ElectroCell). The cells are connected in parallel to a recirculation tank and this, in turn, to a solar photoreactor based on compound parabolic collectors (CPC) with 2 m^2 of illuminated surface. Optimization of the main input variables, pH and current density (*j*), was carried out to maximize onsite

H_2O_2 electrogeneration with the maximum current efficiency (CE). A central composite experimental design was defined, and after the completion of the 19 experiments proposed in the matrix, by means of the statistical analysis of the results, the adjustment model for H_2O_2 concentration was obtained: $[H_2O_2] = 2.19 - 0.31 \cdot pH + 0.81 \cdot j - 0.05 \cdot pH \cdot j + 0.15 \cdot pH^2 - 2.42 \times 10^{-3} \cdot j^2$, as well as for the CE percentage: $\%CE = 61.68 - 0.43 \cdot pH - 0.18 \cdot j - 0.0275 \cdot pH \cdot j$, and the corresponding response surface graphs. Finally, the model was validated, corroborating that, at pH 3 and applying 73.66 mA cm^{-2}, the maximum production of H_2O_2 is achieved (64.9 mg min^{-1}) with a CE associated of 89.3%. Once these parameters were established, the influence of the water and air flows, as well as the concentration of the electrolyte on the H_2O_2 electrogeneration was also studied, reaching the maximum applying a water flow of 5.6 L min^{-1}, an air flow of 10 L min^{-1}, and with 50 mM of Na_2SO_4. Afterwards, preliminary tests were developed assessing the efficiency in the removal of reference compounds, pyrimethanil and methomyl in a concentration of 50 mg L^{-1} and 90 mg L^{-1}, respectively, by the application of the different oxidation processes that are able to be developed in the pilot plant system: anodic oxidation (AO), electro-Fenton (EF) and solar SPEF, having as supporting electrolyte a solution of Na_2SO_4 50 mM. The highest degradation rates were attained by SPEF process: 55% of pyrimethanil and 50% of methomyl after only 5 minutes. This research was performed with the collaboration of Prof. Anastasios J. Karabelas and Dr. Konstantinos V. Plakas of the Chemical Processes and Energy Resources Institute of the Centre for Research and Technology-Hellas (Greece) in the framework of the European project SFERA-II at PSA facilities.

Second objective was focused on a real application of the previously optimized electrochemical pilot plant through its combination with a pre-treatment consisting of a nanofiltration (NF) membrane system. Urban wastewater treatment plant effluent was pre-treated for increasing the concentration of organic microcontaminants (OMCs) in the NF retentate stream, together with reducing the total volume to be treated in the tertiary electro-oxidation system. Also noteworthy is the increase in water salinity achieved after the NF system in the retentate, decreasing ohmic resistance and thus facilitating a subsequent tertiary treatment based on electro-oxidation. For studying the behavior of the SPEF system in highly saline and complex matrices, a recipe of simulated NF concentrate was developed from the characterization of concentrates previously reported in literature. Aiming to work at the effluent natural pH, avoiding the addition of reagents for acidification and neutralization, the use of ethylenediamine-N,N'-disuccinic acid (EDDS) as an iron complexing agent in the electro-Fenton (EF) process was evaluated. It was also checked the stability of Fe^{3+}:EDDS complex in the EF process,

which was degraded after 15 min of treatment, although iron did not precipitate completely until 30 min. Thereupon, the degradation of four OMCs was studied: pentachlorophenol, terbutryn, chlorfenvinphos and diclofenac (at 200 and 500 μg L^{-1} of initial concentration each); by AO, EF, SPEF and solar-assisted AO at natural pH, using Fe^{3+}:EDDS (1:2) at 0.1:0.2 mM in EF and SPEF treatments.

When using simulated NF retentate, whose chloride concentration was 555 mg L^{-1}, the highest degradation of OMCs (500 μg L^{-1} of initial concentration each) was obtained using SPEF reaching 85% of total contaminants removal. The reason is that chlorine species generated by solar-assisted AO were not enough to degrade OMCs (75% of total amount), despite the presence of lower organic matter in solution due to the absence of EDDS. On the other hand, EF process was discarded since no improvement was observed with respect to AO, consuming the hydroxyl radicals produced by the Fenton reaction in the degradation of the EDDS instead of the OMCs.

The evaluation of the SPEF system for the tertiary treatment of actual wastewater, was carried out by collecting effluent from the secondary treatment of El Ejido WWTP (in Almería, South-East of Spain), after its pre-treatment in the NF pilot plant installed at PSA until reducing the initial volume 4 times. The salinity of the effluent increased from 2.1 - 2.3 mS cm^{-1} to 6.1 - 6.8 mS cm^{-1}, and the chloride concentration reached 1182 - 1960 mg L^{-1}. The concentrate was spiked with the four target OMCs (100 μg L^{-1} each) and their degradation was studied by AO, SPEF (with the carbonates naturally contained in the concentrate and reducing them to 20 mg L^{-1} to diminish the scavenger effect on hydroxyl radicals) and solar-assisted AO. The percentages of degradation of the sum of OMCs after 180 minutes of each applied treatment were 84% (AO), 69% (SPEF with carbonates), 75% (SPEF with low carbonates) and 84% (solar-assisted AO), respectively. In this occasion, the highest percentage of degradation with the lowest electricity consumption, 5.3 kWh m^{-3}, was obtained by solar-assisted AO, since the higher concentration of chlorides promoted a higher generation of active chlorine species. Finally, tertiary treatment by applying solar-assisted AO was chosen for the degradation of 44 OMCs actually contained in the secondary effluent of the WWTP and detected by LC-QqLIT-MS/MS, resulting in the elimination of 80% of the sum. This work was performed in collaboration with Prof. Ana Agüera and Dr. Ana Martínez-Piernas from CIESOL (mixed center CIEMAT-UAL) at the University of Almería.

After the experimental program conducted in the electrochemical pilot plant, which began with its start-up and optimization of operation parameters, it was considered to study and

diagnose the state of the cathode surface of the cells used in those tests. While cathode usage hours increased, onsite production of H_2O_2 decreased progressively from 43 mg L^{-1} of accumulated H_2O_2 in 30 min, in the first use of the cathode, to 1.5 mg L^{-1} after several experiments. At the moment an important reduction of the H_2O_2 electrogenerated was observed, making impossible the effective development of EF and SPEF processes, the cell was disassembled and the autopsy of the cathode surface was carried out by means of scanning electron microscopy and X-rays in order to try to identify the main reasons for the contamination of the cathode and the consequent loss of efficiency. In the images obtained, a loss of the carbon-PTFE coating was detected as well as the formation of iron deposits, justifying the drop in H_2O_2 electrogenerated with the loss of the electrode active surface.

In the framework of the Marie Curie - ALICE project "AcceLerate Innovation in urban wastewater management for Climate change", H2020-MSCA-RISE, the PhD candidate carried out a research internship at the Nanotechnology and Integrated BioEngineering Centre (NIBEC) of the University of Ulster (UK), in collaboration with the Photocatalysis Research Team lead by Prof. John Anthony Byrne. The goal of this collaboration was the development and application of a laboratory-scale photoelectrocatalytic reactor for the simultaneous elimination of OMCs and pathogenic microorganisms in natural water. As a core part of the reactor, two nanotube photoanodes of titanium dioxide were manufactured by anodizing a titanium mesh at 30 V for 3 h and then annealing it at 500°C to promote the anatase phase. The reactor consists of a 190 mL cell with a double photoanode of titanium dioxide nanotubes illuminated by a 9 W UV-A lamp through a quartz window, with an applied irradiation of 50 W m^{-2}. The main objective was the simultaneous removal of OMCs (terbutryn, chlorfenvinphos and diclofenac at 500 µg L^{-1} of initial concentration each) and pathogens (*E. coli* as reference bacteria at an initial concentration of 106 CFU mL^{-1}), at the same time that a possible improvement by replacing a counter cathode with no contribution to the degradation process (platinum-coated titanium) by a carbon felt cathode able to electrogenerate H_2O_2, was evaluated. Assessing separately the degradation of OMCs and the inactivation of *E. coli*, when applying the photoelectrocatalytic process with platinum cathode, a clear improvement in the inactivation of bacteria was observed (2 Log reduction after 120 minutes of treatment), compared to the photo-catalytic process on its own (0.8 Log reduction in the same treatment time). However, degradation of OMCs remained at the same ratio; around 70% of the sum after 60 min. Replacement of the platinum cathode by a carbón felt cathode increased the efficiency of *E. coli* inactivation, reducing its concentration in 2.7 Log, although OMCs showed similar degradation percentages. When finally the

degradation of OMCs was carried out simultaneously to the inactivation of bacteria by photoelectrocatalysis with carbon cathode, a significant increase in disinfection was observed, reaching the detection limit of the method through a reduction of 4.5 Log. This improvement could be attributed to the presence of methanol from the stock solution where OMCs were pre-dissolved, that acts as a hole scavenger increasing the photocurrent and getting oxidized so generating formaldehyde, a highly toxic substance for microorganisms (LC_{50} for *E. coli* = 1 mg L^{-1}). As a consequence of this outcome, the effect of hole scavengers presence in disinfection was evaluated, using acetate and methanol at a concentration of 5 mM. In both cases, as described in literature, an increase in the photocurrent was observed under their presence, observing also an increase in the rate of bacteria inactivation, which was greater in the case of methanol due to the generation of formaldehyde.

Finally, as a result of the strong collaboration between the PhD student and the Solar Water Treatment Unit with the electrochemical company DeNora built during transnational access program within SFERA-II project, the evaluation of a commercial electro-oxidation system specially designed for the abatement of chemical oxygen demand in industrial waters and supported by the action of active chlorine spices was carried out. Within the framework of this collaboration, and as part of the objectives developed in this PhD Thesis, the evaluation of a pilot plant equipped with a dimensionally stable anode cell (DSA) manufactured by DeNora was performed, combining it with a solar CPC photoreactor (3.08 m^2), reaching a total capacity of 38 L, and with the aim of evaluating the possible improvement in efficiency of two batches of landfill leachates. These leachates were characterized by high organic loads (>2000 mg L^{-1} of dissolved organic carbon (DOC)) and a high toxicity in one of the batches (53 % of inhibition on activated sludge) so the main purpose was to reduce the toxicity and increase the biodegradability enough for a subsequent combination with a conventional biological treatment (thus reducing the associated operation costs). First step was the treatment of two batches by solar photo-Fenton process, which required an excessive accumulated UV energy (142.2 kJ L^{-1}) to achieve only a 30% reduction of DOC in the first batch of leachate (diluted 1:1 with distilled water). In the second batch it was not possible to perform solar photo-Fenton treatment due to the large amount of foams generated, causing large oscillations of the DOC along the process. Later on, the two batches were treated by electro-oxidation, electro-oxidation by adding H_2O_2 and electro-oxidation combined with solar radiation, being the second batch the one that showed the highest DOC and total nitrogen removal rates, 3.5 g DOC kWh^{-1} and 18 g TN kWh^{-1} in the first batch of leachate and 13.4 g DOC kWh^{-1} and 45.2 g TN kWh^{-1} in the second

batch. After the application of electro-oxidation assisted by solar energy, a reduction on toxicity from 53% to 6% of inhibition, and a sufficient improvement of biodegradability were observed in both batches. This study corroborates the improvement caused by the application of sunlight to the electrochemical treatment of industrial wastewater, which may represent a step forward towards the application of these powerful oxidation systems, presenting themselves as a feasible, sustainable and green alternative to purely electrochemical treatments, with lower operation costs due to lower energy consumption.

Resumen

El ritmo de vida impuesto por la sociedad actual conlleva un alto consumo de recursos naturales, muchos de ellos no renovables, por lo que una gestión inadecuada puede producir una escasez de estos a medio o largo plazo. El caso más evidente es el del agua, que se utiliza tanto para consumo humano, en agua de bebida, aseo y labores domésticas, como en procesos industriales, ya sea como refrigerante o como parte del propio proceso de producción. Hasta el año 2000, este recurso ha sido considerado por las autoridades legislativas como un bien comercial, pero a partir de la implantación de la Directiva Marco de Agua (2000/60/EC) pasó a ser considerado como un patrimonio a proteger, sentando las bases para el desarrollo de una normativa más específica que establece unos límites mínimos de calidad a alcanzar previo a la descarga de efluentes en el medio ambiente.

Específicamente la industria química ha sufrido un fuerte desarrollo por la creciente demanda de nuevos productos que satisfagan las necesidades de los consumidores. La fabricación de fármacos, productos para el cuidado personal, o plaguicidas y fertilizantes para mejorar la producción agrícola, ha dado lugar a la aparición de nuevas sustancias orgánicas. Estas suelen ser tóxicas, no biodegradables y altamente recalcitrantes por lo que no son fácilmente asimilables por los microorganismos, permaneciendo por largos periodos de tiempo en el medio ambiente sin conocer los efectos que pueden generar en el ecosistema.

Por este motivo surge la necesidad de desarrollar y aplicar nuevas tecnologías altamente oxidantes, capaces de reaccionar con estos compuestos degradándolos o mineralizándolos e incluso, dependiendo de su complejidad, mejorando la biodegradabilidad del efluente. Para ello, los procesos electroquímicos suponen una herramienta útil versátil y potente ya que únicamente aplicando una corriente o potencial eléctricos sobre unos electrodos se pueden generar especies altamente oxidantes que interaccionen con esos contaminantes facilitando su eliminación.

Algunos de estos procesos electroquímicos han sido ampliamente utilizados a escala industrial. Por ejemplo, la electrocoagulación supone una ventaja respecto al proceso físico-químico convencional de coagulación-floculación, ya que utiliza un electrodo de sacrificio evitando la adición de reactivos, se genera menos lodo y es más efectivo en la eliminación de coloides. La electrodiálisis, un proceso de membrana asistido eléctricamente, es capaz de separar los iones de un influente generando un efluente de alta calidad con muy baja carga iónica siendo principalmente aplicado en procesos de desalación para la obtención de agua potable.

Pese a presentar importantes ventajas como la facilidad para controlar el proceso y, por tanto su fácil automatización, así como la ausencia de reactivos externos, algunos procesos electro-oxidativos aún no han sido evaluados más que a escala de laboratorio, centrando la mayoría de los estudios recogidos en la literatura en el desarrollo de nuevos materiales para la fabricación de electrodos para la mejora de la efectividad y la reducción de costes asociados a dicha tecnología. Sin embargo, la electro-cloración ha sido el único tratamiento implementado a mayor escala debido al bajo coste de los electrodos.

La escasez de estudios aplicando estas tecnologías en situaciones reales, para la purificación de aguas residuales complejas, ha limitado, desde el punto de vista comercial, las posibilidades de los sistemas electro-oxidativos. Es importante mencionar que, a partir de los diferentes iones presentes de forma natural en determinadas aguas, se pueden generar gran cantidad y variedad de especies oxidantes, lo que conlleva una mejora intrínseca en la eficacia del proceso con respecto a una solución salina cuya única función es permitir el tránsito de electrones. Además, muchas de esas especies electro-generadas son fotoactivas, lo que supone que tan sólo con irradiar con luz ultravioleta la solución, se pueden generar especies aún más oxidantes incrementando la tasa de degradación de los contaminantes. Esto ha provocado que el desarrollo, implementación, puesta en marcha y evaluación de estos sistemas a mayor escala tampoco haya sido abordado en profundidad, lo que dificulta su escalado y aplicación industrial.

En este contexto surge la motivación de la presente Tesis Doctoral, que aborda la aplicación de procesos oxidativos a escala planta piloto en aguas reales, además de estudiar las condiciones de operación que lleven a un incremento en la degradación de contaminantes y depuración de aguas, combinando el sistema electro-oxidativo con una fuente de luz natural y renovable como es la energía solar.

El primer objetivo abordado fue la puesta en marcha, caracterización y optimización de los principales parámetros de operación de una planta piloto de foto electro-Fenton solar (SPEF siglas en inglés) con un volumen máximo de 100 L instalada en la Plataforma Solar de Almería (CIEMAT). El sistema está constituido por cuatro celdas comerciales equipadas con un ánodo de diamante dopado con boro soportado en niobio y un cátodo de difusión de gas de carbono-politetrafluoroetileno (Electro MP-Cells suministradas por ElectroCell). Las celdas están conectadas en paralelo a un tanque de recirculación y éste a su vez a un foto-reactor solar basado en captadores cilindro parabólico compuestos (CPC) con 2 m^{-2} de superficie iluminada. Se llevó a cabo la optimización de

las principales variables de entrada del proceso: el pH y la densidad de corriente (*j*), para maximizar la electro-generación in situ de H_2O_2 con la máxima eficiencia en el empleo de la corriente eléctrica (CE). Se definió un diseño experimental central compuesto, de forma que tras la consecución de una matriz de 19 experimentos y a partir del análisis estadístico de los resultados se obtuvo el modelo de ajuste para la concentración de H_2O_2 generada directamente en el reactor: $[H_2O_2] = 2.19 - 0.31 \cdot pH + 0.81 \cdot j - 0.05 \cdot pH \cdot j + 0.15 \cdot pH^2 - 2.42 \times 10^{-3} \cdot j^2$, y para la CE, $\%CE = 61.68 - 0.43 \cdot pH - 0.18 \cdot j - 0.0275 \cdot pH \cdot j$, así como los gráficos de superficie de respuesta asociados. Finalmente se validó el modelo, corroborando que a pH 3 y aplicando 73.66 mA cm^{-2} se logra la mayor producción de H_2O_2, 64.9 mg min^{-1} con una eficiencia de la corriente aplicada del 89.3%. Una vez establecidos estos parámetros se estudió la influencia del caudal de agua, de aire y la concentración de electrolito en la electro-generación in situ de H_2O_2, alcanzando el máximo con un caudal de agua de 5.6 L min^{-1}, de 10 L min^{-1} de aire, y una concentración de Na_2SO_4 de 50 mM. Posteriormente, se realizaron ensayos preliminares para la evaluación de la eficacia de eliminación de compuestos de referencia, concretamente pirimetanil y metomilo en una concentración de 50 mg L^{-1} y 90 mg L^{-1}, respectivamente, mediante los diferentes procesos de electro-oxidación que podían llevarse a cabo en la planta piloto empleando como electrolito una solución 50 mM de Na_2SO_4, desde oxidación anódica (AO, siglas en inglés) hasta foto electro-Fenton solar (SPEF, siglas en inglés), obteniéndose las mayores tasas de degradación con este último: 55% y 50% de pirimetanil y metomilo, respectivamente, en 5 minutos de tratamiento. Este trabajo se realizó con la colaboración del Prof. Anastasios J. Karabelas y el Dr. Konstantinos V. Plakas del Instituto de procesos químicos y recursos energéticos del Centro para la Investigación y Tecnología-Hellas (Grecia) en el marco del proyecto europeo de capacitación SFERA-II.

El segundo objetivo de esta Tesis Doctoral se centró en abordar la aplicación del sistema experimental a escala planta piloto previamente optimizado a un caso real mediante su combinación con un pre-tratamiento con membranas de nanofiltración (NF) del efluente de una Estación Depuradora de Aguas Residuales (EDAR). De esta manera se buscó aumentar la concentración de microcontaminantes orgánicos (OMCs, siglas en inglés) en la corriente de concentrado a la salida de la NF, a la vez que reducir el volumen total a tratar en el sistema terciario de electro-oxidación. Cabe destacar además el aumento en la salinidad del agua que se logra tras el sistema de NF en la corriente de concentrado, disminuyendo la resistencia óhmica y favoreciendo, por tanto, el tratamiento terciario posterior basado en electro-oxidación. Para estudiar el comportamiento del sistema de SPEF en matrices altamente salinas y complejas, se

desarrolló una receta de simulado de concentrado de NF a partir de la caracterización de concentrados previamente reportados en la literatura. Con el fin de trabajar al pH natural del agua, evitando la adición de reactivos para acidificar y volver a neutralizar, se evaluó el uso de ácido etilenediamina-N,N'-disuccínico (EDDS) como quelante del hierro en el proceso electro-Fenton (EF). A continuación, se estudió la degradación de cuatro OMCs: pentaclorofenol, terbutrina, clorfenvinfos y diclofenaco (a 200 y 500 μg L^{-1} de concentración inicial cada uno); mediante AO, EF, SPEF y AO asistida por luz solar a pH natural, usando Fe^{3+}:EDDS (1:2) a una concentración 0.1:0.2 mM en los tratamientos EF y SPEF.

Cuando se empleó como matriz el agua simulada de concentrado de NF, con una concentración de cloruros de 555 mg L^{-1}, el mayor porcentaje de degradación de los OMCs (500 μgL^{-1} de concentración inicial cada uno), se obtuvo mediante SPEF, alcanzando el 85% de eliminación del total. Esto se debe a que las especies oxidantes del cloro generadas mediante AO asistida por luz solar no fueron suficientes para degradar los OMCs (75% del total), pese a la presencia de menor materia orgánica en disolución debido a la ausencia de EDDS. Por otro lado, el proceso EF fue descartado ya que no se observó mejora con respecto a AO, consumiendo los radicales hidroxilo generados por la reacción Fenton en la degradación del EDDS.

Para la evaluación de este sistema de electro-oxidación en agua real, se recolectó efluente del tratamiento secundario de la EDAR de El Ejido y se pre-trató en el sistema piloto de NF disponible en la Plataforma Solar de Almería, hasta reducir el volumen inicial 4 veces (factor de concentración de 4). La salinidad del agua se incrementó de 2.1 - 2.3 mS cm^{-1} a 6.1 - 6.8 mS cm^{-1}, con una concentración de cloruros final entre 1182 – 1960 mg L^{-1}. El concentrado generado fue fortificado con los cuatro OMCs evaluados en el trabajo previo con agua simulada (100 μg L^{-1} de cada uno) y se estudió su degradación mediante AO, SPEF (con los carbonatos naturalmente contenidos en el concentrado y reduciéndolos a 20 mg L^{-1} para disminuir la interacción con los radicales hidroxilo) y AO asistida por luz solar. Los porcentajes de degradación de la suma total de OMCs tras 180 minutos de tratamiento fueron 84%, 69%, 75% y 84%, respectivamente. En esta ocasión, el mayor porcentaje de degradación con el menor consumo eléctrico, 5.3 kWh m^{-3}, se obtuvo mediante AO asistida por luz solar, ya que la mayor concentración de cloruros promovió una mayor generación de especies activas del cloro. Finalmente, se escogió el tratamiento terciario mediante AO asistida por luz solar para la degradación de 44 OMCs realmente contenidos en el efluente secundario de la EDAR y detectados mediante LC-QqLIT-MS/MS, consiguiendo eliminar el 80% del

total. Este trabajo se llevó a cabo en colaboración con la Prof. Ana Agüera y la Dra. Ana Martínez-Piernas del CIESOL (centro mixto CIEMAT-UAL) en la Universidad de Almería.

Tras el programa experimental realizado en la planta piloto de electro-oxidación iniciando con su puesta en marcha y optimización de parámetros de operación, se consideró estudiar y diagnosticar el estado de la superficie de los cátodos de las celdas empleadas en dichos ensayos. A medida que las horas de uso del cátodo se incrementaron, la producción in situ de H_2O_2 sufrió un progresivo descenso, desde 43 mg L^{-1} de H_2O_2 acumulado en 30 min, en el primer uso del cátodo, a 1.5 mg L^{-1} en el peor de los casos. En el momento en el que se observó una importante reducción de la electrogeneración de H_2O_2 que imposibilitaba el correcto desarrollo de los procesos EF y SPEF, se procedió al des ensamblaje de la celda y se realizó la autopsia de la superficie del cátodo mediante microscopía electrónica de barrido y rayos X, con objeto de intentar discernir los motivos principales del ensuciamiento del mismo y la consiguiente pérdida de eficiencia. En las imágenes obtenidas se observó una pérdida del recubrimiento de carbono-politetrafluoroetileno además de la formación de depósitos de hierro, justificando la caída en electrogeneración de H_2O_2 con la pérdida de superficie activa del electrodo.

Como parte de las actividades recogidas en el proyecto Marie Curie - ALICE “AcceLerate Innovation in urban wastewater management for Climate changE”, H2020- MSCA-RISE, la doctoranda realizó una estancia de investigación en el Centro de Nanotecnología y Bioingeniería Integrada (NIBEC) de la Universidad de Ulster (Reino Unido), en colaboración con el grupo de Investigación en Fotocatálisis liderado por el Prof. John Anthony Byrne. El objetivo de dicha colaboración fue el desarrollo y aplicación de un reactor foto-electro-catalítico a escala de laboratorio, para la eliminación simultánea de OMCs y microorganismos patógenos en agua natural. Como parte fundamental del reactor, se fabricaron dos foto-ánodos de nanotubos de dióxido de titanio mediante la anodización de una malla de titanio a 30V durante 3h y su posterior recocido a 500°C para promover la fase anatasa. El reactor consiste en una celda de 190 mL con un doble foto-ánodo de nanotubos de dióxido de titanio iluminados por una lámpara ultravioleta de 9 W a través de una ventana de cuarzo, con una irradiación aplicada de 50 W m^{-2}. El objetivo del tratamiento fue la eliminación simultánea de OMCs (terbutrina, clorfenvinfos y diclofenaco a 500 µg L^{-1} de concentración inicial cada uno) y patógenos (*E. coli* como bacteria de referencia en una concentración inicial de 10^6 UFC mL^{-1}), evaluando además la posible mejora al sustituir un cátodo sin contribución en el proceso de degradación, titanio recubierto de platino, por uno de fieltro de carbono capaz de electrogenerar H_2O_2. Evaluando por separado la degradación de los OMCs e

inactivación de *E. coli*, en la aplicación del proceso foto-electro-catalítico con cátodo de platino se observa una clara mejora en la inactivación de la bacteria (2 Log de reducción tras 120 minutos de tratamiento), con respecto al proceso foto-catalítico sólo (0.8 Log de reducción en el mismo tiempo de tratamiento). Sin embargo, la degradación de OMCs se mantuvo en el mismo ratio, en torno al 70% del total tras 60 min. Al sustituir el cátodo de platino por uno de fieltro de carbono se incrementó la eficacia en la inactivación de *E. coli*, reduciendo su concentración en 2.7 Log, aunque los OMCs mostraron porcentajes de degradación similares. Cuando finalmente se llevó a cabo la degradación de OMCs de forma simultánea a la inactivación de bacterias mediante foto-electro-catálisis con cátodo de carbono, se observó un aumento significativo en la desinfección, alcanzando el límite de detección del método con una reducción de 4.5 Log. Esta mejora se debe a la presencia de metanol procedente de la solución en la que van pre-disueltos los OMCs, que actúa como neutralizador de huecos aumentando la fotocorriente y que además se oxida generando formaldehido, una sustancia altamente tóxica para los microorganismos (LC_{50} for *E. coli* = 1 mg L^{-1}). Como consecuencia de este resultado, se evaluó el efecto de la presencia de sustancias neutralizadoras de huecos en la desinfección, utilizando para ello acetato y metanol en una concentración de 5 mM. En ambos casos, como está descrito en la literatura, se observó un aumento en la fotocorriente respecto a la alcanzada por el sistema en ausencia de ellos y, por lo tanto, se produjo un incremento en la tasa de inactivación de la bacteria siendo mayor en el caso del metanol por la generación de formaldehido.

Finalmente, y como resultado de la estrecha colaboración de la doctoranda y la Unidad de Tratamientos Solares del Agua en el proyecto SFERA-II con la empresa DeNora, se llevó a cabo la evaluación de un sistema comercial de electro-oxidación especialmente diseñado para la reducción de demanda química de oxígeno en aguas industriales y basado en la acción de las especias activas del cloro. En el marco de esta colaboración, y como parte de los objetivos desarrollados en esta Tesis Doctoral, se llevó a cabo la evaluación de una planta piloto equipada con una celda de ánodos dimensionalmente estables (DSA, siglas en inglés) procedente de DeNora, combinándola con un reactor solar CPC, con una capacidad total de 38 L y con el objetivo de evaluar la posible mejora en la eficiencia del tratamiento de lixiviados de vertedero. Dichos lixiviados presentaban una alta carga orgánica (>2000 mg L^{-1} de carbono orgánico disuelto (DOC)), siendo el objetivo del tratamiento disminuir su toxicidad e incrementar su biodegradabilidad para poder combinar finalmente con un posterior tratamiento biológico (logrando así reducir los costes de operación asociados). En primer lugar se llevó a cabo el tratamiento de los dos lotes de concentrado de lixiviados mediante foto-Fenton solar, observando una

necesidad de energía UV acumulada excesiva (142.2 kJ L^{-1}) para lograr sólo un 30% de reducción del carbono orgánico disuelto (DOC, siglas en inglés) en el primer lote de lixiviados (diluido 1:1 con agua destilada). En el segundo lote no fue posible llevar a cabo el tratamiento de foto-Fenton solar a causa de la gran cantidad de espumas generada, que provocó grandes oscilaciones del DOC imposibilitando su seguimiento. Posteriormente se trataron los lixiviados mediante electro-oxidación, electro-oxidación añadiendo H_2O_2 y electro-oxidación combinada con radiación solar, siendo este último el que mayores tasas de degradación de DOC y de nitrógeno total mostró, 3.5 g DOC kWh^{-1} y 18 g TN kWh^{-1} en el primer lote de lixiviado tratado y 13.4 g DOC kWh^{-1} y 45.2 g TN kWh^{-1} en el segundo lote. Con este tratamiento, el primer lote de lixiviados, que presentaba una toxicidad del 53% de inhibición en la tasa de consumo de oxígeno por parte de fangos activos de EDAR, disminuyó su toxicidad al 6% de inhibición, y en ambos lotes estudiados se incrementó su biodegradabilidad hasta valores adecuados para la posterior aplicación de un tratamiento biológico. Gracias a este estudio se corrobora la mejora que supone la aplicación de la luz solar a los tratamientos electroquímicos de aguas industriales, lo que puede significar un paso adelante hacia la aplicación de estos sistemas altamente oxidantes presentándose como alternativa viable, sostenible y verde, a los tratamientos puramente electroquímicos, suponiendo unos costes de explotación menores debido al menor consumo energético.

Chapter I. Introduction

1. Water challenge

Water is a crucial element to sustain life. All living beings depend on water on one way or another, since it is involved in most of their activities, directly or indirectly. For wildlife water poses a necessary resource for life, since for multiple species of animals and plants pose the medium in which their life cycles are developed. However, especially for humans, water has become into a singular heritage value, being used for hygiene and drinking, for the development of recreational activities, and most importantly, for the irrigation of crops and the performance of industrial activities such as energy production. Due to its relevance, source preservation and correct management of this element must be carefully dealt with considering all the disturbances that human activities could cause on it, ensuring that the effects promoted by them are within a tolerance range that should not be excessive to prevent the resource deterioration in a way that become permanently unusable.

In this context, United Nations (UN), aiming to preserve the integrity of water resources, declares in its Sustainable Development Goal No. 6: “ensure availability and sustainable management of water and sanitation for all” [1]. For monitoring the consecution of this goal UN-Water compiles data provided by the countries that participate into the initiative within 11 global indicators, being able to track them and thus creating a reference baseline to compare and follow the advances towards more sustainable water usages via reports issued to the pertinent authorities annually. The target of these reports is developing tools for the creation of new ways to access drinking and sanitation water worldwide, while, at the same time, improving their availability and correct usage.

Through these reports, water scarcity caused by the increase in consumption and climate change associated effects, has been shown. Moreover the high water stress levels present within the Mediterranean basin and in the countries downstream of big rivers is evidenced. In this context, finding new sources of water becomes a priority aiming the water stress level decrease thus new ways to get drinking water (desalination) or for agriculture activities (water reuse) have been proposed and Food and Agriculture Organization for UN encourages the research, development and implementation of these new technologies.

In the European Union (EU), the main reason behind the efforts to increase water resources availability is population increase. In 2020, EU 27 (after Brexit) had 447.7 million inhabitants [2], the third most populated region after China and India. In consequence, Europe is one of the regions in the world where higher volumes of

industrial and urban effluents are produced which means that there is a strong contamination of water bodies. From the Agricultural activities promoted by the Common Agrarian Policy oriented towards food availability, there has been a neglecting behaviour as intensive food production requires large amounts of fertilizers and pesticides, which in a great portion, have been ending in the surrounding waters around these agricultural areas. E.g. in Almeria (South-East of Spain) characterized for a semi-arid climate and which economy is mainly driven by intensive agricultural production, according to the mentioned UN reports, around 95% of available fresh water is extracted for different uses.

Even so new policies already promote less aggressive techniques aiming it multiple actions towards the reduction or depuration of pollutants contained in water, the greater or lesser success of them led to that the consequences of this contamination are still being felt in many areas.

There are two ways to measure the quality of water. The first method implies assuming as baseline for water quality the source´s status before the human intervention, that is highly complicated as water is naturally mixed with several unknown substances. For this reason, the second and more realistic method is done via standardized water quality levels according to the final use of the water. A list with the most representative, but not all, parameters admitted for measuring the grade of water quality are the following: amongst physical characteristics there are usually used total dissolved solids, solids in suspension, pH, hardness, turbidity and temperature. Within the chemical characteristics the most usual ones are dissolved oxygen, biological oxygen demand (in 5 days) (BOD_5), chemical oxygen demand (COD), total nitrogen, phosphorous, sulphur and chlorine, toxicity and pathogens.

Required capacities for depuration will depend on the persistency of the pollutants and on their possible integration on the ecological cycles, being important not to overcome the self-depuration capacity of the water body. If any of these parameters exceed such capacity, the vulnerability of the ecosystem increases, compromising the water quality in the influenced area thus directly risking the flora and the fauna while diminishing the availability of the resource for future uses.

Recently water-energy nexus has attracted the interest of the scientific community. This term refers to the inexorable link between water and energy, either the water consumed for energy production or the energy consumed for water treatment (purification,

depuration, disinfection, separation, etc.). The constant increase in water requirements and the reduction of available sources due to climate change effects entailed very negative consequences on the energy system. For this reason in 2014, the Environmental Protection Agency (EPA) tasked the United States Department of Energy to develop and issue a report remarking the importance of this nexus and the necessity for joint policies related to the reduction of wastage in energy production and water consumption in order to reduce water stress levels by carrying out the management of energy and water resources simultaneously. The reason behind this document were droughts in the United States of America in 2012 evidencing problems for energy production when water is scarce [3]. In recent years, water-energy nexus has increased its scopes including also the food production, as agriculture is the biggest consumer of water in the world [4] and the Water Energy Food and Ecosystem Nexus (WEFE Nexus) emerged, addressing an integrated approach of the links between water, energy, agriculture, water supply and treatment, as well as the environment.

1.1. Urban wastewaters

Urban wastewater is defined in the Council Directive 91/271/EEC namely Urban Waste Water Treatment Directive (UWWTD) as domestic households effluents within inhabited areas, as well as certain “industrial” waters from commercial activities undertaken within the cities [5].

According to de UWWTD, two categories are defined: properly “domestic water” referring to water that reaches the treatment plants originated exclusively from domestic households, and “urban water” including domestic water and these coming from certain industries typically installed in conurbations which discharge their effluents into the city’s sewage system. Additionally, water runoffs and rainwater fall under the frame of urban water [5]. Both waters are treated into urban wastewater treatment plants (UWWTPs), commonly presenting a first step consisting of a solid-liquid separation via mechanical methods, a subsequent biological treatment and, if recalcitrant compounds are present in the secondary effluent, or pathogens must be removed for reusing purposes, further depuration via tertiary treatments will be needed.

UWWTPs are specifically designed having as a reference the population of a municipality, albeit sometimes received waters from different sources, as hospitals or even from agro-industrial facilities which practices and intensive agriculture involves a strong pressure on the resource by discharging drugs or pesticides with great persistence in the environment. An exhaustive characterization of the substances

contained in the influent will allow the selection of appropriate technologies for their successful and efficient depuration in UWWTPs.

Wide variation on UWWTP influent characteristics appear depending on the population and the specific activities developed on different conurbations. Even in the same UWWTP the influent varies seasonally diluting the contaminants in the rainy season or increasing the organic load in summer or winter if it is a touristic municipality. The main parameters characterizing urban wastewaters effluents are: 500 - 1200 mg L^{-1} of COD, 250 - 560 mg L^{-1} of BOD_5, 30 - 100 mg L^{-1} of total nitrogen, 20 - 75 mg L^{-1} of ammonia, 6 - 25 mg L^{-1} of phosphorus, 250 - 600 mg L^{-1} of total suspended solids and 200 - 480 mg L^{-1} of volatile solids [6].

In order to analyse these data, compare different treatment plants and possible solutions as well as to calculate the size and volume to be treated by the UWWTP, some indicators have been developed. One of them is Population Equivalent (PE) that can be calculated in 2 ways, either in water volume generated as effluents towards the UWWTP or in BOD_5. These two ways of calculating PE indicator are not interchangeable and once one is selected for the design of a UWWTP the authorities shall abide to it. In Europe, a value of 60 mg/day of BOD_5 have been selected as the value for 1 PE [5].

It is important to notice that previously to the implementation of the UWWTD, a great disparity in the population whose waters were depurated before discharge was evidenced ranging from the 11% corresponding to Slovenia population to the 94% of Netherlands. Through the application of this directive, a significant advance in water depuration was observed in 2014, when most of the EU members were able to treat the urban water generated by 50% of their population prior to discharge. Looking specifically at Spain, data reported a water treatment capacity of 50% of the population in 1990, which increased till 85% in 2014 [7]. Figure 1 represents variation among all member countries. Those where a decrease in treated water is observed are countries that in 1990 were not yet in the EU and therefore lacks reliable data [5].

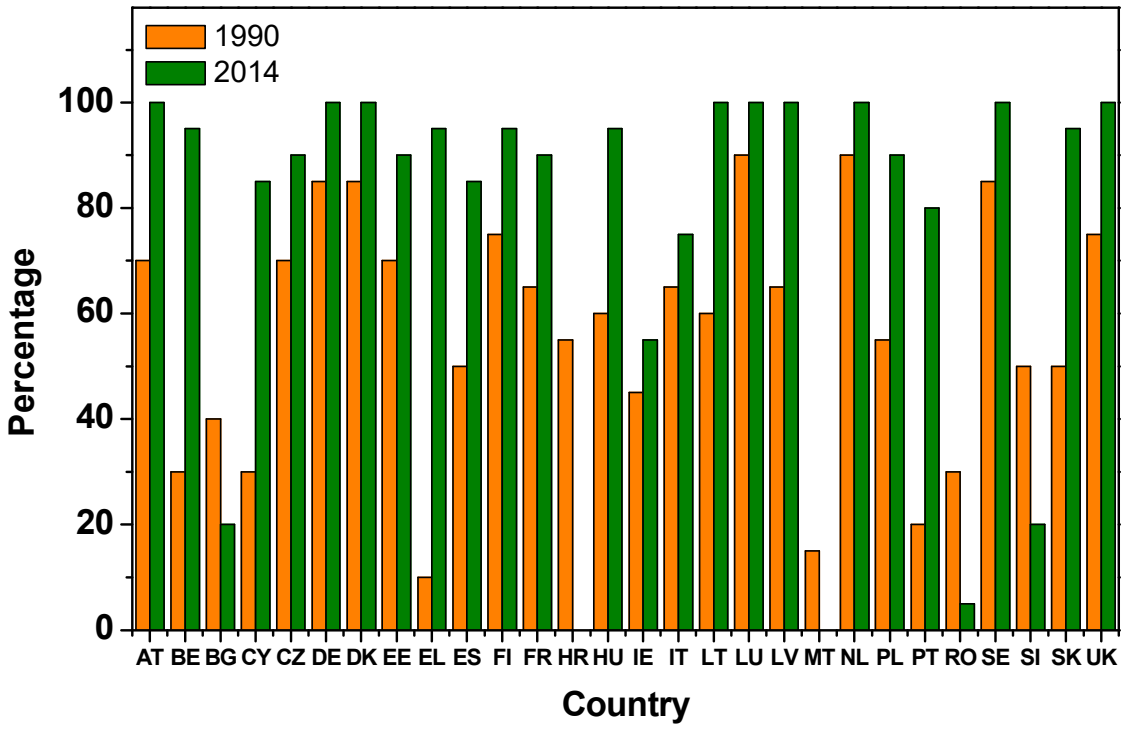

Figure 1. Population percentage whose waters were treated between 1990 and 2014 in each country of the EU (Austria - AT; Belgium - BE; Bulgaria - BG; Croatia - HR; Cyprus - CY; Czech Republic - CZ; Denmark - DK; Estonia - EE; Finland - FI; France - FR; Germany - DE; Greece - EL; Hungary - HU; Ireland - IE; Italy - IT; Latvia - LV; Lithuania - LT; Luxembourg - LU; Malta - MT; Netherlands - PL; Poland - PL; Portugal - PT; Romania - RO; Slovakia - SK; Slovenia - SI; Spain - ES; Sweden - SE).

1.2. Industrial wastewaters

Industrial wastewaters are those that come from an industrial facility used in any of its manufacturing, production, transformation, consumption, cleaning or maintenance processes and their management pose a difficult and costly problem to solve. Specifically, wastewater from chemical industry is one of the main challenges to face for depuration and purification technologies not only for the vast volume produced but the hazardous compounds that are included in the effluents. Nevertheless this fact has made chemical industry one of the most advanced regarding the improvement of wastewater treatments, with the aim of reaching discharge standards described in regulations or to achieve enough quality for their reuse in the own industrial processes. Chemical industries can be further divided into different types regarding the product generated in the process as described below:

- Pharmaceutical and personal care products industry is probably the most important source of organic microcontaminants due to a wide range of chemicals used in the manufacturing and also for the generation of new organic substances, posing a danger for the water reuse [8]. These industrial wastewaters present a variated composition and concentration of different pollutants. Additionally, substances produced in the pharmaceutical industry are mostly complex organic chemicals, most of them very recalcitrant, showing a high resistance to conventional biological degradation.

- Textile Industry is known to demand a high water consumption (7.9 billion m^3 of water in 2017 [9]), at the same time that uses a variety of chemicals for its different processes. Most of the environmental issues come from the bio-refractory nature of the wastewaters from dyeing and finishing stages. On these cases dyestuffs and chemical additives as polyvinyl and surfactants are present in the effluents. Their characteristics are high COD (150 - 10000 mg/L), BOD_5 (100 - 4000 mg/L), high pH (over 6) and colour content [10].

- Pulp and Paper Industry wastewater contains a number of contaminants coming, for example, from wood extracts such as resins, tannins or lignin amongst others. On the other hand during the industrial process other compounds arise as polyphenols, chlorinated organic compounds, aromatic compounds, dioxins and furans. Those wastewater characteristics vary between a COD value of approx. 1500 mg L^{-1} for the wood chipping operation to up to circa 9500 mg L^{-1} just after the first stage of bleaching [11], although they can present differences depending on the origin of the wood and the bleaching process. Compounds directly extracted from the wood are usually non recalcitrant while those coming from the chemical process itself are usually persistent against biological treatments and therefore aggressive oxidative processes are required to be able to achieve current regulations [12].

- Agro-Industrial wastewaters are also highly variable as the come from oil extraction plants, fresh-cut industries, winery or greenhouses for example. The main problem with these wastewaters is the wide and heterogeneous composition of various pollutants, with alcohols, nitrogenised and organic acids as well as many recalcitrant compounds. Additionally, there are many of those pollutants with a marked chelating character leading to an increase of toxic heavy metals in solution unable to be degraded by conventional wastewater treatments.

- Landfill Leachates are produced by rainwater entering the waste deposited in a landfill, dragging all the dissolved substances. The final effluent usually contains harmful and recalcitrant substances which can generate negative impacts in the surroundings if they are not properly treated. The chemical composition vary depending on the landfill composition, but its main characteristics depends on the maturity of the leachate, containing a high organic charge but biodegradable when landfill is young and a low organic charge but non-biodegradable when it is old.

- Bilge and Ballast wastewater are the most common effluents in commercial and naval vessels. They present a big challenge due to their high COD from engine oil and fuel, effluents from the cargo holds and, in case of petrochemical transport vessels, the condensed “spirits” from the manifolds. Years ago, ships directly discharged those waters into international waters, but nowadays such activity is forbidden. Some ports have developed the required infrastructure to receive bilge water from the vessels that arrive to their pier. Ballast water, on the other hand, present a different problem. These waters are taken into the ballast tanks while unloading cargo to maintain stability. The main problem is that this water has to be discharged when loading the ship, which can happen on a very different region. This means that microorganisms, bacteria or algae collected in the port of departure can be discharged on a very different ecosystem. For these reasons, ballast water needs to be depurated to ensure a safety discharge anywhere. With the aim of addressing this problem, the International Maritime Organization, dependent from the UN, issued the “International Convention for the Control and Management of Ships’ Ballast Water and Sediments” regarding the challenges and goals to be attained for maritime operators (ports, vessels, ship-owners and designers) in 2004, entering into force in 2017 [13].

Taking into account the strong interaction between industrial activities and water, in 2002 Hoekstra, A., defined the water footprint, a new indicator that allows evaluating all activities related to water use in companies, contributing to the evaluation and improvement of their sustainability. Water footprint of a product is the volume of water consumed both directly and indirectly (volume of water per unit of time) for its production. The importance of this indicator is that it allows identification of the most efficient products in terms of water consumption.

Water footprint can be complemented with other similar indicators such as the carbon footprint, thus finally obtaining a global view of the sustainability of the company

activities. In fact, in 2014, the International Organization for Standardization (ISO) published the ISO 14046:2014 standard - "Environmental Management - Water Footprint - Principles, requirements and guidelines" laying the foundations for the application of this indicator in the industry and therefore urging companies to reduce it.

Many leading industrial have embraced eco-friendly policies as part of their corporate social responsibility, incorporating a commitment for the reduction of their water footprint. Main actions taken by world-renowned brands are detailed below.

One of the companies working for a reduction in their water footprint is Heineken. In their 2030 goals aims to reduce their 3.5 m^3 of water consumed per m^3 of beer produced to just 2.8 m^3. Along this reduction in the water consumption for beer production, the company is developing a project for a more sustainable harvest and crop growing. In cooperation with the Andalusian regional government they are involved in a mixed olive/barley project located in Jaen and Granada provinces (Spain), enhancing water retention, nutrient renovation and soil value conservation[14].

Coca-Cola Company has also implemented water-sustainable policies in the agro-industry. Among some of their corporate social responsibility goals they proposed to reach an improvement of 25% in 2020 in manufacturing water efficiency referencing as baseline 2010 consumptions, having recently achieved a 1.92 m^3 of water consumption per m^3 of product made. This compromises only part of its water footprint. In 2013, Coca-Cola Company began a project named Sustainable Agriculture Guiding Principles outlining the best practices for the agricultural chain supply within the company. As well as those projects and the treatment of all the process water that doesn't end in the final product, the company "replenishes" the water footprint by funding projects for safe water access and reforestation in order to balance its water consumption [15].

Within the pharmaceutical sector the company Novartis fixed as objective to reduce its water consumption in 2025 to the half of that consumed in 2016 aiming to reach the "neutrality" in 2030, either via water consumption reduction, water replenishment or with the improvement of water quality in the places where they operate [16].

One of the biggest chemical companies in the world, BASF, recognises that its water footprint has to be assessed from the origin of the supplies and that an integral approach from production of raw materials to final consumer has to be undertaken towards achieving their sustainability goals [17].

On the automotive sector, most of the companies are focused on CO_2 footprint reduction, but both Toyota and Nissan have ambitious programs regarding water footprint

reduction. Nissan on their “Nissan Green Program 2022” aims a 30% reduction of process water consumption for 2022 having as reference that consumed in 2011, but the scope of their water footprint goes beyond the pure process [18]. In consequence, autonomous driving and electric vehicles are a point of main effort as improving driving efficiency via automation as well as reducing fuel production will reduce water stress via the water-energy nexus.

Finally, on the shipbuilding industry, water footprint is also concerning shipyards, ship-owners and ports. Ships consume water from their construction stage to their disposal as well as during their operational life (ballast water, cooling water, process water, bilge water and crew running water, amongst fuel, oils and supply production) [19]. Some operators as Maersk and MSC have addressed the problem of ballast water quality installing advanced treatment systems on their ships and designing the new ones for minimal ballast water intake either by the ships design or with logistical route management [20].

1.3. Legislation frame

The EU first recognised on a ministerial seminar about underground waters held in The Hague in 1991 that water should not be seen as a commodity but as a right, since was perceived a global decrease in its quality. Pertinent Resolutions from the Council in 1992 and 1995 demanded a review of the Directive 80/68/CEE on the protection of groundwater against pollution caused by certain dangerous substances, as it dated from 1979. With this in mind, EU decided not only to address the problem of pollution in the frame of underground waters, but provide a comprehensive solution for all kind of waters holding an integral approach. The deadline date given was the year 2000.

In this context the Water Framework Directive (2000/60/EC) (WFD) [21] was developed as the main legal body regarding water issues containing a series of so-called “Strategies against pollution of water” and outlining the guidelines to be followed to guarantee the water quality in all the EU countries. At that moment this was a completely new global approach to the water problem from the legal side, since previously the legislation was targeted to avoid deficiencies in the supply of water, but not in its quality of both supply and discharge into the environment.

For the first time, in WFD water was considered as a “patrimony that members need to protect, defend and treat as such” (WFD, consideration 1). It recognised that the EU needs to protect and deploy the means to supervise the quality and availability of water. Furthermore to reach those goals, it was recommended to all members got involved and

not only from the water overseeing entities but also from the energetic, transport, agriculture, fishing, regional politics and tourism (WFD, consideration 16).

In its Annex X the WFD develops the outline of a comprehensive list of compounds named as “First list of priority substances”. Selected substances were picked according to the Article 16 of WFD that marked out that either by a risk assessment under Directive 91/414/EEC and Directive 98/8/EC or in case that this is not enough, following the methodology descripted in the Regulation 793/3 has to be undertaken in order to ascertain which substances would be included in the list. Nevertheless, the Commission is currently working to improve and simplify the way to recognise and include priority substances in the list, as the existing procedure is complex having to consider different already mentioned directives and regulations.

Apart from WFD, UWWTD regarding the collection, treatment and discharge of urban wastewater was passed, undertaking the challenge of protecting the environment from urban and industrial effluents pollution, and defining the different treatments that could be applied. Despite the effectivity of its implementation, that allowed a reduction in the organic matter and pollutants discharged on natural water bodies, hence improving water quality, this directive is out of date. The current problems found in urban effluents come from the development of new pharmaceutical, personal care and agro-industrial products due to the appearance of persistent organic microcontaminants (OMCs), also known as contaminants of emerging concern, and even microplastics.

UWWTD implements an agenda that all EU members must incorporate to their water policies in order to comply with its objectives. Those countries that do not meet the criteria within the deadline could be subjected to a disciplinary regime.

Aiming to update the old legislation concerning new emergent pollutants, the European Comission issued Directive 39/2013 “as regards priority substances in the field of water policy”. Inside Directive 39/2013, Annex I listed the priority substances to be surveyed marking also the ones that are considered “priority hazardous substances”. In Annex II, it is defined the Environmental Quality Standard for each of these substances and the maximum annual average concentration, maximum allowable concentration and, in case of bioaccumulative pollutants, the maximum allowable concentration present in the biota.

Moreover, on March 2019, the Commission approved a Communication (COM/2019/128 final) concerning the problem regarding pharmaceutical pollutants. This Communication proposes a strategic approach to this kind of pollutants in order to reach an integral vision. By the way, this Communication does not affect the continuation, development or

application of legislation, normative or actions regarding those pollutants by EU members.

One of the countries that have addressed this new topic is Switzerland that has developed the first specific normative regarding micropollutants proposing the depletion of at least 80% of their initial concentration present in urban wastewaters.

Finally, the Parliament and the Council of the EU have passed a Regulation (EU 2020/741, of 25 of May of 2020) on the minimum requirements either in pollutants and pathogens, e.g. *E. coli,* for water reuse. The goals of this regulation are the need to both decrease the pressure on the Union water resources as well as to preserve the quality of water bodies. The regulation includes rulings for the quality to be reached depending on the final use of the reclaimed water and the origin of that reclaimed water.

2. Electrochemical systems for water treatment

Traditionally, water treatments are based on the application of a primary physical treatment consisting on the separation of the biggest solids, fats and sands and later a biological treatment where microorganisms metabolize organic matter contained in the wastewater stream producing CO_2 and water. However, the presence of hazardous and non-biodegradable contaminants has thrusted the development of advanced technologies (as pre-treatment or tertiary treatment stages) for the removal of these substances, such as advanced oxidation processes (AOPs) (based on the generation of $^{\bullet}OH$), membrane processes, ozonation or electrochemical treatments, in which this PhD Thesis is mainly focused.

Electrochemistry addresses all the chemical reactions that occur at the interface of an electrical conductor, known as electrode, and an ion conductor, usually a solution, by applying an external potential between two electrodes. Unlike conventional batteries in which energy is generated from a chemical reaction, where the anode is the negative pole and the cathode is the positive, in electrolytic cells, electrical energy is consumed to promote a chemical reaction, for that reason the polarity of the electrodes reverses, being the anode the positive pole and the cathode the negative one.

Chemical reactions occurring in aqueous solution will depend strongly on the dissolved ionic content, the applied potential between anode and cathode and the electrode composition. Materials conforming the electrodes (metals, mix of metals, semiconductors, etc.) will determined by the electrochemical treatment to be applied,

either coagulation, ion separation or oxidation, and will be a crucial parameter in their effectiveness.

The most widely used electrochemical technologies for water treatment, their mechanism of action and their main operation characteristics are described below.

2.1. Electrocoagulation

Wastewater usually contains suspended solid particles that can settle by their own. However very small particles can be found between 0.001 μm and 1 μm, called colloidal, which are impossible to decant or filter. These colloids have an electrical charge on their surface, commonly negative, so they repel each other preventing their agglomeration and subsequent sedimentation, conferring great stability. Many of pollutants contained in wastewater are colloidal.

To eliminate such particles, the surface of the colloids must be neutralized in order to destabilize and agglutinate them into larger particles that can sediment. For this, metallic cations such as Fe^{3+} or Al^{3+} have traditionally been added in the form of ferric and aluminium sulphates and chlorides what is known as coagulation process. The effectiveness of coagulation will depend on the mixture velocity, the pH and the dose of the coagulant, thus laboratory assays with jar-test equipment are necessary to determine optimal parameter values.

One of the main drawbacks of the chemical coagulation process is the large amount of sludge generated as waste at the end of the process, with very high values of both BOD_5 and COD [22].The direct discharge of this sludge with a high amount of organic matter can cause a severe impact on the environment, thus they must be subsequently treated.

As an improvement of this physicochemical treatment, electrocoagulation (EC) arises. EC does not require the addition of external chemical products since the cations are supplied to the system by means of a sacrificial electrode. Applying an electric current, metal anode (M) of Fe or Al, is oxidized releasing metal cations to the solution by means of reaction 1 producing also O_2 by oxygen evolution reaction (Reaction 2)[23].

$$M \rightarrow M^{n+} + ne^- \qquad \text{(Reaction 1)}$$

$$2H_2O \rightarrow 4H^+ + O_2 + 4e^- \qquad \text{(Reaction 2)}$$

In turn, at the cathode water is hydrolyzed into gaseous hydrogen and hydroxides following reaction 3.

$2H_2O + 2e^- \rightarrow 2H_2 + 2OH^-$ (Reaction 3)

Once in the bulk solution, the metal ions and the hydroxides react in between (Reaction 4), producing metallic hydroxides and polyhydroxides ($Fe(OH)_2$ or $Al(OH)_3$), which are insoluble chemical species.

$M^{n+} + nOH^- \rightarrow M(OH)_n$ (Reaction 4)

These hydroxy complexes are able to adsorb some of the contaminants contained in wastewater, as they form flocs that are separated by sedimentation. [24]. On the other hand, gaseous oxygen produced at the anode and hydrogen produced at the cathode are released as bubbles, interacting with the coagulated particles, attracting and transporting them towards the surface via natural buoyancy [23]. This phenomenon is known as electroflotation. EC process is completely described in detail in figure 2.

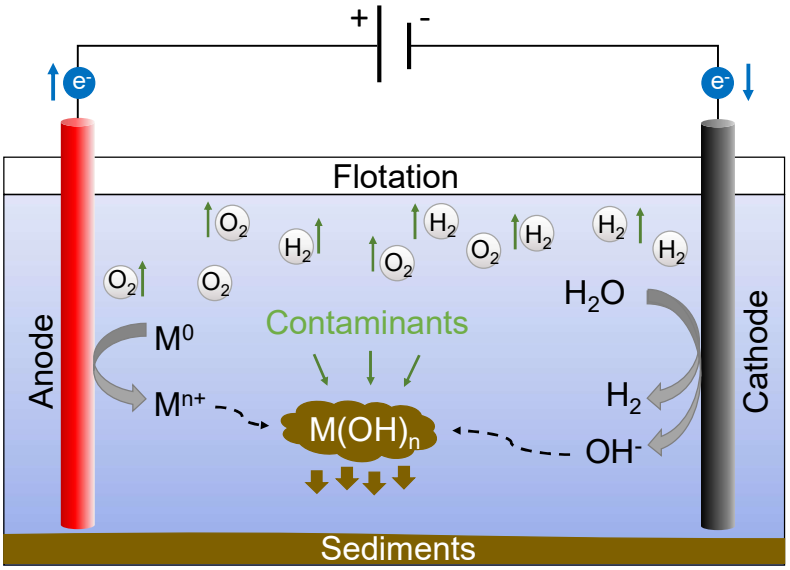

Figure 2. EC mechanism scheme in a cell of two electrodes.

Current density is one of the main parameters of EC since promotes anodic and cathodic reactions and defines the reaction rate, allowing its direct control. The relationship between the applied current density and the amount of metallic electrode dissolved is defined by the Faraday law (Eq. 1), being able to calculate theoretically the mass of Fe^{2+} or Al^{3+} added to the solution [22].

$$n = \frac{it}{zF}$$ (Equation 1)

being *n* the amount of dissolved metal (moles), *i* the current density (A), *t* the electrolysis time (s), *F* is the Faraday constant (96 485 C mol^{-1}), and *z* the charge of the cation (2+ for Fe and 3+ for Al).

However, actual concentration of cations found in solution is usually higher than the calculated, which is known as "superfaradic efficiency" [22]. This phenomenon may be due to the development of reactions at the cathode that favour Fe and Al dissolution and/or to the changes in pH caused by the oxidation and water reduction reactions favouring also the dissolution of ions.

The use of EC processes entails several advantages regarding conventional physicochemical treatment [23, 25]:

- More effective organics removal. EC process is faster and the flocs produced are bigger, more stable and resistant to pH variations.
- It can be applied to wastewater in low temperature and low turbidity conditions, where conventional coagulation is not very effective.
- Treatment is developed in a pH range between 4 and 9, so pH control is not necessary, except for extreme values.
- Addition of reagents is avoided, thus there is no pollution for their discharge neither final neutralization of the effluent is necessary.
- The amount of sludge produced is lower than in chemical coagulation and with greater content of dry and hydrophobic solids.
- The equipment is very simple and easy to operate.

However, this treatment also presents some disadvantages:

- As anodes are dissolved in the bulk solution they must be frequently replaced.
- Electrodes passivation can inhibit the electrolytic process.
- The price of required electricity can limit the application of the treatment.
- A high ionic strength is necessary to favour electron circulation.

2.2. Electrodialysis

First electrodialysis (ED) system was developed at the end of the 19th century as a combination of electrolysis and dialysis aiming for the elimination of harmful substances. Due to this duality, it is considered as an electrically driven membrane process [26]. The action mechanism is based on the principle that by applying a direct current (DC) to a

raw water stream, cations would move towards the cathode or negative pole, while the anions would move towards the anode or positive pole.

If several anion and cation exchange membranes are arranged in the space between electrodes, different compartments are created within the ED system. When an electrolyte is pumped inside the cell and an electrical field is applied, ions present in the aqueous solution are directed towards the electrodes according to their polarity (Fig. 3). Cations migrate towards the cathode, passing through the cation exchange membrane (CEM) but being retained by the anion exchange membrane (AEM). Likewise, anions migrate towards the anode through the AEM albeit the CEM will retain them [27]. As a result, two streams are obtained, a clean effluent depleted of ions and an enriched stream containing both cations and anions. Each unit built around an AEM, a CEM, a dilute channel and a concentrate channel is known as a cell pair. An ED stack is formed by the number of cells pairs required according to their application and two electronic compartments, which promotes the conversion of the current of ions into a current of electrons by means of an external DC circuit.

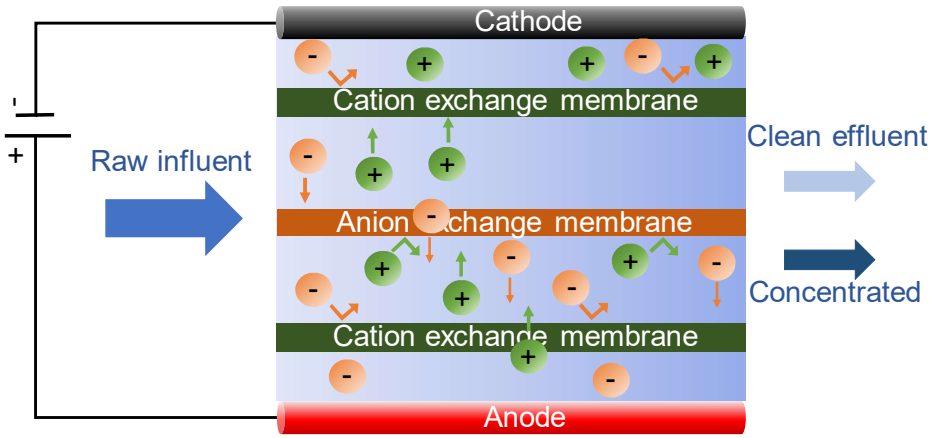

Figure 3. Simplified scheme of the electrodialysis procedure.

Conventional ED stack systems consist on a plate-and-frame electro-cell. Flow channels for the depleted and the concentrated solutions are created by interposing ionic exchange membranes between the net spacers, maintaining a fixed inter-membrane distance and allowing ionic flow through them. Spacers are provided with gaskets sealing the channels. Holes in the spacers generate differentiated ducts for the two hydraulic circuits which distribute each solution on the corresponding channel. ED device is closed with two end plates and compressed by bolts and nuts [28].

Despite being an electrically-assisted treatment, the main components of ED systems are membranes. Type of membrane and its characteristics define the performance of the process and the efficiency of the treatment, leaving the role of electrodes in the background.

ED directly competes with other membrane separation processes, such as reverse osmosis (RO), nanofiltration (NF), ultrafiltration (UF) and microfiltration (MF), presenting the disadvantage of the high cost of electrodes and ion exchange membranes, which also have a relatively short life time when working within a high-density electric field [29]. Consequently, despite being apt for multiple effluent treatment applications , its industrial commercialization has been relegated to desalination for drinking water production and to the recovery of substances from the concentrated stream such as heavy metals [30].

2.3. Capacitive deionization

Capacitive deionization (CDI) process was developed as a non-polluting, energy-efficient, and cost-effective alternative to desalination technologies [31]. Also, due to its high efficiency to remove ions from water, CDI can be applied to produce ultra-pure water without involving high costs.

This emerging technique works via electro-adsorption avoiding the high-pressure pumps required for separation membrane process. The history of this treatment dates back to 1960 when the first conceptual studies and electrode materials where developed, nevertheless it is not until 2010 that the first commercial units where developed from Voltea and not until 2017 that the first units for domestic use had been released [32].

The principle of the process is based on an electrical potential difference over a pair of electrodes thus removing ionic species from the stream of water according to their electrical charge. There are 4 main architectures (Fig. 4). The first two are basic, CDI architectures with a flow between electrodes (Fig. 4a) or a flow through one (Fig. 4b). On the first one, the stream is fed between the electrodes and the clean stream departs from the other extreme. On the latest, the flow passes through the electrodes that are in this case porous to water. In these two methods, adsorbing filters need replacement with time as active sites are being filled and coped with ionic charge

In recent years this technology has been further improved in both removal and energy efficiency resulting in the so-called advanced CDI systems membrane-CDI (MCDI), which is a modified CDI cell that integrates ion exchange membrane on the surface of

the electrodes (Fig. 4d). This method presents better desalination due to the prevention of co-ion impact.

To regenerate electrodes, the potential applied has to be inverted. As ion exchange membranes allow only passing cations or anions, ions are released from the electrodes unable to cross the membrane into the other, so they exit the stream concentrated and need disposal (Fig. 4e). During this time, the plant is not operating [33].

Recently, Flow-CDI process has been developed which uses a slurry solution of activated carbon as an electrode and filter (Fig. 4c). As this slurry can be later desalinated in a continuous flow when it reaches its storage tank, better efficiency removal can be achieved as desorption phase does not mean the stop of the plant.

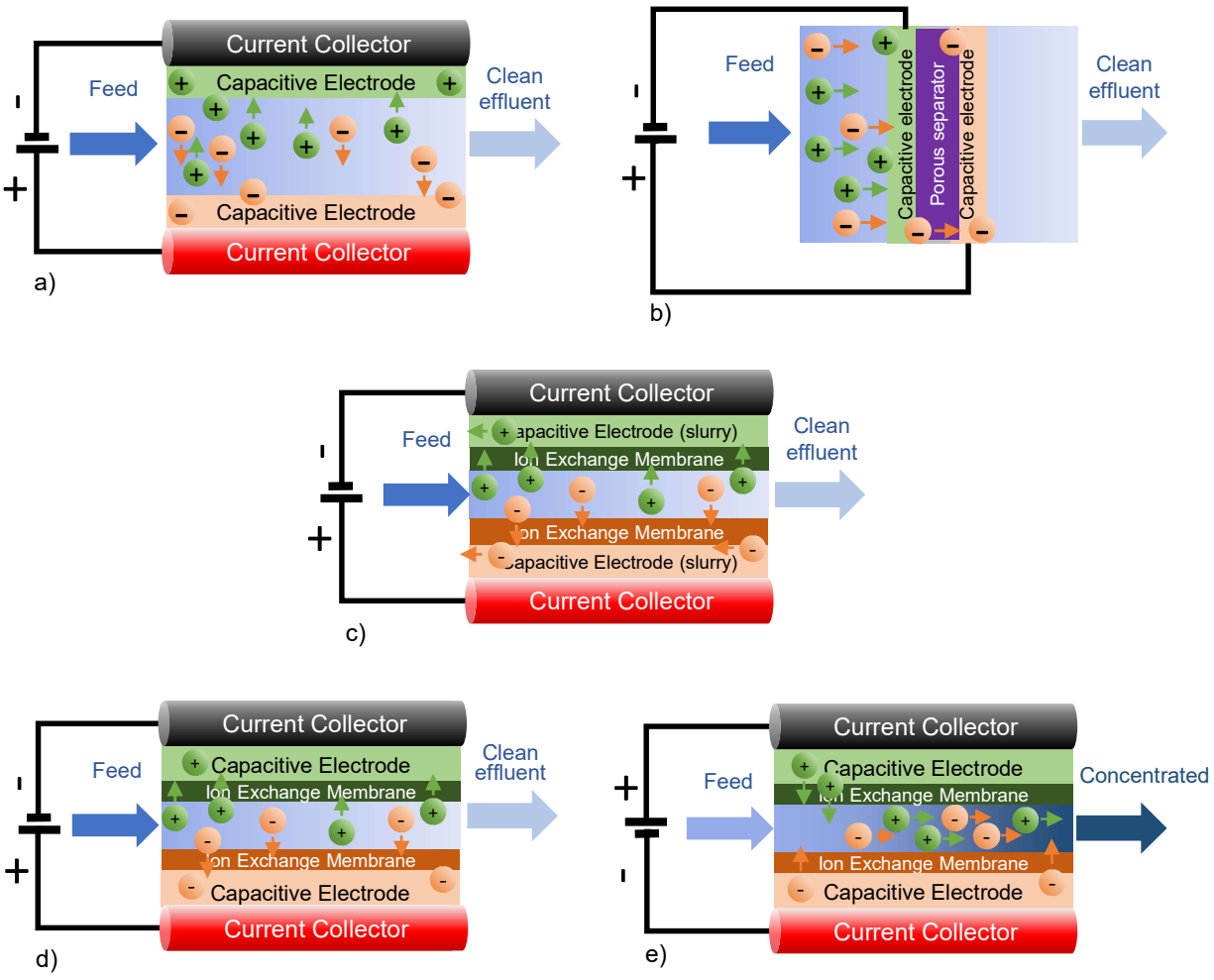

Figure 4. CDI systems configurations. a) flow between, b) flow through, c) carbon flow electrodes, d) MCDI purifying and e) MCDI – regenerating.

The most important and defining element of this treatment is electrodes composition, both for cost and efficiency reasons. From the 1970s, mostly used material has been activated carbon, being the base for the development of new electrodes. Several studies addressed carbon-based electrodes modification aiming to increase their porosity, and therefore increasing the reactive surface, and their reactivity by its doping with other element.

Two latest developments related to electrode materials are carbon nanotubes as well as graphene based electrodes [32]. Those two electrode materials show a substantial improvement thanks to an increased surface for interaction with the stream, thought they present manufacturing high costs.

The most common actual application of CDI is after a RO system obtaining a very high quality water stream.

2.4. Electroreduction

Electroreduction is a relatively new process studied since the end of the 20th century. Many of the core mechanisms driving involved reactions are still being under study. Actually, this technology has not been deployed further than laboratory scale yet, but under controlled conditions.

2.4.1. Electroreduction of Halogenated Compounds

One of the first steps that must be faced when treating halogenated compounds is the kind of material to be used for electrodes preparation, the solvent and the supporting electrolyte. Carbon, steel, mercury, copper, tin and several noble metals are used for electrode construction albeit nowadays several other nanomaterials and neo-composites have been also developed. Nevertheless, silver, even with its high associated cost, has been picked up as one of the preferred electrodes for the reduction of halogenated organic compounds due to its capacity to reductively cleavage of carbon-halogen bonds. The selection of the supporting electrolyte and solvent has to be decided based on the chemical compatibility with the substrate, cost, stability, inertness, toxicity, ease of purification [34]. On top of this, they must be conductive so significantly positive and negative potentials can be applied [35].

The following reaction represents the process (Reaction 5).

$$2RX + 2e^- \rightarrow R_2 + 2X^- \qquad \text{(Reaction 5)}$$

The reduction of the carbon-halogen bond can be done either directly or with aid of a catalyst. In order to address this topic, the energy for the bonds shall be considered. Enthalpies are shown on table 1.

Table 1. Halogenated compounds bonds and their corresponding enthalpy energy.

Bond	Enthalpy (kJ mol^{-1})
C-I	213
C-Br	285
C-Cl	327
C-F	566

Up to a C-Cl bond, a direct cleavage reaction has been achieved, while C-F bond cleavage has been never observed to occur directly. For this reason, the use of a catalyst is necessary, in order to reach the enthalpy for C-F separation. Instead of adding a direct reagent, in-situ electrogeneration of the catalyst is desirable, taking into account that the catalyst must be able to break the target bond and the precursor must be easier to reduce than the substrate, that is, to have a lower reduction potential.

One of the most important compounds treated by electroreduction is Chlorofluorocarbons (CFCs). In 1986, Montreal Protocol on Substances that Deplete the Ozone Layer was introduced and made compulsory the elimination of CFCs. To achieve the removal of chlorine atoms from those compounds there are two main possibilities: high-temperature incineration or electroreduction. Electroreduction shows lower reaction energy and operation costs, while being better at target product selectivity. It is known that incineration can produce other pollutants, mainly carbon dioxide and hydrogen halides [35]. Also, when treated with electroreduction, CFCs remediation products are more environmentally friendly or converted in propellants via electro-synthetic processes [34].

Disinfection Byproducts (DBPs) can be also treated by electroreduction. Trihalomethanes (THMs) and haloacetic acids are the two most common DBPs. DBPs are generated in drinking water, posing a threat to human lives and creating the necessity of removing them from wastewater effluents and water reservoirs. They are mainly formed via reaction of chlorine with organic matter. Other two ions that can also react and form DBPs are bromine and iodine, each of them even more dangerous than chlorine in the risk they pose to human life. Each compound removal has been investigated with different types of electrodes, for example THMs have been reduced at

silver cathode in a 50/50 mixture of acetonitrile and water [36], Radjenovic et al. [37] worked on a resign-impregnated graphite cathode that was able also to reduce THMs.

Pesticides, fungicides and bactericides can also be treated via electroreduction. These compounds are significantly dangerous for health and they are required to be eliminated from water flows. Amongst them, organophosphates, as dichlorvos or tetraclorvinphos are treated with silver cathodes[38]. Dicarboximide pesticides pose a great risk as they disrupt the endocrine system and have reproductive development effects. Sreedhar et al. [39] used a mercury cathode to reduce such compounds and render them harmless. Dichloro-diphenyl-trichloroethane (DDT), for example, and their degradation products have been studied under different electrodes. For this specific case, glassy carbon and silver have been the most used to dechlorinate DDT and silver has showed its capability to cleave C-X bond at lower potentials than glassy carbon [35].

Finally, flame retardants can be also considered being made from a wide range of brominated compounds known as persistent organic pollutants. They mostly fall into two categories. The first of them is brominated phenols. Rondinini et al. [40] managed to degrade bromophenol using silver cathodes in an acetonitrile medium while Xu et al. [41] used constant current electrolyses with surface-roughened silver cathodes instead of polished ones, yielding better results. Second category is hexabromocyclodecane (HBCD), the most widely used brominated flame retardant in the market [35]. Again, silver electrodes by using direct reduction is the preferred method able to completely reduce HBCD.

2.4.2 Electroreduction of Nitrates

Specifically for nitrates, electroreduction pose several advantages over other treatments, since no sludge is produced, investment cost is low and it is able to treat highly concentrated waters [42]. The most common pathway followed for the reduction of nitrates is a direct reduction on the cathode surface[43]. Products obtained after nitrates electroreduction are nitrites, ammonia and nitrogen (Reactions 6-8) [42] which are not desirables products, nevertheless those are easy to be oxidized on the anode.

$NO_3 + H_2O + 2e^- \rightarrow NO_2^- + 2OH^-$ (Reaction 6)

$NO_2^- + 2H_2O + 3e^- \rightarrow ½\ N_2 + 4OH^-$ (Reaction 7)

$NO_2^- + 5H_2O + 6e^- \rightarrow NH_3 + 7OH^-$ (Reaction 8)

Various studies reported in literature [42, 43] showed also that the process is accelerated when higher potentials are applied, but an excess of potential results in the reduction of

nitrogen into ammonia, a compound that is mentioned before as non-desirable albeit poses no problem as it can be oxidized in the anode [44, 45]. Another operating factor that influences the reaction is the pH. It has been determined that reactions are positively affected from a low pH, but this affects metallic electrodes due to high corrosion. To address the later, different materials have been tested.

In the case of indirect reduction (driven by reducing intermediates), different approaches have been tackled. Pronkin et al. [46] used bimetallic nanoparticles. In this study, supported Cu/Pd/C electrodes were used on a solution containing 0.1 M H_2SO_4 and 0.1 M $NaNO_3$, observing an increase in the catalytic activity. Other studies, like the one made by Reddy and Lin [47] used palladium, platinum, and rhodium on carbon substrate obtaining with rhodium the highest efficiency for nitrate removal. Graphite felt was used as an electrode by Ding et al. [42] begin highly resistance to corrosion under electroreduction processes, especially if they are under heavy stress.

2.5. Electrochemical oxidation

Electro-oxidative processes are a very effective tool for the degradation of recalcitrant organic substances having great versatility. They can be applied as a tertiary treatment for the degradation of OMCs along with the disinfection of pathogenic microorganisms. They are also suitable for the depuration of very complex waters with high organic load, salinity, toxicity and low biodegradability. In fact, they are widely applied in industrial environments to treat bilge water, landfill leachates or membrane rejections.

Moreover, electrochemical processes can be combined with a biological treatment. In this case, electro-oxidative treatment would be applied as a pre-treatment until making the effluent biocompatible.

This PhD Thesis is based on the application of electrochemical processes, therefore different electro-oxidative treatments, as well as their performance mechanisms, are described in detail in the following sections.

2.5.1. Direct oxidation on anode surface

In direct electro-oxidation process (Fig. 5) target contaminants are adsorbed on the anode surface where they are oxidized by the transfer of electrons from de molecule to de anode avoiding the intervention of any mediator.

This treatment is theoretically possible as long as the applied potential is low and keeps below the oxygen evolution potential. As a consequence degradation kinetics are also low and strongly depend on the anode electrocatalytic activity [48].

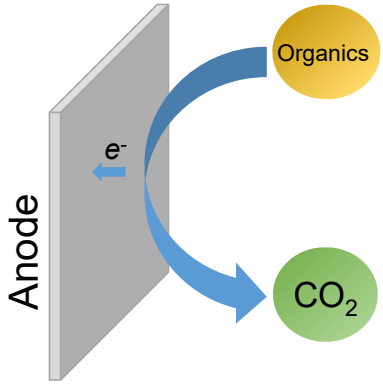

Figure 5. Description of organics degradation applying direct oxidation process.

To increase the reaction rate, electrocatalytic anodes, such as Pt or Pd have been proposed. However, another drawback of the application of low potentials is evidenced by a decrease on the anode activity when time of operation is increasing due to the formation of a layer of polymer on the surface. This phenomenon is known as poisoning or deactivation. Likewise, this polymer can be eliminated by the application of a highly oxidative potential, thus regenerating the anode surface [48, 49].

Another crucial point to achieve high process efficiency is to ensure that target contaminants reach the electrode surface so that they can be oxidized [50], if not reaction rate will be limited by mass transfer.

Modelling of direct oxidation processes has been widely described. Complexity of the model will be defined by the type of process and the level of description of the system that we want to achieve. The greater the number of characteristics described in the model, the greater number and complexity of resulting equations [50].

However, modelling the system in actual operation conditions is very limited, being practically unfeasible since the composition of wastewater reaching the treatment plant is usually unknown and/or highly variable.

2.5.2. Indirect oxidation by electrogenerated oxidants at anode surface

In indirect oxidation (Fig. 6) electrons from organic pollutants are not exchanged directly on the anode surface [48]. Instead, oxidizing species are electrogenerated on the anode

and transport to the bulk solution to oxidize organic matter, so they can be considered as the intermediaries transferring electrons between the anode and the organic contaminants.

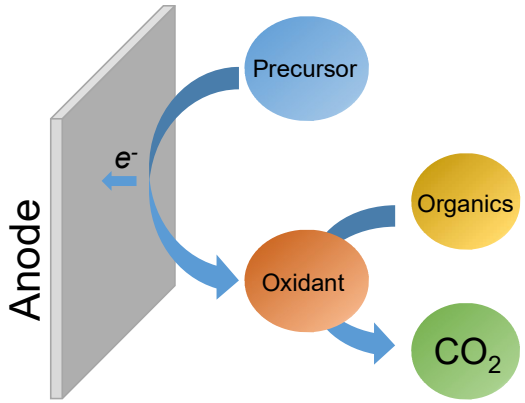

Figure 6. Mechanism of organic contaminants removal by indirect oxidation process.

These oxidizing species can be generated from two sources, from the intermediates generated (•OH) as result of the oxygen evolution reactions described in section I.2.5.2.1 or from the ionic species dissolved in water (mainly ClO^- from Cl^-) addressed in sections I.2.5.2.2 and I.2.5.2.3.

2.5.2.1. Intermediates of Oxygen Evolution Reaction

Mechanism for the indirect electrochemical oxidation of organics at high potential by means of intermediates of oxygen evolution reaction was proposed in the 90s [51]. The process consisted on water discharge on the anode surface producing •OH, which remain adsorbed on the surface (Reaction 9) and are able to oxidize organic compounds (Reaction 10). S [·] represents the surface sites where •OH species can be adsorbed and OP the oxidized products.

$$S[\cdot] + H_2O \rightarrow S[^{\bullet}OH] + H^+ + e^- \quad \text{(Reaction 9)}$$

$$S[^{\bullet}OH] \rightarrow S[\cdot] + OP + H^+ + e^- \quad \text{(Reaction 10)}$$

It has been checked that the material conforming the electrode, the experimental conditions and the composition of the wastewater strongly influence the oxidation process [48, 52]. Above all, the material nature will define the interaction of hydroxyl radicals with the electrode surface and therefore determine the reaction rate.

The nature of the electrodes will determine their interaction with •OH, being able to clearly differentiate between two types: [49, 53, 54]

a) "Active" anodes: in the electrode areas (commonly of metal oxide, MO_x) where higher oxidation states above the standard potential for oxygen evolution (1.23 V) are available, adsorbed hydroxyl radicals can interact with the anode leading to the so-called superior oxide (MO_{x+1}) (Reaction 11).

$$MO_x (^{\bullet}OH) \rightarrow MO_{x+1} + H^+ + e^- \quad \text{(Reaction 11)}$$

Thus, on the anode surface, the couple MO_{x+1}/MO_x is present, known as chemisorbed active oxygen (oxygen in the lattice of the MO_x anode), that will act as a mediator in the selective conversion or oxidation of refractory organic compounds (R) (Reaction 12) into oxidized products (OP) which probably are more biodegradable than their precursors.

$$MO_{x+1} + R \rightarrow MO_x + OP \quad \text{(Reaction 12)}$$

Typically, electrodes materials that show this behaviour are carbon, graphite, RuO_2, IrO_2 or Pt.

b) "Non-active" anodes: electrode lacks the ability to oxidize presenting a weak interaction between the anode and $^{\bullet}OH$ leaving these physio-adsorbed on the anode surface. This means a high reactivity for the non-selective oxidation of organic compounds so enabling to even reach a complete mineralization (Reaction 13) with a high degree of efficiency. Most common non-active anodes are made of PbO_2, SnO_2 or boron-doped diamond (BDD).

$$MO_x (^{\bullet}OH) + R \rightarrow MO_x + mCO_2 + nH_2O + H^+ + e^- \quad \text{(Reaction 13)}$$

Figure 7 shows a general diagram of organic compounds oxidation and oxygen evolution reaction in both types of anodes, active and non-active, presented for the first time by Conminellis 1994. Different states are defined below: (1) water electron discharge to form $^{\bullet}OH$, (2) formation of metal oxide MO_{x+1}, (3) selective oxidation of organic compounds, (4) decomposition of metal oxide following oxygen evolution, (5) mineralization of organic compounds, (6) electrochemical oxidation of $^{\bullet}OH$ ending to the oxygen evolution.

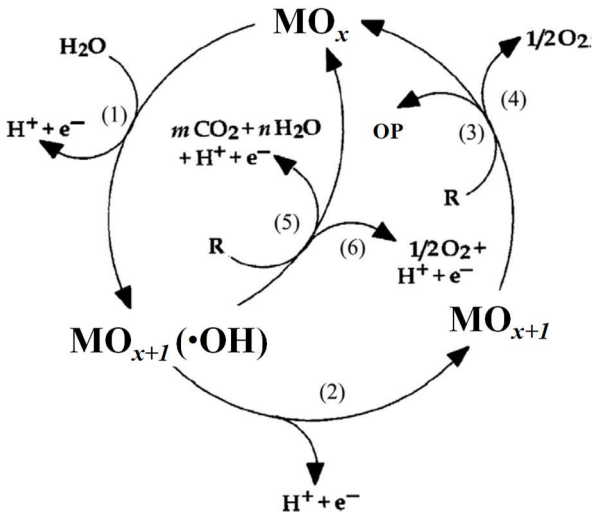

Figure 7. Scheme of organic compounds removal mechanism by active and non-active anodes simultaneously proposed by Conminellis in 1994 [49]

Anodic materials can be also classified according to their oxidation potential (Table 2). There is a directly proportional relation between the anode oxidation potential and the over-potential for oxygen evolution. At the same time, it is inversely proportional to the enthalpy of •OH adsorption on the anode surface. Therefore, higher oxidation potential of an electrode entailed higher over-potential for oxygen evolution and lowest enthalpy of •OH adsorption, thus •OH are highly available to react with the organic compounds and oxidizing power is greater.

Table 2. Classification of the main anodic materials according to their oxidation potential ([52, 55]).

Electrode material	Oxygen evolution potential (V)	Adsorption enthalpy of M-•OH	Oxidation power of the anode
RuO_2	1.47	(Chemisorption of •OH) Highest	Lowest
IrO_2	1.52		
Pt	1.60		
PbO_2	1.90		
SnO_2	1.90		
BDD	2.30	Lowest (Physisorption of •OH)	Highest

As a general rule, active anodes are characterized by a low oxygen evolution over-potential thus present a high electrochemical activity towards oxygen evolution reaction, while non-active anodes have a high oxygen evolution over-potential and its activity for oxygen evolution reaction is very low.

One of the electrode materials widely applied for water depuration in the last decades is BDD. This material has excellent properties for electrochemical processes. It has an inert character meaning that it is chemically, mechanically and thermally resistant, avoiding corrosion even when a high electrical charge is applied [56]. Furthermore, it shows a very low activity for oxygen evolution (Reactions 14 and 15) due to its high over-potential for this reaction, 2.2 – 2.6 V on p-Si/BDD anodes [57], entailing a higher electrochemical window than any other known material [56]. The main drawback of BDD is the high cost of their production both due to the cost of the BBD itself and due to the necessity of a support made of Tantalum, Niobium or Tungsten.

$BDD + H_2O \rightarrow BDD(^{\bullet}OH) + H^+ + e^-$ (Reaction 14)

$2BDD(^{\bullet}OH) \rightarrow 2BDD + O_2 + 2H^+ + 2e^-$ (Reaction 15)

BDD systems behaviour has been deeply studied for the removal of organics. In Kapalka et al. [52] a kinetic model able to predict COD removal trend, current efficiency (CE) and energy consumption of the process are detailed. From it, working in batch mode and under galvanostatic conditions, two differentiated regimes were observed:

- When applied j is low or organic concentration is high enough (applied *j* < limiting *j*), electrolysis is under current limited control which means that organics decrease linearly, generating a huge amount of intermediates, and the CE achieves 100%.

- When applied *j* is high or organic concentration is low (applied *j* > limiting *j*), electrolysis is controlled by mass transfer and organic compounds are directly mineralized. However, secondary reactions (as oxygen evolution) begin reducing CE. Under these conditions, organic removal follows an exponential trend. [53]

Limiting *j* is the maximum rate that can be achieved in a mass-transfer controlled system, calculated according to equation 2:

$$j_{\lim} = nFk_mC_{org} \quad \text{(Equation 2)}$$

being j_{lim} the limiting *j* for organic removal (A m^{-2}), *n* the number of electrons involved in the degradation reaction, *F* the Faraday's constant (96 485 C mol^{-1}); k_m the coefficient for mass transfer (m s^{-1}), and C_{org} the concentration of target organics (mol m^{-3}).

2.5.2.2. Chemical intermediates

Indirect electro-oxidation process can be carried out by using as mediators the oxidative species electrogenerated from the oxidation at the anode of ions dissolved in target wastewater.

These oxidant species have a crucial role in electro-chemical processes since allows the degradation of organics in the bulk solution, even far of the anode surface surroundings. The kind of oxidant produced (Fig. 8) depends on wastewater composition but also on the wide potential window of the electrode material. For this reason non-active anodes, and specifically BDD anodes, are able to generate the highest number of different oxidants [56] while in active anodes the main oxidant generated is chlorine [58].

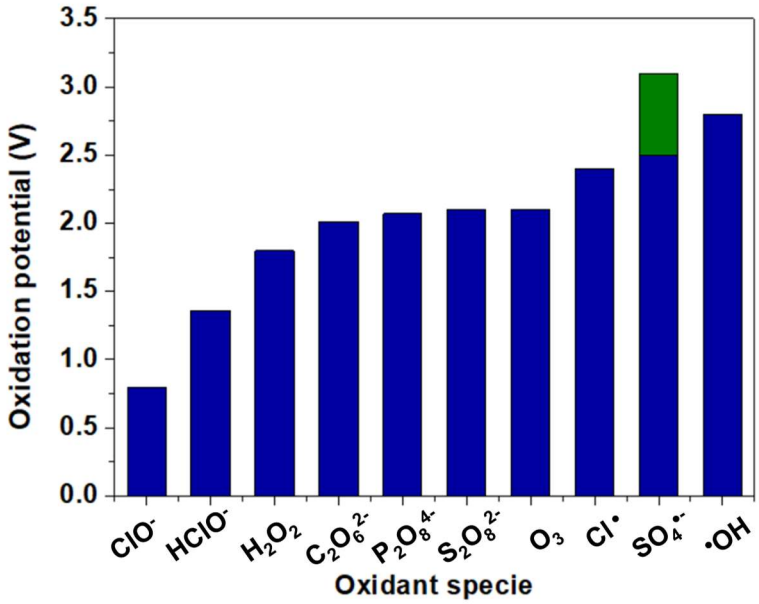

Figure 8. Redox potential (V) of the oxidant species that are commonly electrogenerated.

Chlorine

One of the main ions that can be naturally found in waters is chloride. When a contaminated water containing this ion undergoes an electrochemical depuration process, oxygen can reach organics thought two pathways: on the electrode surface via adsorbed oxychloro species such as chloro (Reaction 16) and oxychloro radicals or by long-lifetime oxidants, which remains in the solution, resultant from the oxidation of chlorides (Reactions 17 - 19) [53]

$Cl^- \rightarrow Cl^{\bullet}_{(ads)} + e^-$ (Reaction 16)

$2Cl^- \rightleftarrows Cl_{2(aq)} + 2e^-$ (Reaction 17)

$Cl_{2(aq)} + HO^- \rightarrow ClO^- + Cl^- + H^+$ (Reaction 18)

$HClO \rightleftarrows ClO^- + H^+$ (Reaction 19)

The solution pH determines the species of active chlorine that will be present in wastewater. At pH below 7.55 (pKa), the main specie is HClO (E^0 = 1.49) and at higher values ClO^- (E^0 = 0.86 V) is predominant (Reaction 19). Chlorine speciation according to pH is shown in figure 9.

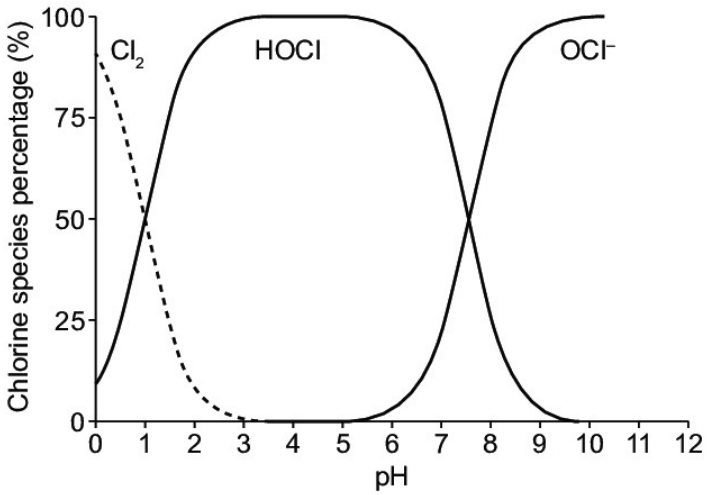

Figure 9. Presence of chlorine species as function of pH for a chloride concentration of $5 \cdot 10^{-3}$ M. From Deborde and von Gunten 2008 [59].

Despite the wide use of these active chlorine species (ACS) as intermediate for the degradation of organics, electrochemical and chemical reactions occurring during the electro-oxidative process are partially unknown [53]. Nonetheless Bonfatti et al. [60] proposed some modifications to Comninellis model [49] for the intermediates of oxygen evolution reaction (Fig. 7), aiming to include the cases in which oxygen transfer is mediated by adsorbed chloro and oxychloro species (Fig. 10).

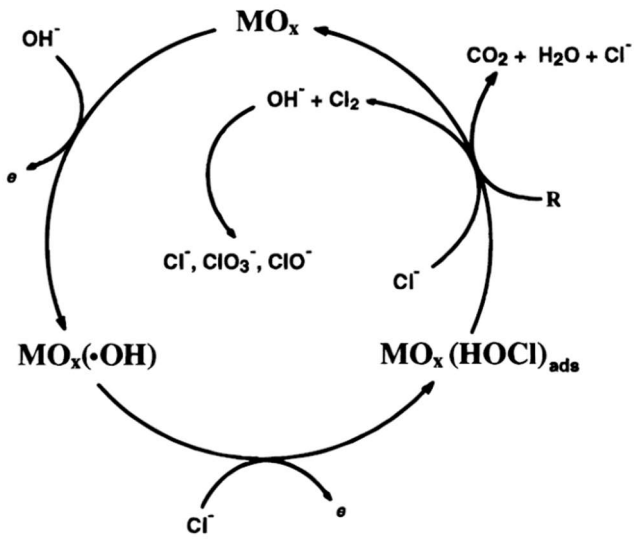

Figure 10. Model proposed by Bonfatti et al. [60] including the role of chloro and oxychloro species adsorbed on the electrode surface as intermediates for organics oxidation.

Electrochemically-assisted chlorine treatment, commonly known as electrochlorination, present several advantages regarding conventional chlorination where ACS are added as a reagent [25]:

- Transport and storage of chlorine are not necessary thus the risk associated is avoided.
- Organics removal is faster than in chemical oxidation.
- Overall costs are much lower.

As the process starts, ACS react with organic matter as soon as they are electro-generated so free available chlorine (FAC) concentration remains low, however when the organic matter is completely eliminated, FAC begins to accumulate and so oxidation process ends. A high presence of FAC can lead into the generation of undesirable chlorine by-products, mainly ClO_2^-, ClO_3^- or CO_4^-, coming from the oxidation of ClO^- (Reactions 20-22) [61] which must be assessed since these species are highly toxic and entail a serious risk for the ecosystems and human beings.

$ClO^- + {}^\bullet OH \rightleftarrows ClO_2^- + H^+ + e^-$ (Reaction 20)

$ClO_2^- + {}^\bullet OH \rightleftarrows ClO_3^- + H^+ + e^-$ (Reaction 21)

$ClO_3^- + {}^\bullet OH \rightleftarrows ClO_4^- + H^+ + e^-$ (Reaction 22)

When a BDD anode is used for the removal of organics in a high chloride wastewater, BDD high over-potential for oxygen evolution leads in the generation of a huge amount of •OH, thus promoting the oxidation of ACS to undesired ClO_3^- and ClO_4^- (Reactions 20 to 22) [62] reducing the oxidative power of the process and increasing water toxicity. For that reason, with BDD electrodes it is important to control the production of •OH. Regulating the applied current according to the amount of organic matter, the system can be kept under charge transfer limit (applied *j* < limiting *j*) avoiding the generation of an excess of •OH that could react with ACS.

In this context it is concluded that the most suitable electrodes for electrochlorination are the non-active anodes. Specifically the most used electrodes are dimensionally stable anodes (DSA) consisting on a titanium base coated with a conducting thin layer of metal oxide or a mix of them (such as RuO_2 or TiO_2). Since their development in 1960s, DSA electrodes have been widely studied in literature addressing the use of new materials for the metal oxide layer and the application of new methods for coating. In fact, several authors have reported their used for organic removal by means of ACS electrogeneration [48] being applied mainly in highly complex or recalcitrant waters.

Ozone

Ozone is a strong oxidant (E^0 = 2.1 V) widely used for water disinfection. It can also be applied for the removal of organic contaminants, but against •OH, it shows a selective behaviour being more effective for the degradation of some contaminants.

In conventional systems, ozone is produced by corona discharge, which means an electrical discharge realized through dry oxygen or air. Ozone is generated in gaseous phase, thus to ensure the reaction with the microorganisms as well as contaminants, a proper mass transfer between the gas and liquid phase is required. However, this transfer usually presents a low efficiency, being the main limitation of this treatment.

In order to overcome this drawback, electrochemical ozone production emerged. This technology is based on the application of a potential which generate ozone directly and continuously in the aqueous solution by reaction 23.

$$3H_2O \rightarrow O_3 + 6e^- + 6H^+ \qquad \text{(Reaction 23)}$$

Nevertheless, when applying this type of treatment, it must be considered that the oxygen evolution reaction is presented as the main competitor to ozone generation. Thermodynamically oxygen evolution reaction is widely favoured regarding ozone

production, E^0 = 1.23 V vs E^0 = 1.51 V, therefore ozone will only be electrogenerated in anodes with a high oxygen over-potential [62], so by using mainly BDD electrodes.

Peroxydisulphate, peroxydicarbonate and peroxydiphosphate

When water purification is carried out by cells equipped with high oxygen evolution over-potential anodes, organic contaminants are removed mainly by the oxidizing action of electrogenerated hydroxyl radicals as described in section I.2.5.2.1. However, if the effluent to be treated is an actual wastewater which contains a wide variety of dissolved salts, these are also oxidized on the anode releasing oxidants that can favour the degradation process. The main electrogenerated oxidizing species come from the oxidation of sulphate, carbonate and phosphate ions, as described by reactions 24-26:

$2SO_4^{2-} \rightleftarrows S_2O_8^{2-} + 2e^-$ (Reaction 24)

$2CO_3^{2-} \rightleftarrows C_2O_6^{2-} + 2e^-$ (Reaction 25)

$2PO_4^{3-} \rightleftarrows P_2O_8^{4-} + 2e^-$ (Reaction 26)

The main advantage of these oxidants is that they are dissolved in the aqueous solution, so that oxidative process extends beyond the areas adjacent to the anode, thus avoiding the limitation of mass transfer and increasing the efficiency of the process [53]. In fact, at the beginning of the treatment, in which the concentration of organic pollutants is high and the system is under load transfer control, no significant differences are found regarding the presence or absence of sulphate, carbonate and phosphate ions. Nevertheless, when the concentration of organics is low and the system is limited by mass transfer, the degradation process will be faster in wastewater with higher content of these ions.

2.5.2.3. Generation of new oxidants by the application of light irradiation to electrogenerated species

Many of electrogenerated species on the anode surface are able to be activated by different methods, being the irradiation with light the most widely applied. Due to this phenomenon, new species with a high oxidizing power can be generated, leading on an increase in the treatment efficiency.

This is the case of ACS which undergo photolysis when radiation is applied generating $Cl^{\bullet}$ (E^0 = 2.4 V) and $^{\bullet}OH$ following reaction 27 in the case of $HClO^-$ and reactions 28 and 29 for ClO^-.

$HClO + h\nu \rightarrow Cl^{\bullet} + {}^{\bullet}OH$ (Reaction 27)

$ClO^- + h\nu \rightarrow Cl^\bullet + {}^\bullet O^-$ (Reaction 28)

${}^\bullet O^- + H_2O \rightarrow {}^\bullet OH + OH^-$ (Reaction 29)

These reactions have been studied in detail mainly at 254 nm of irradiation [63], in the UV-C range of the spectra, which is the most energetic one. However, chlorine photolysis probably could occur at other wavelengths depending on the molar absorption of ACS, though maybe with lower quantum efficiency (Fig. 11). In fact, in the case of ClO^- photolysis, it can take place even under solar radiation since the molar absorption spectrum of ClO- overlaps with UV-B and UV-A region of the solar spectrum (from 280 to 400 nm) [64], which suggests that sunlight can be applied in solutions containing ACS at pH higher than 7.5 aiming an enhancement in the treatment oxidative capacity.

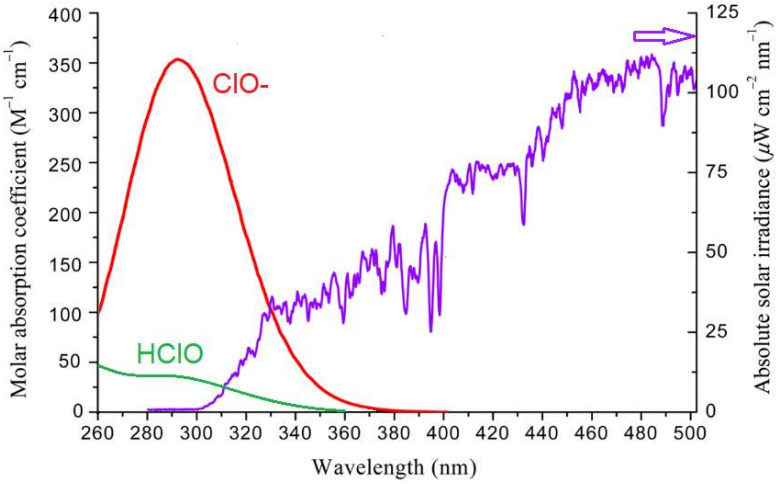

Figure 11. Molar absortion of HClO and ClO^- vs solar irradiance spectrum at noon. Modified from Shu et al 2014 [64].

On the other hand, $S_2O_8^{2-}$ can be activated either by increasing temperature, by adding a transition metal catalyst or by irradiating with light at 254 nm according to reaction 30. Hence $SO_4^{-\bullet}$ is produced, which has a very high redox potential E^0 = 2.5 – 3.1 V, in the same range as ${}^\bullet OH$. For this reason, sulphate-based treatments has been described in depth in literature for the removal of OMCs and for bacteria inactivation [65]. However, mechanism involving $SO_4^{-\bullet}$ generation and its role during electro-oxidative treatment is still under study.

$S_2O_8^{2-}$ + heat / UV-C light / metal catalyst $\rightarrow 2SO_4^{-\bullet}$ (Reaction 30)

Electrogenerated ozone can be also photo-activated, resulting in the generation of ${}^\bullet OH$ according to reaction 31 [55].

$O_3 + H_2O + h\nu \rightarrow 2^{\bullet}OH + O_2$ (Reaction 31)

Combination of an electrochemical treatment with a light source, whether artificial as a lamp or natural as sunlight, leads to the promotion of electrogenerated oxidative species to still more oxidizing ones. Therefore, efficiency of electrochemical processes could be enhanced jointly with a reduction on the energy cost which is one of the major drawbacks of electro-oxidative treatments.

2.6 Electro-Fenton and photo electro-Fenton

AOPs are based in the production of strong oxidants for the elimination of recalcitrant compounds contained in wastewater streams that are unable to be removed by biological processes. To generate these oxidants different technologies can be used, such as UV photolysis, heterogeneous photocatalysis or Fenton-based processes being the last widely reported in the scientific literature.

The so-called Fenton reaction (reaction 32) consist in the mixture of H_2O_2 and a ferrous iron salt to generate $^{\bullet}OH$. It was defined by Henry John Horstman Fenton at the end of the 19th century, who observed and enhancement in the oxidation of organic acids in the presence of these two reagents [66].

$H_2O_2 + Fe^{2+} \rightarrow Fe^{3+} + OH^- + {}^{\bullet}OH$ (Reaction 32)

However, as the reagents are consumed, their continuous addition becomes necessary for allowing the process going on and ensuring the availability of enough $^{\bullet}OH$. Moreover, this involves the generation of a huge amount of ferric sludge which composition depends on the pH of the solution (Fig. 12) and that has to be finally removed and treated [67].

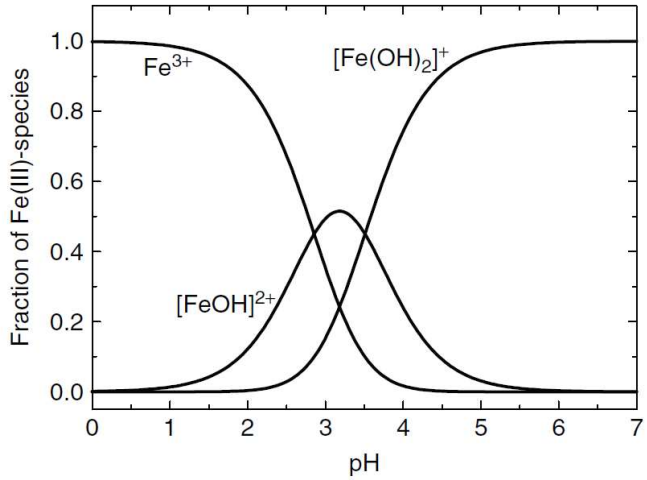

Figure 12. Speciation of Fe(III) in water as function of the pH value in absence of complexing agents. Reproduced from Hoffman 2005 [68].

Electrochemistry is presented as a versatile tool for Fenton's reaction control. The combination of both is known as electro-Fenton (EF) process. In this treatment, the anode generates oxidant species on its surface, as described in previous sections, and simultaneous electrogeneration of H_2O_2 occurs by two-electron reduction of O_2 on the cathode surface (reaction 33), thus only with the addition of an iron salt Fenton reaction is promoted. Furthermore, ferric iron obtained after Fenton reaction can be also reduced to ferrous iron on the cathode, regenerating the catalyst (reaction 34) [69, 70] which is able to react again with electrogenerated H_2O_2, closing the cycle of the catalytic process [71]. By means of the applied energy (current or potential) to the electrochemical cell, the generation of oxidant species as well as Fenton reagents can be controlled, allowing adapting the treatment according to the target wastewater characteristics.

$O_2 + 2H^+ + 2e^- \rightarrow H_2O_2$ (Reaction 33)

$Fe^{3+} + e^- \rightarrow Fe^{2+}$ (Reaction 34)

As it happens with the anodes, the selection of cathode material is of outmost relevance for H_2O_2 electrogeneration since it requires the use of specific and selective materials with a high over-potential for H_2 evolution. Specifically, the most used material is carbon-based, such as carbon-polytetrafluoroethylene (PTFE), carbon felt, reticulated vitreous carbon or graphene, which are good electrical conductors, non-toxic, stable, low-cost and shows a high over-potential for H_2 evolution with a low catalytic activity for H_2O_2 reduction [67]. To facilitate the cathodic production of H_2O_2 it is convenient to have as much O_2 in solution as possible thus, in filter-press cells, it is common to install an air

chamber in the back side of the cathode, working in a slightly higher pressure than water flow forcing the diffusion of O_2 to the aqueous solution. These kind of electrodes are known as Gas Diffusion Electrodes (GDE).

EF process was the first technology considered as an electrochemical advanced oxidation process (EAOP), presenting several advantages [12]:

- The in situ generation of reagent poses cost saving as well as avoid risks associated to their transport and storage.
- The oxidation of contaminants can be easily controlled by means of varying the current or potential applied.
- Easy automation and monitoring of working parameters.

As electrogenerated oxidants can be activated by irradiation, as described in section I.2.5.2.3, EF can also be enhanced by the application of a light source. When working at acidic pH, ferric sludge is mainly conformed of $[Fe(OH)]^{2+}$ (Fig. 12) which interacts with UV light to produce ferrous iron (reaction 35), thus increasing the regeneration rate of the iron source. This process is known as photo electro-Fenton (PEF) when the irradiation source is a lamp and as solar photo electro-Fenton (SPEF) when it is developed under sunlight.

$$[Fe(OH)]^{2+} + h\nu \rightarrow Fe^{2+} + {}^{\bullet}OH \qquad \text{(Reaction 35)}$$

Nonetheless, most of the published studies address EF, PEF and SPEF process at laboratory scale, with small surface electrodes applied in very low working volumes, focusing mainly on the development of new electrode materials. This evidences the lack of studies carried out at larger scale, which would serve as a preliminary step to a real application of these systems. In such a context, this PhD Thesis covers the star-up and optimization of a SPEF pilot plant assessing the effectiveness of the process and the effects provoked by changing different parameters at pilot plant scale, as described in detail in section V.1.

2.7 Photoelectrocatalysis

Heterogeneous photocatalysis is based on the reactions that occur at the interface of different phases, solid-liquid or solid-gas of a solid photocatalyst. Specifically in solid semiconductor materials, the incidence of photons on the solid surface promotes an electron transfer from valence band to the conduction band (e_{CB}^-), achieving a

photoexcited state and generating a positive charge hole (h_{VB}^+) [72] thus resulting in oxidation and reduction reactions [73].

Although different semiconductors can be applied in water depuration, the most commonly used is TiO_2 since owns suitable properties as low cost, low toxicity, and a wide band gap of 3.2 eV, which results in good stability and prevents photo-corrosion [72]. When TiO_2 is illuminated with a UV source, excited electrons and holes are produced (reaction 36). From that holes, water is oxidized generating $^{\bullet}OH$ (reaction 37), which are responsible of organic contaminants oxidation and bacteria inactivation.

$TiO_2 + h\nu \rightarrow e_{CB}^- + h_{VB}^+$ (Reaction 36)

$h_{VB}^+ + H_2O \rightarrow {}^{\bullet}OH + H^+$ (Reaction 37)

The main drawback of this photocatalyst lays on its recovery once treatment is ended and the low efficiency that could be observed due to recombination of e_{CB}^- and h_{VB}^+. To solve these problems many works have studied different supported TiO_2 photocatalyst, but when such support is performed of an electrical conductive material, either a current density or a bias potential can be applied to enhance the separation of photogenerated e_{cb}^- and h_{vb}^+. The external circuit extracts photoexcited e_{CB}^- from the anode [72] thus reducing recombination and the subsequent loss of efficiency [74] (Reactions 38 and 39) having a higher amount of h_{VB}^+ available to produce $^{\bullet}OH$.

$e_{CB}^- + h_{VB}^+ \rightarrow TiO_2 + Heat$ (Reaction 38)

$e_{CB}^- + {}^{\bullet}OH \rightarrow OH^-$ (Reaction 39)

As well as $^{\bullet}OH$, other oxidant species can be generated from oxidation of ions dissolved in the target wastewater as it was described in section I.2.5.2.2, however when using TiO_2 photoanodes the oxidation is carried out by h_{VB}^+ instead of the anode surface itself. Analogously, besides promoting photoexcitation of electrons, UV light contribute to the photoactivation of electrogenerated reactive species [55] (section I.2.5.2.3).

3. Perspectives for an actual application of electrochemical treatments

The large treatment capacity of electrochemical processes and their clear advantages, mainly the ease of operation and the absence of additives, have made them to be widely studied in literature. Since the year 2000, more than 7500 articles have been published on the use of electrochemical treatments for water purification (keywords: "electrochemical" "treatment" and "water") (Fig. 13) with a significant increase since 2012. Most of these works are mainly focused on the development of new materials for the manufacture of electrodes and the effectiveness achieved in the degradation of a reference contaminant in a simple water matrix. However, works addressing the application of these electrochemical processes in actual water matrices are below 500 (keywords: "electrochemical" "treatment" “real” "actual" and "water"), evidencing a scarcity that hinder its upgrade to pilot-plant scale.

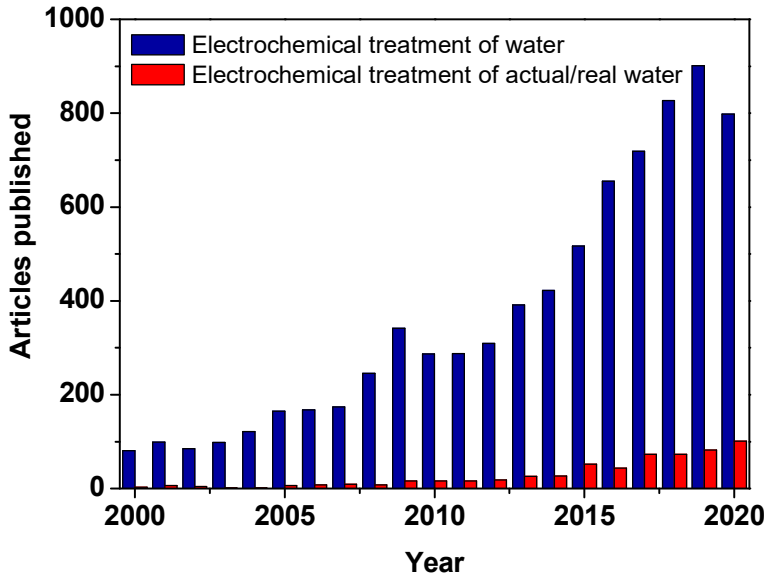

Figure 13. Articles from Scopus DataBase focused on the study of electrochemical treatments since 2000 (Revised on August 2020).

Furthermore, this has meant a limitation to deepen in the possible improvements through the application of a light source. When using specific simulated saline solutions as a support electrolyte, the degradation of organics is carried out by means of $^{\bullet}OH$. In that cases, there are not a huge variety of ions to electrogenerate oxidizing species in the bulk solution that could be photoactivated, thus the degradation process is limited to the anode surface.

One of the most recent reviews undertaken electrochemical technologies focused on the depuration of actual wastewaters was published by Garcia-Segura et al. [75] in 2018. Table 3 covers some of the latest advances achieved in this field, according to the application of electrochemical process as pre-treatment of wastewater originated in industrial processes aiming to remove the high organic load and refractory substances that hinder the direct implementation of a biological treatment, as a treatment itself for the depuration of a contaminated effluent or as a tertiary treatment or post-treatment commonly used in combination with membrane systems.

Table 3. Some of the latest studies published addressing electrochemical treatments of actual wastewaters.

Electrochemistry as pre-treatment				
Type of Water	**Treatment**	**Conditions**	**Organics removed**	**Ref.**
Actual herbicide wastewater	AO	PbO_2 anode - Ti cathode A: gap: 1 cm *j*: 4 A dm^{-2} pH 4 V: 1 L	87% COD, from 7519 to 980 mg L^{-1}	[76]
Electronic industry effluent + 50 mM of K_2SO_4	EF	Nb-BDD anode 20 cm^2 Carbon brush cathode 80 cm^2 gap: 3 cm *j*: 2.5 mA cm^{-2} pH: 3 $[Fe^{2+}]$ = 0.2 mM t: 4 h V = 0.4 L	94% of TOC	[77]
	EF	Carbon-PTFE anode 21 cm^2 Carbon brush cathode 80 cm^2 gap: 3 cm *j*: 1.25 mA cm^{-2} pH: 3 $[Fe^{2+}]$ = 0.2 mM t: 4 h V = 0.4 L	76.5% of TOC	

Electrochemistry as main treatment				
Type of Water	**Treatment**	**Conditions**	**Organics removed**	**Ref.**
Industrial textile wastewater-Acid Blue 29	SPEF	DSA anode/ Carbon-PTFE air-diffusion cathode A= 50 cm^{-2} gap: 1.5 cm *j*: 25 mA cm^{-2} pH: 3 [Fe^{2+}] = 0.5 mM t: 6 h V = 10 L Adding Na_2SO_4 CPC illuminated volume: 700 mL Irradiation: 30 W m^{-2}.	93% of TOC	[78]
Sugar beet wastewater	AO	BDD anode/Stainless steel cathode A= 109 cm^2 gap: 1 cm *j*: 49.1 mA cm^{-2} pH: 5 t: 294 min V: 1 L Adding NaCl	75% COD	[79]
Olive oil mill wastewater	Sequential EC and photoelectro-Fenton (PEF)	EC: Fe anode/stainless steel cathode A= 10 cm^{-2} gap: 1cm *j*: 3 mA cm^{-2} pH: natural t: 20 min V = 150 mL + PEF: Si-BDD anode /carbon-PTFE cathode A = 3 cm^{-2} gap: 1cm; *j*: 25 mA cm^{-2}, pH: 3 [Fe^{2+}] = 0.5 mM V: 100 mL 6W UV-A lamp (5 W m^{-2})	97% of TOC	[80]
Urban wastewater with benzophenone-3 (BP-3) (0.024 mM)	Sequential EC and PEF	EC: Fe anode/stainless steel cathode A= 10 cm^{-2} gap: 1cm *j*: 15 mA cm^{-2} pH: 8 t: 20 min V = 150 mL	EC+PEF ~80% of TOC and BP-3: >99%	[81]

		+ PEF: Si-BDD anode /carbon-PTFE cathode A = 3 cm^{-2} gap: 1cm; *j*: 33.3 mA cm^{-2} pH: natural t: 360 min; V: 100 mL UV-A lamp (5 W m^{-2})		
Washing machine effluent	AO	Nb-BDD anode/Ti cathode A: 63.5 cm^{-2} gap: *j*: 16.6 mA cm^{-2} t: 360 min V: 1 L	71% of COD	[82]
	AO	Nb-BDD anode/Ti cathode A: 63.5 cm^{-2} *j*: 66.6 mA cm^{-2} *t*: 180 min Adding 7 g L^{-1} of Na_2SO_4	88.5% of COD	

Electrochemistry as tertiary treatment				
Type of Water	**Treatment**	**Conditions**	**Organics removed**	**Ref.**
RO concentrate of petrochemical industry	AO	Nb-BDD anode / stainless steel AISI 304L cathode A: 0.01 m^2 *j:* 20 mA cm^{-2} pH: 8 t: 5 h V: 1.5 L	71% of COD	[83]
RO concentrate of print and dyeing wastewater	AO	PbO_2-Ti anode / Ti mesh-plate cathode. A: 300 cm^2 gap: 1cm *j:* 10 mA $cm^{-2;}$ pH: 8.3 t: 40 min V: 1 L Q_{sp}: 2.45 Ah L^{-1}	72% of COD	[84]
Slaughterhouse effluent from secondary treatment	AO AO + UV-C AO + H_2O_2	Nb-BDD anode / Pt cathode. A: 10 cm^2 gap: 3.7 mm *j:* 100 mA $cm^{-2;}$ pH: 7.5 t: 480 min	AO + H_2O_2 + UV-C COD: < 10 mg L^{-1}	[85]

	AO + H_2O_2 + UV-C	V: 1.4 L Q_{sp}: 7.3 Ah L^{-1} Low pressure UV-C lamp 11 W		
Oxyfluorfen solution, raw (234 mg L^{-1}) and ultrafiltration retentate	AO	BDD anode / Stainless Steel AISI 304 cathode A: 78 cm^2 gap: 9 mm j: 500 mA cm^{-2} V: 0.6 L 590 kWh kg^{-1} Adding 1 g L^{-1} of Na_2SO_4	50% of Oxyfluorfen raw solution	[86]

4. References

[1] U.N. Water, Sustainable Development Goal 6 synthesis report on water and sanitation, Published by the United Nations, New York, 10017 (2018).

[2] EUROSTAT, Population on 1 January, (2020). https://ec.europa.eu/eurostat/databrowser/view/tps00001/default/table?lang=en (Accessed August 2020).

[3] U.S. Department of Energy, The Water-Energy Nexus: Challenges and Opportunities (2014).

[4] P. D'Odorico, K.F. Davis, L. Rosa, J.A. Carr, D. Chiarelli, J. Dell'Angelo, J. Gephart, G.K. MacDonald, D.A. Seekell, S. Suweis, The global food-energy-water nexus, Rev. Geophys., 56 (2018) 456-531.

[5] European Union, Council Directive 91/271/EEC of 21 May 1991 concerning urban waste water treatment, Official Journal, 135 (1991) 40-72.

[6] M. Henze, Y. Comeau, Wastewater characterization, in: M. Henze, M.C.M. van Loosdrecht, G.A. Ekama, D. Brdjanovic (Eds.) Biological wastewater treatment: Principles modelling and design, (2008) 33-52.

[7] European Commision, Executive summary of the evaluation of the Council Directive 91/271/EEC of 21 May 1991 concerning urban waste-water treatment, (2019).

[8] M. Helmecke, E. Fries, C. Schulte, Regulating water reuse for agricultural irrigation: risks related to organic micro-contaminants, Environ. Sci. Eur., 32(1) (2020) 4.

[9] N. Šajn, Environmental impact of the textile and clothing industry: What consumers need to know, European Parliamentary Research Service (2019).

[10] A. Asghar, A.A. Abdul Raman, W.M.A. Wan Daud, Advanced oxidation processes for in-situ production of hydrogen peroxide/hydroxyl radical for textile wastewater treatment: a review, J. Clean. Prod., 87 (2015) 826-838.

[11] M. Kamali, Z. Khodaparast, Review on recent developments on pulp and paper mill wastewater treatment, Ecotoxicol. Environ. Saf., 114 (2015) 326-342.

[12] K.V. Plakas, A.J. Karabelas, Electro-Fenton applications in the water industry, in: M. Zhou, M.A. Oturan, I. Sirés (Eds.) Electro-Fenton Process, Springer, 2017, pp. 343-378.

[13] I.M.O., International Convention For The Control And Management Of Ships' Ballast Water And Sediments, in International Conference on Ballast Water Management for Ships, BWM/CONF/36, 16 February 2004. Organization International Maritime (2004).

[14] Red para la Sostenibilidad Agroalimentaria (REDSOSTAL), Heineken define sus objetivos 2030 para proteger las fuentes de agua (2019). http://redsostal.es/Heineken-objetivos2030-fuentes-agua-Redsostal (Accessed July 2020)

[15] The Coca-Cola Company, Improving our water efficiency. Meeting goals and moving goalpost (2018). https://www.coca-colacompany.com/news/improving-our-water-efficiency (Accessed July 2020)

[16] Novartis, Water (2020). https://www.novartis.com/our-company/corporate-responsibility/environmental-sustainability/water (Accessed July 2020)

[17] BASF Online Report, Water (2019). https://report.basf.com/2019/en/managements-report/responsibility-along-the-value-chain/environmental-protection-health-and-safety/water.html# (Accessed July 2020)

[18] Nissan Motor Corporation, Water Scarcity. https://www.nissan-global.com/EN/ENVIRONMENT/GREENPROGRAM/WATERSCARCITY/ (accessed July 2020)

[19] International Maritime Organization, Annex 17, Resolution Mepc.269(68), Guidelines For The Development of The Inventory of Hazardous Materials (2015).

[20] MSC, Sustainability Report 2018 (2019).

[21] Directive 2000/60/EC of the European Parliament and of the Council of 23 October 2000 establishing a framework for Community action in the field of water policy, Official Journal 327 (2000) 1-73.

[22] C.E. Barrera-Díaz, P. Balderas-Hernández, B. Bilyeu, Electrocoagulation: Fundamentals and Prospectives, in: C.A. Martínez-Huitle, M.A. Rodrigo, O. Scialdone (Eds.) Electrochemical Water and Wastewater Treatment, 2018, pp. 61-76.

[23] H. Liu, X. Zhao, J. Qu, Electrocoagulation in Water Treatment, in: C. Comninellis, G. Chen (Eds.) Electrochemistry for the Environment, Springer, New York, 2010, pp. 245-262.

[24] N. Gonzalez-Rivas, H. Reyes-Pérez, C.E. Barrera-Díaz, Recent Advances in Water and Wastewater Electrodisinfection, ChemElectroChem, 6 (2019) 1978-1983.

[25] C.A. Martinez-Huitle, E. Brillas, Decontamination of wastewaters containing synthetic organic dyes by electrochemical methods: A general review, Appl. Catal. B-Environ., 87 (2009) 105-145.

[26] S. Al-Amshawee, M.Y.B.M. Yunus, A.A.M. Azoddein, D.G. Hassell, I.H. Dakhil, H.A. Hasan, Electrodialysis desalination for water and wastewater: A review, Chem. Eng. J., 380 (2020).

[27] H. Strathmann, Electrodialysis, a mature technology with a multitude of new applications, Desalination, 264 (2010) 268-288.

[28] A. Campione, L. Gurreri, M. Ciofalo, G. Micale, A. Tamburini, A. Cipollina, Electrodialysis for water desalination: A critical assessment of recent developments on process fundamentals, models and applications, Desalination, 434 (2018) 121-160.

[29] T. Xu, C. Huang, Electrodialysis-based separation technologies: A critical review, AIChE J., 54 (2008) 3147-3159.

[30] F. Fu, Q. Wang, Removal of heavy metal ions from wastewaters: a review, J. Environ. Manage., 92 (2011) 407-418.

[31] A. Subramani, J.G. Jacangelo, Emerging desalination technologies for water treatment: a critical review, Water Res., 75 (2015) 164-187.

[32] S.S. Gupta, M.R. Islam, T. Pradeep, Capacitive Deionization (CDI): An Alternative Cost-Efficient Desalination Technique, in: S. Ahuja (Ed.) Advances in Water Purification Techniques, 2019, pp. 165-202.

[33] J. Choi, P. Dorji, H.K. Shon, S. Hong, Applications of capacitive deionization: Desalination, softening, selective removal, and energy efficiency, Desalination, 449 (2019) 118-130.

[34] S. Rondinini, C. Locatelli, A. Minguzzi, A. Vertova, Electroreduction, in: C.A. Martínez-Huitle, M.A. Rodrigo, O. Scialdone. Electrochemical Water and Wastewater Treatment, 2018, pp. 3-28.

[35] E.T. Martin, C.M. McGuire, M.S. Mubarak, D.G. Peters, Electroreductive Remediation of Halogenated Environmental Pollutants, Chem. Rev., 116 (2016) 15198-15234.

[36] G. Fiori, S. Rondinini, G. Sello, A. Vertova, M. Cirja, L. Conti, Electroreduction of volatile organic halides on activated silver cathodes, J. Appl. Electrochem., 35 (2005) 363-368.

[37] J. Radjenovic, M.J. Farre, Y. Mu, W. Gernjak, J. Keller, Reductive electrochemical remediation of emerging and regulated disinfection byproducts, Water Res., 46 (2012) 1705-1714.

[38] A.A. Isse, L. Falciola, P.R. Mussini, A. Gennaro, Relevance of electron transfer mechanism in electrocatalysis: the reduction of organic halides at silver electrodes, Chem. Commun., (2006) 344-346.

[39] M. Sreedhar, T.M. Reddy, K. Balaji, S.J. Reddy, Electrochemical Reduction Behavior and Polarographic Determination of Methoxy Triazine Herbicides in Environmental Samples, Anal. Lett., 43 (2010) 674-686.

[40] S. Rondinini, P.R. Mussini, V. Ferzetti, D. Monti, Electrochemical reduction of α-D-glycopyranosyl bromides on a mercury cathode, Electrochim. Acta, 36 (1991) 1095-1098.

[41] Y. Xu, Y. Zhu, F. Zhao, C.-a. Ma, Electrocatalytic reductive dehalogenation of polyhalogenated phenols in aqueous solution on Ag electrodes, Appl. Catal. A-Gen., 324 (2007) 83-86.

[42] J. Ding, W. Li, Q.-L. Zhao, K. Wang, Z. Zheng, Y.-Z. Gao, Electroreduction of nitrate in water: Role of cathode and cell configuration, Chem. Eng. J., 271 (2015) 252-259.

[43] T. Suzuki, M. Moribe, Y. Oyama, M. Niinae, Mechanism of nitrate reduction by zero-valent iron: Equilibrium and kinetics studies, Chem. Eng. J., 183 (2012) 271-277.

[44] D. Reyter, D. Belanger, L. Roue, Optimization of the cathode material for nitrate removal by a paired electrolysis process, J. Hazard. Mater., 192 (2011) 507-513.

[45] E. Lacasa, J. Llanos, P. Cañizares, M.A. Rodrigo, Electrochemical denitrificacion with chlorides using DSA and BDD anodes, Chem. Eng. J., 184 (2012) 66-71.

[46] S.N. Pronkin, P.A. Simonov, V.I. Zaikovskii, E.R. Savinova, Model Pd-based bimetallic supported catalysts for nitrate electroreduction, J. Mol. Catal. A: Chem., 265 (2007) 141-147.

[47] K.J. Reddy, J. Lin, Nitrate removal from groundwater using catalytic reduction, Water Res., 34 (2000) 995-1001.

[48] M. Panizza, Importance of electrode material in the electrochemical treatment of wastewater containing organic pollutants, in: C. Comninellis, G. Chen (Eds.) Electrochemistry for the Environment, Springer, New York, 2010, pp. 25-54.

[49] C. Comninellis, Electrocatalysis in the electrochemical conversion/combustion of organic pollutants for waste water treatment, Electrochim. Acta, 39 (1994) 1857-1862.

[50] M.A. Rodrigo, P. Cañizares, J. Lobato, C. Sáez, Modeling of Electrochemical Process for the Treatment of Wastewater Containing Organic Pollutants, in: C. Comninellis, G. Chen (Eds.) Electrochemistry for the Environment, Springer, New York, 2010, pp. 99-124.

[51] J. Feng, D.C. Johnson, Electrocatalysis of Anodic Oxygen-Transfer Reactions: Fe-Doped Beta-Lead Dioxide Electrodeposited on Noble Metals, J. Electrochem. Soc., 137 (1990) 507-510.

[52] A. Kapałka, G. Fóti, C. Comninellis, Basic principles of the electrochemical mineralization of organic pollutants for wastewater treatment, in: C. Comninellis, G. Chen (Eds.) Electrochemistry for the Environment, Springer, New York, 2010, pp. 1-23.

[53] M. Panizza, G. Cerisola, Direct and mediated anodic oxidation of organic pollutants, Chem. Rev., 109, 12 (2009) 6541–6569.

[54] A. De Battisti, C.A. Martínez-Huitle, Electrocatalysis in Wastewater Treatment, in: C.A. Martínez-Huitle, M.A. Rodrigo, O. Scialdone (Eds.) Electrochemical Water and Wastewater Treatment, 2018, pp. 119-131.

[55] C. Barrera-Díaz, P. Cañizares, F.J. Fernández, R. Natividad, M.A. Rodrigo, Electrochemical advanced oxidation processes: an overview of the current applications to actual industrial effluents, J. Mex. Chem. Soc., 58 (2014) 256-275.

[56] P. Rychen, C. Provent, L. Pupunat, N. Hermant, Domestic and industrial water disinfection using boron-doped diamond electrodes, in: C. Comninellis, G. Chen (Eds.) Electrochemistry for the Environment, Springer, New York, 2010, pp. 143-161.

[57] B. Marselli, J. Garcia-Gomez, P.A. Michaud, M.A. Rodrigo, C. Comninellis, Electrogeneration of hydroxyl radicals on boron-doped diamond electrodes, J. Electrochem. Soc., 150 (2003) D79.

[58] C. Sáez, M.A. Rodrigo, A.S. Fajardo, C.A. Martínez-Huitle, Indirect Electrochemical Oxidation by Using Ozone, Hydrogen Peroxide, and Ferrate, in: C.A. Martínez-Huitle, M.A. Rodrigo, O. Scialdone (Eds.) Electrochemical Water and Wastewater Treatment, 2018, pp. 165-192.

[59] M. Deborde, U. von Gunten, Reactions of chlorine with inorganic and organic compounds during water treatment-Kinetics and mechanisms: a critical review, Water Res., 42 (2008) 13-51.

[60] F. Bonfatti, S. Ferro, F. Lavezzo, M. Malacarne, G. Lodi, A. De Battisti, Electrochemical incineration of glucose as a model organic substrate. II. Role of active chlorine mediation, J. Electrochem. Soc., 147 (2000) 592.

[61] M.E.H. Bergmann, Drinking water disinfection by in-line electrolysis: Product and inorganic by-product formation, in: C. Comninellis, G. Chen (Eds.) Electrochemistry for the Environment, Springer, New York, 2010, pp. 163-204.

[62] K. Groenen Serrano, Indirect Electrochemical Oxidation Using Hydroxyl Radical, Active Chlorine, and Peroxodisulfate, in: C.A. Martínez-Huitle, M.A. Rodrigo, O. Scialdone (Eds.) Electrochemical Water and Wastewater Treatment, 2018, pp. 133-164.

[63] Y. Feng, D.W. Smith, J.R. Bolton, Photolysis of aqueous free chlorine species (HOCl and OCl^-) with 254 nm ultraviolet light, J. Environ. Eng. Sci., 6 (2007) 277-284.

[64] Z. Shu, C. Li, M. Belosevic, J.R. Bolton, M.G. El-Din, Application of a solar UV/chlorine advanced oxidation process to oil sands process-affected water remediation, Environ. Sci. Technol., 48 (2014) 9692-9701.

[65] I. Sánchez-Montes, I. Salmerón García, G. Rivas Ibañez, J.M. Aquino, M.I. Polo-López, S. Malato, I. Oller, UVC-based advanced oxidation processes for simultaneous removal of microcontaminants and pathogens from simulated municipal wastewater at pilot plant scale, Environ. Sci-Wat. Res., (2020).

[66] H.J.H. Fenton, LXXIII.—Oxidation of tartaric acid in presence of iron, J. Chem. Soc., Trans., 65 (1894) 899-910.

[67] N. Oturan, M.A. Oturan, Electro-Fenton Process: Background, New Developments, and Applications, in: C.A. Martínez-Huitle, M.A. Rodrigo, O. Scialdone (Eds.) Electrochemical Water and Wastewater Treatment, 2018, pp. 193-221.

[68] P. Hoffmann, 2.9 Speciation of Iron, in: R. Cornelis (Ed.) Handbook of Elemental Speciation II–Species in the Environment, Food, Medicine and Occupational Health, John Wiley & Sons, 2005.

[69] I. Sirés, E. Brillas, M.A. Oturan, M.A. Rodrigo, M. Panizza, Electrochemical advanced oxidation processes: today and tomorrow. A review, Environ. Sci. Pollut. R., 21 (2014) 8336-8367.

[70] E. Brillas, I. Sirés, M.A. Oturan, Electro-Fenton process and related electrochemical technologies based on Fenton's reaction chemistry, Chem. Rev., 109 (2009) 6570-6631.

[71] E. Brillas, A review on the photoelectro-Fenton process as efficient electrochemical advanced oxidation for wastewater remediation. Treatment with UV light, sunlight, and coupling with conventional and other photo-assisted advanced technologies, Chemosphere, 250 (2020) 126198.

[72] E.V. dos Santos, O. Scialdone, Photo-electrochemical technologies for removing organic compounds in wastewater, in: C.A. Martínez-Huitle, M.A. Rodrigo, O. Scialdone (Eds.) Electrochemical Water and Wastewater Treatment, 2018, pp. 239-266.

[73] J. Byrne, P. Dunlop, J. Hamilton, P. Fernández-Ibáñez, I. Polo-López, P. Sharma, A. Vennard, A review of heterogeneous photocatalysis for water and surface disinfection, Molecules, 20 (2015) 5574-5615.

[74] R.J. Ramírez, C.A.P. Arellano, A.A.Á. Gallegos, A.E.J. González, S.S. Martínez, H_2O_2-assisted TiO_2 generation during the photoelectrocatalytic process to decompose the acid green textile dye by Fenton reaction, J. Photoch. Photobio. A., 305 (2015) 51-59.

[75] S. Garcia-Segura, J.D. Ocon, M.N. Chong, Electrochemical oxidation remediation of real wastewater effluents—a review, Process Saf. Environ. Prot., 113 (2018) 48-67.

[76] L. Zhang, F. Wei, Q. Zhao, S. Lv, Y. Yao, Real herbicide wastewater treatment by combined means of electrocatalysis application and biological treatment, Chem. Ecol., 36 (2020) 382-395.

[77] E. Mousset, Z. Wang, H. Olvera-Vargas, O. Lefebvre, Advanced electrocatalytic pre-treatment to improve the biodegradability of real wastewater from the electronics industry—A detailed investigation study, J. Hazard. Mater., 360 (2018) 552-559.

[78] R. Salazar, J. Gallardo-Arriaza, J. Vidal, C. Rivera-Vera, C. Toledo-Neira, M.A. Sandoval, L. Cornejo-Ponce, A. Thiam, Treatment of industrial textile wastewater by the solar photoelectro-Fenton process: Influence of solar radiation and applied current, Sol. Energy, 190 (2019) 82-91.

[79] S. Sharma, H. Simsek, Sugar beet industry process wastewater treatment using electrochemical methods and optimization of parameters using response surface methodology, Chemosphere, 238 (2020) 124669.

[80] N. Flores, E. Brillas, F. Centellas, R.M. Rodríguez, P.L. Cabot, J.A. Garrido, I. Sirés, Treatment of olive oil mill wastewater by single electrocoagulation with different electrodes and sequential electrocoagulation/electrochemical Fenton-based processes, J. Hazard. Mater., 347 (2018) 58-66.

[81] Z. Ye, J.R. Steter, F. Centellas, P.L. Cabot, E. Brillas, I. Sirés, Photoelectro-Fenton as post-treatment for electrocoagulated benzophenone-3-loaded synthetic and urban wastewater, J. Clean. Prod., 208 (2019) 1393-1402.

[82] F.E. Durán, D.M. de Araújo, C. do Nascimento Brito, E.V. Santos, S.O. Ganiyu, C.A. Martínez-Huitle, Electrochemical technology for the treatment of real washing machine effluent at pre-pilot plant scale by using active and non-active anodes, J. Electroanal. Chem., 818 (2018) 216-222.

[83] S. Wohlmuth da Silva, C.D. Venzke, J. Bitencourt Welter, D.E. Schneider, J. Zoppas Ferreira, M.A. Siqueira Rodrigues, A. Moura Bernardes, Electrooxidation Using Nb/BDD as Post-Treatment of a Reverse Osmosis Concentrate in the Petrochemical Industry, Int J. Environ. Res. Public Health, 16 (2019).

[84] J. Wang, T. Zhang, Y. Mei, B. Pan, Treatment of reverse-osmosis concentrate of printing and dyeing wastewater by electro-oxidation process with controlled oxidation-reduction potential (ORP), Chemosphere, 201 (2018) 621-626.

[85] P. Alfonso-Muniozguren, S. Cotillas, R.A.R. Boaventura, F.C. Moreira, J. Lee, V.J.P. Vilar, Single and combined electrochemical oxidation driven processes for the treatment of slaughterhouse wastewater, J. Clean. Prod., 270 (2020).

[86] G. Acosta-Santoyo, J. Llanos, A. Raschitor, E. Bustos, P. Cañizares, M.A. Rodrigo, Performance of ultrafiltration as a pre-concentration stage for the treatment of oxyfluorfen by electrochemical BDD oxidation, Sep. Purif. Technol., 237 (2020).

Chapter II. Objectives and experimental plan

1. Objectives

The objective of this PhD Thesis lies in the application of novel technologies based on electrochemical oxidation processes enhanced by its combination with solar energy for the treatment of industrial wastewater as well as for the elimination of OMCs contained in urban wastewater. In addition, the combination with other technologies such as membrane NF systems is also considered for efficiency improvement.

To achieve the general objective, the following specific objectives (defined as targets) are proposed, which have been developed in each of the papers that conforms this PhD Thesis:

- ***Target 1:*** Characterization, modelling and start-up of a SPEF pilot plant consisting on Electro MP-Cells from ElectroCell with Nb-BDD as anode and carbon-PTFE GDE as cathode for onsite generation of H_2O_2. Optimization of the main operating parameters (pH and *j*) by using Response Surface Methodology. Addresed in Salmerón, I., Plakas, K. V., Sirés, I., Oller, I., Maldonado, M. I., Karabelas, A. J., Malato, S. *Optimization of electrocatalytic H_2O_2 production at pilot plant scale for solar-assisted water treatment.* Applied Catalysis B: Environmental, 242 (2019) 327-336.
- ***Target 2.*** Combination of a NF membrane system with the SPEF pilot plant as a tertiary treatment of UWWTP retentate. Evaluation of different electro-oxidative processes combined or not with solar energy for the elimination of OMCs in simulated and actual NF retentate. Addressed in Salmerón, I., Rivas, G., Oller, I., Martinez-Piernas, A., Agüera, A., Malato, S*. Nanofiltration retentate treatment from urban wastewater secondary effluent by solar electrochemical oxidation processes.* Separation and Purification Technology.
- ***Target 3.*** Examination, diagnosis and preliminary autopsy of carbon-PTFE GDE cathode surface by scanning electron microscopy (SEM) and X-ray microanalysis. Assessment of H_2O_2 onsite production variations. Addressed in Salmerón, I., Oller, I., Plakas, K. V., Malato, S*. Degradation of carbon-based cathodes in electro-Fenton treatment.* Submited.
- ***Target 4.*** Development and application of new photoelectrocatalytic processes at laboratory scale for the simultaneous elimination of OMCs and pathogens in freshwater. Assessment of the enhancement achieved when a Pt counter cathode is replaced by a carbon felt cathode able to electrogenerate H_2O_2. Addressed in Salmerón, I., P. K. Sharma, P.K., Polo-López, M.I., Tolosana, A., Oller, I., Byrne, J.A., Fernández-Ibañez, P. *Electrochemically Assisted*

Photocatalysis for the Simultaneous Degradation of Organic Micro-Contaminants and Inactivation of Microorganisms in Water. Process Safety and Environmental Protection. *Under Review: mayor revisions.*

- ***Target 5.*** Pre-treatment of complex industrial wastewaters by electrogenerated chlorine species by using commercial DSA, made of a titanium base coated with a conducting layer of a metal oxide or a mix of them, and combined with solar energy at pilot plant scale. Main objective lays on increasing biodegradability enough for the subsequent application of a lower-cost biological treatment. Addressed in Salmerón, I., Oller, I., Malato, S. *Electro-oxidation process assisted by solar energy for the treatment of wastewater with high salinity.* Science of The Total Environment, 705 (2020) 135831.

2. Experimental plan

For the successful achievement of the proposed objectives, the tasks detailed below have been set out and performed:

Task 1. Optimization of an electrochemical pilot plant equipped with four Electro-Cells of Nb-BDD anodes for the onsite generation of H_2O_2 and carbon-PTFE GDE cathode.

1.1 Modelling and optimization of H_2O_2 electro-generation by Response Surface Methodology.

Application of a Central Composite Experimental Design for the optimization of main operation parameters of the electro-oxidation pilot plant: pH and current density. A set of 19 runs will be defined on the experimental matrix, setting variations of pH among 3, 5 and 7, and *j* among 30, 65 and 10 mA cm^{-2}. The statistical analysis of the results will allow obtaining a second-order regression model and the optimal operating conditions for maximizing the electrogeneration of H_2O_2 with the lowest energy consumption.

1.2 Establishment of the best operation conditions.

Once the main parameters are optimized (pH and *j*), several tests are carried out to evaluate the effect of other process parameters on the SPEF pilot plant performance, such as water flow, air flow and different ionic strengths, in order to describe their influence on H_2O_2 electrogeneration.

Task 2. Evaluation of the optimized electrochemical process for the removal of reference organic contaminants.

Preliminary tests are carried out with organic reference compounds (pyrimethanil and methomyl at 50 and 90 mg L^{-1}, each), which degradation behaviour by other AOPs is well known, in order to assess the performance of the electrochemical process and its enhancement by solar energy. Experimental operation conditions will be those stablished by the previous optimization, by using Na_2SO_4 as supporting electrolyte. Parameters to be monitored through the experiments are: concentration of H_2O_2 and iron (total and dissolved), FAC, DOC and the organic compounds (analysed by HPLC-UV).

Task 3. First approach to the combination of technologies, application of Nb-BDD electro-cells with carbon-PTFE GDE cathodes and NF membrane system for the degradation of OMCs contained in UWWTP effluents.

3.1 Development of a simulated NF retentate receipt.

A synthetic recipe of NF membrane retentate from the effluent of an UWWTP is developed according with previous characterizations reported on literature, which is used as water matrix for the removal of the target OMCs (pentachlorophenol, terbutryn, chlorphenvinfos and diclofenac).

3.2 Working at natural pH by studying the use of ethylenediamine-N,N'-disuccinic acid as iron complexing agent in EF and SPEF processes.

Electrochemical treatments are applied at natural pH being crucial the use of an iron complexing agent to maintain it in solution. Ethylenediamine-N,N'-disuccinic acid (EDDS) is selected for showing high biodegradability and stability in demineralized water at neutral pH as demonstrated in previous published works. The suitability of the complex formed by Fe^{3+} and EDDS is evaluated under 1:2 ratio (0.1:0.2 mM), studying its stability in highly salted concentrated streams, its interaction with cations contained in the water matrix, as well as its behaviour during electro-oxidative processes.

3.3 OMCs removal in the SPEF pilot plant.

Different electrochemical processes assisted or not by solar energy, are evaluated for the removal of selected OMCs from the priority substances of the Directive 2013/39/EU: pentachlorophenol, terbutryn, chlorphenvinfos and diclofenac at initial concentrations of 200 and 500 µg L^{-1}. Simulated NF retentate is used as water matrix.

Task 4. Tertiary treatment of actual UWWTP effluents by the combination of NF system and electrochemical processes.

NF membrane system is applied as pre-concentration stage in a tertiary treatment line for the increase of OMCs concentration in the retentate stream as well as the reduction of the total volume to be treated, at the same time that a high quality permeate stream is produced, which could be directly reused for different purposes. In consequence, its combination with an electrochemical treatment envisages the reduction of the ohmic resistance with a subsequent decrease of the electrical cost related to the energy needed in the electrochemical treatment.

4.1 Combined technologies assessment by fortification of actual NF retentate with target OMCs.

Tests are carried out on an actual NF retentate from an UWWTP effluent, obtained in a pilot plant available at Plataforma Solar de Almería (PSA) facilities (conformed by FilmTec NF90 2540 commercial NF membranes) and spiked with the selected OMCs (pentachlorophenol, terbutryn, chlorphenvinfos and diclofenac at initial concentration of 100 μg L^{-1}). Electrochemical treatments: AO and EF, combined with solar energy (solar-assisted AO and SPEF) are evaluated in order to find the most suitable process according to the water matrix characteristics. Furthermore, the influence of the carbonates in the degradation process by electrochemical treatments is also addressed.

4.2 Combined technologies for the removal of OMCs contained in the actual NF retentate stream.

Effectiveness assessment of the most promising tertiary electrochemical treatment selected in the previous task will be studied for the elimination of OMCs actually present in the NF retentate stream. OMCs are detected and monitored by using liquid chromatography coupled to mass spectrometry.

Task 5. Examination, diagnosis and degradation assessment of Carbon-PTFE GDE cathode.

5.1 Evolution study of H_2O_2 electrogenerated in the SPEF pilot plant.

The stability and robustness of carbon-PTFE cathodes is studied by monitoring the accumulated H_2O_2 electrogenerated after several tests carried out along the PhD Thesis. Their capacity to produce H_2O_2 and their suitability for EF and SPEF processes performance are also evaluated.

5.2 Cathodes cleaning procedure and evaluation of H_2O_2 electrogeneration capability recovery.

Disassembled of different pieces of the cell for a visual evaluation of physical changes observed on the cathode surface and the formation of salt inlays is planned. Removal of the inlays is performed by the cathode immersion in HCl solution 1:2 during 24 h. After cleaning procedure, the concentration of accumulated H_2O_2 electrogenerated is compared to the one attained when the cathode was new for the assessment of cleaning effectiveness for a possible cathode reuse.

5.3 SEM and X-ray analysis of cathode surface.

Cathode surface is studied after the cleaning procedure for analysing the loss of reactive surface provoked by the detachment of carbon-PTFE from the cloth support and by the possible remaining salt inlays. Detailed characterization of the cathode composition as well as the inlays will be tackled.

Task 6. Assessment of a photoelectrocatalytic process with innovative and newly developed TiO_2 nanotubes (TiO_2-NT) photoanodes for the purification of fresh water at laboratory scale.

6.1 Manufacture of new TiO_2-NT photoanodes at laboratory scale.

A titanium mesh is immersed in a specific electrolyte consisting on NH_4F (0.3 wt%) in distilled water (3.0 vol%) and ethylene glycol (97 vol%). By applying a potential of 30 V during 3 h, the growing of TiO_2-NT over the entire surface of the mesh is promoted. Then the electrodes are assembled in a cell with a quartz window and an anode-anode-cathode configuration.

6.2 Definition of operation conditions for testing the electrocatalytic efficacy of the new developed cell with TiO_2-NT.

Best working potential is determined by scanning a range of potentials from 0.1 to 1.5 V till reaching the maximum photo-current when illuminating the photoanodes with a UV-A lamp of 9 W at an irradiation of 50 W m^{-2}.

6.3 Evaluation of the new cathode effectiveness for OMCs and pathogens removal in natural water.

A comparison between OMCs degradation (terbutryn, chlorphenvinfos and diclofenac at 500 µg L^{-1} each) and disinfection results (*E. coli* at 10^6 CFU mL^{-1}) reached by the

photoelectrocatalytic lab scale system using a counter cathode of Pt, and the possible improvement that could be obtained by replacing it by a carbon-based one able to electrogenerate H_2O_2 onsite is addressed. For this, tests will be carried out with OMCs and bacteria, following the degradation and inactivation rates along treatments.

6.4 Hole scavengers effect in disinfection by new lab scale photoelectrocatalytic system.

Methanol and acetate, well known hole scavengers, are added to the target natural water at 5 mM each aiming to check their influence in the photo-current achieved and in bacteria inactivation through the photoelectrocatalytic treatment.

Task 7. Pre-treatment of complex industrial wastewaters by electrogenerated chlorine species using commercial DSA electrodes.

7.1 Characterization of industrial wastewaters: two different batches of landfill leachate.

A complete characterization of target industrial wastewaters will be carried out, addressing physicochemical parameters such as chemical oxygen and biological oxygen demands, dissolved organic carbon and concentration of ionic species. Toxicity and biodegradability are carried out by means of respirometry (oxygen uptake rate measurement) with active sludge from an UWWTP.

7.2 Landfill leachates treatment with a commercial device based on DSA electrolyzer.

Two different batches of landfill leachate are depurated applying the stand-alone electrolyzer until improving toxicity and biodegradability enough to allow a subsequent conventional biological treatment.

7.3 Commercial DSA electrolyzer assisted by solar energy.

DSA electrolyzer is combined with a solar compound parabolic collector (CPC) photoreactor available at PSA, in order to evaluate the benefits and/or disadvantages of the application of solar energy to the electrochemical process, aiming to reduce toxicity and increase biodegradability in a more efficient way.

To complete the feasibility study, landfill leachates treatment by commercial DSA electrolyzer, assisted and not by solar energy, was compared with solar photo-Fenton process.

Chapter III. Materials and Methods

1. Chemicals

1.1. Organic microcontaminants

Pyrimethanil and methomyl have been used as model compounds in the optimization, tuning and validation of an electrochemical pilot plant as their degradation had been widely previously studied in detail by different AOPs [1-4].

A selection of target micropollutants to be studied in this work has been carried out based on Directive 2013/39/EU which addresses priority substances for water policy. OMCs have been chosen according to their abundance in UWWTP effluents, their solubility in water, their stability against hydrolysis and photolysis, and to the ease of their analysis. pentachlorophenol, terbutryn and chlorphenvinfos were picked up as targets as they represent a mixture of different anthropogenic substances that can be easily found in a water effluent. DCF has been also selected as part of the OMCs mixture due to its high presence in wastewater coming from its extended use as a nonsteroidal anti-inflammatory (painkiller) in humans. Main characteristics of all target selected compounds are gathered in table 4.

Fortification of water matrices with OMCs: pentachlorophenol, terbutryn, chlorphenvinfos and diclofenac was carried out by preparing two stock solutions of 2.5 and 6.25 g L^{-1} (of each OMC) in methanol, aiming to add similar amount of DOC from methanol in experiments at low or high concentration of OMCs but always maintaining DOC in the range of what is normally found in UWWTP effluents.

Table 4. Reference compound characteristics.

Pyrimethanil	
Systematic name (IUPAC):	N-(4,6-dimethylpyrimidin-2-yl)aniline
CAS number:	53112-28-0
Linear Formula:	$C_{12}H_{13}N_3$
Molecular weight (g mol^{-1}):	199.28
Solubility in water (mg L^{-1}):	110
Class:	Fungicide
Acute Toxicity (oral); LD_{50} (mg kg^{-1}) in rats:	4150
Effects in humans	Endocrine disrupter, Eye irritant, Affects reproduction and development, Neurotoxicant, Possible human carcinogenic (USEPA)

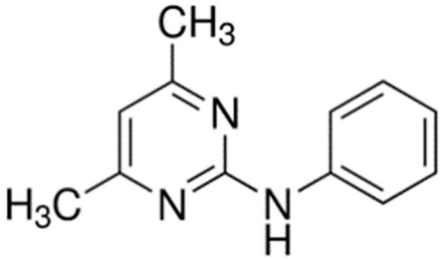

Methomyl	
Systematic name (IUPAC):	S-methyl (EZ)-N-(methylcarbamoyloxy)thioacetimidate
CAS number:	16752-77-5
Linear Formula:	$C_5H_{10}N_2O_2S$
Molecular weight (g mol^{-1}):	162.21
Solubility in water (mg L^{-1}):	55000
Class:	Insecticide
Acute Toxicity (oral); LD_{50} (mg kg^{-1}) in rats:	30; High
Effects in humans	Eye and respiratory tract irritant. Cholinesterase inhibitor

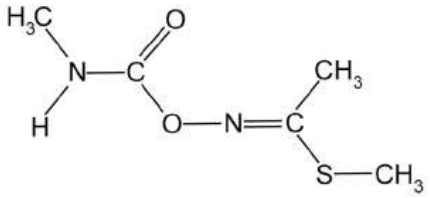

Pentachlorophenol	
Systematic name (IUPAC):	2,3,4,5,6 – pentaclorofenol
CAS number:	87-86-5
Linear Formula:	C_6HCl_5O
Molecular weight (g mol^{-1}):	266.34
Solubility in water (mg L^{-1}):	10
Class:	Multi-action pesticide and herbicide
Acute Toxicity (oral); LD_{50} (mg kg^{-1}) in rats:	80; High
Effects in humans	Carcinogen Endocrine disrupter Skin, eyes and respiratory tract irritant Affects reproduction and development Neurotoxicant Bioaccumulates

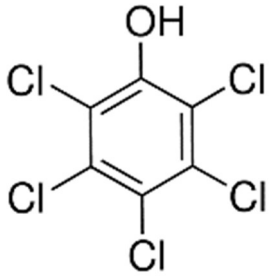

Terbutryn	
Systematic name (IUPAC):	N2-tert-butyl-N4-ethyl-6-methylthio-1,3,5-triazine-2,4-diamine
CAS number:	886-50-0
Linear Formula:	$C_{10}H_{19}N_5S$
Molecular weight (g mol^{-1}):	241.36
Solubility in water (mg L^{-1}):	25
Class:	Herbicide
Acute Toxicity (oral); LD_{50} (mg kg^{-1}) in rats:	> 2500; Low
Effects in humans	Endocrine disrupter, Eyes irritant, Possible human carcinogenic (USEPA)

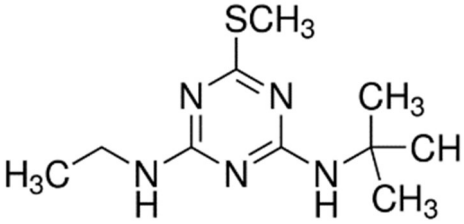

Chlorfenvinphos	
Systematic name (IUPAC):	(EZ)-2-chloro-1-(2,4-dichlorophenyl)vinyl diethyl phosphate
CAS number:	470-90-6
Linear Formula:	$C_{12}H_{14}Cl_3O_4P$
Molecular weight (g mol^{-1}):	359.6

Solubility in water (mg L^{-1}):	145
Class:	Insecticide
Acute Toxicity (oral), LD_{50} (mg kg^{-1}) in rats:	12, High
Effects in humans	Endocrine disrupter, Neurotoxicant, Cholinesterase inhibitor

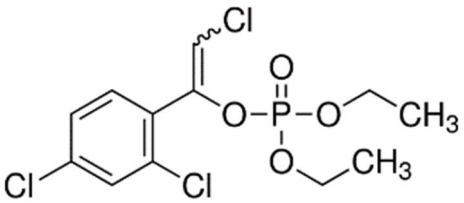

Diclofenac	
Systematic name (IUPAC):	2-[2-(2,6-dichloroanilino)phenyl]acetic acid
CAS number:	15307-79-6
Linear Formula:	$C_{14}H_{11}Cl_2NO_2$
Molecular weight (g mol^{-1}):	296.15
Solubility in water (mg L^{-1}):	2.73
Class:	Drug

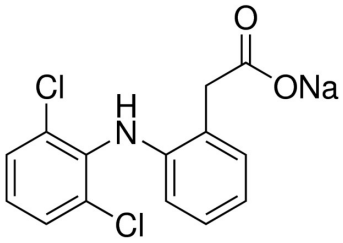

Source: Pesticides Properties DataBase[5]

1.2. Reagents

In this PhD Thesis a large number of reagents has been used mainly for elaboration of the synthetic water matrices (see section III.1.3.4), appart from those normally required for samples analysis and monitroing of physico-chemical parameters. The reagents used are listed below (Table 5).

Table 5. List of substances used to undertake the experiments, detailing their use and their supplier.

Reagent	To be used for/as	Supplier
Sodium sulphate anhydrous ≥99%	Supporting electrolyte and Simulated Nanofiltration Retentate components	Honeywell
Sodium chloride	Simulated Nanofiltration Retentate components	Merk
Calcium nitrate		Sigma-Aldrich
Potassium sulphate		Merck Millipore
Calcium sulphate		Panreac
Ammonium sulphate		Merck Millipore
Sodium phosphate dibasic		Panreac
Sulfuric acid 95-97%	pH adjustments and to lower carbonates	J.T. Baker
Sodium hydroxide	pH adjustments	J.T. Baker
Hydrogen peroxide 30% (p/v)	Fenton reagent and cleaning of photoelectrocatalytic cell	Panreac
Titanium (IV) oxysulfate solution 1.9-2.1%	H_2O_2 measurement	Fluka
Bovine liver catalase	Quencher of H_2O_2	Sigma-Aldrich

Reagent	To be used for/as	Supplier
2300 units mg^{-1}		
Iron (II) sulphate heptahydrate 99%	Catalyst. Fenton reagent	Panreac
Iron (III) sulphate hydrate 75%	Catalyst in Fenton-like processes at natural pH. Used with EDDS as chelant	Panreac
Ethylenediamine-N,N'-disuccinic acid (EDDS) 35% (w/v) in water	Chelant. Fe^{3+} complexing agent	Sigma-Aldrich
1,10 Phenanthroline chloride monohydrate	Iron measurements reactive.	Merck
Ammonium acetate >98%	Buffer solution for Iron measurements	Riedel-de-Haën
Acetic Acid 99-100%		J.T.Baker
N, N-diethyl-p-phenylenediamine (DPD) pillow for Free Chlorine	Free chlorine measurements	Hach
Sodium thiosulphate pentahydrate	Quencher of chlorine species	Merck
Methanol >99.9%	Solvent for the stock solutions and mobile phase in HPLC	J.T.Baker
Acetonitrile >99.9%	Organic mobile phase for HPLC	Sigma-Aldrich
Formic acid 98-100%	Preparation of HPLC aqueous mobile fase	Merk
Sodium acetate anhydrous	Reference in toxicity test	Merck
N-Allylthiourea 98%	Nitrification inhibition in biodegradability analysis	Sigma-Aldrich
Chloridric acid 37%	Electrocells cleaning	Panreac
Oxalic acid dehydrated 99.8%	Cleaning of the CPC photoreactors	Guinama

Ethylenediamine-N,N'-disuccinic acid

Fenton and Fenton-like processes at neutral pH have been tackled by using EDDS as chelant agent to complex iron (III) and keep it in solution as long as possible.

When iron is presented in ferric form it is able to generate complexes with natural substances such citrate and oxalate. However, a synthetic organic substance such as ethylenediaminetetraacetic acid (EDTA) has been the most commonly used as a complexing agent in the context of Fenton-like processes for its great capacity to form chelates due to the presence of four carboxyl and two amino groups within the molecule. But, in view of the non-biodegradable nature of EDTA and its recent clasification as a persistent pollutant, the use of this compound had been ruled out. In this situation, EDDS

appears as an alternative, since it is structurally an isomer of EDTA, it is also able to form chelates with ferric iron and highly biodegradable, presenting, in addition, greater efficiency when degrading OMCs compared to natural chelants such as citrate [6].

The optimum molar rate between Fe^{3+} and EDDS (1:2) in Fenton-like processes to degrade OMCs has been studied previously by Klamerth et al. [7]. Nevertheless, it is important to hihglight that EDDS enters into competition with OMCs in the degradation process. In this PhD Thesis, EF and SPEF experiments were developed at natural pH with a concentration of 0.1 mM of Fe^{3+} which meant an addition of 0.2 mM of EDDS to form an stable complex.

The complex was prepared just before every experiment following steps detailed below:

- In a glass beaker, a low volume of water is acidified till pH 2.8 depending on the amount of iron and the volume of the reactor. Usually between 40 and 50 mL of acidified water for a concentration of 0.1 mM of Fe^{3+} in a total volume of 30 L.
- Iron (III) sulphate hydrate salt is weighed and added to the acidified water keeping it stirred till being totally dissolved, that is, when it shows a light and clear yellow colour.
- The glass beaker is wholly covered with aluminium foil and the corresponding amount of EDDS is added, stirring vigorously until the complex is completely formed, what is evidenced when the solution takes a strong yellow colour.

Catalase to remove remaining hydrogen peroxide

Elimination of the residual oxidants, such as hydrogen peroxide, remaining in the sample under analysis was necessary in order to prevent the oxidation reaction further develop, for an accurate measure of the degradation in the specific sampling time and to avoid possible interferences in the different analytical techniques applied.

Catalase is an oxidoreductase enzyme whose purpose is to neutralize H_2O_2 during cellular metabolism, producing water and molecular oxygen (Reaction 40).

$$2\ H_2O_2 \rightarrow 2\ H_2O + O_2 \qquad \text{(Reaction 40)}$$

Despite that its mechanism of action is not defined, it is known that a catalase unit breaks down 1.0 µmol of hydrogen peroxide per minute at pH 7 and at approximately 25ºC, showing activity at pH values between 5 and 8. To neutralize residual H_2O_2 in samples, the procedure described below was followed.

In order to have a catalase solution as fresh as possible and to guarantee enzyme activity, a solution of 1 g L^{-1} of Bovine liver catalase in ultrapure water was prepared before each experiment. For each sample to be neutralized residual H_2O_2 concentration was measured and, in those cases in which pH was above or below the activation range of the enzyme it was adjusted to a value around neutrality. Generally, 0.5 mL of catalase solution must be added to a 25 mL of sample with a 20 mM residual H_2O_2 concentrationand left to react for 10 minutes. Finally, concentration of H_2O_2 in samples must be measured again to assure absence of residual oxidant.

Reagents for neutralization of active chlorine species

Neutralization of ACS has been extensively studied since chlorination is one of the most widespread methods for drinking water. Commonly used methods to eliminate ACS in water facilities are focused in the addition of reducing agents as sulphur dioxide, sodium bisulphite, and sodium thiosulphate. Lately, even ascorbic acid (Vitamin C) has begun to be used as a neutralizer as it entails less risk during operation.

In this PhD Thesis sodium thiosulphate has been selected to remove chlorine species, since this salt is less dangerous than conventional methods based on the addition of sulphur salts. Reactions that occur between sodium thiosulphate and ACS are shown below (Reactions 41 - 43):

$$Na_2S_2O_3 + 4\ HClO + H_2O \rightarrow 2\ NaHSO_4 + 4\ HCl \quad \text{(Reaction 41)}$$

$$Na_2S_2O_3 + HClO \rightarrow Na_2SO_4 + S + HCl \quad \text{(Reaction 42)}$$

$$2Na_2S_2O_3 + HClO \rightarrow Na_2S_4O_6 + NaCl + NaOH \quad \text{(Reaction 43)}$$

The amount of thiosulfate required to neutralize chlorine can vary depending on the target water pH. In our study, pH of the treated water was not modified, being naturally between 7 and 8, so according to what is stated in Wang et al. 2006 [8], 2 parts of thiosulfate were necessary to neutralize one part of FAC. Accordingly, sodium thiosulfate was added when required from a 20mM stock solution.

1.3. Water matrices

Different water matrices have been employed along the experimentation carried out within this PhD Thesis. From demineralized to natural and simulated wastewater to finally move to an application closer to actual conditions with more complex matrices.

1.3.1. Ultrapure water

Ultrapure quality water (milliQ) was obtained from demineralized water treated by an ultrapure water system Milli-Q® from Merck Millipore. Water obtained presented a conductivity of 0.054 µS cm^{-1} and a maximum COD of 0.3 mg L^{-1}.

1.3.2. Demineralized water

PSA has a membrane distillation plant that supplies demineralized water to all facilities. Demineralized water characterization is: conductivity below 10 µS cm^{-1}, chlorides between 0.7 and 0.8 mg L^{-1}, 0.5 mg L^{-1} of nitrate and an organic carbon below 0.5 mg L^{-1}.

1.3.3. Natural water

Natural water at PSA is supplied by a well in Los Llanos de Tabernas, Almería. This water is characterized for having a high hardness and a high ionic charge. Detailed parameters are described in table 6.

Table 6. Characterization of the natural water at PSA facilities.

Main parameters	***Value***
pH	7.4 - 7.6
Conductivity (mS cm^{-1})	2.4 - 2.6
DOC (mg L^{-1})	1.2 - 3.2
Ionic species	***mg L^{-1}***
HCO_3^-	813
Cl^-	254 - 334
SO_4^{2-}	169 - 240
Na^+	383 - 471
Ca^{2+}	73 - 96
NH_4^+	0
Mg^{2+}	50 - 66
K^+	2.3 - 7.9
NO_3^-	11 - 15
HPO_4^{2-}	0

1.3.4. Synthetic electrolytes

Electrochemical processes have to be applied in waters with medium to high conductivity to allow electrons flux, so initially, experiments were developed with demineralized water with a solution 50mM of Na_2SO_4. This specie is commonly used in electrochemical

treatments in order to achieve a high ionic strength avoiding Cl^-, which can electrogenerate also ACS not being able to evaluate the effect of $^{\bullet}OH$ by itself.

Simulated nanofiltration retentate (SNR) was also defined based on the characterization of NF retentates obtained by Miralles-Cuevas et al. [6] when treated UWWTP effluents from El Ejido in batch mode, reducing by four times the volume of water to be treated. Simulated effluent was carachterized by maximum 500 mg L^{-1} of Cl^-, 1500 mg L^{-1} of SO_4^{2-}, 1050 mg L^{-1} of Na^+, 213 mg L^{-1} of Ca^{2+}, 20 mg L^{-1} of NH_4^-, 50 mg L^{-1} of Mg^{2+}, 40 mg L^{-1} of K^+ and 100 mg L^{-1} of NO_3^-.

Under this conditions, SNR recipe contained the following reagents (see Table 5): 82 mg $L^{-1}$of $Ca(NO_3)_2$, 1420 mg L^{-1} of Na_2SO_4, 87 mg L^{-1} of K_2SO_4, 340 of $CaSO_4$, 497 mg L^{-1} of NaCl , 66 mg L^{-1} of $(NH_4)_2SO_4$ and 21 mg L^{-1} of Na_2HPO_4. All of them were dissolved in natural water from PSA reaching a conductivity between 5.5 - 6 mS cm^{-1}. Characterization of natural water and SNR is shown in table 7.

Table 7. Deailed description of the SNR composition.

	Natural water (mg L^{-1})	**Addition of reagents (mg L^{-1})**	**Final concentration in SNR (mg L^{-1})**
HCO_3^-	813	-	813
Cl^-	254	301	555
SO_4^{2-}	169	1296	1465
Na^+	389	661	1050
Ca^{2+}	73	140	213
NH_4^+	0	18	18
Mg^{2+}	50	-	50
K^+	7	39	46
NO_3^-	11	62	73
HPO_4^{2-}	0	14	14

1.3.5. Actual wastewaters

Scaling up to actual electrochemical applications by treating actual wastewater is one of the goals addressed in this PhD Thesis. Three different types of water were used along the whole PhD: UWWTP effluent, surface water (low levels of pollution and a source of drinking water) and landfill leachate selected as a reference of complex, toxic and biorecalcitrant wastewater from industrial origin. In the following sections they are described in more detail.

1.3.5.1. UWWTP effluent

UWWTP effluent was collected from El Ejido UWWTP in Almería, Spain. These facilities were designed to treat an organic load of 100 000 p.e. and a water flow of 12 459 m^3 per day.

This UWWTP is located in an intensive agricultural production area, with almost 13 000 hectares of greenhouses, involving a high input of chemicals for the success of each harvest. Taking into account that this UWWTP collect wastewater from both the municipality and from intensive agriculture, it is expected to found in the effluent a wide variety of biocides, pesticides, herbicides, as well as a huge amount of pharmaceuticals.

Main physicochemical parameters of UWWPT effluent are: DOC around 12 mg L^{-1}, COD in the range from 17 to 50 mg L^{-1}, low turbidity (3.1 - 5.9 NTU) and conductivity between 2.1 and 2.3 mS cm^{-2}. Ions contained in wastewater are shown in table 8.

Table 8. Characterization of the ionic content of the UWWTP effluent

Ionic species	***mg L^{-1}***
HCO_3^-	264 - 440
Cl^-	423 - 460
SO_4^-	127 - 140
Na^+	254 - 264
Ca^{2+}	96 - 105
NH_4^+	22 - 35
Mg^{2+}	66 - 67
K^+	23 - 25
NO_3^-	12 - 31

1.3.5.2. Surface water

Surface waters are those that are above the earth's surface open to the atmosphere and subjected to surface runoff. This source of waters can be presented in form of lotic water systems as streams and rivers, or in form of lentic water bodies as reservoirs, wetlands lakes and oceans.

New developed TiO_2-NT photoanodes efficiency was finally assessed for the elimination of OMCs and pathogens in surface water at laboratory scale. Surface water was collected from a natural stream in Whiteabbey (Newtownabbey, UK) along the collaboration stay of the PhD candidate with the University of Ulster. In table 9 is show its characterization.

Table 9. Detailed characterization of the surface water.

Main parameters	***Value***
pH	7.3
Conductivity	697 µS cm^{-1}
DOC	6.9 mg L^{-1}
Turbidity	0.1 NTU
Ionic species	***mg L^{-1}***
HCO_3^-	83
Na^+	15
NH_4^+	0.2
Mg^{2+}	13
Ca^{2+}	50
K^+	1.2
Cl^-	18
NO_2^-	0.1
NO_3^-	2.8
HPO_4^{2-}	1.3
SO_4^{2-}	111

1.3.5.3. Landfill leachate

Leachates are liquids, whether from rainfall or groundwater, that percolate through the solid residues in a landfill, washing them and carrying large amounts of compounds from the residues and their degradation products (e.g. ammonium or toxic metals), so if they are not collected nor treated entail an important pollutant source.

The composition of a leachate depends on the type of waste deposited, its compaction, the climatic conditions of the region, the time elapsed since the formation of the deposit, etc. According to this, two types of leachate are differentiated:

- ***Young:*** from landfills with an age of 1-2 years. The pH is usually low, in the range between 4.5 and 7.5. High COD and BOD_5, in the range of several g L^{-1}.

- ***Mature:*** from landfills over 5 years old. pH range is between 6.5 - 7.5. COD and BOD_5 had been substantially reduced by anaerobic microorganisms remaining only the most recalcitrant organics. Moreover, the ionic content (e.g. sulphates, chlorides) significantly increases.

In this PhD Thesis, the treatment of two mature leachates from different sources was addressed by a commercial electrochemical system. A detailed characterization of them is shown in table 10.

Table 10. Landfill leachates characterization.

	Leachate 1	**Leachate 2**
Main parameters		
pH	7-8	7-8
Conductivity (mS cm^{-1})	50-70	25-35
COD (g L^{-1})	8.1 – 8.4	8.8 - 11
DOC (g L^{-1})	2 - 2.5	2 – 3.2
TN (g L^{-1})	6 – 6.5	3.9 - 4.7
Turbidity (NTU)	35	200-300
Toxicity	53%	0%
Biodegradable	No	No
Iron (mg L^{-1})	70 - 115	38 - 44
Ionic species (g L^{-1})		
Cl^-	6.4 – 8.2	4.5 - 5.2
SO_4^-	23 - 27	8.2 - 9
Na^+	5.7 - 7.3	2.3 - 2.8
Ca^{2+}	0.3 - 0.4	0.1 - 0.3
NH_4^+	6.6 - 8.5	2.6 - 3.2
Mg^{2+}	0.2 - 0.4	N.D
K^+	3.5 - 4.4	2.3 - 2.8

**N.D. non detected*

2. Microorganisms

Escherichia coli (*E. coli*) is a gram-negative bacterium generally used as biological indicator of disinfection efficiency in water systems [9]. Specifically the *E. coli* strain used in this study is K12, commonly selected as model pathogen since it has been modified to be unable to infect humans permitting its manipulation without running into eventual health risk. It was obtained from the Spanish Culture Collection (CECT 4624).

Previous day to disinfection experiments, fresh liquid cultures were prepared adding one colony from a stock dish (prepared weekly) into 14 mL of Tryptone Soya Broth CM0129

(from OXOID). Then the solution was incubated in a rotary shaking at 37°C, and after 20h the stationary phase at 10^9 Colony-Forming Unit (CFU) mL^{-1} was reached. Once the inoculum was ready, two procedures were followed depending on the type of experiment:

(i) In the experiments developed to test the efficiency of the new photoelectrocatalytic system described in section III.4.5 (at laboratory scale), 190 µL of these liquid culture was diluted directly into the reactor attaining an initial concentration of 10^6 CFU mL^{-1}, increasing the DOC to 6.7 mg L^{-1} due to the addition of the nutrient broth.

(ii) In hole-acceptors experiments, the inoculum was centrifuged at 3000 rpm for 10 min in a 15 mL Falcon conical centrifugal tube obtaining 2 phases: a pellet with the bacteria and nutrient broth. Broth was then removed and the pellet was re-suspended in Phosphate Buffer Saline (PBS) solution. Then 190 µL of this solution was diluted directly into the reactor (total volume of 190 mL), achieving the initial concentration of 10^6 CFU mL^{-1} but avoiding any DOC increase noted in the previous method.

As occurs with the addition of the inoculum, two different methods were used to enumerate bacteria in water samples according to the experiment:

(i) When testing new photoelectrocatalytic reactor efficiency (at lab scale), samples were enumerated using the standard plate counting method with Tryptone Soya Agar CM0131 0 (from OXOID) as culture media. Six 20 µL drops of each dilution were plated entailing a detection limit (DL) of 9 CFU mL^{-1}. Petri-dishes were incubated at 37 °C for 24 h counting the colonies once finalized the incubation time.

(ii) For hole-aceptor experiments, samples were enumerated using the standard plate counting method with ChromoCult®Coliform Agar (from Merck) a selective culture media specific for enumeration of *E. coli* and *Coliform* bacteria. Samples were diluted in serial within PBS (10-fold) spreading volumes ranged between 50 - 500 µL onto Petri-dishes surface achieving a detection limit of 2 CFU mL^{-1}. Colonies were counted after 24 h of incubation at 37 ºC.

3. Analysis

3.1. Physical-chemical parameters

3.1.1. pH measurement

As occurs in all chemical processes, pH will determine the species present in the solution. Particularly in electrochemical processes will determine the concentration of HClO or ClO^- according to the pKa (7.5) and in Fenton and Fenton-like reactions the presence of dissolved iron available to react.

pH was measured using a potentiometric method based in the measurement of the potential through a pH electrode. This electrode commonly combines a pH electrode that contains the reference and measuring electrode in the same glass body. Measuring electrode is composed of a glass bulb selective for hydronium ions filled with an electrolyte, usually a solution of KCl, with a metallic thread of silver or silver chlorine inside it. Reference electrode is a metallic thread of silver or silver chlorine with a protective joint, usually of glass or ceramic, that avoids the mixing with the filling electrolyte while allows closing the circuit.

The equipment used in this study was a LAQUAact PH110 (HORIBA) portable pH-meter (Fig. 14), calibrated periodically with standards solutions of pH 4.01, 7 and 10.01 from HORIBA (pH buffer solutions 560-4; 560-7 and 560-10 respectively).

Figure 14. Portable pH-meter LAQUAact PH110 used for pH determinations.

3.1.2. Electrical conductivity measurement

Electrical conductivity is the ability of a substance to allow electrical current pass through it, measured in S m^{-1}. In an aqueous medium it is related to the presence of salts whose dissociation generates positive and negative ions able to transport the electrons which

is crucial since it determines the resistance of the solution to their transport and, therefore, energy consumption.

For the measurement of the electrical conductivity of a solution it is used a conductivity meter. Its operation consists on the application of an electrical field between two electrodes submerged in the target solution determining the electrical resistance. In this study a GLP 31 Conductivity meter from CRISON (Fig. 15) was used.

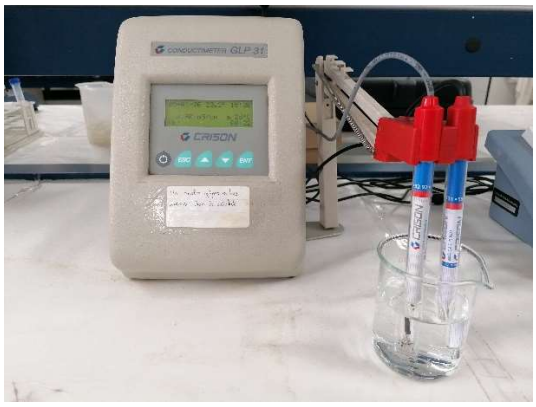

Figure 15. Conductivity meter available in the Water Technologies Laboratory at PSA.

3.1.3. Turbidity measurement

Turbidity is defined as the optical property of a suspension that causes the light dispersion avoiding its transmission through the solution. Higher amount of suspended solids in liquid entails higher degree of turbidity which in drinking water and wastewater involves lower quality. Its easy determination makes turbidity one of the most suitable parameters to define water quality.

In this PhD study, turbidity of target water must be considered as it determines the amount of photons that are able to pass across the solution and react with the substances contained on it, influencing the production of oxidant species and subsequently the degradation rates. Hence, water with high turbidity as well as a strong dark colour presents greater difficulty for decontamination when treated with solar processes and thereby, the use of a reactor with a small tube diameter may be promoted.

Measurements were undergone by nephelometry following Method 180.1 from USEPA. This method consists on measuring the radiation dispersed by the particles in the solution. A light beam is applied to the solution and the scattered light is measured with a detector at 90° angle from the incident beam. The particle density is calculated as a function of the light scattered in the detector and the results are expressed in nephelometric turbidity units (NTU).

A 2100AN Turbidimeter from Hach (Fig. 16) was used for the measurements allowing a quantification from 0.1 to 4000 NTU. The calibration of the equipment was done following manufacturer procedure, using at Hach 2100AN (IS StablCal® Stabilized Formazin standars).

Figure 16. Equipment for turbidity measuments (2100N turbidimeter from Hach) available in the Water Technologies Laboratory at PSA

3.2. UV/VIS spectrophotometry.

3.2.1. Iron measurement

One of the reagents involved in Fenton reactions is iron. Iron measurement was performed following ISO 6332 by the spectrometric method using 1,10-phenanthroline. This procedure is based on the reaction between the dissolved Fe^{2+} and three molecules of 1,10-phenanthroline (reaction 44) forming a red complex which absorbance is measured at 510 nm.

$$3C_{12}H_8N_2 + Fe^{2+} \rightarrow [(C_{12}H_8N_2)Fe]^{2+} \quad \text{(Reaction 44)}$$

To safeguard a correct complex formation, an acidic pH is needed. That means that for this procedure, a buffer solution of acetic acid and ammonium acetate is used so pH value varies between 3 and 3.5 supporting all reactions from ferrous iron.

This kind of analysis are executed by adding 4 mL of sample, 1 mL of 1,10-phenanthroline in a concentration of 1 g L^{-1}, 1 mL of buffer solution with 250 g L^{-1} of ammonium acetate and 700 mL L^{-1} of acetic acid. Next to leaving the solution to react during a few minutes, samples are measured at 510 nm in a quartz cuvette of 1 cm with an Evolution 220 UV-Visible spectrophotometer from Thermo Scientific (Fig. 17)

Figure 17. Evolution 220 spectrophotometer available in Water Technologies Laboratory of PSA facilities.

In order to measure the total iron, it is necessary to reduce the Fe^{3+} formed during the Fenton reaction to Fe^{2+} by adding a little spoon of ascorbic acid to the sample.

Depending on the target of the analysis, either if it is the dissolved and precipitated iron or only dissolved iron, the samples are measured directly or after filtration by a 0.45 µm nylon filter from ASIMIO.

If the sample is colourless, the blank in the equipment is made with distilled water. If, the water is coloured, blank is made with a solution of 4 mL of sample mixed with 1 mL of buffer solution and 1 mL of distilled water. Iron concentration results are obtained directly from an internal calibration curve, y = 0.132x (R^2= 0.999) in the range of 0.25 to 7.5 mg L^{-1}, diluting the sample when needed.

3.2.2. Hydrogen peroxide measurement

Hydrogen peroxide analyses were developed following DIN 38409 H15. This method is based in the reaction of Titanium (IV) Oxysulfate with hydrogen peroxide in solution. Measurements were developed by adding 0.5 mL of Titanium (IV) Oxysulfate to 5 mL of sample previously filtrated by a 0.45µm nylon filter, forming instantaneously the complex $[Ti(O_2)(OH)(H_2O)_3]^+$ of yellow colour that is measured spectrophotometrically at 410 nm (Evolution 220).

Calibration curve is y = 0.0226x addressing a concentration range from 0.5 till 60 mg L^{-1}. Samples with a higher concentration must be diluted with distilled water before its analysis.

3.2.3. Free Available Chlorine measurement

A crucial parameter in electrochemical treatments is FAC. From chlorides dissolved in solution ClO^- is electrogenerated (pH >7.5) (described in section I.2.5.2.2.), known for its use as disinfectant and being potentially able to degrade OMCs. The evolution of this parameter during treatment produces information useful to determine the state of the oxidation process.

FAC contained in samples is determined by means of its reaction with DPD shown in figure 18. DPD amine is oxidized through chlorine towards two oxidation products. When the pH values are close to neutrality the primary product from this oxidation reaction is a semi-quinoid cationic compound known as Würster dye. The amount of chlorine present is directly related to the pink colouration of the solution due to the formation of Würster dye. DPD can be further oxidized originating a colourless imine. A small chlorine presence in the sample will promote the formation of Würster dye over imine while on more oxidizing conditions the formation of imine will be predominant, resulting in the dimming of the solution pink colour.

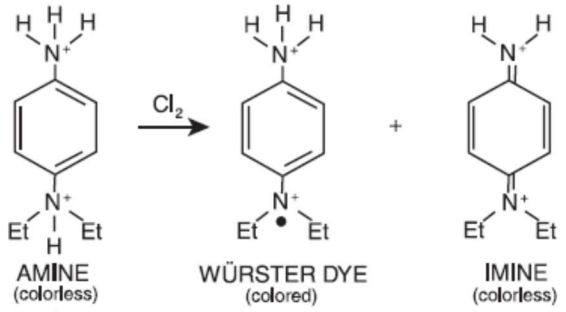

Figure 18. Description of the reaction of DPD with Cl_2. [10]

FAC was determined following Hach Method 10069 approved by USEPA, using DPD powder pillows. These pillows contained reactive DPD and the buffer in form of powder. Analyses were developed taking 25 mL of sample in a glass vessel adding directly a powder pillow. The mixture was shaken for 30 seconds in which the colour of the sample turned towards pink (Fig. 19) and then measured at 530 nm (Evolution 220) before 1 min of reaction. The calibration curve was $y = 0.1989x$ ($R^2 = 0.999$) in a range from 0.1 till 10 mg L^{-1}.

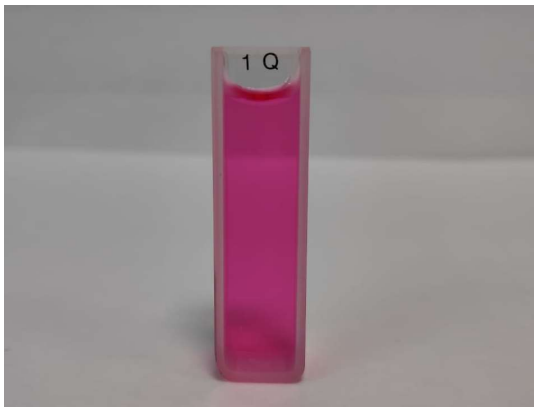

Figure 19. Würster dye generated from the reaction of DPD powder pillows with FAC contained in a sample.

3.2.4. •OH determination by p*-nitrosodimethylaniline*

p-nitrosodimethylaniline (RNO) is a strong yellow organic dye which absorbance peak at 440 nm makes it measurable by UV/VIS spectroscopy.

In literature RNO had been reported to show high selectivity against oxidation by •OH. Despite that the specific oxidation pathway is still unknown, it has been suggested that it is carried out via reaction described in figure 20, causing loss of colour on the solution. In fact, the absolute rate constant of the reaction between •OH and RNO has been determined on 1.25×10^{10} M^{-1} s^{-1} [11].

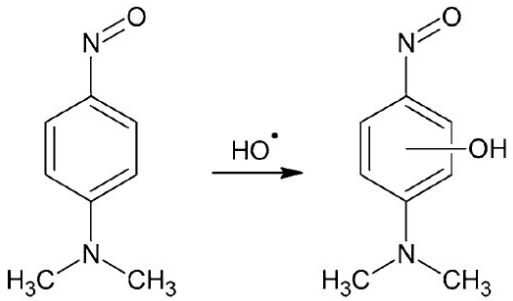

Figure 20. RNO reaction with •OH. From Muff et al. [12].

Due to the simplicity of its analysis, •OH determination method has been widely applied in water photocatalytic treatments. However, when this method is applied to electro-oxidative processes, interferences with ACS have been found. In fact, the study developed by Muff et al. [12], showed that ACS themselves, without intervention from •OH, are able to produce bleaching of the solution, despite that the mechanism of the reaction is likewise as the previous one unknown.

For this reason RNO cannot be used to properly measure •OH in electro-oxidative processes albeit it provides information on the electrochemical oxidizing power.

This technique was used to determine the oxidative power of the photoelectrocatalytic system developed in collaboration with the Nanotechnology and Integrated BioEngineering Centre (NIBEC), at Ulster University (UK), described in section III.4.5. For this purpose a photoelectrocatalytic test was developed with a solution of 17 μM RNO (from Sigma-Aldrich) in surface water as target, measuring the absorbance at 440 nm of the solution every 2 min. Quantification was made in the range from 1 to 20 μM with a 6300 UV-Visible spectrophotometer from Jenway (Fig. 21), and the calibration curve was y = 30.259x (R^2 = 0.999).

Figure 21. Spectrophotometer model 6300 from Jenway installed at NIBEC facilities.

3.2.5. Chemical Oxygen Demand determination

COD is defined as the amount of oxygen needed to oxidize the organic matter. In COD tests, potassium dichromate is used as an oxidant adding silver sulphate as a catalyst and in acidic medium. Potassium dichromate is a hexavalent chromium salt, of orange colour, known as a very strong oxidant able to degrade almost 100% of organic matter. Once it oxidizes a substance, it is transformed to a trivalent form of chromium, of green colour, according to reaction 45:

$$Cr_2O_7^{2-} + 14\ H^+ + 6e^- \rightarrow 2\ Cr^{3+} + 7\ H_2O \qquad \text{(Reaction 45)}$$

When dichromate oxidizes an organic molecule it loses 6 electrons while an oxygen molecule loses 4 (Reaction 46), so the oxidation of 1 mol of dichromate is equivalent to the consumption of 1.5 moles of molecular oxygen. According to this equivalence, results can be expressed as mg L^{-1} of COD or mg L^{-1} of O_2

$$O_2 + 4\ H^+ + 4\ e^- \rightarrow 2\ H_2O \qquad \text{(Reaction 46)}$$

COD measurements were performed as stated in ISO 15705. Depending on the expected COD, two different COD Cell Test Spectroquant® (from Merck) were used: for lower COD values, Cell Test range from 25 to 1500 mg L^{-1} (Ref. 1.14541.0001) was used and for the higher ones the range from 500 to 10000 mg L^{-1} (Ref. 1.14555.0001). According to manufacturer instructions, 1 or 3 mL of sample were added to the cell (according to the range), shaking gently to ensure the mixture and introducing it into a Thermoreaktor TR300 (from Merck) at 148ºC for 2 hours. After 30 minutes, once the sample was at room temperature the absorbance was measured at 605 nm in a spectrophotometer NOVA 60A (from Merck) (Fig. 22). Calibration curves are recorded in the equipment by the manufacturer, obtaining the COD concentration directly in the display.

In order to avoid interferences in the method due to high concentration of H_2O_2 or chloride ions, samples were quencher and/or diluted before their analysis.

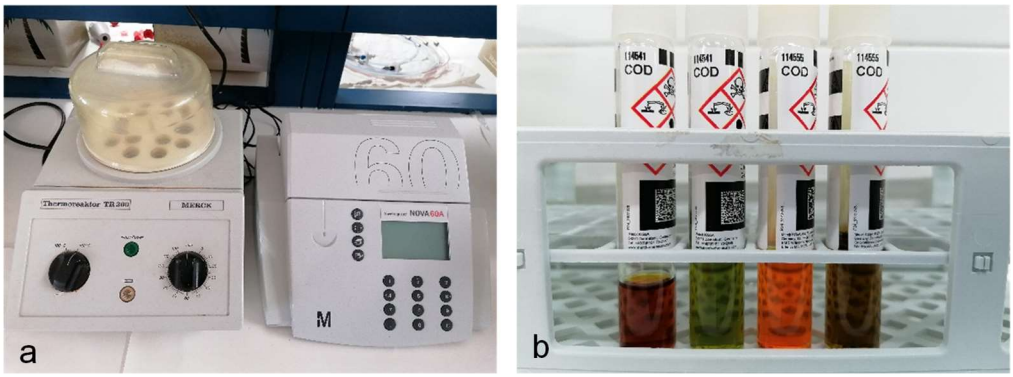

Figure 22. a) Thermoreaktor and spectrophotometer used for COD measurements and b) COD cells test: first vial new, second after measure in the lower range and third vial new, fourth after measure in the upper range.

3.3. Dissolved organic carbon and total nitrogen measurements

DOC is the quantity of organic carbon contained in a water sample after filtration through 0.45 µm filter. This parameter was measured in a Total Organic Carbon Analyser TOC-V CSN from Shimadzu equipped with an ASI-V sampler (Fig. 23). DOC is obtained from the difference between Total Dissolved Carbon (TDC) and Dissolved Inorganic Carbon (DIC) measured on the target water.

Figure 23. Shimatzu TOC-V CSN in Water Technologies Laboratory at PSA.

TDC is first analyse by direct oxidation to CO_2 in a combustion chamber of tubular form that is filled with platinum catalyser. This platinum catalyser is fixed on alumina spheres and once the sample has been introduced the chamber reaches a temperature of 680ºC. Generated gases of the aforementioned reaction are pulled via high purity air at 150 mL min^{-1} after which they are cooled down and dried so a Non-Dispersive Infra-Red (NDIR) detector is able to evaluate the amount of generated CO_2.

The second stage is the measurement of DIC which is based on the decomposition of carbonates and bicarbonates when the sample is introduced inside a reactor where air is pumped in presence of phosphoric acid (25% p/V). Again, NDIR is used after dragging generated CO_2 with high purity air.

Calibration with analytical standards is neccesary to have internal calibration curves available in the software so letting the equipment giving concentration values directly. A solution of potassium hydrogen phthalate in ultra-pure water was used to determine TDC and a solution of 50-50% Na_2CO_3 and $NaHCO_3$ to determine DIC. Calibration curve ranges are: 1-10, 10-50, 50-250, 250-1.000 y 1.000-4.000 mg L^{-1} for TDC and 0,5-2,5, 2,5-15, 15-75, 75-250 and 250-1.000 mg L^{-1} for DIC. R^2 is close to 1 for all the ranges with a standard deviation around 1.5%.

When TDC and DIC in a sample are very similar, since DOC is calculated as the difference between both, it is greatly influenced by the error of the equipment, obtaining even negative DOC values. To avoid this error, it is necessary to remove DIC of the sample by adding two or three drops of acid and letting stirring before its injection. Then TDC measured will correspond directly to DOC.

Total nitrogen (TN) is also measured in the same equipment with a TNM-1 module from Shimatzu. During the analysis nitrogen species are oxidised to NO and NO_2 that, in turns, reacts with ozone generating an excited state of NO_2. When this product reverts to a non-excited state it emits light that is measured by a chemo-luminescence detector, determining the amount ofnitrogen. As in TDC and TIC, the software gives directly the concentration of TN, being calibrated in two ranges: 1-10 and 10-100 mg L^{-1}.

Before analysis, all samples are filtrated through a nylon filter of 0.45 µm (ASIMIO).

3.4. Toxicity and biodegradability analysis

To guarantee water quality after pre-treatment of complex wastewaters and/or post-treatment (tertiary) of UWWTP effluents for reusing purposes, it is necessary to develop a toxicity (acute and chronic) and biodegradability evaluation. Respirometry analyses have been carried out in this work to check both by means of a SURCIS BM-Advanced Respirometer (Fig. 24), composed by a glass vessel with a dissolved oxygen (DO) and pH probes, aeration and recirculation stirring, temperature control and H_2SO_4 and NaOH dosing pumps to control pH when required. Respirometric tests are defined as a direct measure of the biological activity of activated sludge from a UWWTP. It is based on the consumption of DO by microorganisms from activated sludge when are fed with a specific wastewater.

Figure 24. SURCIS BM-Advanced Respirometer used to perform toxicity and biodegradability assays

Two respirometry assays were carried out:

- OUR (Oxygen Uptake Rate) mode is the traditional method, corresponding to an LSS (liquid phase principle, static gas, static liquid) respirometry. It consists in the monitorization of the DO evolution in the sludge once it is fed with an organic substrate but, during this kind of test, activated sludge is not recirculated and aeration is stopped so there is not an extra supply of oxygen, only that found in solution is the one that is available to metabolize the substrate. It is measured in mg O_2 L^{-1} h^{-1}.
- R mode corresponds to an LFS (liquid phase principle, flowing gas, static liquid) respirometry in which the system can be considered a batch reactor. In this kind of test when the system is fed with the sample agitation and aireation is maintained so a continuos supply of oxygen occurs. DO in the liquid phase is continuously measured. Main parameters that are defined in this test are Rs (Dynamic Respiration Rate) (mg O_2 $L^{-1}h^{-1}$); CODb (Biodegradable COD) (mg O_2 L^{-1}) and CODu (COD removal rate) (mg COD L^{-1} h^{-1}).

These tests are carried out with actual activated sludge, which is characterized before its use. The total content of solids and volatile solids are analysed. For total solids measurement, glass microfiber filters without binder (GF 52 090) from Albet LabScience (able to filtrate particles below 1µm from liquids) were used, previously washed with distilled water and dried in the oven at 106ºC for 1 hour. Then, the washed filter is weighed and a representative amount of sample was filtered and put into the stove at 106°C for 2 hours. After this, sample on the filter was weighed, obtaining the amount of total solids according to equation 3.

$$Total\ Solids = \frac{\mathrm{B-A}}{V} \qquad \text{(Equation 3)}$$

where *A* is the weigh of the filter after cleaning (g), *B* is the weigh of the filter once the sample was filtered and after 2 h in the stove at 106°C (g) and *V* is the volume of sample analyzed (L).

Sample is then introduced into the furnace, calcining at 550ºC for 30 minutes ensuring that all volatile content had been eliminated. Volatile solids are calculated according to equation 4.

$$Volatile\ Solids = \frac{\mathrm{C-B}}{V} \qquad \text{(Equation 4)}$$

where *B* is the weight of the filter after sample filtration and 2 hours in the stove (g), *C* is the weight of the filter after sample filtration and 30 min in the furnace at 550 °C (g) and *V* the volume of sample analyzed (L).

Respirometric analyses were carried out with activated sludge from El Ejido UWWTP (Almeria, Spain) containing between 7 and 8.5 g L^{-1} of volatile solids. Before performing the toxicity and biodegradability tests, it was necessary to keep them under continous aeration for 24 hours to achieve endogenous phase. Water samples must also be pre-conditioned by adjusting their pH between 6.5 and 7.5 and eliminating the possible oxidants residue they could contain.

Toxicity analyses were performed by means of an R test according to the following procedure: 1 L of activated sludge is introduced into the respirometer glass vessel under stirring and aeration. Once DO is stable, activated sludge is fed with 30 mL of a solution that contains 0.5 g of sodium acetate per gram of volatile solids in distilled water, which is a highly biodegradable organic reference substance. Then toxicity test starts and Rs (mg O_2 $L^{-1}h^{-1}$) starts to increase till reach a plateau. At that moment 30 mL of the sample is added to the activated sludge (Fig. 25). Change in Rs profile gives the percentage of inhibition (or stimulation if the sample not only is not toxic but contain highly biodegradable organic carbon) related to the OUR of the activated sludge.

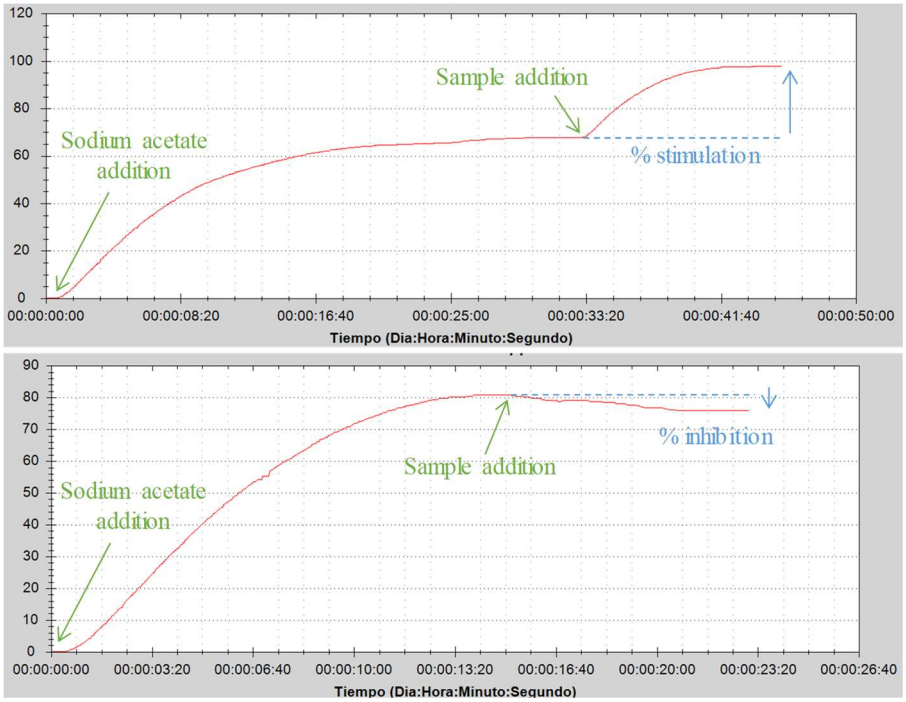

Figure 25. Examples of Rs evolution during R tests to determine the toxicity of different wastewater samples. a) Non-toxic sample with stimulation of the activated sludge b) Toxic sample that produces inhibition in the activated sludge.

Biodegradability analyses (Fig. 26) were also done in R test mode by adding 900 mL of activated sludge into the respirometer vessel together with 2.5 mL of a solution of N-Allylthiourea (1.02 g L^{-1}) per gram of volatile solids, in order to inhibit nitrification processes leaving 30 min to ensure its reaction. After, 100 mL of sample (previously filtered and aireated along 30 minutes) was added to the reactor starting the test. Rs increased till reach a maximum, and from that point started to decrease till a residual constant value, pointing out that the analysis ended. The software of the equipment calculates CODb by itself (according to internal conversion factors and total volatile solids introduced in the software by the operator) which must be compared with the total COD of the sample. According to the equipment protocol, when the ratio CODb/COD is higher than 0.2 the sample can be considered biodegradable.

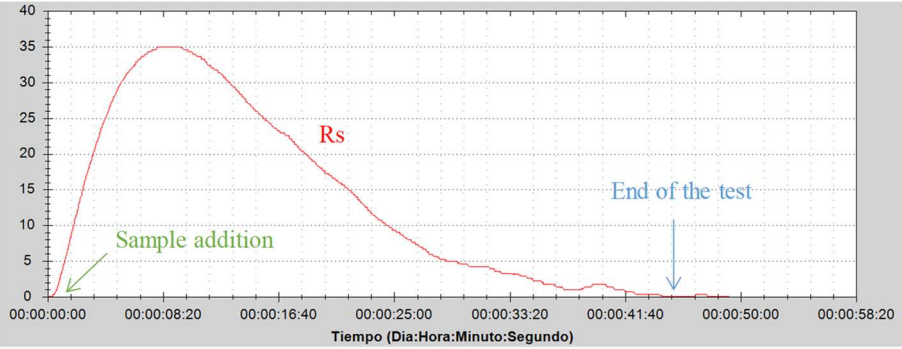

Figure 26. Briodegradability test of a water sample.

3.5. Ionic cromatography

Ions present in the solution have a double function in electrochemical processes. On the one hand they determine the conductivity and therefore the electrical consumption. On the other hand, ionic species will suffer oxidation by the action of the anode generating new species that, in turn, can have redox potential high enough to degrade organic matter. The clearest example is chloride, precursor of ACS and whose initial concentration will determine the amount of ACS that will be electrogenerated.

Ions concentration were determined by ion exchange chromatography, a method able to measure ions and polar molecules dissolved in an aqueous solution. The analysis is based in the separation of molecules according to their electrical charge properties. It consists of two phases: the stationary phase or ion exchanger, and the mobile phase. The stationary phase is an ion exchange resin that contains ionic functional groups fixed on the surface which interact reversibly with opposite charged ions of the analyte. The

mobile phase consists on an aqueous solution of ions (dissolved in ultrapure Milli-Q water) competing with the analytes of the stationary phase active points.

Depending on the target ion charge, two different techniques are defined:

- Cation exchange chromatography: stationary phase shows a negatively charged functional groups in order to retain positively charged cations, commonly sulfonic acid ($H^+SO_3^-$ strong acid) and carboxylic acids (H^+COO^-, weak acid).
- Anion exchange chromatography: stationary phase contains positively charged functional groups, such as a quaternary amine ($N(CH_3)_3^+OH^-$, strong base) or primary amines ($NH_3^+OH^-$, weak base) retaining negatively charged anions.

When a sample pass across these columns, ions are separated showing different retentions times according to their interactions with the stationary phase. After that, the sample passes through a conductivity detector.

In this PhD Thesis an ionic chromatograph (IC) Metrohm 850 Professional IC was employed (Fig. 27). For anions determination, it was used Metrosep A Supp 7 150/4.0 column thermoregulated at 45˚C with a solution of 3.6 mM of sodium carbonate as mobile phase in a flow of 0.7 mL min^{-1}. For cations analyses the column was Metrosep C6 150/4.0 with a solution of 1.7 mM nitric acid and 1.7 mM dipicolinic acid as eluent with a flow of 1.2 mL min^{-1}.

Figure 27. Metrohm 850 Professional IC used for the determination of ionic species contained in water samples.

Before each set of samples analysis, standards of 10 mg L^{-1} of each ion were injected ensuring the accuracy of the measurements. Samples werefiltered by a 0.45 µm nylon filter from ASIMIO before injection in the IC. Calibration curves and retention times for each ionic specie in the range of 0.1 to 20 mg L^{-1} is detailed in the table below (Table 11):

Table 11. Ionic species measured by IC and calibration.

Ionic specie	Calibration curve	Retention time (min)
F^-	$y = 0.109 + 0.027x$	4.3
Cl^-	$y = -0.049 + 0.019\,x$	6.7
NO_2^-	$y = -0.028 + 0.012\,x$	8.9
Br-	$y = -0.033 + 8.46 \cdot 10^{-3}x$	10.7
NO_3^-	$y = -0.038 + 0.01x$	12.2
PO_4^{3-}	$y = -0.066 + 5.66 \cdot 10^{-3}x$	15.9
SO_4^-	$y = -0.052 + 0.013x$	17.6
Na^+	$y = 0.01 + 5.17 \cdot 10^{-3}\,x$	5.4
NH_4^+	$y = 5.03 \cdot 10^{-3} + 5.92 \cdot 10^{-3}x$	6.2
K^+	$y = 2.74 \cdot 10^{-3} + 2.71 \cdot 10^{-3}x$	9.6
Ca_2^+	$y = 6.49 \cdot 10^{-5} + 3.99 \cdot 10^{-3}x$	12.5
Mg_2^+	$y = 0.013 + 9.41 \cdot 10^{-3}x$	17.3

3.6. High or ultra performance liquid chromatography

OMCs were determined using high performance liquid chromatography (HPLC) and ultra-performance liquid chromatography (UPLC) in reverse phase, that are essential analytical techniques able to identify and quantify the substances contained in an aqueaous mixture. They are based in the separation of the mixture components according to their polarities, by means of their hydrophobic interactions with the absorbent particles of a stationary phase (or column), provoking different elution rates when they flow out of the column. The column contains a non-polar granular material, mainly silica or polymers. The mobile phase or eluent is a polar solution, typically a mixture of water and an organic solvent such as acetonitrile or methanol, that pass through the column driven by a pump being able to achieve very high pressures, up to 400 bar in HPLC and 1000 bar in UPLC. An injector introduces the sample into the mobile phase that flows to the column and then to the detector. One of the most commoly used is diodo array detector (DAD), consisting on a two lamps, one of tungsten (source of visible light) and other of deuterium (UV fraction) that incides on a flow cell attenuating the intensity of light at certains wavelengths according to the absorption of the different

OMCs contained in the sample and their concentration. After the cell, the light beam is dispersed by the diffraction grating and, in the diodo array, the light intensity of each wavelength is converted in an electrical signal.

Reference compound (pyrimethanil and methomyl) were monitored with an UPLC/UV Agilent Technologies Series 1200, equipped with a reverse phase column ZORBAX XDB C-18. (4.6 x 50 mm, 1.8 µm particle size, Agilent Technologies). The analytical method used ultrapure water as eluent A and acetonitrile as eluent B. The method started with an isocratic phase of 15% of B till 4 min. After that, a gradient was applied achieving at 8 min 80% of B which was maintained until 15 min. Re-equilibration time was 3 min. Flow rate was 1 mL min^{-1}, the injection volume 50 µL and the temperature of the column 30 ºC. Analytical characteristics of PYR and MET are shown in table 12.

Samples preparation for their injection in the UPLC system consist in the filtration of 9 mL of sample through a 0.22 µm hydrofobic PTFE membrane filter from Millipore Millex. Then, the filter was washed with 1 mL of acetonitrile in order to extract any absorbed compound, and the acetonitrile is mixed with the water sample.

Table 12. External calibration curves were prepared for pyrimethanil and methomyl.

OMCs	Retention time (min)	LOQ* (µg L^{-1})	Curve	Maximum absorption (λ)
Pyrimethanil	8.4	100	y = 0.425x	270 nm
Methomyl	1.9	200	y = 0.1689x	230 nm

LOQ: Limit of quantification

OMCs (pentachlorophenol, terbutryn, chlorphenvinfos and diclofenac) concentration were determined with two equipments: an UPLC/UV Agilent Series 1200 with ZORBAX Eclipse XDB-C18 analytical column installed in the Water Technologies laboratory of the PSA and the second an HPLC/UV Agilent Technologies Series 1100 with an analytical column Luna C18 (4.6 x 150 mm, 3 µm particle size, Phenomenex) located at NIBEC in Ulster University.

Same method was employed consiting on formic acid 25 mM in ultrapure water as eluent A and acetonitrile as eluent B. The gradient starting with 10% of eluent B, reaching 100% of B in 14 min at a flow rate of 1 mL min^{-1}. Sample inyection volume was 100µL. In table 13 the analytical characteristics of each OMCs detection is shown.

Table 13. Retention time, LOQ, and maximum absorption of studied OMCs

OMCs	Retention time (min)	LOQ (μg L^{-1})	Curve	Maximum absorption (λ)
UPLC series 1200				
Pentaclorophenol	10.8	10	y = 0.6056x	220 nm
Terbutryn	7.7	10	y = 7195x	230 nm
Chlorfenvinphos	10.4	10	y = 1384x	240 nm
Diclofenac	9.6	10	y = 2114x	285 nm
*HPLC series 1100**				
Terbutryn	10.6	130	y = 1.5994x	230 nm
Chlorfenvinphos	13.5	170	y = 8.7711x	240 nm
Diclofenac	12.7	40	y = 5.0619	285 nm

**As LOQ of pentaclorophenol in HPLC Series 1100 was very high its analysis was discarded*

Fe^{3+}:EDDS concentration was determined by a HPLC Agilent Technologies Series 1100 with a reversed-phase column Luna C18 (150 x 3.00 mm, 5μm particle size) available in the Water Technologies laboratory at PSA. It was followed an isocratic method consisting of 95% of a buffer solution, containing 2mM tetrabutylammonium bisulphate and 15 mM of sodium formate, and 5% of methanol. The duration of the method was 7 minutes with a flow rate of 0.5 mL min^{-1} and an injection volume of 20 μL. Fe^{3+}:EDDS have maximum absorption peak at 240 nm. The external calibration curve was: y = 20930 x (R^2=0.999) with a LOQ of 0.005 mM.

3.7. Liquid chromatography coupled to mass spectrometry

OMCs found in actual wastewaters appear at very low concentrations, in the range of μg L^{-1} to ng $L^{-1,}$ thus their analysis requires highly accurate and selective detection techniques as mass spectrometry, commonly used for trace compounds since it is able to provide information on actual concentration of a great number of compounds simultaneously from a water sample.

Monitoring of OMCs contained in target UWWTP effluent retentate after NF pre-treatment as well as to follow their degradation during electro-oxidative process in this PhD Thesis, a HPLC coupled to a mass spectrometry system equipped with a hybrid quadrupole/linear ion trap tandem mass analyzer (QqLIT-MS/MS) was used.

Firstly, HPLC system separates OMC mixture as described in the previous section, and then the liquid sample withstands an electrospray ionization (ESI), the interface between liquid chromatography and mass spectrometry. In this technique, sample passes through

a capillary that is under the effect of a high electrical potential causing at the capillary outlet the dispersion of the solution as a spray formed by small charged drops which evaporate at a fast pace, releasing molecules protonated into the gas phase. The forementioned generated ions can then be protonated in multiple ways, giving rise to different species for the same molecule. Generated ions go to the triple quadrupole analyser. A quadrupole consists of four parallel cylindrical bars acting as electrodes. Opposite bars are electrically connected, one pair to the positive pole of a variable direct current supply and the other pair to the negative pole. Different Alternating Current Potential are applied to each pair of bars, 180º out of phase, so the ions are accelerated through the quadrupole. Direct and alternating current voltages increase simultaneously keeping their ratio constant, only those ions that have an adequate mass-to-charge ratio (m/z) maintain a stable path and pass to the detector, the rest end up colliding with the bars.

In a triple quadrupole analyzer three quadrupoles are installed sequentially, acting the first and last one, Q_1 and Q_3, as a normal quadrupole while the second (Q_2) works as a collision cell. Into the cell a small amount of gas, usually He or Ar, is introduced so the entering ions collide with them, being fragmented. Finally, ions formed go to Q_3 for their analysis.

The equipment used in this PhD Thesis is located in the facilities of Solar Energy Research Center (CIESOL, joint center between CIEMAT and the University of Almería) consisting on an HPLC (Agilent Technologies Series 1200) coupled to a QqLIT-MS/MS 5500 QTRAP® (Sciex Instruments). HPLC contained a Kinetex C18 (150 x 4.6 mm, 2.6-µm particle size from Phenomenex) and analyses were developed following gradient in which eluent A was 0.1% formic acid in ultrapure water and eluent B was methanol. The gradient started with 20% of B during 0.5 min, increasing till 50% of B within 3 min, reaching 100% in 9.5 min, keeping constant for 3.5 min and reducing to 20% of B in 0.1 min. Flow rate was 0.5 mL min^{-1} and the volume of injection 10 µL. Total analysis time was 13.1 min and 6 min for re-equilibration time. Electrospray source (from TurboIon Spray) was operated in positive polarity with the following settings: ionspray voltage 5000 V; curtain gas 25 (arbitrary units); GS1 50 psi; GS2 40 psi; and 500 ºC. N_2 was used as nebulizer, curtain and collision gas.

OMCs were analysed by Multiple Reaction Monitoring applying the Schedule MRM™ algorithm, with a retention time window of 40 s per transition to increase the sensitivity of the analytical method. The optimal MS/MS parameters for each compound are

summarized in table 14. Data acquisition and processing was done by a Sciex Analyst version 1.6.2 software and MultiQuant 3.0.1 software was used for quantification.

Table 14. Optimal LC-QqLIT-MS/MS conditions for OMCs multi-residue analysis.

Compound	Rt (min)	Precursor ion	Quantifier/ qualifyer	DP[a] (V)	EP[b] (V)	CE[c] (eV)	CXP[d] (V)
10,11 - Dihydrocarbamazepine	9.31	239.3	194.1	66	12	32	10
			180.2	150	10	47	11
4 -AA	5.3	204.2	56.2	45	5	30	2
			159.2	45	5	16	2
4 -AAA	6.62	246.2	228.1	46	5	18	2
			83.1	46	5	40	2
4 -DAA	5.1	232.2	113.2	48	5	17	2
			111.2	48	5	21	2
4 -FAA	6.54	232.2	214.2	60	5	18	2
			77	60	5	50	2
4 -MAA	4.75	218.2	56.1	35	5	30	2
			97.2	35	5	16	2
9-Acridinecarboxilic acid	11.63	224.2	196	63	12	36	11
			167.2	63	12	54	11
			180	63	12	42	10
Acetaminophen	5.8	152.1	110.1	40	5	20	2
			64.8	40	5	45	2
Acetamiprid	7.84	223	126	100	10	30	4
			128	50	13	25	7
Acetanilide	8	136	94	70	10	24	15
			77	70	11	40	10
Alfuzosin	7.17	390.3	235.1	50	12	40	12
			156.1	50	12	37	10
Amitriptyline	8.8	278.4	91.2	30	5	35	2
			233.1	30	5	22	2
Amoxicilin	4.91	366.1	114	70	12	30	19
			208	70	12	13	8
			349.1	70	6	18	11
Antipyrine	7.41	189.2	77.1	48	5	51	2
			104.1	48	5	32	2
Atenolol	3.41	267.3	145.2	70	5	35	2
			190.2	70	5	27	2
Atrazine	9.93	216	174	100	13	25	10
			176	40	8	25	10
Azithromycin	7.07	749.5	83.1	50	11	110	20
			591.4	50	12	40	13
			573.3	50	8	47	14

Compound	Rt (min)	Precursor ion	Quantifier/ qualifyer	DP[a] (V)	EP[b] (V)	CE[c] (eV)	CXP[d] (V)
Azoxystrobin	9.93	404.1	372.2	100	10	20	10
			329	56	10	42	6
Betamethasone	9.76	393.3	373.1	70	10	13	20
			355	70	11	18	20
			147	70	10	39	15
Buprofezin	11.69	306	201	20	11	17	5
			116	20	13	22	6
			106	20	13	40	6
C13 Caffeine	6.95	198.1	140.1	40	5	30	2
			112.2	40	5	35	2
C13 -Phenacetin	8.68	181.3	110.3	150	10	47	11
			139.3	150	10	47	11
Caffeine	6.95	195	138	20	4	27	4
			110	20	5	31	13
			123	20	5	45	5
Carbamazepine	9.38	237.2	194.3	80	5	25	2
			192.1	80	5	35	2
Carbendazim	6.15	192.3	160.1	100	10	27	4
			132.2	100	10	41	4
Cefalexin	6.43	348	158.1	60	12	13	8
			174.1	60	11	20	11
			106.1	150	10	47	11
Cefotaxime	6.76	456.1	324.1	40	5	15	3
			396.1	40	5	10	2
			241.3	40	5	20	2
Cetirizine	9.31	389.4	201	48	12	30	12
			166.2	48	12	55	8
Chlorfenvinphos	10.95	359.1	99	60	10	50	6
			155	100	8	18	10
Chlorpyriphos	12.19	352	97	55	10	55	7
			197.9	96	10	26	6
Chlortetracycline	7.37	479.2	444	100	9	31	10
			462	100	9	24	11
Ciprofloxacin	6.47	332.2	314.3	50	5	25	2
			231.2	50	5	48	2
Citalopram	7.88	325.3	109.1	100	5	30	2
			262.1	100	5	25	2
Clarithromycin	8.87	748.4	158.4	45	5	35	2
			590.4	45	5	26	2
Clindamycin	7.88	425.2	126.1	80	11	35	7
			377.1	80	12	28	9
Clomipramine	9.05	315.2	86.1	40	5	27	2
			58.1	40	5	60	2
Clotrimazole	9.06	344.9	277.3	30	5	15	2

Compound	Rt (min)	Precursor ion	Quantifier/ qualifyer	DP[a] (V)	EP[b] (V)	CE[c] (eV)	CXP[d] (V)
			165	30	5	43	2
Cotinine	3	177	80	45	5	36	2
			98	45	5	26	2
Cyclophosphamide	8.67	261.2	140	40	12	23	12
			233.2	40	8	30	8
			106	40	8	25	6
Cyprodinil	10.83	226	77	120	12	63	9
			93	120	12	80	9
D10-Carbamazepine	9.37	247.2	204.3	150	10	47	11
			202.1	150	10	47	11
Danofloxacin	6.48	358.2	340.2	100	8	31	12
			314.3	100	8	26	11
Dextromethorphan	8.1	272.4	215.1	150	10	47	11
			171.1	150	10	47	11
			173	150	10	47	11
Diatrizoic acid	5.03	632	361	80	9	35	8
			233.1	80	8	55	12
Diazepam	10.37	285.2	193.2	100	12	42	10
			154.2	100	12	36	10
Difloxacin	6.67	400.3	299	70	8	42	17
			356	70	8	30	20
Dimethoate	7.96	230	199.1	100	10	13	4
			125.1	100	10	28	4
			171	50	7	19	9
Dimethomorph	10.32	388	301	100	10	30	8
			165	100	10	45	8
			303	130	10	29	7
Diphenhydramine	8.01	256.4	167.2	40	12	21	9
			152	40	12	50	7
Diuron	10.04	233	72	60	7	50	12
			72	110	6	36	10
Domperidone	7.56	426.2	175	37	12	35	10
			147.1	37	11	55	7
Donepezil	7.51	380.4	91	65	12	63	9
			151.1	65	14	40	8
Doxycycline	7.98	445.3	428.2	90	10	28	9
			410.2	90	10	34	10
			154.1	90	10	39	10
EDDP	7.96	278.6	234	30	11	42	14
			249.2	30	12	31	12
Enrofloxacin	6.48	360.3	245.2	80	10	37	10
			316.2	80	10	27	12
Eprosartan	8.01	425.2	135.1	79	11	47	9
			207.1	79	12	35	10

Compound	Rt (min)	Precursor ion	Quantifier/ qualifyer	DP[a] (V)	EP[b] (V)	CE[c] (eV)	CXP[d] (V)
			163.2	79	10	44	5
Erithromicyn	8.45	734.6	158.3	58	5	40	2
			576.5	58	5	28	2
Famotidine	3.42	338	189.3	25	5	24	2
			259.4	25	5	15	2
Fenhexamid	10.51	302	97	80	14	30	12
			55	80	8	60	7
Fenofibrate	11.87	361.2	233.1	60	5	25	2
			139.1	60	5	35	2
Fenofibric acid	10.98	319.1	233.1	65	5	22	2
			139.1	65	5	42	2
Flecainide	7.84	415.2	301	48	12	49	7
			398.1	48	12	35	9
			98	48	12	36	15
Flumequine	9.38	262.3	244.08	50	5	21	14
			202.3	50	5	41	12
Fluoxetine	8.73	310.3	44.2	30	5	25	2
			148.2	30	5	10	2
Gabapentin	5.96	172.4	154.1	50	9	18	9
			137.2	50	9	22	7
Ifosfamide	8.49	261.1	91.9	60	5	33	2
			154.3	60	5	29	2
Imazalil	8.54	297	159	80	12	31	8
			255	80	12	25	7
Imazalil d6	8.54	302.1	159	60	10	32	4
			203	60	10	26	4
			255.1	60	10	26	4
Imidacloprid	7.45	256.1	175.1	100	10	27	4
			209.2	100	10	25	4
Iminostilbene	9.31	194	179	150	10	47	11
			167	150	10	47	11
			152	150	10	47	11
Indomethacin	10.91	358.2	139.1	50	5	25	2
			174.3	50	5	15	2
Irbesartan	9.82	429.3	207	55	12	34	5
			195	55	12	32	14
Isoproturon	9.88	207	72	60	8	25	12
			165	60	8	20	10
Josamycin	8.77	828.6	174.2	54	12	46	13
			229.1	54	11	43	11
			600.2	54	11	37	14
Ketolorac	9.76	256.2	105.1	70	5	25	2
			178.1	70	5	34	2
Ketoprofen	10.03	255.2	105.1	47	5	33	2

Compound	Rt (min)	Precursor ion	Quantifier/ qualifyer	DP[a] (V)	EP[b] (V)	CE[c] (eV)	CXP[d] (V)
			209.2	47	5	16	2
Labetalol	7.45	329.1	162.1	32	12	33	9
			90.9	32	12	67	8
			294.2	32	12	27	15
			311.2	32	12	21	7
Lansoprazole	9.29	370	252.2	45	5	15	2
			119.2	45	5	27	2
Levofloxacin	6.25	362.1	261.2	80	8	40	10
			318.2	80	8	26	15
Lidocaine	6.52	235	86	70	7	20	5
			58	70	8	50	4
Lincomycin	5.86	407.1	126.3	50	5	45	2
			359.3	50	5	23	2
Loratadine	10.7	383.1	337.3	50	5	29	2
			267.2	50	5	40	2
Mefanamic acid	11.68	242.2	224.2	36	5	34	2
			180.2	36	5	53	2
Memantine	8.1	180.3	163.1	28	12	22	10
			107.1	28	12	36	9
Mepivacaine	6.67	247.4	98.1	28	5	23	2
			70.1	28	5	53	2
Metalaxyl	9.76	280	220	85	12	20	12
			220	100	12	19	9
			192	70	12	25	9
Methadone	8.55	310.2	265.1	70	13	22	7
			105	70	11	40	20
			223	70	13	30	11
Methiocarb	10.33	226	169	44	14	13	9
			121	44	9	25	6
			107	44	9	51	5
Methotrexate	6.1	455.2	308	80	12	28	15
			175	90	12	55	15
			134	90	12	48	15
Metoclopramide	6.57	300	184	80	6	42	11
			141	80	11	66	10
Metoprolol	6.9	268.2	116.2	30	5	25	2
			159.2	30	5	28	2
Metronidazol	5.63	172.1	128.1	35	5	20	2
			82.1	35	5	30	2
Mevastatin	11.4	391.3	185.2	55	5	25	2
			159.3	55	5	30	2
Myclobutanil	10.38	289.2	70.2	100	10	36	4
			125.1	100	10	44	4
Nadolol	6.15	310.2	254.4	45	5	30	2

Compound	Rt (min)	Precursor ion	Quantifier/ qualifyer	DP[a] (V)	EP[b] (V)	CE[c] (eV)	CXP[d] (V)
			201.2	45	5	30	2
Nalidixic acid	9.25	233.2	187	45	10	35	12
			104	45	10	55	11
Naproxen	10.23	231.2	185.1	86	5	17	10
			170.1	86	5	35	10
N-desmethylcitalopram	7.85	311.3	109.1	66	12	31	7
			262.1	66	11	23	13
Nicotinamide	3.16	123.1	53.1	35	8	42	10
			80	35	12	28	8
			78	35	12	33	12
Nicotine	2.77	163.3	130	60	4	26	7
			132	60	10	20	7
			106	60	15	23	6
Nicotinic acid	3.34	124	80.1	76	6	29	13
			78.1	76	8	30	12
Nitrendipine	10.46	361	315	80	10	18	17
			329.1	80	10	15	15
			254.2	80	10	45	15
Norfloxacin	6.41	320	302.2	220	12	33	17
			233.1	220	12	33	5
O-desmethyltramadol	5.91	250.3	58.1	70	12	45	7
			232.2	70	13	17	11
O-desmethylvenlafaxine	6.76	264.1	57.9	190	9	50	6
			107	190	13	25	6
Oxcarbamazepine	8.68	253	180	73	10	44	11
			208.1	73	10	28	13
			235.9	150	10	47	11
Oxytetracycline	6.62	461.3	426.1	90	10	27	11
			443.1	90	10	19	11
Paraxanthine	6.19	181.2	124.2	50	5	25	2
			69.2	50	5	43	2
Paroxetin	8.46	330.3	192.2	70	5	25	2
			151.2	70	5	30	2
Pentoxifylline	8.02	279	181	60	10	23	10
			138	60	10	35	10
Phenacetin	8.68	180.3	110.1	70	10	29	6
			138	70	10	22	9
			152	70	10	21	7
Pirimicarb	8.02	239	72.1	100	10	38	4
			182.1	100	10	23	4
Primidone	8.02	219.2	91.1	35	5	35	2
			162.3	35	5	16	2
Prochloraz	10.94	376.1	308	80	10	18	4

Compound	Rt (min)	Precursor ion	Quantifier/ qualifyer	DP[a] (V)	EP[b] (V)	CE[c] (eV)	CXP[d] (V)
			266	80	10	23	4
Propafenone	8.47	342.4	116	69	8	32	7
			98.1	69	12	29	6
Propamocarb	4.97	189.1	101.9	29	10	25	4
			144.1	29	10	16	4
Propanolol	7.93	260	116.2	35	5	23	2
			183.2	35	5	23	2
Propyphenazone	9.43	231.3	189.2	55	5	22	2
			201.2	55	5	30	2
Pyrimethanil	10.13	200.1	107	246	12	33	6
			82.1	246	8	35	7
Quinmerac	8.37	222	204	47	10	25	12
			141	47	13	45	10
			206	46	10	24	6
Quinoxyfen	12.25	308	197	300	12	49	5
			162	300	12	61	8
Ranitidine	3.94	315.3	176.2	38	5	21	2
			130.1	38	5	30	2
Roxithromycin	8.91	837.5	158	140	8	43	15
			679.4	140	8	31	10
Salbutamol	3.42	240.3	148.2	44	5	26	2
			222.2	44	5	14	2
Sertraline	7.87	360.3	158.9	21	12	40	8
			275.1	21	12	18	6
Simazine	9.37	202.1	132	45	5	26	2
			124.2	45	5	23	2
Simvastatin	11.96	419.1	285.3	45	5	15	2
			199.1	45	5	15	2
Sotalol	3.4	273.3	255.2	45	6	14	2
			133.2	45	6	37	2
Sulfadiazine	5.68	251.2	92.1	40	5	35	2
			108.1	40	5	30	2
Sulfamethazine	6.8	279	186.2	42	5	20	2
			156.1	42	5	26	2
Sulfamethizole	6.76	271.1	156.1	80	6	20	8
			92	80	6	37	10
			108.1	80	6	34	10
Sulfamethoxazole	7.21	254.2	156.1	47	5	21	2
			108.1	47	5	30	2
Sulfapyridine	6.06	250.1	156.1	47	5	21	2
			108.3	47	5	34	2
Sulfathiazole	5.87	256.2	156	45	5	18	2
			92.2	45	5	34	2
Sulpiride	3.66	342.3	112	47	11	34	15

Compound	Rt (min)	Precursor ion	Quantifier/ qualifyer	DP[a] (V)	EP[b] (V)	CE[c] (eV)	CXP[d] (V)
			214.1	47	12	48	11
Tamoxifen	9.69	372	72	50	10	32	8
			70	50	8	75	10
			129	50	6	38	7
Tebuconazole	10.95	308	70	80	7	50	11
			125	80	10	50	6
			70	80	10	63	10
Telmisartan	9.14	515.5	497.3	40	12	47	11
			305.2	40	12	58	15
			276.2	40	12	60	7
Terbutaline	3.42	226.3	152.2	47	5	20	2
			107.1	47	5	40	2
Terbutryn	10.05	242	186	100	13	27	10
			68	100	12	60	4
Tetracycline	6.47	445.2	154.2	75	10	40	11
			410.2	75	10	27	9
Theophylline	6.45	181.1	124.2	50	8	24	19
			69.1	50	8	35	12
Thiabendazole	6.72	202	131.1	150	10	47	11
			175.1	150	10	47	11
Tramadol	6.85	264	246.1	15	8	15	3
			58	15	8	7	3
Tramadol N-oxide	7.04	280.4	135.1	70	13	32	11
			201.1	70	13	27	10
			58	70	14	47	15
			159	70	13	37	10
Trazodone	7.4	372.4	148.1	73	12	48	8
			176	73	12	35	10
Triamterene	6.66	254.6	238.1	29	12	39	12
			168.1	29	12	47	10
Trigonelline	2.65	138.2	78.2	45	8	33	12
			92.2	150	10	47	11
Trimethopim	5.95	291.3	230.2	45	5	28	2
			123.2	45	5	30	2
Vancomycin	4.75	725.3	100.3	150	10	47	11
			144.3	150	10	47	11
Venlafaxine	7.71	278.4	58.1	50	5	45	2
			260.4	50	5	15	2
Verapamil	8.07	455.5	303.3	52	10	36	8
			260	52	12	41	14

[a]DP: Declustering Potential; [b]EP: Entrance Potential; [c]CE; Collision Energy; [d]CXP: Collision Cell Exit Potential

3.8. Scanning electron microscopy

In electrochemical processes basic oxidation-reduction reactions occur directly on the electrodes surface, so it is necessary to check their status for ensuring their proper operation.

SEM is an electron microscopy technique able to produce high-resolution images of a sample surface by using electron-matter interactions.

In this technique instead of light beam, an electron beam is used to form the images, allowing to achieve greater amplifications than with the optical microscopes, since the wavelength of electrons is much smaller than that of photons from the visible range.

Specifically, in SEM technology the electron beam is generated by means of a tungsten cathode. Generated electrons pass through a column where they are accelerated by and electromagnetic field produced by the application of a potential, aiming to exploit the wave-behavior of the electrons. At higher potentials, higher resolution will be obtained since the wavelength reached will be smaller, but for operation this parameter is conditioned by its nature and its resistance, and also if it is insulated. Accelerated electrons are focused by the condenser and objective lenses, reducing the diameter of the electron beam as much as possible in order to achieve a better resolution. After that, the baffle coil sweeps the electron beam across the entire surface of the sample.

Electron beam interacts with the sample surface atoms, resulting in a loss of energy that can be expressed in different ways as X-ray, heat or secondary electrons. These secondary electrons are collected in a detector creating an image that reflects the surface of the sample, providing information o shapes and textures. Additionally, we can also acquire the X-ray signal in order to perform a subsequent spectrographic analysis of the sample composition.

In this PhD Thesis two equipments were used: a Hitachi SU5000, installed at NIBEC in Ulster University, for the characterization of developed TiO_2-NT photoanode used in photoelectrocatalysis study working at 10 kV and an energy dispersive X-ray (EDX) analysis in an Oxford Instruments EDX. Secondly, a Hitachi S-3500N (Fig. 28) operated at 15 kV with an EDX analyser Oxford INCAx-sight were employed for the autopsy carried out to the cathodes conforming the electrochemical pilot plant available at PSA facilities.

Figure 28. Hitachi S-3500N SEM and Oxford INCAx-sight EDX at University of Almería.

3.9. Solar radiation measurement

Depending on the wavelength, solar energy is classified mainly in ultraviolet (from 100 to 400 nm), visible light (400 to 700nm) and infrared (greater than 700nm). Only UV radiation promotes photocatalytic processes which represents a small part of the solar spectrum, between 3.5 and 8% [13].

Photochemical reaction rates will be determined by the number of photons that interact with the catalyst hence it is necessary to quantify the incident radiation as it is a limiting factor in such processes. For this purpose, global UV radiation at PSA facilities is measured by a pyranometer titled 37º regarding the horizontal since CPC photoreactors used in this study are also titled 37º according to PSA coordinates (37ºN, 2.4ºW) The equipment used is a CUV 5 pyranometer from Kipp & Zonen (Fig. 29) covering the wavelength region from 280 nm to 400 nm and possessing a sensitivity of 301 μV W^{-1} m^{-2}. The irradiance value (E_{Solar}, in W m^{-2}) was calculated dividing the output signal of the pyranometer (U_{emf}, in μV) by its sensitivity (S, μV W^{-1} m^{-2}) as shown in equation 5. This irradiance values were registered at 1 min intervals.

$$\mathrm{E_{solar}} = \frac{\mathrm{U_{emf}}}{\mathrm{S}} \qquad \text{(Equation 5)}$$

To integrate properly solar UV radiation in contaminant degradation kinetics it is required the calculation of a standardized parameter which considers all the quantifiable factors that influence the system (incident UV radiation, treatment time, photoreactor surface and volume), permitting the comparison of experiments carried out on different days,

seasons or weather conditions. This parameter is known as Quv and it is calculated according to equation 6.

$$Q_{UV,n} = Q_{UVn-1} + \Delta t_n \cdot \overline{UV}_{G,n} \cdot A_i / V_t ; \quad \Delta t_n = t_n - t_{n-1} \qquad \text{(Equation 6)}$$

Where $Q_{UV,n}$ (kJ L^{-1}) is the accumulated UV energy per unit of volume, $\overline{UV}_{G,n}$ (W m^{-2}) is the average solar ultraviolet radiation (280 - 400 nm) measured in an specific period of time Δt_n (between t_n and t_{n-1}, being n the number of sample), A_i is the irradiated surface of the reactor and V_t is the total volume treated.

Figure 29. Pyranometer CUV 5 from Kipp & Zonen used for UV radiation measurements.

4. Experimental Set-up and methodology

4.1. Filtration system

Although UWWTP effluents undergo secondary decantation after having passed through secondary biological treatment, large particles in suspension are still present on this effluent that must be removed to protect tertiary treatments correct performance against blockages, fouling and abrasion.

Filtration unit used in this study (Fig. 30) comprised a polypropylene feeding tank with a capacity up to 1 m^3. Connected to this tank there two centrifugal pumps Techno 15 5 M from ESPA supplying wastewater to a sand filter of 75 µm SETA 16x44 (PEVASA). Following this first filtration, the liquid is sent through two string wound filter cartridges

(from AMETEK) installed sequentially, of 25 µm and 5 µm pore size. Filtered solution is then stored into a second polypropylene tank.

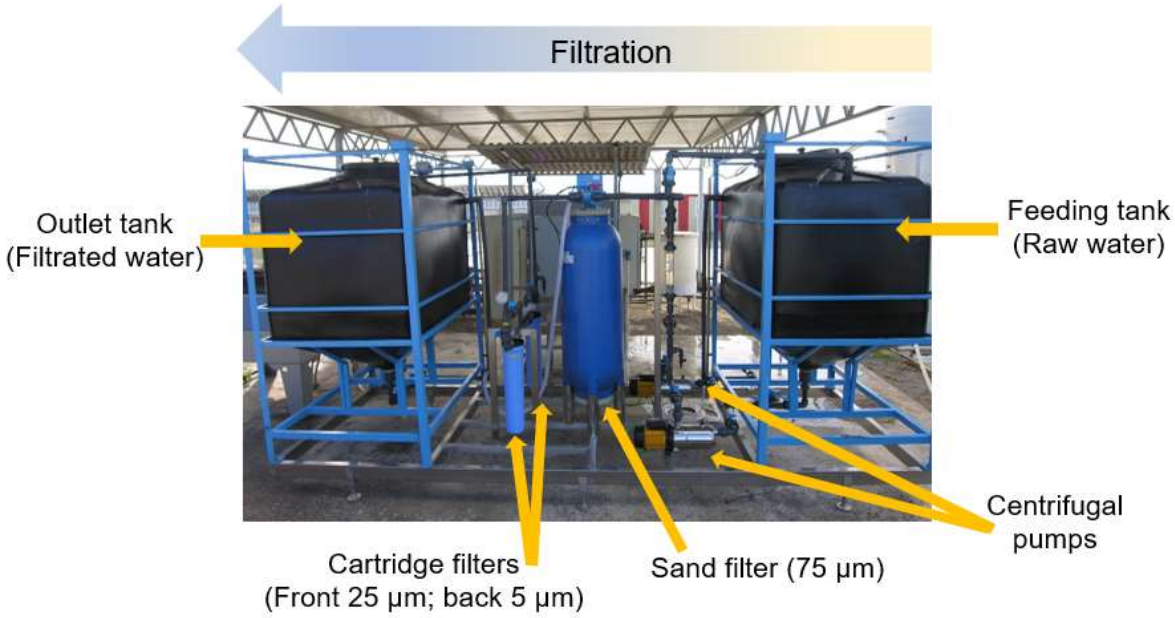

Figure 30. Detail of the filtration system for actual UWWTP effluent pretreatment at PSA facilities.

Sand filter presents an automatic operation and washing system, a flowmeter and two WIKA 232.50 manometers with a range from 0 to 6 bar to monitor the pressure both at inlet and outlet. When the difference of pressure between both manometers is higher than 0.7 bar it implied that the filter is clogging and so cleaning is necessary to regenerate it.

In addition, the circuit has two other WIKA 232.50 manometers installed at the outlet of both 25 µm and 5 µm filters. The same working principle is applied for these two manometers, when differential pressure between both exceeds 0.7 bar filters needed to be replaced.

Operation details

Effluent was collected from the UWWTP in batches of $1m^3$. As soon as the effluent arrived at PSA facilities, raw water was introduced into the feeding tank of the filtration system and pumped to the filters at 1 m^3 h^{-1}.

4.2. Nanofiltration pilot plant

Physical water treatments include membrane systems which are based on the separation of a raw influent with a high content of pollutants and/or bacteria in a clean and safe permeate and a rejection stream with all contaminating substances and salts.

Among membrane systems, UF and NF are highly applied on water separation. NF membranes require the application of around 5 bar of pressure to pass water through it, operating with a cross-flow while retaining the compounds according to their molecular weight. Specifically in this kind of membranes the pore size varies from 1 to 10 nm being mainly applied for organic substances removal (Fig. 31).

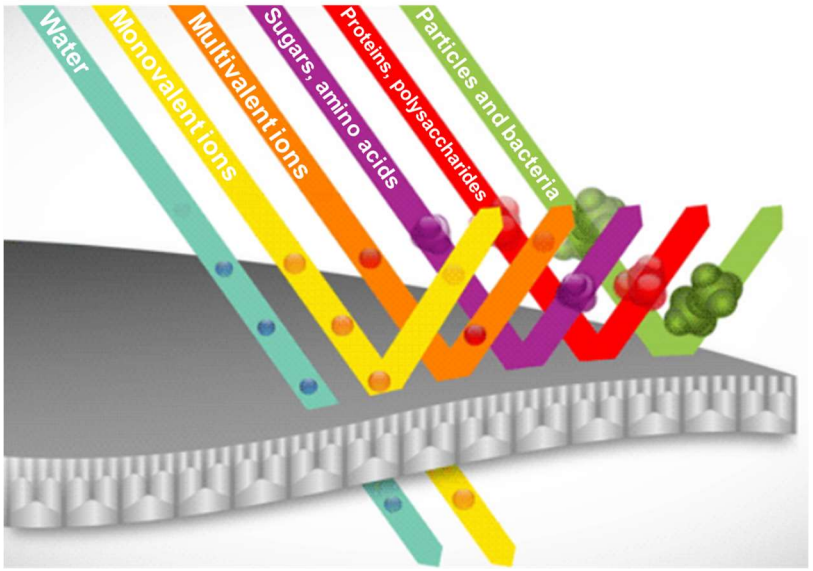

Figure 31. Description of a NF membrane rejection. Modified from Synder Filtration, Inc. [14]

The NF pilot plant used in this PhD Thesis and available at PSA facilities (Fig. 32a) is composed by three FilmTec NF90 2540 spiral membranes from DUPONT installed in parallel (Fig. 32b) thought the flow system allow to use them in series. However, in this study only one of them was used, number 1 from figure 32b.

Membrane's model material is Polyamide Thin-Film of 2.6 m^2 surface wound as a spiral. Size pore is 1 nm that was able to reach 97% of salt rejection. Specifically this membrane is recommended for the application in small industrial water treatment plants as it is able to obtain a high quality permeate. Main characteristics of the membrane are shown in table 15.

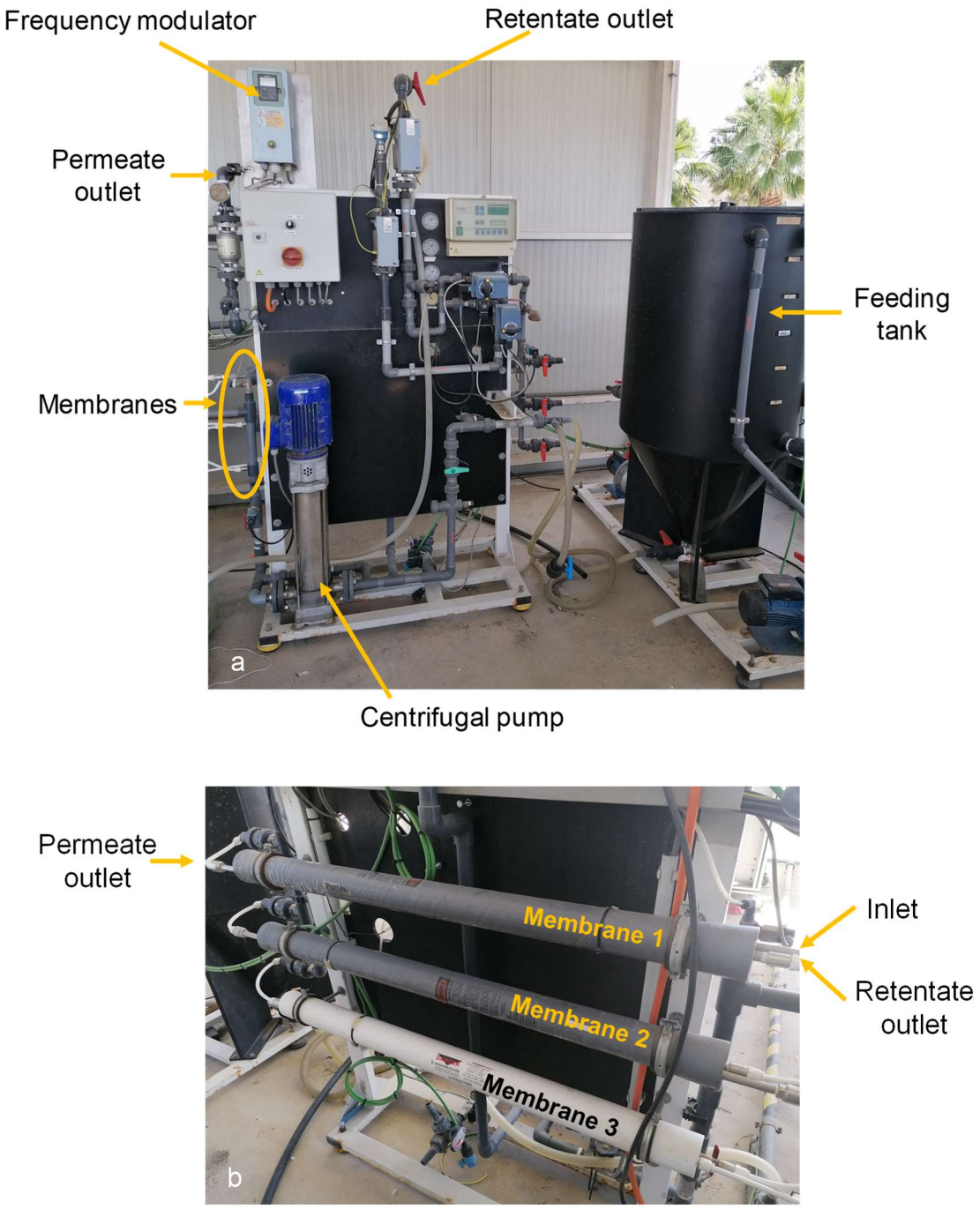

Figure 32. NF pilot plant at PSA facilities a) Main components of the system b) detail of the three membrane frames.

Table 15. Operation limits according to product data sheet of FilmTec membranes (DUPONT).

Maximum temperature (ºC)	45
Maximum pressure (bar)	41
Maximum feed flow rate ($m^3 h^{-1}$)	1.4
Maximum pressure drop (bar)	0.9

pH range in operation	2 - 11
Maximum feed silt density index	5
FAC tolerance (mg L^{-1})	< 0.1

NF membrane was fed from a 400 L polypropylene tank connected to a centrifugal pump built by DP Pumps driven from a VACON frequency modulator. In order to increase the inlet pressure on the membrane, to maintain the trans-membrane pressure, an internal retentate recirculation was installed with a variable flow rate up to 2 m^3 h^{-1}. Pressure regulation was monitored with a pair of MEGA manometers with a range from 0 to 10 bar installed in the inlet and outlet of the membranes. Monitoring of retentate, permeate and recirculation flows was undertaken with three DFM 3530 flowmeters from Stübbe. Two conductivity sensors were additionally installed both at the outlet of retentate and permeate streams. Temperature probe was installed in the recirculation circuit.

Plant monitoring and operation control of the main process parameters were carried out through a Supervisory Control and Data Acquisition (SCADA) system developed in collaboration with the Instrumentation Deparment of the PSA.

Operation details

In this PhD Thesis the NF membrane was used to pre-concentrate OMCs and reduce the volume of wastewater to be treated by electro-oxidative processes, reducing at the same time the ohmic resistance of the solution so as the electric consumption.

For this purpose the NF pilot plant was operated in batch mode by pumping the retentate stream into the feeding tank, while the permeate stream was discarded. In each experiment from 1 m^3 of effluent previously filtrated (see section III.3.5.1) 250 L of retentate was obtained entailing a Volume Retention Factor (VRF) of 4.

At the begging of the separation and pre-concentration process, pressure at membrane inlet remained between 5 and 6 bar while the permeate outlet remained between 4 and 5 bar, keeping transmembrane pressure below 0.9 bar according to manufacturer recommendations. While operating in batch mode, feeding water increased its conductivity gradually, from values around 2.2 mS cm^{-1} till values around 6.5 mS cm^{-1}. Consequently, the volume rejected by the membrane was higher while the permeate volume was reduced. To increase the permeate flowrate, an increase of the pressure at the inlet of the membranes was needed, reaching up to 8 - 9 bar in the final stage of the experiment. (In any case, during the nanofiltration performance, the permeate conductivity remained below 200 µS cm.)

NF plant cleaning after experiments was faced by adding demineralized water into the feed tank and passing through the membranes until obtaining permeate and retentate conductivity on the vicinity of 5 uS cm^{-1} for both elements. After that, the membrane was kept in humid conditions until next experiment. When it is forseen a long stop of the plant, biocide in a concentration directly related to estimated downtime is added [15].

4.3. Solar photoelectro-Fenton pilot plant

BDD electrodes main characteristic is a high oxigen evolution over-potential promoting the generation of •OH. However this material also presents other advantages that make it very attractive for water treatment purposes that is a low absorption on the anode surface which allows a high reactivity of physisorbed •OH with organics substances. Also it presents stability against corrosion [7] even in strong acidic media in which Fenton reaction is usually developed.

For this reason their use combined with carbon-based electrodes capable to electrogenerate H_2O_2 (Reaction 32 section I.2.6), has attracted researchers´ attention since they allow highly oxidizing Fenton-like processes being developed by adding iron as a catalyst. Furthermore when combined with a solar photoreactor, consumed iron is continuously regenerated what is known as SPEF.

SPEF processes at pilot plant scale has been designed and installed in combination with a solar CPC photoreactor by the Solar Treatment of Water Unit at PSA facilities. The flow diagram is shown in figure 33. The electrochemical system consisted of four commercial plate-and-frame Electro MP-Cells, from ElectroCell (Fig. 34a) installed in parallel and connected to a 100 L tank and to a solar CPC photoreactor (Fig. 34b). This configuration confers great versatility to the system, as it allows the development of electrochemical tests (with the desired number of cells) with and without the combination with the CPC photoreactor. Alternatively it can lead to the development of a solar test avoiding the pass of the solution through the electrochemical cells.

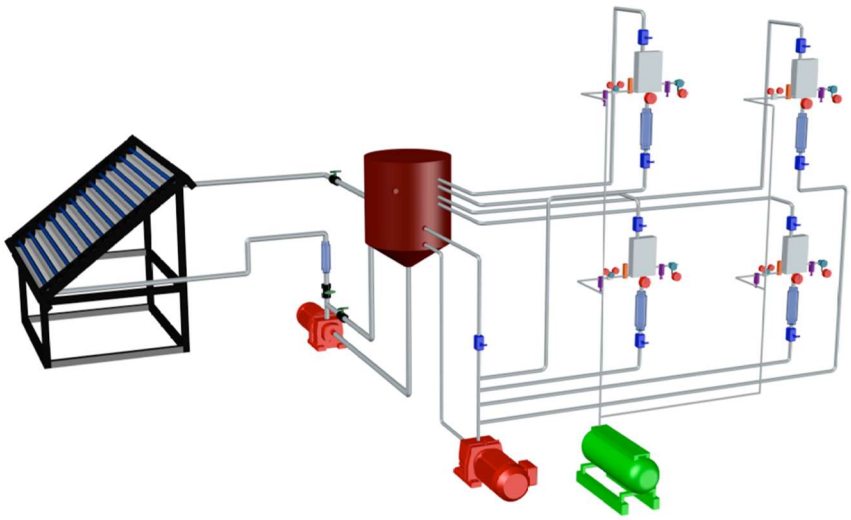

Figure 33. Flow diagram of the SPEF pilot plant installed at PSA facilities.

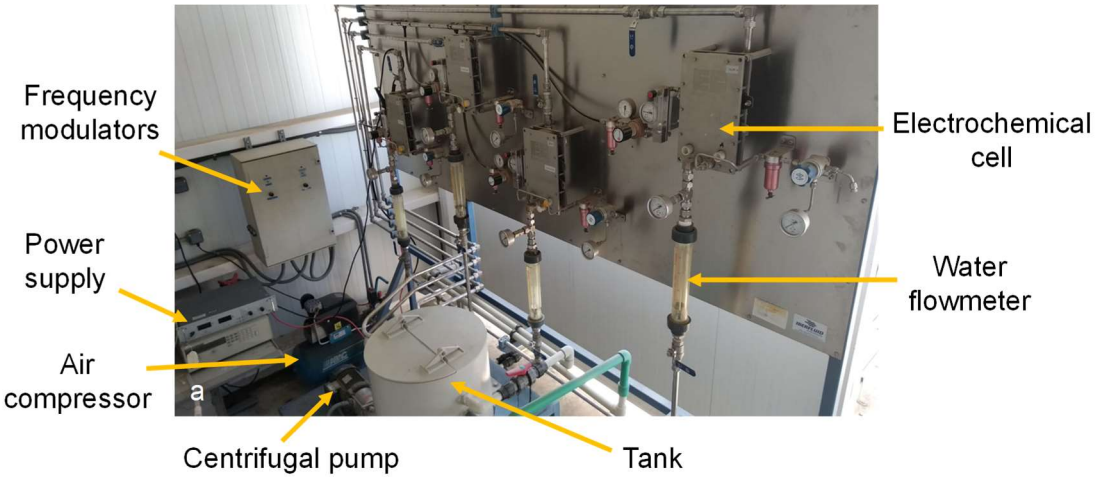

Figure 34. Images of the main components of the electrochemical pilot plant a) Electro MP-Cells b) Solar CPC photoreactor.

Each electrochemical cell (Fig. 35) is conformed by a niobium mesh covered with a thin film of BDD as anode, and a GDE of carbon-PTFE as cathode, both with a surface of 0.010 m^2. The cell has a filter-press configuration so it was necessary to use plastic flow frames both to keep the electrodes separate from each other and to separate them from the initial and final parts of the cell. Each of them has 6 mm of width. These flow frames, in turn, have specific input and output channels so that air and water flows can be directed as required. In this case, it was ensured that air passed behind the carbon-PTFE cathode to supply it with oxigen and that water flow passed through the anode. In order to avoid leaks, rubber gaskets (1 mm width) were used when assembling the different components, applying a maximum torque of 10 Nm preventing the deformation and breakage of plastic parts.

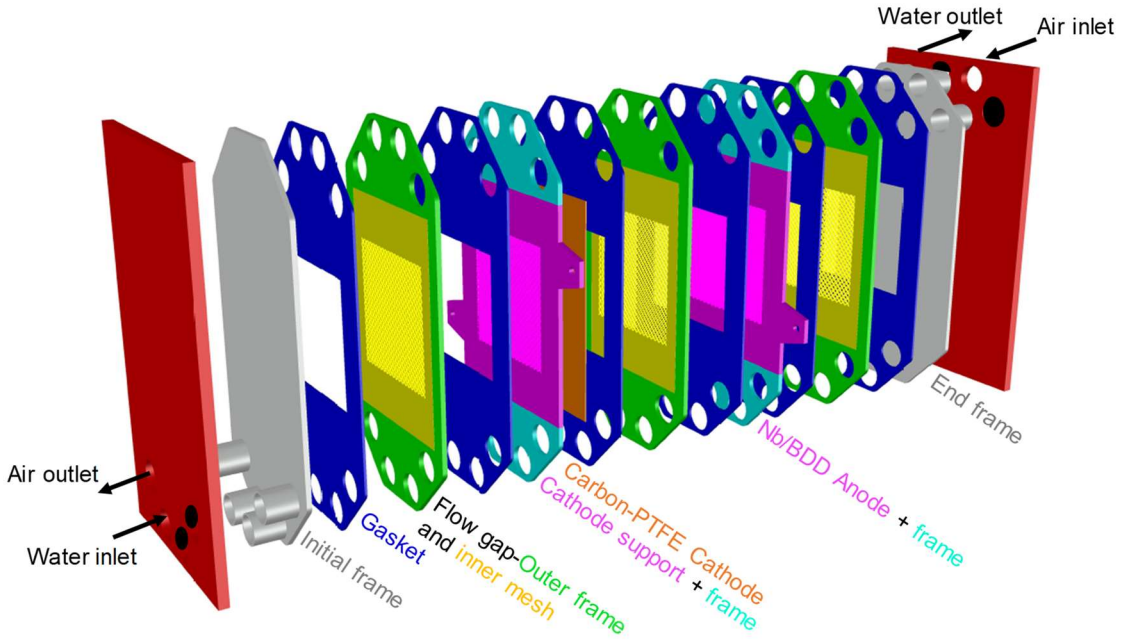

Figure 35. Detailed diagram of each internal piece that conforms a disassembled electrochemical cell.

An ABAC 1.5 kW air compressor supplied oxigen to the GDE cathode. Inlet air to the cell (Fig. 36) was regulated with a Spectrotec pressure regulator LT2000 NG and a flowmeter Tecfluid 2100 establishing a fixed pressure and flow in each case.

A LAFERT ST 90L L2, 1.8 kW pump circulate water to be treated to the cell through stainless steel pipes of 3/4” diameter. At the water inlet, a flowmeter Tecfluid PT11 and a manometer AISI 316L (from Manometría e Instrumentación) were installed to monitor these parameters, but along the experiments carried out in this PhD Thesis, the flow was

regulated through the power of the pump, controlled by a frequency modulator ACS355-03E-05A6-4 (from ABB). When operating the system it is crucial to guarantee that air pressure was always higher than water pressure to prevent it passing into the air circuit.

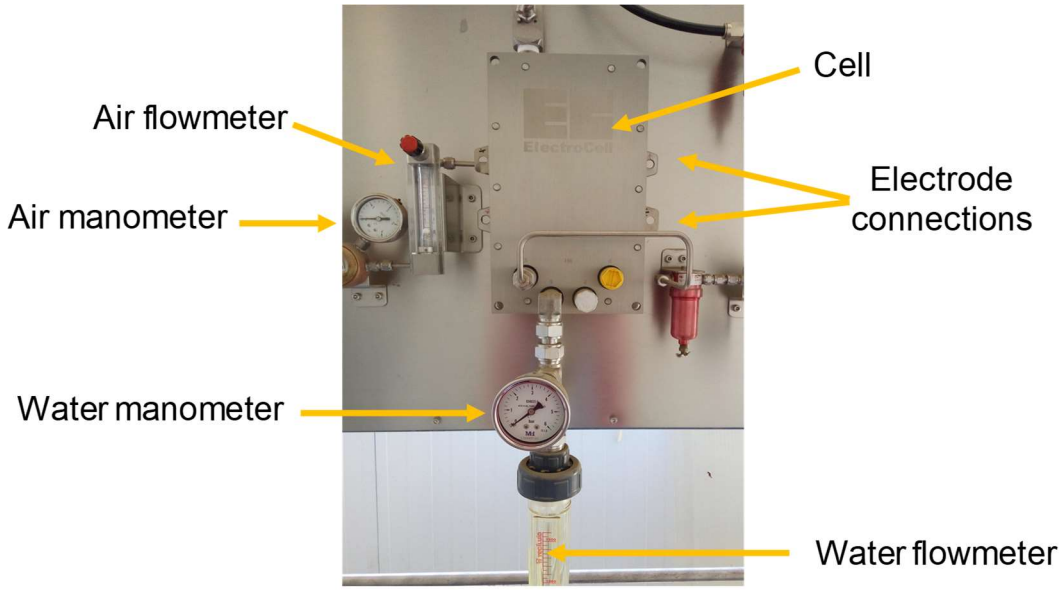

Figure 36. Instrumentation to monitor air and water inlets to the cell as well as electrode connections to the power supply.

Electrodes were connected to a Delta Electronika 70 – 22 power supply unit with a limit output of 70 V and 22 A. When active, this unit supplied a constant current to the system, while displaying the cell voltage drop.

Solar CPC photoreactor was fed directly from the tank throught 1” pipes of high density poliethylene with a 0.75 kW PAN World magnetic pump regulated by a frequency modulator VAT-3FD (from General Electric) monitoring the flow with a Tecfluid PT11 flowmeter. The solar CPC photoreactor has a total illuminated area of 2 m^2, with 10 borosilicate glass tubes of 150 cm of length and 4.5 cm of inner diameter involving an irradiated volume of 23 L. The photoreactor was installed in an aluminium platform tilted 37º according to PSA geographical coordinates (37º N, 2.4º W).

Finally, the pilot plant was coupled to an automatic temperature control system developed by ECOSYSTEM S.L., that contained a water chiller and two electric resistances in order to keep temperature controlled throughout the experiments.

Wastewater volume treated on stand-alone electro-oxidation experiments was 30 L while when combining with the CPC solar photoreactor the total volume increased to 75 L.

Operation details

In this PhD Thesis, wastewater treated with the electrochemical pilot plant was the retentate stream obtained from a NF membrane, showing the kindness of high salinity and containing a great amount of OMCs in higher concentrations than that found naturally in UWWTP secondary effluents.

The experiments were carried out following the procedure here described:

- Wastewater addition to the tank, 30L in the case of the application of electrochemical treatments such as AO and EF, and 75 L in the case of SPEF or solar-assisted AO. Let 15 - 20 minutes for correct homogenization.
- Connecting temperature control system to keep water temperature at 25 (±5) ºC along the experiment.
- If necessary, pH adjustment according to the process operation conditions by adding H_2SO_4.
- If wastewater was spiked by target OMCs, pre-dissolved contaminants from a methanol-concentrated mother solution was added.
- If the experiment developed was an EF or SPEF treatment, iron was required. When testing at pH 3, Fe^{2+} was added pre-dissolved in an acid solution. But when testing at natural pH, EDDS was used as complexing agent by previous formation of Fe^{3+}:EDDS complex.
- Operation parameters were then adjusted. Water flow was adjusted triggering the power of the pump and air pressure and flow were adjusted by regulable valves, keeping air pressure slightly above of water pressure.
- Once all the operation parameters were stable, an initial sample was taken and the experiment started. EF and AO treatments were initated by turning on the power supply of electrodes, and for SPEF and solar-assisted AO, CPC must be directly uncovered too.
- Samples were taken at shorter time intervals at the beginning of the experiment, spacing them in time until it was taken every 30 min, since degradation kinetics were expected to be faster at the beginning of the treatments.

Once each experiment was over, the system was cleaned with an acidic solution at pH 3, by mixing HCl and demineralized water, and then the whole pilot plant was rinsed 3 times with demineralized water.

4.4. Electro-oxidative pilot plant

The key parameters that determine the oxidant species being electrogenerated from target water is the material of the anode. It is known that, when using mixed metal oxide anodes, chlorine formation is expected primarily against water oxidation as they show low ability to electrogenerate •OH [16, 17]. It is within this group that falls the so-called DSA consisting of a titanium base covered with a thin layer of conducting metal oxide or a mix of metal oxides. [18].

In this PhD Thesis a commercial electrochemical cell consisting of a monopolar electrolyzer (Fig. 37) has been studied. It is composed from five DSA and counter cathodes, settled in an alternative pattern with a total anodes surface of 0.324 m^2. An Alinten S2750 Power Supply unit is connected to the cell, rated for a maximum 110 A on 25 V in Direct Current.

The reactor consists on an open tank of polypropylene with the electrodes submerged directly in the solution. Water is recirculating with a centrifugal pump IWAKI MD-70RZ maintaining a flow rate around 150 L h^{-1} and passing through a string wound filter and a cooling coil. The electrochemical system is able to treat up to 15 L.

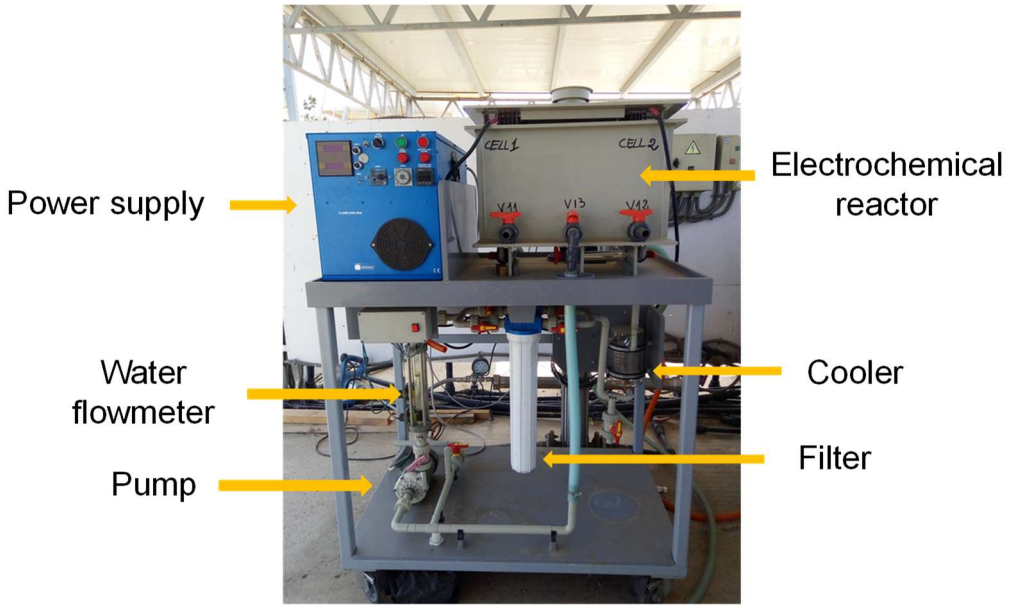

Figure 37. Commercial electrochemical device with DSA electrodes available at PSA facilities.

The electrochemical system was connected to a solar CPC photoreactor (Fig. 38) composed by 24 borosilicate glass tubes of 3.2 cm diameter and 150 cm length. The CPC reactor was tilted 37º from the horizontal with an illuminated area of 3.08 m^2 for a

total lit up volume of 22 L. The CPC volume was added to the one of the electrochemical side of the circuit going to a total volume of 38 L in the combined system.

Figure 38. Solar CPC photoreactor combined with the electrochemical device during the treatment of a landfill leachate in the facilities of PSA.

Operation details

Due to the high oxidative power of this system, target wastewater were landfill leachates described in section III.1.3.5.3. The plant was designed with the objective of using a minimum amount of additives. Thus the operation procedure for performing the experiments was filling the tank with the wastewater, let recirculate until homogenization and then turned on the cell, establishing a fixed current density of 25 mA cm^{-2} according to manufacturer's specifications for this kind of wastewater.

Two main disadvantages were overcomed during the operation of the electrochemical pilot plant, the generation of foams and pH collapse to strong acid values. Due to agitation and high organic load of target wastewater (landfill leachates) a large amount of foams were produced during operation. These foams had to be re-dissolved and then returned to the circuit, causing fluctuations in the DOC as function of foam generation-re-dissolution cycle. Furthermore, as strong acidification of the solution was promoted along electrochemical process, addition of NaOH was necessary to avoid pH falling under 3.5. That limiting value was necessary to maintain in order to avoid the formation of Cl_2 as it is a well known toxic agent that entails a serious risk for the operator and people in the surroundings. This, at the same time, had the undesired effect of provoking precipitation and re-disolution of some species due to pH change so string wound filter

cartridge must be used to remove any precipitates that could be generated to avoid damaging electrodes.

On the other hand, mainly in tests combining electrochemical and solar reactors, temperature of leachate being treated could rise above 45 ºC near solar noon, causing the decomposition of oxidizing species such as H_2O_2. To avoid this, the coiling coil was connected to an external cold-water circuit, always keeping the leachate below that temperature value.

After finishing each experiment, the system was cleaned with a HCl solution on demineralized water at pH 3 and then rinsed 3 times with demineralized water.

4.5. Photoelectrocatalysis at laboratory scale

TiO_2 photocatalyst has been widely studied for water depuration and purification due to its low cost and high effectiveness. Thus TiO_2 photoanodes have been developed as an upgrade to traditional treatment based on suspended TiO_2, since the main two drawbacks of these process are addressed: preventing the recombination of the electron-hole pairs due to the application of an electrical bias, and avoiding its recovery at the end of the treatment as it is supported on the anode.

As TiO_2 particles and photoelectrodes are governed by same fundamental principles and show the same behaviour, its application is limited to relatively clean waters with little colour and low turbidity, since they must allow the photons reach the anode surface in order to promote electrons from the valence band to the conduction band of the semiconductor.

Aiming to depurate surface wastewater, a new photoelectrocatalytic reactor was designed, assembled and tested in collaboration and in the facilities of NIBEC of Ulster University (UK) at laboratory scale.

The main component of the reactor (Fig. 39) is a double photoanode of TiO_2-NTs. To build it two titanium meshes of 75 x 95 mm from Sigma-Aldrich underwent a washing-anodizing-annealing process. Meshes were immersed and sonicated in a 5% Decon90 detergent solution, in distilled water and finally in an ethanol solution for washing. The electrochemical anodization was performed following the procedure described in Shin and Lee, 2008 [19]. Titanium meshes were immersed in a polypropylene container holding a solution of ethylene glycol (97 vol%) and NH_4F (0.3 wt%) in distilled water (3.0 vol%) as electrolyte. As a cathode, a Pt coated Ti mesh was used, placing it between the two photoanodes, obtaining an anode-cathode-anode configuration. Electrodes were

connected to a PLH120 Power Supply applying 30V for 3h. After that, the same procedure was repeated on the other side of meshes in order to have nanotubes on both sides avoiding mistakes during assembly. At the end of the process, photonodes were cleaned rinsing them several times with distilled water.

Finally, annealing of the nanotubes was carried out in order to obtain an anatase structure, in a Lenton AWF 12/5 Chamber Furnace at 500°C in air for 20h with a ramp of 2°C min^{-1} up and 1°C min^{-1} down.

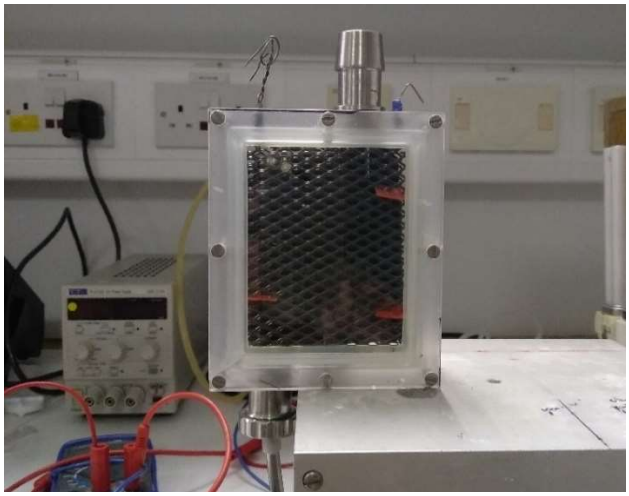

Figure 39. Lab-scale reactor designed for surface wastewater depuration in NIBEC.

A diagram of the reactor configuration and a picture of the flow system are shown in figures 40 and 41. The cell was made of a plastic outer shell with a 75x95 mm (71.25 cm^2) quartz window at the front that allowed the ultraviolet radiation pass through and into the reactor. Inside, the electrodes were arranged in an anode-anode-cathode configuration immediately behind the quartz window. Approximately half the area of the photonodes corresponded to the holes of the mesh, thus the first photoanode interacted with 50% of the photons, while the second, due to the shadow effect of the first, did so with 25%. Two cathodes were tested, a Ti-Pt mesh from Sigma-Aldrich and a carbon felt Sigracet GDL 28 BC from Ion Power in order to study the possible advantages of H_2O_2 electrogeneration in the oxidation process.

Photoelectrocatalytic cell has a total volume of 190 mL and it was operated in batch mode. An air-blower with a flowmeter was connected to the bottom of the cell in order to supply oxygen to the reactor (0.36 mL min^{-1}), being also useful to stir the solution. Electrodes were fed with a PLH120 Power Supply connected to two multimeters to accurately monitor the potential applied and current density. They were illuminated with

two 9W UVA blacklight lamps (Phillips, Actinic BL PL-S 9W/10/2P; 370 nm-peak wavelength).

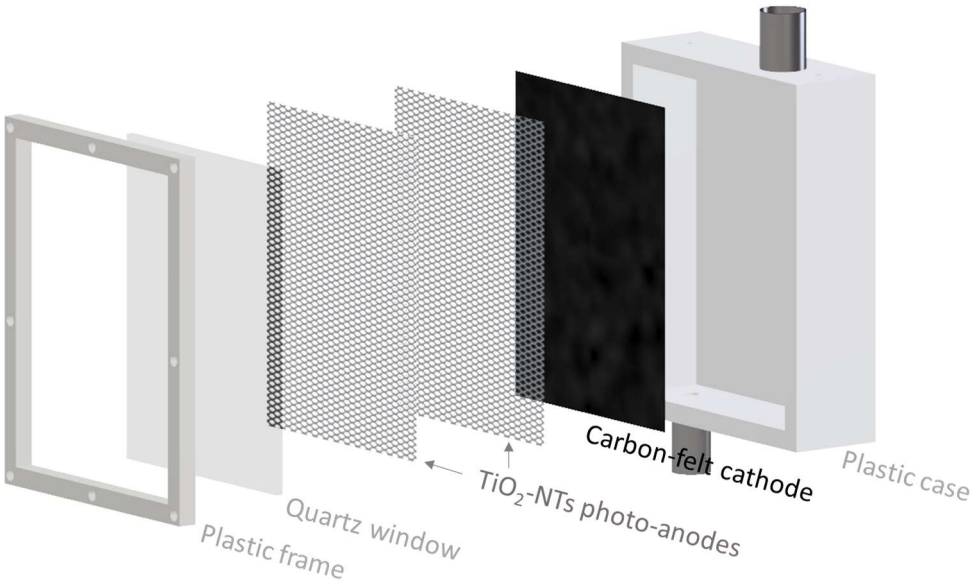

Figure 40. Components of the photoelectrocatalytic reactor designed and built in NIBEC, using carbón felt as cathode.

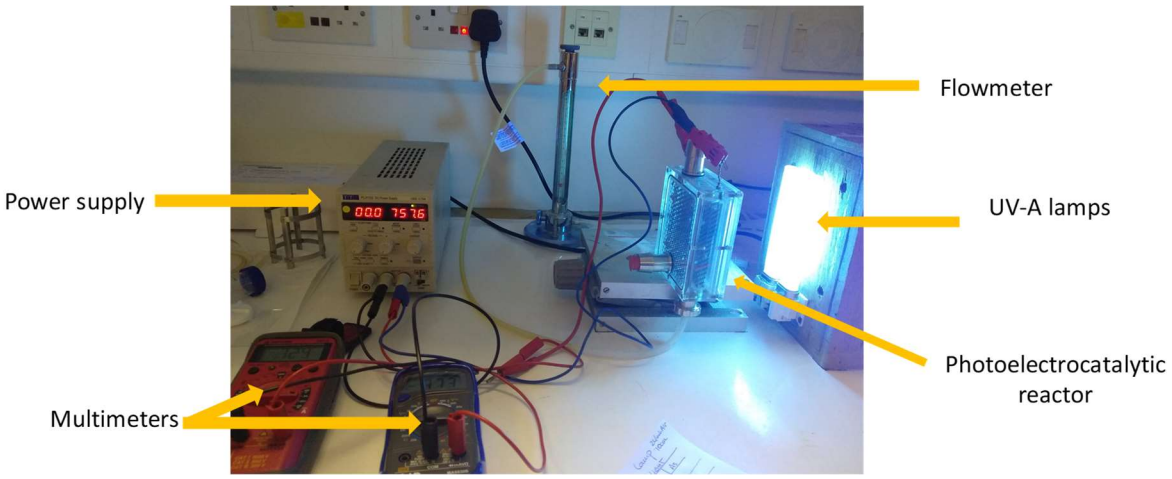

Figure 41. Main components of the photoelectrocatalytic system in NIBEC.

Irradiation selected for the experiments was 50 W m^{-2}, considered as the highest irradiation in the equator. In order to find the distance between the lamps and the cell which integration in the UV-A range (from 320 to 400 nm) was the target irradiation, lamps profiles were done at different distances (Fig. 42), reaching 50 W m^{-2} in the UV-A at 6.5 cm of the light source.

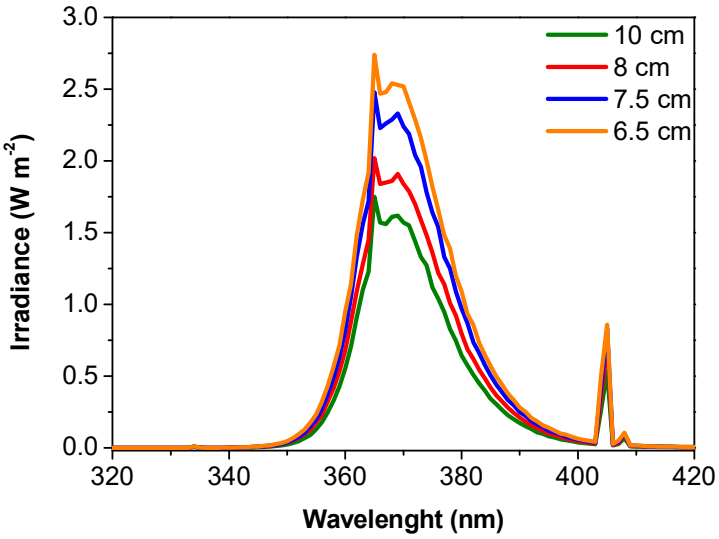

Figure 42. Irradiance profiles of the lamps at different distances of the source.

Operation details

Performance of this photoreactor was tested for the simultaneous removal of contaminants and bacteria from a surface wastewater. Target wastewwater characteristics were detailed in section III.1.3.5.2, spiked with three contaminants (terbutryn, chlorphenvinfos and diclofenac), and with *E.coli* K12 as reference pathogen.

Photoelectrocatalytic reactor was cleaned before each experiment with a solution of 10 mg L^{-1} H_2O_2 in distilled water, whirling it in order to homogenize and disinfect the entire cell, and then rinsed 3 times with distilled water.

Experiments were carried out by filling the reactor with surface wastewater, and by adding bacteria and/or target OMCs in a concentration of 10^6 CFU mL^{-1} and/or 500 mg L^{-1} of each contaminant, respectively. An air stream was bubbled into the system homogenizing the solution, working parameters (air flow, potential and distance to the light source) were henceforth set in a specific value and the initial sample was taken. The experiment started by turning on the power supply and removing the wooden cover of the cell that avoided the incidence of photons from the lamps, which had been previously switched on. Each experiment had a maximum duration of 2 h and at the end, the cell was cleaned again with a 10 mg L^{-1} H_2O_2 solution in distilled water, rinsing three times with distilled water.

4.6. Current efficiency calculation

CE for an electro-oxidative process can be defined as the proportion of the total applied current that is effectively taken for the completion of the oxidative process for a determined period of time as shown in equation 7.

$$CE = \frac{I_{effective}}{I_{applied}} \quad \text{(Equation 7)}$$

This concept was developed to be applied for the elimination of the organic matter contained in an effluent. The upgrading of CE calculation considers the whole amount of organic matter removed as COD and the different variables that cause an influence on the process as well as their relationship according to equation 8 [20].

$$CE(\%) = \frac{(\Delta COD)_t \, F \, V_T}{8 \, I \, t} \quad \text{(Equation 8)}$$

where $(\Delta COD)_t$ is the COD variation during a certain period of time expressed in mol O_2 m^{-3}, F is Faraday's constant (96 485 C mol^{-1}); 8 comes as a result of including the equivalent mass of oxygen ing eq^{-1}, I is the applied current and V_T is the volume of the electrolyte in m^3.

For each specific OMC, its CE required for its degradation can be calculated through the mineralization of the compound, having DOC as a reference. To calculate the mineralization CE, we need to upgrade the COD equation given before resulting in the following equation 9 [20, 21].

$$MCE(\%) = \frac{(\Delta DOC)_t \, n \, F \, V_T}{4.323 \cdot 10^7 \, m \, I \, t} \quad \text{(Equation 9)}$$

where $(\Delta DOC)_t$ is the DOC decay (mg C L^{-1}) for an specific period of time, n is the number of electrons exchanged in the mineralization process, $4.32 \cdot 10^7$ is the conversion factor for units homogenization (3600 s h^{-1} × 12 000 mg C mol^{-1}) and m is the number of carbon atoms of the OMC molecule.

This methodology can be also adapted to determine the value of CE for H_2O_2 electrogeneration and calculated according to equation 10.

$$CE(\%) = \frac{[H_2O_2] \, n \, F \, V_T}{1000 \, M \, (H_2O_2) Q} \quad \text{(Equation 10)}$$

where $[H_2O_2]$ is the accumulated H_2O_2 (mg L^{-1}) electrogenerated in an specific time, $M(H_2O_2)$ is the molecular weight of H_2O_2 (34 g mol^{-1}), and Q is the charge applied during the electrolysis.

In this PhD Thesis, CE for H_2O_2 electrogeneration was stablised as response variable on which electrochemistry system must be optimized by following an experimental design procedure (described in the following section).

4.7. Optimization by Response Surface Methodology experimental design

The Response Surface Methodology (RSM) is a set of mathematical and statistical techniques given for the treatment of problems in which a response of interest (output variable) is influenced by several independent factors (input variables) of a quantitative nature.

The initial phase of these techniques consists on designing a serie of experiments to assess the way the system response (output) as the factors (inputs) change. Then collected data is used to determine which mathematical model best fits experimental data. The final objective is determining the factor values that allows optimization of the response variables.

Central composite design (CCD) is the experimental design mostly used for optimization as it is able to adjust second-order regression models (Fig. 43). Specifically, CCD is built in modules (Fig. 44) thus allowing the reduction of experimentation time hence saving costs. First, a 2^k design (where k is the number of factors) address the interaction between the factors at diferent levels (from low or -1 to high or +1). If the curvature is confirmed to be significant according to the P-value (<0.05) from an ANOVA analysis, then a centre point is added which joins the blocks previously studied and allows an error estimation. If this shows that curvature is still significant (P-Value <0.05) then axial points are added, which are tasked to fit the components to the square.

Those axial points are at an alpha (α) distance that ensures the rotability of the design. Alpha value is dependent on the number of factors and it is calculated according to equation 11, where F is the number of factors

$$\alpha = F^{1/4} \qquad \text{(Equation 11)}$$

When alpha value is stablished at 1 for a CCD it is said that we are working on a Face Centered Design (FCD). This kins of analysis locate the axial points in the centre of each face within the factor space. For this design modality level 3 for each factor is required.

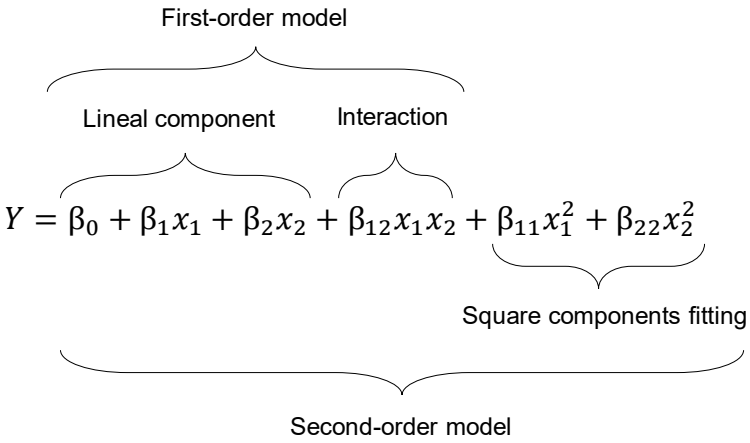

Figure 43. Second-order regression model components.

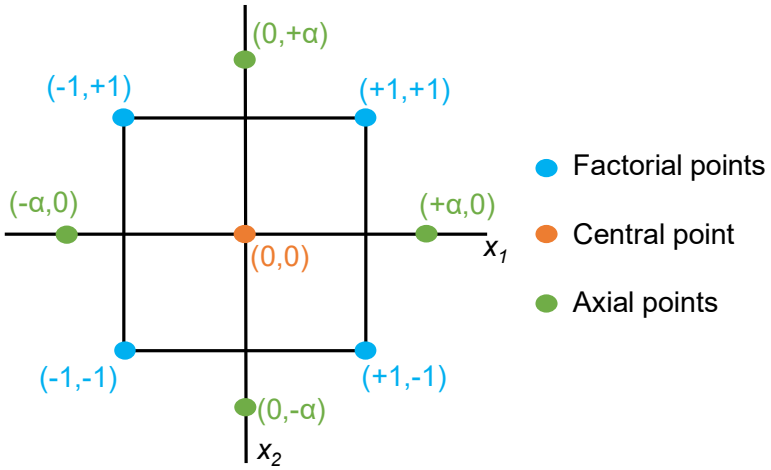

Figure 44. Scheme of the spatial distribution of CCD points.

In this PhD Thesis, target was the optimization of the electrogenerated H_2O_2 through a RSM using a FCD. For this purpose, pH and current density (*j*) were selected as factors (input variables) and the simultaneous maximization of both H_2O_2 concentration and CE as response (output) variables.

Each factor was studied at three levels, low, central and high, (Table 16) selecting each value according to the literature and published know-how on this electrochemical systems.

Table 16. Input variables range studied in the experimental design.

Variable	Levels and value		
	Low (-1)	Center (0)	High (+1)
pH	3	5	7
j (mA cm^{-2})	30	65	100

Statistical software used was Desing Expert 7.0.0 (from Stat-Ease Inc.). The experiments to be done for the FCD are sumarized in table 17, consisting in the combination of all the levels between them with two replicas per combination and three replicas in the central point resulting in 19 experiments.

Table 17. Experimental design to be run for the optimization of H_2O_2 electrogeneration obtained with Desing Expert 7.0.0 software, having pH and *j* as input factors.

Experiment	pH	*j* (mA/cm^2)
1	3	100
2	7	30
3	5	65
4	7	100
5	3	30
6	3	100
7	5	65
8	5	100
9	3	65
10	7	100
11	5	100
12	5	30
13	5	65
14	5	30
15	3	30
16	7	65
17	3	65
18	7	65
19	7	30

4.8. Ratio between mineralization degree and electric energy: r_e parameter

When facing the treatment of complex wastewater as landfill leachates, a huge amount of organic substances of very different nature is present so its depuration must be monitorized in terms of organic matter removal (COD) or mineralization degree (DOC).

On the other hand, in electrochemical processes already operating under optimum conditions, crucial parameter is applying the required electrical energy to reach organic

compounds degradation, that is similar as Quv role in photo-Fenton processes. Furthermore, electrical energy, against solar energy, entails economical cost associated to the supply from the electrical network. This means that small variations on this parameter can lead to big savings or cost increase, thus its weight in the process is even higher.

Aiming to address simultaneously this two concepts, removal of DOC and electrical energy, for comparison of different electro-oxidative processes, r_e parameter was described (equation 12) stablishing the relationship between the mineralization degree and the electrical energy required to reach it.

$$r_e = \frac{\Delta DOC}{e} \qquad \text{(Equation 12)}$$

being r_e (g DOC kWh^{-1}) the degradation rate, ΔDOC the removal of DOC (g DOC m^{-3}) reached and e the electrical normalized energy applied per treated volume (kWh m^{-3}).

As r_e parameter can be consider a rate of removed mass vs energy, it can be applied to other parameters as TN or a single OMC allowing to compare electrochemical processes and its efficiencies from different points of view.

5. References

[1] I. Oller, W. Gernjak, M.I. Maldonado, L.A. Perez-Estrada, J.A. Sanchez-Perez, S. Malato, Solar photocatalytic degradation of some hazardous water-soluble pesticides at pilot-plant scale, J. Hazard. Mater., 138 (2006) 507-517.

[2] I. Oller, S. Malato, J.A. Sánchez-Pérez, M.I. Maldonado, R. Gassó, Detoxification of wastewater containing five common pesticides by solar AOPs–biological coupled system, Catal. Today, 129 (2007) 69-78.

[3] A. Zapata, I. Oller, E. Bizani, J.A. Sánchez-Pérez, M.I. Maldonado, S. Malato, Evaluation of operational parameters involved in solar photo-Fenton degradation of a commercial pesticide mixture, Catal. Today, 144 (2009) 94-99.

[4] A. Zapata, I. Oller, L. Rizzo, S. Hilgert, M.I. Maldonado, J.A. Sánchez-Pérez, S. Malato, Evaluation of operating parameters involved in solar photo-Fenton treatment of wastewater: Interdependence of initial pollutant concentration, temperature and iron concentration, Appl. Catal. B-Environ., 97 (2010) 292-298.

[5] University of Hertfordshire. Agriculture and Environment Research Unit (AERU), Pesticides Properties DataBase (PPDB) (2007). https://sitem.herts.ac.uk/aeru/ppdb/en/index.htm (Accessed July 2020)

[6] S. Miralles-Cuevas, I. Oller, J.A.S. Perez, S. Malato, Removal of pharmaceuticals from MWTP effluent by nanofiltration and solar photo-Fenton using two different iron complexes at neutral pH, Water Res., 64 (2014) 23-31.

[7] N. Klamerth, S. Malato, A. Aguera, A. Fernandez-Alba, G. Mailhot, Treatment of municipal wastewater treatment plant effluents with modified photo-Fenton as a tertiary treatment for the degradation of micro pollutants and disinfection, Environ. Sci. Technol., 46 (2012) 2885-2892.

[8] L.K. Wang, Y.T. Hung, N.K. Shammas. Handbook of Environmental Engineering: Advanced Physicochemical Treatment Processes, Humana Press, 2006.

[9] A. Rincon, C. Pulgarin, Effect of pH, inorganic ions, organic matter and H_2O_2 on *E. coli* K12 photocatalytic inactivation by TiO_2 Implications in solar water disinfection, Appl. Catal. B-Environ., 51 (2004) 283-302.

[10] D.L. Harp, Current technology of chlorine analysis for water and wastewater: Technical information series–Booklet no. 17, Hach, Loveland, Colorado, (2002) 2-8.

[11] J.H. Baxendale, A.A. Khan, The pulse radiolysis of p-nitrosodimethylaniline in aqueous solution, International Journal for Radiation Physics and Chemistry, 1 (1969) 11-24.

[12] J. Muff, L.R. Bennedsen, E.G. Søgaard, Study of electrochemical bleaching of p-nitrosodimethylaniline and its role as hydroxyl radical probe compound, J. Appl. Electrochem., 41 (2011) 599-607.

[13] J. Blanco, S. Malato, Solar detoxification, UNESCO Publishing, France, 2003.

[14] Synder Filtration, Inc., What are Nanofiltration Membranes?. https://synderfiltration.com/nanofiltration/membranes/ (Accessed July 2020)

[15] S.M. Cuevas, Eliminación de micro-contaminantes mediante combinación de sistemas de membrana (nanofiltración) y procesos avanzados de oxidación, (2015).

[16] I. Sirés, E. Brillas, M.A. Oturan, M.A. Rodrigo, M. Panizza, Electrochemical advanced oxidation processes: today and tomorrow. A review, Environ. Sci. Pollut. R., 21 (2014) 8336-8367.

[17] C.A. Martinez-Huitle, E. Brillas, Decontamination of wastewaters containing synthetic organic dyes by electrochemical methods: A general review, Appl. Catal. B-Environ., 87 (2009) 105-145.

[18] M. Panizza, Importance of electrode material in the electrochemical treatment of wastewater containing organic pollutants, in: C. Comninellis, G. Chen (Eds.) Electrochemistry for the Environment, Springer, New York, 2010, pp. 25-54.

[19] Y. Shin, S. Lee, Self-Organized Regular Arrays of Anodic TiO_2 Nanotubes, Nano Lett., 8 (2008) 3171-3173.

[20] E. Brillas, I. Sirés, M.A. Oturan, Electro-Fenton process and related electrochemical technologies based on Fenton's reaction chemistry, Chem. Rev., 109 (2009) 6570-6631.

[21] F.C. Moreira, R.A.R. Boaventura, E. Brillas, V.J.P. Vilar, Electrochemical advanced oxidation processes: a review on their application to synthetic and real wastewaters, Appl. Catal. B-Environ, 202 (2017) 217-261.

Chapter IV. Results and Discussion

Target 1. Optimization of electrocatalytic H_2O_2 production at pilot plant scale for solar-assisted water treatment

Applied Catalysis B: Environmental 242 (2019) 327–336

Contents lists available at ScienceDirect

Applied Catalysis B: Environmental

journal homepage: www.elsevier.com/locate/apcatb

Optimization of electrocatalytic H_2O_2 production at pilot plant scale for solar-assisted water treatment

Irene Salmerón[a,b], Konstantinos V. Plakas[c], Ignasi Sirés[d], Isabel Oller[a,b,*], Manuel I. Maldonado[a,b], Anastasios J. Karabelas[c], Sixto Malato[a,b]

[a] Plataforma Solar de Almería-CIEMAT, Ctra Senés km 4, 04200, Tabernas, Almería, Spain
[b] CIESOL, Joint Centre of the University of Almería-CIEMAT, 04120, Almería, Spain
[c] Chemical Process and Energy Resources Institute, Centre for Research and Technology – Hellas (CERTH), 6th Km Charilaou-Thermi Road, Thermi, Thessaloniki, GR 57001, Greece
[d] Laboratori d'Electroquímica dels Materials i del Medi Ambient, Departament de Química Física, Facultat de Química, Universitat de Barcelona, Martí i Franquès 1-11, 08028, Barcelona, Spain

ARTICLE INFO

Keywords:
Boron-doped diamond
Gas-diffusion electrode
Hydrogen peroxide electrogeneration
Solar photoelectro-Fenton
Wastewater treatment

ABSTRACT

This manuscript summarizes the successful start-up and operation of a hybrid eco-engineered water treatment system, at pilot scale. The pilot unit, with 100 L capacity, has been devised for the efficient electrocatalytic production of H_2O_2 at an air-diffusion cathode, triggering the formation of $^{\cdot}OH$ from Fenton's reaction with added Fe^{2+} catalyst. These radicals, in combination with those formed at a powerful boron-doped diamond (BDD) anode in an undivided cell, are used to degrade a mixture of model pesticides. The capability of the plant to produce H_2O_2 on site was initially optimized using an experimental design based on central composite design (CCD) coupled with response surface methodology (RSM). This aimed to evaluate the effect of key process parameters like current density (j) and solution pH. The influence of electrolyte concentration as well as liquid and air flow rates on H_2O_2 electrogeneration and current efficiency at optimized j and pH was also assessed. The best operation conditions resulted in H_2O_2 mass production rate of 64.9 mg min^{-1}, 89.3% of current efficiency and 0.4 kWh m^{-3} of energy consumption at short electrolysis time. Performance tests at optimum conditions were carried out with 75 L of a mixture of pesticides (pyrimethanil and methomyl) as a first step towards the elimination of organic contaminants by solar photoelectro-Fenton (SPEF) process. The combined action of homogeneous ($^{\cdot}OH$) and heterogeneous (BDD($^{\cdot}OH$)) catalysis along with photocatalysis (UV photons collected at a solar CPC photoreactor) allowed the removal of more than 50% of both pesticides in 5 min, confirming the fast regeneration of Fe^{2+} catalyst through cathodic reduction and photo-Fenton reaction.

1. Introduction

The extraordinary development of chemicals manufacturing and their widespread use in all human activities is intimately associated with contamination of aquatic environment. Water quality monitoring programs underline the seriousness of the problem worldwide and highlight the potential hazards posed by mixtures of synthetic organic contaminants (SOCs) and their metabolites in surface water and groundwater [1–4]. Typically, SOCs include solvents, preservatives, pharmaceuticals and personal care products, lubricants, dyes or active substances for plant protection [5]. Among the latter, methomyl (MET) and pyrimethanil (PYR) are ubiquitous in intensive agriculture, which is worrisome since they are classified as persistent organic pollutants (POPs) [6] and are considered extremely toxic [7,8]. This issue has prompted the application of advanced oxidation processes (AOPs) for the fast and complete removal of SOCs from polluted water streams [9], based on the in situ production of hydroxyl radical ($^{\cdot}OH$) as main reactive oxygen species (ROS).

Fenton's reaction between ferrous ions (Fe^{2+}) and hydrogen peroxide (H_2O_2), so-called Fenton's reagent, is the most popular source of $^{\cdot}OH$ for practical applications [10]. As an upgraded approach, the electro-Fenton (EF) process allows overcoming two key limitations of the conventional chemical method [11–13]: (i) it ensures the continuous regeneration of Fe^{2+} through cathodic reduction of Fe^{3+}, thus requiring a much lower amount of catalyst to perform the treatment, and (ii) it avoids the handling, storage and transportation of H_2O_2 produced industrially, since this reagent can be electrosynthesized on site through Reaction (1) by using appropriate cathode materials.

* Corresponding author.
E-mail address: isabel.oller@psa.es (I. Oller).

https://doi.org/10.1016/j.apcatb.2018.09.045
Received 12 June 2018; Received in revised form 11 September 2018; Accepted 15 September 2018
Available online 29 September 2018
0926-3373/

$$O_{2(g)} + 2H^+ + 2e^- \rightarrow H_2O_2 \quad (1)$$

Electrocatalytic H_2O_2 generation is becoming a hot topic because the combination of electrochemistry with new catalysts enables a more eco-friendly and less energy-intensive production of this commodity [14,15]. Several prospective electrocatalysts have been developed, with noble metals and metal alloys like Pd-Au, Pt-Hg and Pt/Pd-Hg as particularly prominent options [14,16,17]. Non-precious Co-based particles are very active promoters of Reaction (1) as well, at smaller cost [18]. Unfortunately, none of these catalysts is viable for large-scale water treatment due to their high cost and toxicity, which has fostered the investigation on inexpensive carbonaceous materials [14,19,20]. Unmodified carbon-based catalysts exhibit appealing characteristics as cathodes, such as non-toxicity and high stability, conductivity and durability. H_2O_2 production with such inexpensive materials is particularly interesting for developing small- or medium-size decentralized units where the chemical is generated on demand [21]. This can be achieved using graphite felt, reticulated vitreous carbon, activated carbon fiber or carbon nanotubes as cathode, completely immersed into the solution to generate H_2O_2 from dissolved O_2 [22–24]. However, much greater H_2O_2 concentrations are attained upon implementation of an air-chamber in the electrochemical reactor, since it allows continuous air-feeding through a hydrophobized carbon-based gas-diffusion electrode (GDE) [15,18,25–28]. Worth noting, the vast majority of studies on Fenton-based electrochemical AOPs (EAOPs) reporting data on H_2O_2 production at GDE have been carried out either at laboratory scale or in small pre-pilot plants of 2.5 L [29] and 5 L [30,31]. Only one work reported the use of a bigger plant with 25 L capacity, but it was mainly focused on aniline degradation [32].

Undivided electrochemical cells are preferred to perform all these studies on water treatment because the use of a separator would increase the cell voltage and hence, the energy consumption. In addition, in such cells, the combination of carbonaceous cathodes with electrocatalytic materials that promote the anodic production of heterogeneous hydroxyl radical enhances the performance of EF process. Boron-doped diamond (BDD) thin film on Si substrate is the best anode to oxidize H_2O to physisorbed $^{\cdot}OH$ via Reaction (2) [11,13,33], owing to its large overpotential for O_2 evolution. However, Ti and Nb substrates are more suitable for plant-scale applications due to their much higher mechanical and chemical resistance.

$$BDD + H_2O \rightarrow BDD(^{\cdot}OH) + H^+ + e^- \quad (2)$$

The best performance among Fenton-based EAOPs for SOCs degradation is attained upon continuous irradiation of the treated solution with UV/Vis light. This is feasible employing a UVA lamp in photoelectro-Fenton (PEF) process [11,13], since it promotes: (i) a high regeneration rate of Fe^{2+}, with concomitant production of homogeneous $^{\cdot}OH$, from photoreduction of the main Fe(III) species at pH ~ 3.0 (Reaction (3)), (ii) the photodegradation of Fe(III)-carboxylate complexes formed as intermediates (Reaction (4)), and (iii) the direct photolysis of some pollutants and/or their oxidation by-products [11,34].

$$[Fe(OH)]^{2+} + h\nu \rightarrow Fe^{2+} + {}^{\cdot}OH \quad (3)$$

$$[Fe(OOCR)]^{2+} + h\nu \rightarrow Fe^{2+} + CO_2 + R^{\cdot} \quad (4)$$

In order to achieve the synergy between electrocatalytic and photolytic reactions at an affordable cost, UVA lamps have been lately replaced by direct sunlight irradiation, yielding the promising solar PEF (SPEF) process. Its great oxidation capability arises from: (i) the higher UV photon flux from sun if the solar collector design is adapted to the photoreactor, which upgrades the $^{\cdot}OH$ production, along with (ii) the additional illumination within the visible range ($\lambda > 400$ nm), promoting Reaction (3) (also active in the visible range) and accelerating the photolysis of refractory Fe(III)-carboxylate complexes (Reaction (4)) [34]. Very good degradation results by SPEF with GDE were obtained using a recirculation small pilot plant of 2.5-L capacity equipped with a flat-plate photoreactor [35–37], also employed to treat pesticides like mecoprop [35], diuron [38] or tebuthiuron and ametryn [39]. Replacement by a more efficient photoreactor based on compound parabolic collectors (CPC) could increase the efficiency of SPEF due to the greater photon flux supply to the solution. At present, CPC is the most popular photoreactor, as confirmed by its integration in most of the SPEF units for treating 2.2 L [40], 6 L [41], 8 L [42] and up to 10 L [43–48], which is the largest volume investigated so far.

Based on the excellent performance of SPEF at limited scale, a larger pilot plant has been developed for the treatment of SOCs by EAOPs with H_2O_2 electrogeneration. The system, with capacity to treat up to 100 L, consists of four undivided Nb-BDD/GDE filter-press cells coupled with a solar CPC, and has been installed and tested at Plataforma Solar de Almería (PSA), the largest European facility to test solar technologies. As a first step toward the treatment of real wastewater, this work is focused on the optimization of pilot plant main operation variables for the electrocatalytic H_2O_2 production, including current density (j), solution pH, liquid flow rate, air flow rate and electrolyte concentration. This was made with the aid of central composite design (CCD) coupled to response surface methodology (RSM). The plant was further validated by performing degradation trials under optimum conditions using a mixture of fungicide PYR and insecticide MET spiked into conductive water at high concentrations to simulate real agricultural wastewater. Note that these pesticides have only been studied before by AOPs like solar TiO_2 photocatalysis and solar photo-Fenton at pilot scale [6] and EF at lab scale [8].

2. Materials and methods

2.1. Chemicals

Heptahydrated ferrous sulfate (Sigma-Aldrich) used as catalyst and anhydrous sodium sulfate (Fluka) employed as background electrolyte were of analytical grade. PYR (IQV, AgroEvo, 98% purity) and MET (Aragonesas Agro, 99.5% purity) were of reagent grade and used without further purification. Mixtures of the two pesticides were prepared with deionized water (conductivity < 10 μS cm^{-1}, dissolved organic carbon (DOC) < 0.5 mg L^{-1}) and the electrolyte, and their pH was adjusted with analytical grade sulfuric acid (J.T. Baker). Organic solvents and other chemicals employed for HPLC analysis of the pesticides were of analytical grade from Sigma-Aldrich.

2.2. Pilot plant

Images of the filter-press type electrochemical cells and the CPC photoreactor, along with a schematic diagram of the pilot plant, are shown in Fig. 1. The plant consisted of four plate-and-frame electrochemical reactors (Electro MP-Cells from ElectroCell) coupled to a purpose-made solar CPC. Each cell contained an anode made of BDD thin film deposited on a niobium mesh (Nb-BDD) and a carbon-polytetrafluoroethylene (PTFE) GDE as the cathode, both with 0.01 m^2 effective area. The CPC photoreactor had a total illuminated area of 2 m^2, corresponding to an irradiated volume of 23 L. It was comprised of 10 borosilicate glass tubes (150 cm length × 4.5 cm inner diameter) mounted in an aluminum frame on a platform tilted 37° (PSA, 37 °N, 2.4 °W). The working volume was 25 L to carry out the optimization of H_2O_2 electrogeneration, and 75 L to perform the degradation experiments. The unit was equipped with two magnetic drive pumps (PAN World, 0.75 kW), one for pumping the solution from the feed tank (maximum capacity of 100 L) to the electrochemical cells, and the other for the liquid recirculation to and from the CPC. The GDE was fed with compressed air (ABAC air compressor, 1.5 kW) at a pressure and flow rate regulated with a back-pressure gauge and a flowmeter, respectively, in order to avoid the flooding of the air chamber. The experiments were made at constant j using a Delta Electronika power supply (limited to 70 V and 22 A).

Global ultraviolet solar radiation (UV_G) was measured using a radiometer (Kipp & Zonen, model CUV 3) mounted on a platform tilted 37°, the

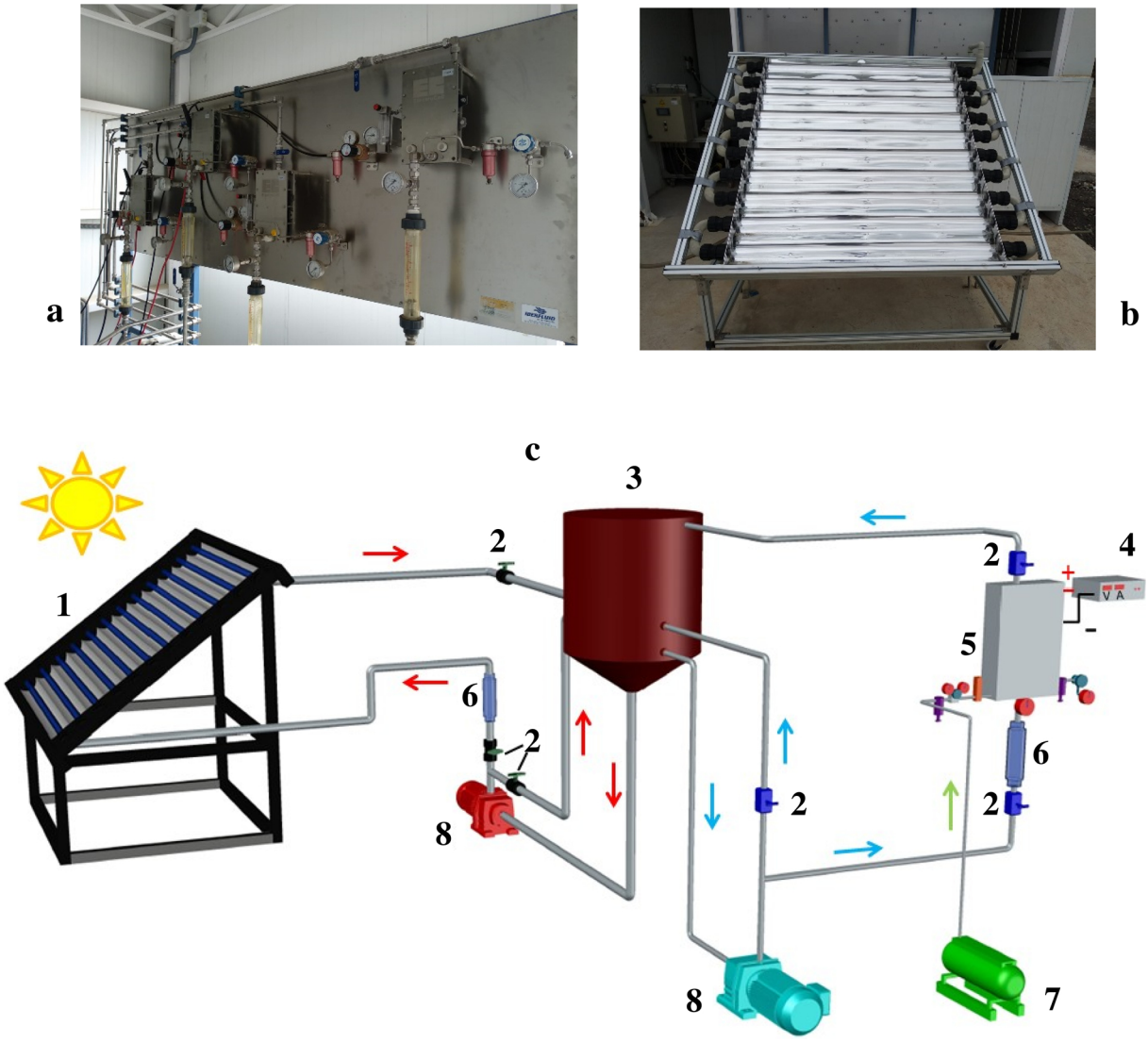

Fig. 1. Front view of (a) the four filter-press type electrochemical cells of the pilot unit, and (b) the CPC photoreactor. In (c), schematic diagram of the pilot unit equipped with one cell (examined in this work), showing: (1) CPC photoreactor, (2) valve, (3) feed tank, (4) power supply, (5) electrochemical reactor, (6) liquid flowmeter, (7) air compressor, (8) magnetic pump.

same angle as the photoreactor, which provided data in terms of incident irradiance ($W_{UV}\,m^{-2}$). This informs about the energy reaching any surface in the same position with regard to the sun. Eq. (5) allows combining the data from trials performed in different days, thus enabling comparison with results obtained in other photocatalytic experiments [49].

$$Q_{UV,n} = Q_{UV,n-1} + \Delta t_n \bullet \bar{UV}_{G,n} \bullet A_r \bullet V_T \quad (5)$$

where Q_{UV} is the accumulated UV energy per unit of volume ($kJ\,L^{-1}$), $\bar{UV}_{G,n}$ (in $W\,m^{-2}$) is the average UV radiation measured during Δt_n ($= t_n - t_{n-1}$), A_r is the irradiated surface area ($2\,m^2$) and V_T is the total volume treated in the pilot plant.

2.3. Experimental design

Experimental design by RSM was employed to optimize the in situ electrogeneration of H_2O_2. Trials were performed with one of the four identical electrochemical cells of the pilot, assuming that the resulting optimum conditions would be also valid for the other three cells. Two optimization criteria were considered: (a) maximization of the concentration of the produced H_2O_2, and (b) maximization of the current efficiency (CE, in percentage), defined as the ratio between the electricity consumed by the electrode reaction of interest and the total electricity supplied. CE can be calculated via Eq. (6), where *n* represents the stoichiometric number of electrons transferred in Reaction (1), F is the Faraday constant ($96{,}487\ C\ mol^{-1}$), $[H_2O_2]$ the concentration of H_2O_2 accumulated in bulk solution ($mg\ L^{-1}$), V_T the volume of the treated solution (L), $M(H_2O_2)$ the molecular weight of H_2O_2 ($34\,g\,mol^{-1}$), and Q the charge consumed during the electrolysis (C).

$$\%\,CE = \frac{nF\,[H_2O_2]V_T}{1000\,M(H_2O_2)Q} \times 100 \quad (6)$$

RSM was first used to assess the relationship between response (H_2O_2 concentration or % CE) and two independent variables, namely the solution pH (factor A) and *j* (factor B), as well as to optimize the relevant conditions in order to predict the best value of responses. CCD, the most widely used approach of RSM and, more specifically, a face centered composite (FCC) design, was employed to determine the effect of the two variables. Design Expert® v.7.0.0 software (Stat-Ease Inc., USA) was used. Three levels between -1 and +1 were established for the two independent variables (Table 1). Ranges were chosen based on preliminary experiments (data not shown here), background knowledge, and some constraints arising from the cathodic H_2O_2 electrogeneration and the nature of the electrode materials. For example, the production of H_2O_2 is favored at acidic pH (Reaction (2)), whereas the use of GDE and BDD

Table 1
Experimental range and levels of independent variables.

Variable	Factor	Units	Level and Range		
			Low (-1)	Central (0)	High (+1)
pH	A	–	3	5	7
j	B	mA cm^{-2}	30	65	100

anode limits the operation cell voltage to less than 25 V to prevent surface damage, which would cause the loss of electrocatalytic properties, and keep a reasonable CE [50]. This means that maximum current that can be applied is 10 A (j = 100 mA cm^{-2}).

For the CCD, a 2^3 full factorial design with 3 replicates at the center point (resulting in 19 experiments) was used to determine the optimum values of independent variables. These experiments were carried out by recirculating synthetic solutions of 50 mM Na_2SO_4 at a liquid flow rate of 4.4 L min^{-1}, and they were randomly performed to minimize the effect of systematic errors. Analysis of variance (ANOVA) of the data was performed to identify significant values (p-value < 0.05). The quality of the fit of polynomial model was expressed by the value of correlation coefficient (R^2). The main indicators demonstrating the significance and adequacy of the used model include the model F-value (Fisher variation ratio), probability value (Prob > F), and adequate precision. The optimal region of the independent variables was determined by plotting three-dimensional response surfaces of the independent and dependent variables. Additionally, numerical optimization of the independent variables was carried out using the same software.

A second set of experiments was carried out aiming to assess the effect of electrolyte concentration as well as liquid and air flow rates, under the optimum pH and j conditions. The best operation conditions were finally applied to degrade mixtures of pesticides, in the absence or presence of iron catalyst. In SPEF, the pesticide solution was irradiated when circulating through the CPC photoreactor.

2.4. Instruments and analytical methods

The concentration of H_2O_2 accumulated during the electrolysis was determined by adding Ti(IV) oxysulfate to the sample and measuring the absorbance at 410 nm, according to DIN 38,409 H15. Iron concentration was measured by using 1,10-phenanthroline, following ISO 6332. In both cases, a Unicam UV/Vis UV2 spectrophotometer was employed. Dissolved organic carbon (DOC) was measured after sample filtration through a 0.22 μm Nylon filter, on a Shimadzu TOC-VCSN analyzer. The degradation rate of the two pesticides was monitored on a UPLC/UV Agilent Technologies Series 1200, equipped with a C-18 ZORBAX XDB C-18 analytical column. The column was kept at 30 °C and the injection volume was 50 μL. A linear gradient profile with water and acetonitrile (ACN) eluted at a flow rate of 1 mL min^{-1} was established as follows: 0–4 min, isocratic at 85/15 (v/v) H_2O/ACN; 4–8 min, gradient from 85/15 to 20/80 (v/v); 8–15 min, isocratic at 85/15 (v/v). Re-equilibration time was 3 min. The UV signals for MET and PYR were monitored at the wavelength of their maximum absorption, 230 nm and 270 nm, respectively. For UPLC analyses, 9 mL of sample were filtered through a 0.22 μm PTFE syringe filter. Then, it was washed with 1 mL of UPLC grade ACN to extract any compound adsorbed on the filter. The pH of the treated solution was monitored by means of a Crison 25 pH-meter.

3. Results and discussion

3.1. Influence of independent experimental variables on the in situ H_2O_2 electrogeneration

The results obtained from the experimental design matrix including the two independent variables (pH, j) are shown in Table 2. The

Table 2
Design of experiments and results.

Run	Independent variables		Responses (t = 5 min)		Responses (t = 30 min)	
	pH	j (mA cm^{-2})	[H_2O_2] (mg L^{-1})	% CE	[H_2O_2] (mg L^{-1})	% CE
1	3	100	15.11	71.40	48.12	37.90
2	7	30	4.97	78.30	18.06	47.05
3	5	65	10.41	75.70	34.85	42.30
4	7	100	8.88	42.00	31.55	24.90
5	3	30	5.93	93.40	19.67	51.70
6	3	100	13.41	63.40	45.25	35.70
7	5	65	9.23	67.20	31.42	38.10
8	5	100	9.71	45.90	34.25	27.00
9	3	65	8.93	65.00	33.59	40.70
10	7	100	8.45	40.00	30.16	23.80
11	5	100	8.36	39.60	29.90	23.60
12	5	30	6.23	98.20	21.15	55.60
13	5	65	8.67	63.10	30.55	37.00
14	5	30	5.49	86.60	19.80	52.00
15	3	30	5.75	90.70	19.85	52.20
16	7	65	7.71	56.10	27.85	33.80
17	3	65	9.67	70.30	33.38	40.50
18	7	65	6.58	47.90	24.54	29.80
19	7	30	4.84	76.30	17.89	47.00

responses (H_2O_2 concentration and % CE) are presented at two electrolysis times, 5 and 30 min, corresponding to approximately one and five circulations of the initial feed solution volume (25 L) through the electrochemical cell, respectively. The average values of the two responses at 30 min are illustrated in Fig. 2a, whereas the changes in H_2O_2 mass production rate over the electrolysis time are depicted at constant pH = 3.0 (Fig. 2b) or j = 100 mA cm^{-2} (Fig. 2c).

As expected, a higher accumulation of H_2O_2 was found as the electrolyses were prolonged, although this occurred in concomitance with current efficiency decrease (Table 2). This is also confirmed from the profiles of the H_2O_2 production rates with time, since the highest values were attained at the beginning of the electrolyses until quasi-steady values were observed at longer times, regardless of the j (Fig. 2b) or the pH (Fig. 2c) studied. According to Eq. (6), the gradual lower efficiency with electrolysis time is related to the reduced [H_2O_2]/Q ratio as a result of nonlinear increase of the accumulated H_2O_2. This kind of behavior can be partly explained by the use of batch operation mode, since the H_2O_2 production rate at the air-diffusion cathode from Reaction (1) becomes equal to its decomposition rate by parasitic reactions that can take place in the cell. For example, the continuous recirculation of H_2O_2 accumulated in the solution may promote its electrochemical reduction at the cathode surface (Reaction (8)) and, to much lesser extent, its spontaneous disproportion in the bulk (Reaction (9)) [11].

$$H_2O_2 + 2H^+ + 2e^- \rightarrow 2H_2O \quad (8)$$

$$H_2O_2 \rightarrow ½\ O_{2(g)} + H_2O \quad (9)$$

Furthermore, considering that an undivided electrochemical reactor is employed, other additional parasitic reactions occur, as for example the oxidation of H_2O_2 to O_2 at the Nb-BDD anode surface via $HO_2^{\cdot}$ as an intermediate, according to the following reactions:

$$H_2O_2 \rightarrow HO_2^{\cdot} + H^+ + e^- \quad (10)$$

$$HO_2^{\cdot} \rightarrow O_{2(g)} + H^+ + e^- \quad (11)$$

In addition, it is worth mentioning that H_2O_2 decomposition is promoted as the solution pH becomes more alkaline, according to the following reaction:

$$H_2O_2 + OH^- \rightarrow H_2O + HO_2^- \quad (12)$$

As a consequence of these undesired reactions, the accumulated H_2O_2 concentration is always below the theoretical maximum. As explained

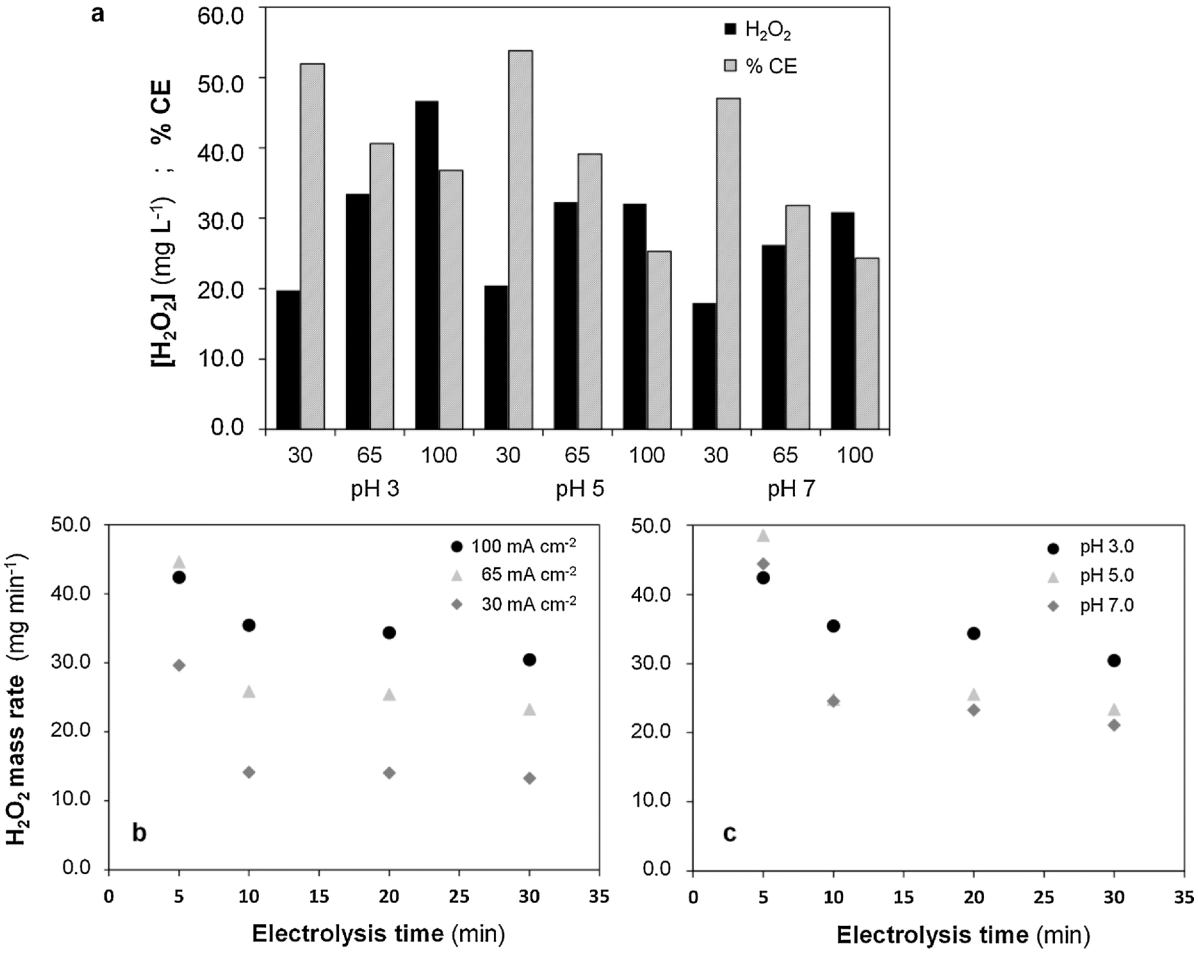

Fig. 2. (a) Accumulated H_2O_2 concentration and current efficiency (% CE) at different pH values and current densities (j). The values were obtained after 30 min of continuous recirculation of a 50 mM Na_2SO_4 solution at a liquid flow rate of 4.4 L min^{-1} and air flow rate of 5 L min^{-1}. (b) H_2O_2 production rate as function of electrolysis time, at constant pH = 3.0 and various j values. (c) H_2O_2 production rate as function of electrolysis time, at constant j = 100 mA cm^{-2} and varying pH.

in the Introduction, undivided reactors are the best choice for water treatment, but divided ones should be employed for industrial electrochemical H_2O_2 production. Note that similar trends for H_2O_2 accumulation have been reported by Brillas and co-workers, as shown during the electrolysis of Na_2SO_4 solutions in a similar batch filter-press BDD/GDE reactor at j values between 50 and 150 mA cm^{-2} [29].

In addition, Fig. 2b and c show that the maximum H_2O_2 production was achieved at 100 mA cm^{-2} and pH 3.0. This agrees with the fact that a higher electron and proton supply promotes a faster O_2 reduction from Reaction (1).

3.2. Validation of the correlation models

With the aid of Design Expert software, the models that best correlated the responses and the independent variables shown in Table 2 were:

(i) Quadratic model:

$$[H_2O_2] = 2.19 - 0.31 \cdot pH + 0.81 \cdot j - 0.05 \cdot pH \cdot j + 0.15 \cdot pH^2 - 2.42 \times 10^{-3} \cdot j^2 \quad (12)$$

- Two-factor interaction model (2FI):

$$\% \text{ CE} = 61.68 - 0.43 \cdot pH - 0.18 \cdot j - 0.0275 \cdot pH \cdot j \quad (13)$$

Both models were validated by the analysis of variances (ANOVA), and the results are summarized in Table 3. The statistical significance was assessed by means of Fisher's test. The F-values calculated for the lack of fit of the quadratic and the 2FI models were 30.44 and 60.89, respectively, suggesting that they are satisfactory. Similar conclusions can be drawn from the low probability values (p-value) at a 95% confidence level (< 0.0001) for both models. The statistical significance of the two models is also verified from Fig. 3, since the actual values of the accumulated H_2O_2 concentration and current efficiency are randomly distributed around the mean of predicted values. Moreover, good linear correlations between the predicted and observed values for H_2O_2 concentration and % CE, with corresponding R^2 values of 0.932 and 0.924, were obtained.

According to the ANOVA analysis (Table 3), the effects of the independent variables (A-pH, B-j) were obvious and the effective order was j > initial pH, whereas the interaction of the two variables (AB) was not obvious (p-value > 0.1). This can also be deduced from Fig. 2b and c, which show that the H_2O_2 production is more substantially affected by j (Fig. 2b) rather than by solution pH, with the latter showing only a slight superiority at pH 3.0 as compared to neutral pH (Fig. 2c). This is important, since the adjustment of pH when treating wastewater complicates the process and increases the water salinity and the operation cost (for acidification and subsequent neutralization).

3.3. Optimization by response surface methodology

To better assess the effect of pH and j on H_2O_2 production and current efficiency and identify their optimum values, 3D response

Table 3
ANOVA results for response surface of the Quadratic and 2FI models.

Source	Sum of squares	Degree of freedom	Mean square	F-value	p-value	
Quadratic model	1225.26	5	245.05	30.44	< 0.0001	significant
A-pH	206.75	1	206.75	25.68	0.0002	
B-*j*	880.82	1	880.82	109.41	< 0.0001	
AB	98.63	1	98.63	12.25	0.0039	
A^2	1.56	1	1.56	0.19	0.6673	
B^2	38.61	1	38.61	4.80	0.0474	
Residual	104.66	13	8.05			
Lack of fit	73.34	3	24.45	7.80	0.0056	not significant
Pure error	31.33	10	3.13			
2FI model	1723.02	3	574.34	60.89	< 0.0001	significant
A-pH	228.38	1	228.38	24.21	0.0002	
B-*j*	1466.34	1	1466.34	155.45	< 0.0001	
AB	28.31	1	28.31	3.00	0.1037	
Residual	141.49	15	9.43			
Lack of fit	102.41	5	20.48	5.24	0.0127	not significant
Pure error	39.08	10	3.91			

surfaces and contour maps were developed with the aid of Design Expert software. The response surface plot shown in Fig. 4 implies that the generation of H_2O_2 increases with j at acidic pH values. On the other hand, the current efficiency (Fig. 5) decreases as j is raised, regardless of the initial pH of the electrolyte solution. As explained above, this is attributed to the batch operation mode in an undivided cell configuration, which promotes the activation of detrimental side reactions. Four sets of optimum pH and j values were proposed by the statistical software (Table 4), yielding maximum H_2O_2 production and current efficiency. Among the four solutions proposed, solution number 1, requiring electrolyte pH = 3.0 and j = 73.66 mA cm^{-2} (~74.0), was selected as the optimum one. Under these conditions, a set of experiments was conducted aiming to validate the two correlation models (Eqs. (12) and (13)) and to investigate the effect of other operation conditions like liquid and air flow rates, as well as electrolyte concentration. The main goal was to fully optimize the electrocatalytic H_2O_2 production at plant scale, eventually yielding the most effective (highest H_2O_2 production rate), efficient (maximum CE percentage) and profitable (lowest energy consumption) process at large scale.

The results of two replicate experiments under the aforementioned optimum conditions are summarized in Table 5. The relative errors were below 5% for both, H_2O_2 generation and % CE (3.69% and 4.38%, respectively), demonstrating the excellent fitting of the experimental results (actual values) with those predicted by the two models.

3.3.1. Effect of liquid flow rate

The feed flow rate is closely related to the hydraulic residence time (HRT) of the treated solution within the electrochemical cell. This is of great significance under continuous operation mode, where the feed solution is continuously treated and discharged. For batch operation, as is the case of the experiments carried out in this work, the recirculation flow rate does not necessarily match the HRT, but it rather affects the mixing and may create turbulent flow within the electrochemical cell. This, in turn, may intensify the mass transport induced by the higher local concentration of molecular oxygen dissolved in the aqueous phase. Indeed, when the flow rate was doubled (from 2.8 to 5.6 L min^{-1}), H_2O_2 production was gradually greater at each given time (Fig. 6b), finally increasing by 28.8% at 30 min (Fig. 6a, [H_2O_2] in mg min^{-1}). Current efficiency also increased in the same proportion, as a result of the higher H_2O_2 generation at similar charge consumption (note that energy consumption varied between 1.97 and 2.00 kWh m^{-3} for all pilot runs) (Fig. 6a).

3.3.2. Effect of air flow rate

Large feeding of air or pure O_2 to the air chamber is often needed to counterbalance the existing pressure on the wet face of the GDE, thereby avoiding flooding that would stop the H_2O_2 production. If correctly adjusted, an increase in air flow rate may upgrade the H_2O_2 accumulation. As found for the pilot plant studied in this work, a rise in

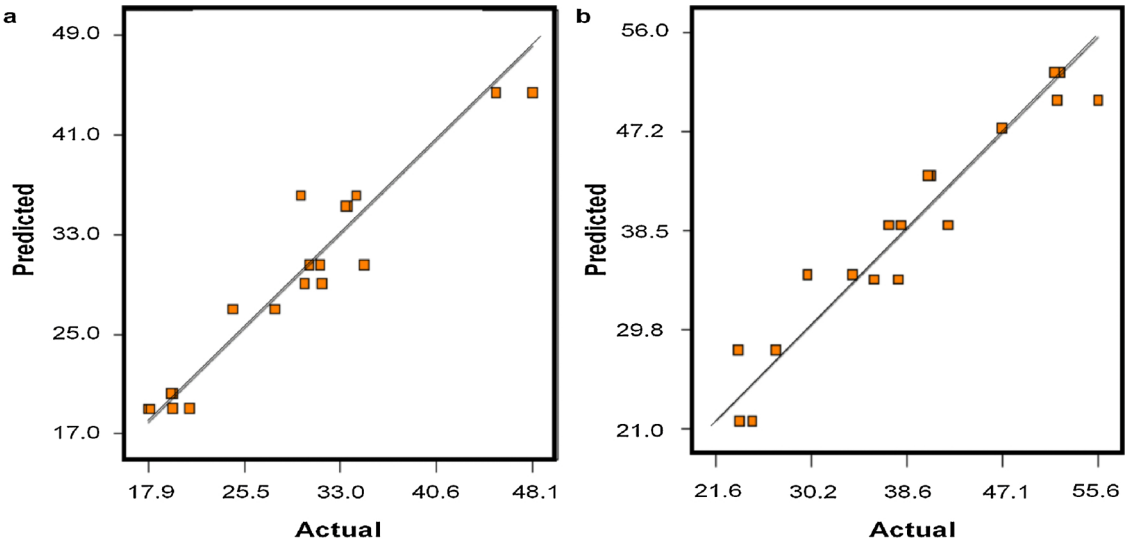

Fig. 3. Comparison of the actual results obtained experimentally regarding (a) H_2O_2 production and (b) current efficiency (in %), with those predicted via central composite design Eqs. (12) and (13), respectively.

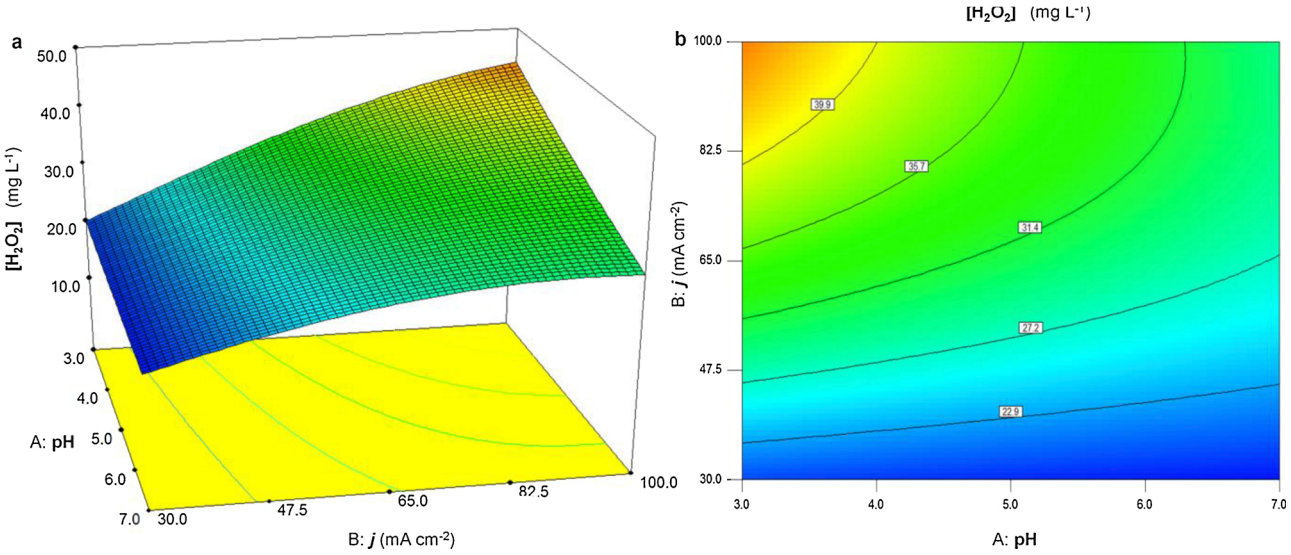

Fig. 4. (a) 3D surface plot and (b) contour plot for the H_2O_2 production as function of the initial pH (A) and current density (B). Experimental data correspond to 30-min electrolyses under continuous recirculation of a 50 mM Na_2SO_4 solution at liquid flow rate of 4.4 L min^{-1} and air flow rate of 5 L min^{-1}.

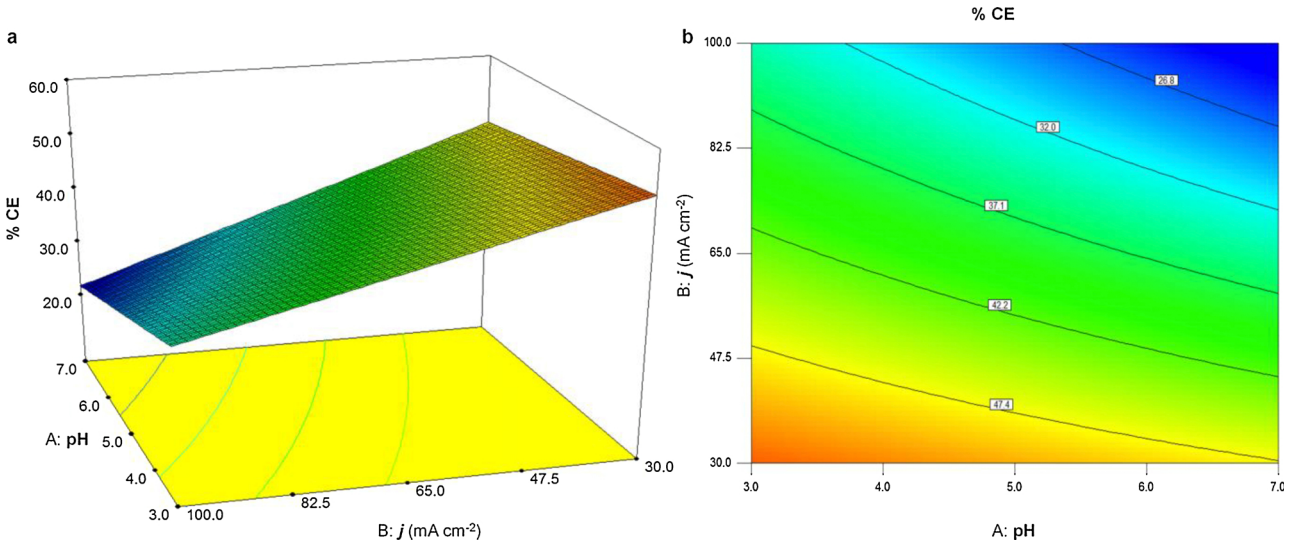

Fig. 5. (a) 3D surface plot and (b) contour plot for current efficiency (in %), as in Fig. 4.

Table 4
Optimum operation conditions proposed by Design Expert 7.0.0 software to attain maximum H_2O_2 concentration and current efficiency at 30 min of electrolysis.

Test number	pH	j (mA cm^{-2})	[H_2O_2] (mg L^{-1})	% CE	Desirability	
1	3.00	73.66	38.0961	41.0744	0.604	Selected
2	3.00	74.16	38.2467	40.9437	0.604	
3	3.00	72.82	37.8392	41.2949	0.604	
4	3.00	70.00	36.9532	42.0343	0.603	

Table 5
Models validation under optimum conditions, with experimental data obtained after 30 min of electrolysis under continuous recirculation of 50 mM Na_2SO_4 solution at pH 3.0, 74 mA cm^{-2}, liquid flow rate of 3.3 L min^{-1} and air flow rate of 5 L min^{-1}. Two independent runs were performed.

	Run		Average actual values	Predicted values	Relative error (%)
	a	b			
H_2O_2 (mg L^{-1})	35.51	38.07	36.79	38.20	3.69
% CE	37.80	40.60	39.20	40.99	4.38

the air flow rate from 2.5 and 5 L min^{-1} to 10 L min^{-1}, resulted in an enhanced H_2O_2 production by 23.1% and 15.6% at 30 min, respectively (Fig. 7a and b). Moreover, the kinetics of H_2O_2 production was faster at the maximum air flow rate of 10 L min^{-1} (Fig. 7b), with no negative effect on the corresponding energy consumption, which was similar at all air flow rates examined. This is interesting, since one might presume that an excessive air feeding could generate too many bubbles within the electrochemical reactor, thereby increasing the ohmic drop and also affecting the stability of the liquid flow rate, which did not occur.

Based on these results, as well as on the better performance of the plant at high electrolyte flow rates, it can be concluded that the combined increase of air and liquid flow rates may effectively enhance the fraction of oxygen consumed for H_2O_2 production (Reaction (1)) over the total amount of air fed. Indeed, under the optimum operation conditions, namely 50 mM Na_2SO_4 solution at pH 3.0 treated at 74 mA cm^{-2}, with liquid flow rate of 5.6 L min^{-1} and air flow rate of 10 L min^{-1}, the highest H_2O_2 mass production rate and current efficiency were

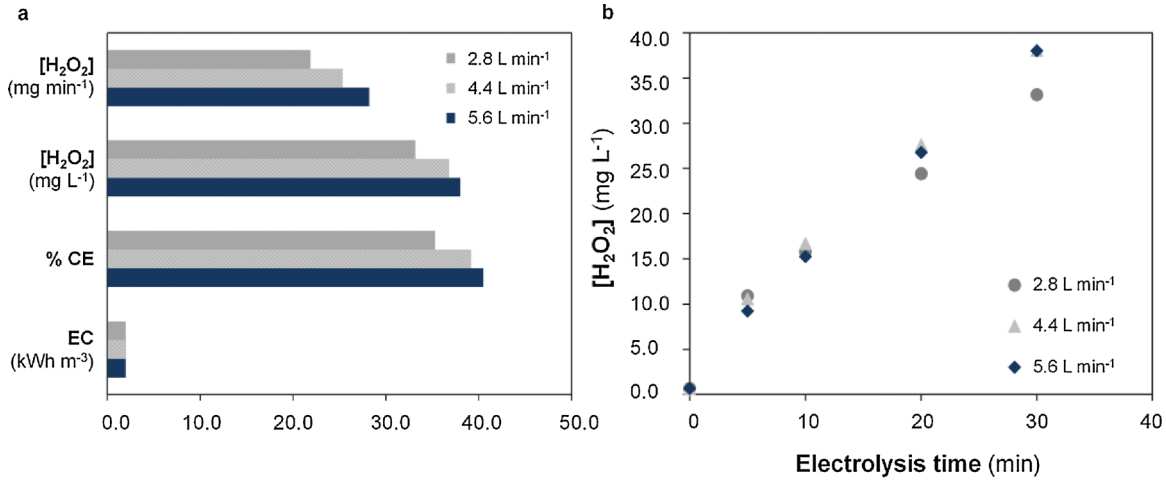

Fig. 6. (a) Effect of liquid flow rate on various process efficiency parameters, corresponding to 30-min electrolyses; (b) accumulated H_2O_2 as a function of electrolysis time, at three different liquid flow rates. Fixed parameters: 50 mM Na_2SO_4 at pH 3.0, j = 74 mA cm^{-2}, air flow rate of 5 L min^{-1}.

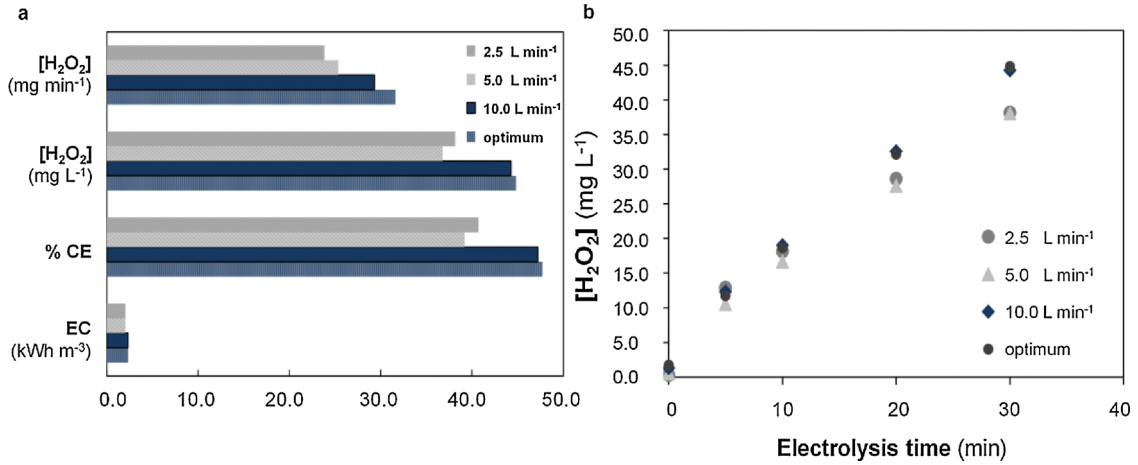

Fig. 7. (a) Effect of air flow rate on various process efficiency parameters, corresponding to 30-min electrolyses; (b) accumulated H_2O_2 as function of electrolysis time, at different air flow rates. Fixed parameters: 50 mM Na_2SO_4 at pH 3.0, j = 74 mA cm^{-2}, liquid flow rate of 4.4 L min^{-1}. The optimum trial corresponds to the same conditions but using a liquid flow rate of 5.6 L min^{-1} and air flow rate of 10 L min^{-1}.

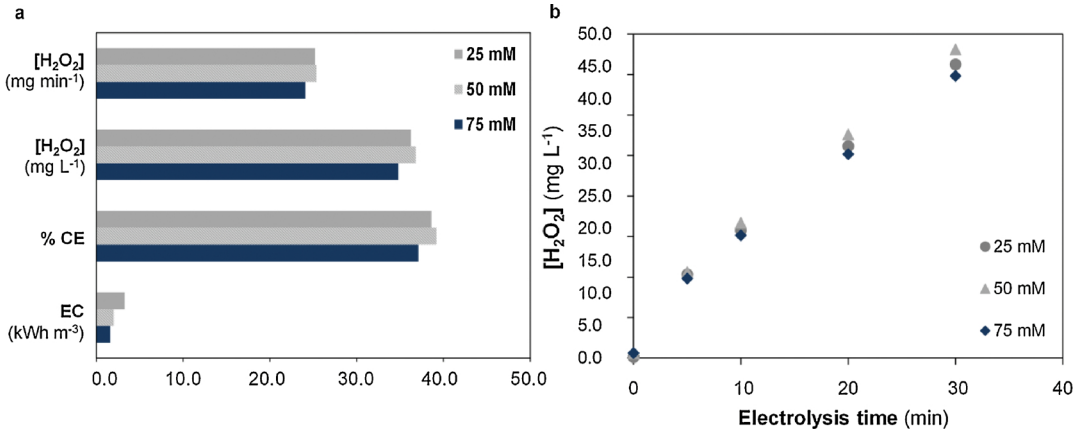

Fig. 8. (a) Effect of Na_2SO_4 molar concentration on various process efficiency parameters, corresponding to 30-min electrolyses; (b) accumulated H_2O_2 as a function of electrolysis time, at three different electrolyte concentrations. Fixed parameters: electrolyte solution at pH 3.0, j = 74 mA cm^{-2}, liquid flow rate of 4.4 L min^{-1} and air flow rate of 5 L min^{-1}.

obtained. In the first 5 min of electrolysis, these conditions led to H_2O_2 production with a mass rate of 64.9 mg min^{-1}, 89.3% current efficiency and energy consumption of 0.4 kWh m^{-3}. These values are among the best achieved with similar system configurations. For example, Flox et al. [29] reported a production rate of ca. 23 mg min^{-1} at 30 min in 50 mM Na_2SO_4 at pH 3.0, 100 mA cm^{-2} and liquid flow rate of 3 L min^{-1}, whereas Fig. 7a shows a higher H_2O_2 electrogeneration rate of 32 mg min^{-1} at that time.

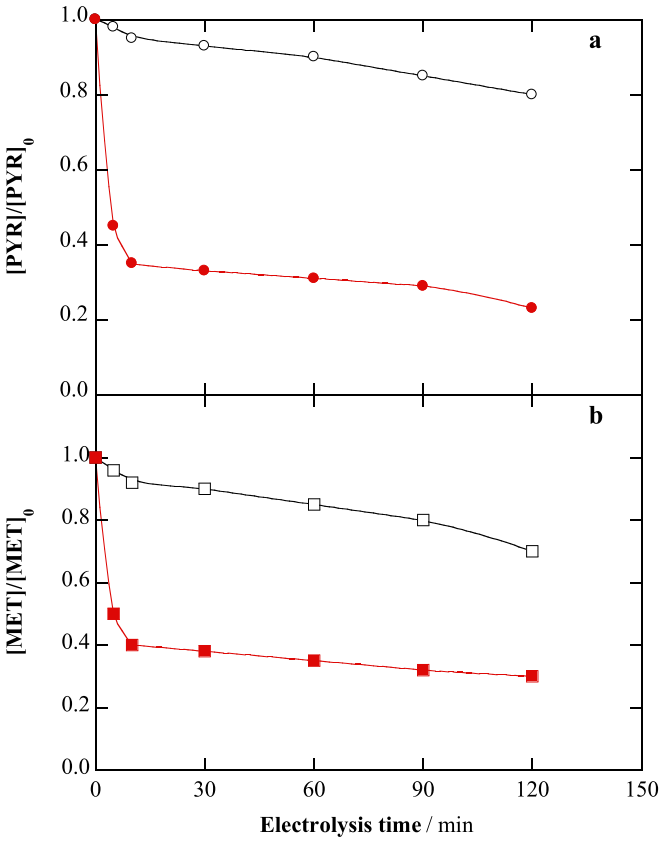

Fig. 9. Normalized concentration decays of pesticides (a) pyrimethanil (PYR) and (b) methomyl (MET) versus electrolysis time during the (○,□) electro-oxidation (EO) and (●,■) solar photoelectro-Fenton (SPEF) treatment of 75 L of mixtures of both pesticides (71 mg L^{-1} DOC) in deionized water with 50 mM Na_2SO_4 at pH 3.0 using the pilot plant at j = 74 mA cm^{-2}, liquid flow rate of 5.6 L min^{-1} and air flow rate of 10 L min^{-1}. SPEF treatment was performed in the presence of 0.5 mM Fe^{2+} as catalyst.

3.3.3. Effect of electrolyte concentration

Considering the rather small electrode gap (6 mm) between the anode and cathode in the electrochemical cell, it was assumed that the solution conductivity would not significantly affect the production of H_2O_2. Therefore, a set of experiments was made to determine the possible influence of electrolyte concentration. It was observed that, within the range of 25–75 mM of Na_2SO_4, which is equal to a solution conductivity range of 4.6–12.3 mS cm^{-1}, the accumulation of H_2O_2 was quite analogous, being only slightly higher in the case of 50 mM (Fig. 8). However, a rather substantial effect is observed regarding the energy consumption, since a higher conductivity led to a gradually lower consumption; i.e. 3.24, 2.00 and 1.61 kW h m^{-3} at 25, 50 and 75 mM Na_2SO_4, respectively. This was expected, since the increase of electrolyte concentration causes a reduction of the ohmic resistance in the bulk solution, and accelerates the electron transfer, thus decreasing the overall charge consumption. From these findings, it can be concluded that the system would be more efficient at higher water conductivity. Therefore, future industrial application of this technology should focus on high conductivity wastewater or be coupled with membrane technologies for treating membrane concentrates.

3.4. Treatment of a mixture of pesticides

After the optimum operation conditions were determined for attaining the best balance between H_2O_2 production and current efficiency, the plant performance was validated by carrying out several tests to assess its capability to degrade a mixture of two model SOCs, namely PYR and MET, which were treated by sun-assisted AOPs like solar photo-Fenton [6,51]. All the assays were made with 75 L of mixtures of both pesticides in water with 50 mM Na_2SO_4 under optimized conditions: pH 3.0, 74 mA cm^{-2} and air flow rate of 10 L min^{-1}.

First, a mixture containing 50 mg L^{-1} PYR and 90 mg L^{-1} MET (i.e., 71 mg L^{-1} DOC) was treated by EO with electrogenerated H_2O_2. The influence of liquid flow rate (2.8, 4.4 and 5.6 L min^{-1}) was investigated, aiming to promote a larger oxidation of both organic contaminants either by increasing the HRT (at a lower flow rate) or by enhancing the mass transport of pollutants to the anode surface (at a higher flow rate). However, no significant effect of this parameter was found, which suggests that the amount of BDD(˙OH) produced via Reaction (2) at 74 mA cm^{-2} was high enough to react with both pesticides regardless of the hydrodynamic conditions (within the studied range). Fig. 9a and b depict the normalized decays of PYR and MET concentrations at a liquid flow rate of 5.6 L min^{-1}, respectively. As can be seen, the degradation by EO-H_2O_2 was very slow, only attaining 20% and 30% of PYR and MET removal after 120 min. The larger degradation of MET could be explained by the greater electrocatalytic behavior of BDD with this pesticide as a result of a more favorable adsorption on its surface, thus reacting more quickly with physisorbed BDD(˙OH). At the end of the electrolysis, almost no mineralization was achieved in EO process, in agreement with the refractory nature of typical reaction by-products like carboxylic acids [10–13]. In all these trials, the energy consumption was around 10 kW h m^{-3}.

The same pesticides mixture was treated by EF, using the optimized parameters with liquid flow rate of 5.6 L min^{-1}, in the presence of different amounts of Fe^{2+} as catalyst (not shown). After 120 min, a higher degradation percentage was reached for both pesticides, with up to 35% and 40% for PYR and MET, respectively. This demonstrates that the H_2O_2 produced under optimized conditions reacted with added Fe^{2+} according to Fenton's reaction, yielding homogeneous ˙OH that enhanced the degradation because this radical acted concomitantly with BDD(˙OH). The former was confined into the reactor, whereas the latter radical was transported throughout the whole volume. In contrast, DOC abatement only attained 8% as maximum, which agrees with the high stability of Fe(III)-carboxylate complexes formed as intermediates [11]. Worth mentioning, a much larger mineralization was achieved working with a pesticide mixture that accounted for 20 mg L^{-1} DOC, using 1.0 mM Fe^{2+}. In this case, 32% DOC removal was attained at 120 min. It is also important to note that the Fe^{2+} concentration remained almost constant during all these EF trials, which confirms the capability of the cathode to regenerate it from Fe (III) reduction.

Finally, the mixtures with 71 mg L^{-1} DOC were comparatively treated by SPEF using the best Fe^{2+} concentration (i.e., 0.5 mM). In these experiments, required accumulated UV energy, Q_{UV}, was 7.1 kJ L^{-1}. As it can be observed in Fig. 9, 55% and 50% removal of PYR and MET was reached in only 5 min, which confirms the fast Fe^{2+} photoregeneration with additional ˙OH production from Reaction (3). At longer time, the degradation was much slower, but ended in 77% and 70% removal, respectively, at 120 min. This is a much better performance as compared to EO and EF, which was further confirmed by DOC abatements higher than 15%, in agreement with the powerful action of UV/Vis photons on Fe(III)-carboxylate complexes according to Reaction (4).

4. Conclusions

The successful performance of the largest SPEF pilot plant existing to date has been demonstrated in this work. The core of the plant, the filter-press electrochemical reactor, is comprised of a Nb-BDD anode and a GDE as cathode. Optimization of main operation parameters has been carried out according to a thorough experimental design, in order to maximize the electrocatalytic H_2O_2 production with a high current efficiency. Optimum values obtained for the key parameters were: pH 3.0,

74 mA cm^{-2}, liquid flow rate of 5.6 L min^{-1} and air flow rate of 10 L min^{-1}. Their application yielded a mass rate of up to 64.9 mg H_2O_2 min^{-1}, current efficiency of 89.3% and energy consumption of 0.4 kWh m^{-3} during the first minutes. The SPEF treatment of 75 L of pesticides mixtures allowed the removal of more than 50% of each pesticide in only 5 min, whereupon further degradation as well as mineralization of by-products and their Fe(III) complexes became much slower but always superior to EO and EF treatments. Further optimization of the SPEF process for treating different kind of wastewater in the integrated pilot system is in progress.

Acknowledgments

The authors wish to thank the EU funded SFERA-II project (7th Framework Programme, Grant Agreement n. 312,643), a Transnational Access program which aims at boosting scientific collaboration among the leading European institutions in solar concentration systems. Financial support from project CTQ2016-78616-R (AEI/FEDER, EU) is also acknowledged.

References

[1] R. Loos, B.M. Gawlik, G. Locoro, E. Rimaviciute, S. Contini, G. Bidoglio, Environ. Pollut. 157 (2009) 561–568.
[2] The NORMAN Network, (2012) (Accessed 15 May 2018), http://www.norman-network.net/?q=Home.
[3] J.-Q. Jiang, Z. Zhou, V.K. Sharma, Microchem. J. 110 (2013) 292–300.
[4] B. Petrie, R. Barden, B. Kasprzyk-Hordern, Water Res. 72 (2015) 3–27.
[5] C. Postigo, D. Barceló, Sci. Total Environ. 503–504 (2015) 32–47.
[6] I. Oller, S. Malato, J.A. Sánchez-Pérez, M.I. Maldonado, R. Gassó, Catal. Today 129 (2007) 69–78.
[7] D.J.E. Costa, J.C.S. Santos, F.A.C. Sanches-Brandão, W.F. Ribeiro, G.R. Salazar-Banda, M.C.U. Araujo, J. Electroanal. Chem. 789 (2017) 100–107.
[8] M. Popescu, C. Sandu, E. Rosales, M. Pazos, G. Lazar, M.A. Sanromán, J. Electroanal. Chem. 808 (2018) 455–463.
[9] C. Comninellis, A. Kapałka, S. Malato, S.A. Parsons, I. Poulios, D. Mantzavinos, J. Chem. Technol. Biotechnol. 83 (2008) 769–776.
[10] M.A. Oturan, J.-J. Aaron, Crit. Rev. Environ. Sci. Technol. 44 (2014) 2577–2641.
[11] E. Brillas, I. Sirés, M.A. Oturan, Chem. Rev. 109 (2009) 6570–6631.
[12] L. Feng, E.D. van Hullebusch, M.A. Rodrigo, G. Esposito, M.A. Oturan, Chem. Eng. J. 228 (2013) 944–964.
[13] C.A. Martínez-Huitle, M.A. Rodrigo, I. Sirés, O. Scialdone, Chem. Rev. 115 (2015) 13362–13407.
[14] S. Chen, Z. Chen, S. Siahrostami, T.R. Kim, D. Nordlund, D. Sokaras, S. Nowak, J.W.F. To, D. Higgins, R. Sinclair, J.K. Nørskov, T.F. Jaramillo, Z. Bao, ACS Sustain. Chem. Eng. 6 (2018) 311–317.
[15] T. Pérez, G. Coria, I. Sirés, J.L. Nava, A.R. Uribe, J. Electroanal. Chem. 812 (2018) 54–58.
[16] S. Siahrostami, A. Verdaguer-Casadevall, M. Karamad, D. Deiana, P. Malacrida, B. Wickman, M. Escudero-Escribano, E.A. Paoli, R. Frydendal, T.W. Hansen, Ib Chorkendorff, I.E.L. Stephens, J. Rossmeisl, Nature Mater. 12 (2013) 1137–1143.
[17] E. Pizzutilo, O. Kasian, C.H. Choi, S. Cherevko, G.J. Hutchings, K.J.J. Mayrhofer, S.J. Freakley, Chem. Phys. Lett. 683 (2017) 436–442.
[18] C. Ridruejo, F. Alcaide, G. Álvarez, E. Brillas, I. Sirés, J. Electroanal. Chem. 808 (2018) 364–371.
[19] G.-L. Chai, Z. Hou, T. Ikeda, K. Terakura, J. Phys. Chem. C 121 (2017) 14524–14533.
[20] V. Čolić, S. Yang, Z. Révay, I.E.L. Stephens, Ib Chorkendorff, Electrochim. Acta 272 (2018) 192–202.
[21] S. Yang, A. Verdaguer-Casadevall, L. Arnarson, L. Silvioli, V. Čolić, R. Frydendal, J. Rossmeisl, Ib Chorkendorff, I.E.L. Stephens, ACS Catal. 8 (2018) 4064–4081.
[22] A. Dirany, I. Sirés, N. Oturan, A. Özcan, M.A. Oturan, Environ. Sci. Technol. 46 (2012) 4074–4082.
[23] M. Panizza, A. Dirany, I. Sirés, M. Haidar, N. Oturan, M.A. Oturan, J. Appl. Electrochem. 44 (2014) 1327–1335.
[24] G. Coria, T. Pérez, I. Sirés, J.L. Nava, J. Electroanal. Chem. 757 (2015) 225–229.
[25] K.V. Plakas, S.D. Sklari, D.A. Yiankakis, G.Th. Sideropoulos, V.T. Zaspalis, A.J. Karabelas, Water Res. 91 (2016) 183–194.
[26] A. Galia, S. Lanzalaco, M.A. Sabatino, C. Dispenza, O. Scialdone, I. Sirés, Electrochem. Commun. 62 (2016) 64–68.
[27] Z.G. Aguilar, E. Brillas, M. Salazar, J.L. Nava, I. Sirés, Appl. Catal. B: Environ. 206 (2017) 44–52.
[28] S. Lanzalaco, I. Sirés, M.A. Sabatino, C. Dispenza, O. Scialdone, A. Galia, Electrochim. Acta 246 (2017) 812–822.
[29] C. Flox, J.A. Garrido, R.M. Rodríguez, P.-L. Cabot, F. Centellas, C. Arias, E. Brillas, Catal. Today 129 (2007) 29–36.
[30] G.R. Agladze, G.S. Tsurtsumia, B.-I. Jung, J.-S. Kim, G. Gorelishvili, J. Appl. Electrochem. 37 (2007) 375–383.
[31] M. Giomo, A. Buso, P. Fier, G. Sandonà, B. Boye, G. Farnia, Electrochim. Acta 54 (2008) 808–815.
[32] E. Brillas, J. Casado, Chemosphere 47 (2002) 241–248.
[33] B. Chaplin, Environ. Sci.: Processes Impacts 16 (2014) 1182–1203.
[34] E. Brillas, J. Braz. Chem. Soc. 25 (2014) 393–417.
[35] C. Flox, P.L. Cabot, F. Centellas, J.A. Garrido, R.M. Rodríguez, C. Arias, E. Brillas, Appl. Catal. B: Environ. 75 (2007) 17–28.
[36] A. Thiam, I. Sirés, E. Brillas, Water Res. 81 (2015) 178–187.
[37] J.R. Steter, E. Brillas, I. Sirés, Appl. Catal. B: Environ. 224 (2018) 410–418.
[38] A.R.F. Pipi, I. Sirés, A.R. De Andrade, E. Brillas, Chemosphere 109 (2014) 49–55.
[39] F. Gozzi, I. Sirés, A. Thiam, S.C. de Oliveira, A. Machulek Jr., E. Brillas, Chem. Eng. J. 310 (2017) 503–513.
[40] F.C. Moreira, J. Soler, A. Fonseca, I. Saraiva, R.A.R. Boaventura, E. Brillas, V.J.P. Vilar, Appl. Catal. B: Environ. 182 (2016) 161–171.
[41] G. Coria, T. Pérez, I. Sirés, E. Brillas, J.L. Nava, Chemosphere 198 (2018) 174–181.
[42] C. Espinoza, J. Romero, L. Villegas, L. Cornejo-Ponce, R. Salazar, J. Hazard. Mater. 319 (2016) 24–33.
[43] L.C. Almeida, S. Garcia-Segura, N. Bocchi, E. Brillas, Appl. Catal. B: Environ. 103 (2011) 21–30.
[44] E. Isarain-Chávez, R.M. Rodríguez, P.L. Cabot, F. Centellas, C. Arias, J.A. Garrido, E. Brillas, Water Res. 45 (2011) 4119–4130.
[45] S. Garcia-Segura, E. Brillas, Electrochim. Acta 140 (2014) 384–395.
[46] V.S. Antonin, S. Garcia-Segura, M.C. Santos, E. Brillas, J. Electroanal. Chem. 747 (2015) 1–11.
[47] S. Garcia-Segura, E. Brillas, Appl. Catal. B: Environ. 181 (2016) 681–691.
[48] T. Pérez, I. Sirés, E. Brillas, J.L. Nava, Electrochim. Acta 228 (2017) 45–56.
[49] S. Malato, J. Blanco, A. Campos, J. Cáceres, C. Guillard, J.M. Herrmann, A.R. Fernández-Alba, Appl. Catal. B: Environ. 42 (2003) 349–357.
[50] M. Panizza, G. Cerisola, Chem. Rev. 109 (2009) 6541–6569.
[51] A. Zapata, T. Velegraki, J.A. Sánchez-Pérez, D. Mantzavinos, M.I. Maldonado, S. Malato, Appl. Catal. B: Environ. 88 (2009) 448–454.

Target 2. Nanofiltration retentate treatment from urban wastewater secondary effluent by solar electrochemical oxidation processes

Contents lists available at ScienceDirect

Separation and Purification Technology

journal homepage: http://ees.elsevier.com

Nanofiltration retentate treatment from urban wastewater secondary effluent by solar electrochemical oxidation processes

I. Salmerón [a,b], G. Rivas [a,b], I. Oller [a,b], A. Martínez-Piernas [b], A. Agüera [b], S. Malato [a,b]

[a] Plataforma Solar de Almería-CIEMAT. Ctra Senés km 4, 04200 Tabernas (Almería), Spain
[b] CIESOL, Joint Centre of the University of Almería-CIEMAT, 04120 Almería, Spain

ARTICLE INFO

Keywords
Boron doped diamond
Electrochemistry
Micropollutants
Solar-assisted electrooxidation
Wastewater regeneration

ABSTRACT

Comparison of electrochemical processes at pilot plant scale for the elimination of organic microcontaminants in actual urban wastewater treatment plant secondary effluents pre-treated by nanofiltration ($[Cl^-]$ = 1100–2000 mg L^{-1}) membranes (for reducing total volume to be treated and increase water salinity), has been addressed. Anodic oxidation (AO), solar-assisted AO, electro Fenton (EF) and solar photoelectro-Fenton (SPEF) processes have been evaluated by using, when required, ethylenediamine-N,N'-disuccinic acid (EDDS) as complexing agent to maintain iron in solution at natural pH. Target water was spiked with a mix solution of microcontaminants: pentachlorophenol, terbutryn, chlorfenvinphos and diclofenac at initial concentrations of 500 and 100 μg L^{-1}, each. AO and EF processes obtained similar degradation rates as added EDDS competed with microcontaminants for oxidant species. SPEF and solar assisted AO showed that high chloride concentrations was a crucial factor since chlorine species generated by solar-assisted AO were enough for efficient microcontaminant removal avoiding the addition of EDDS. Degradation monitoring of microcontaminants contained in actual urban wastewater treatment plant effluents was carried out by liquid chromatography coupled to hybrid quadrupole-linear ion trap-mass spectrometry.

1. Introduction

The growth of chemical industry based on the development of products for personal care, pharmaceuticals or pesticides, involves the widespread in the environment of new recalcitrant substances unable to be removed by conventional secondary biological reactors in urban wastewater treatment plants. These substances are known as organic microcontaminants, which, despite being in low concentrations, in the range of ng L^{-1} - μg L^{-1}, can represent a serious concern to water bodies. Their direct impact on the ecosystem is still unknown and they can even affect humans due to their potential bioaccumulation. For this reason, the removal of microcontaminants is one of the main issues in wastewater regeneration, being crucial for the sustainability of modern chemical processes, the reuse of treated wastewater and the quality of water bodies [1].

Separation processes have been widely applied on water regeneration. Nanofiltration or reverse osmosis commercial membranes have been applied for the removal of personal care products, drugs and pesticides from various water matrices [2] obtaining a very good quality permeate stream but also a retentate enriched with ions and microcontaminants [3–5]. Specifically, composite polyamide membranes exhibit greater rejection performance compared to other materials [2].

Electrochemical treatments can be considered highly interesting to be combined with membrane processes. They can be applied before membranes with the aim of reducing fouling [6] to prevent pore wetting enhancing the operational life of membranes [7] or after them for the treatment of the rejection streams. The main benefit when applied to the retentate is the reduction on the total volume to be treated, also involving an increase of microcontaminant concentration jointly with a decrease of the electrolyte ohmic resistance (increase of salinity), and so requiring lower cell voltage which would reduce the consumption of energy [8]. Accordingly, a higher concentration of ionic species in the retentate entails a higher electrogeneration of oxidants, increasing the capacity to remove recalcitrant organic compounds [9].

Regarding electrodes material, boron doped diamond (BDD) anodes present several characteristics that make them the most suitable for wastewater depuration: (i) capability of self-cleaning through fouling oxidation [10], (ii) high corrosion resistance, (iii) stability up to high anodic potentials, (iv) high oxygen evolution over-potential, involving high reactivity towards organics oxidation and (v) higher efficient use of electrical energy regarding other electrode materials [9,11–13].

In the regeneration of high salinity wastewaters by BDD anodes, additionally to the generation of hydroxyl radicals ($^{\bullet}OH$) (E^0 = 2.8 V) at the anode surface, it is promoted the formation of a large number of oxidants in the bulk solution from dissolved ions. They are mainly active chlorine species (hypochlorous acid and hypochlorite ion, E^0 = 1.49 V, E^0 = 0.86 V, respectively) and chloride radicals (E^0 = 2.4 V) from chlorides (reactions (1)–(4)) [14], sulphate radicals (E^0 = 2.5–3.1 V) (reaction (5)) [15], and even ozone (E^0 = 2.07 V) as product of low-saline water electrolysis (below 20 μS cm^{-1}) (reaction (6)) [16,17], increasing the oxidative treatment capacity. The formation of oxidants in the bulk solution is limited by mass transfer as reactions are produced on the surface of the anode with limited contact area.

$$2Cl^- \rightarrow Cl_{2(aq)} + 2e^- \quad \text{(R.1)}$$

https://doi.org/10.1016/j.seppur.2020.117614
Received 21 May 2020; Received in revised form 12 August 2020; Accepted 17 August 2020

$$Cl_{2(aq)} + HO^- \rightarrow ClO^- + Cl^- + H^+ \quad (R.2)$$

$$HClO \rightleftarrows ClO^- + H^+ \quad (R.3)$$

$$Cl^- \rightarrow Cl^{\bullet} + e^- \quad (R.4)$$

$$SO_4^{2-} \rightarrow SO_4^{\bullet} + 2e^- \quad (R.5)$$

$$3H_2O \rightarrow O_3 + 6e^- + 6H^+ \quad (R.6)$$

The use of a gas diffusion electrode as cathode allows on-line H_2O_2 electrogeneration by O_2 reduction (reaction (7)), so by adding iron, Fenton reactions are promoted and the process is known as electro-Fenton (EF) (reactions (8) & (9)), producing an extra source of $^{\bullet}OH$ in the bulk solution [18–21]. EF together with the potentially great amount of oxidizing species that could be generated in the anode, is considered as a powerful technology for the depuration of high saline waters as it was recently demonstrated by Tawabini et al. [22].

$$O_{2(g)} + 2H^+ + 2e^- \rightarrow H_2O_2 \quad (R.7)$$

$$Fe^{2+} + H_2O_2 \rightarrow Fe^{3+} + {}^{\bullet}OH + OH^- \quad (R.8)$$

$$Fe^{3+} + H_2O_2 \rightarrow Fe^{2+} + HO_2^{\bullet} + H^+ \quad (R.9)$$

Furthermore, this process can be improved by the application of solar light, regenerating Fe^{3+} to Fe^{2+} and so allowing to occur photo-Fenton process, which is known as solar photoelectro-Fenton (SPEF) (reaction (10)). SPEF also promotes the formation of chlorine radicals from the active chlorine species by radiation at 310 and 313 nm [23,24] (reactions (11) and (12)).

$$[Fe(OH)]^{2+} + h\nu \rightarrow Fe^{2+} + {}^{\bullet}OH \quad (R.10)$$

$$ClO^- + H_2O + h\nu \rightarrow Cl^{\bullet} + {}^{\bullet}OH + OH^- \quad (R.11)$$

$$HClO + h\nu \rightarrow Cl^{\bullet} + {}^{\bullet}OH \quad (R.12)$$

Working at neutral pH along EF and SPEF processes require the addition of a complexing agent to avoid iron precipitation. In this sense, EDDS is highly used as a safe and environmentally benign complexing agent in Fenton-like processes [25]. However, since Fe^{3+}:EDDS complex is photosensitive its stability under photocatalytic processes is limited, being degraded till $Fe(OH)_3$ that immediately precipitates. A detailed study of Fe^{3+}:EDDS photodecarboxylation mechanism during solar photo-Fenton processes has been developed by Soriano-Molina et al. [26] which can be simplified in reactions (13)–(17)[27].

$$Fe^{3+}\text{:EDDS} + h\nu \rightarrow [Fe^{3+}\text{:EDDS}]^* \quad (R.13)$$

$$[Fe^{3+}\text{:EDDS}]^* \rightarrow Fe^{2+}\text{:EDDS} + H^+ \quad (R.14)$$

$$Fe^{2+}\text{:EDDS} + H_2O_2 \rightarrow Fe^{3+}\text{:EDDS} + {}^{\bullet}OH + OH^- \quad (R.15)$$

$$Fe^{2+}\text{:EDDS} + \rightarrow Fe^{2+} + \text{EDDS}^{3-\bullet} \quad (R.16)$$

$$Fe^{2+} + H_2O_2 \rightarrow Fe(OH)_3 + {}^{\bullet}OH + OH^- \quad (R.17)$$

An exhaustive literature review has evidenced a scarce number of works focused on the evaluation of solar-assisted electrochemical processes for the depuration of real and complex wastewaters, finding only purely electrochemical processes [9,28–30]. In consequence, it must be highlighted that one of the key strong points of the present study is the application of electrooxidation treatments not only at pilot plant scale but also to different actual wastewaters.

The present work addresses the comparison of different electrochemical treatments: anodic oxidation (AO), EF, SPEF and AO assisted by solar energy, in order to find the best alternative for the treatment of nanofiltration retentates. Two different water matrices were evaluated: a synthetic retentate with medium content of chlorides (in the range of 550 mg L^{-1}, from natural water) and an actual wastewater with higher concentration of chlorides (in the range of 1200–2000 mg L^{-1}, after nanofiltration pre-concentration of an urban wastewater treatment plant effluent), spiked with a mix of four microcontaminants (pentachlorophenol, terbutryn, chlorphenvinfos, and diclofenac). All the processes were tested at natural pH. In the case of EF and SPEF, iron was kept in solution at natural pH by the addition of the commercial chelate Ethylenediamine-N,N'-disuccinic acid (EDDS) as iron complexing agent [31]. Once the most suitable electrochemical treatment was selected, an assay was carried out to verify the effectiveness of the process for the removal of microcontaminants actually contained in the nanofiltration retentate of an urban wastewater treatment plant effluent. Microcontaminant degradation was monitored by liquid chromatography coupled to a hybrid quadrupole/linear ion trap mass spectrometer.

2. Materials and methods

2.1. Water matrices

2.1.1. Simulated nanofiltration retentate

A synthetic recipe of simulated nanofiltration retentate was developed according to the composition described by Miralles-Cuevas et al. [32], of the retentate obtained from an urban wastewater treatment plant effluent from El Ejido (Almería, Spain) operating in batch mode after achieving a volume retention factor of 4. This means reducing 4 times the initial effluent volume, taking into account that nanofiltration membranes do not retain monovalent ions. Maximum values for main ions were stablished as follows: 500 mg L^{-1} of Cl^-, 1500 mg L^{-1} of SO_4^{2-}, 1050 mg L^{-1} of Na^+, 213 mg L^{-1} of Ca^{2+}, 20 mg L^{-1} of NH_4^-, 50 mg L^{-1} of Mg^{2+}, 40 mg L^{-1} of K^+ and 100 mg L^{-1} of NO_3^-. To avoid a strong $^{\bullet}OH$ scavenger effect, inorganic carbon was established at 160 mg L^{-1}, which corresponds to the natural inorganic carbon found in the tap water at the Plataforma Solar de Almería, Spain.

According to these premises, simulated nanofiltration retentate was formulated by using 82 mg L^{-1} of $Ca(NO_3)_2$ (from Sigma-Aldrich), 1420 mg L^{-1} of Na_2SO_4 (from Sigma-Aldrich), 87 mg L^{-1} of K_2SO_4 (from Merck Millipore), 340 mg L^{-1} of $CaSO_4$ (from Panreac), 497 mg L^{-1} of NaCl (from Sigma-Aldrich), 66 mg L^{-1} of $(NH_4)_2SO_4$ (from Merck Millipore) and 21 mg L^{-1} of Na_2HPO_4 (from Panreac) dissolved in natural water. The final ionic composition of the simulated nanofiltration retentate and natural water are shown in Table SI-1 (see supplementary information).

2.1.2. Urban wastewater treatment plant effluent

Actual urban wastewater treatment plant secondary effluent was collected from El Ejido (Almería, Spain) during dry season, (April - July 2019). Before experimentation, wastewater was filtered through a 75 μm sand filter and two polypropylene wound filter cartridges of 25 and 5 μm, respectively. Most significant physicochemical measured parameters were: 2.1–2.3 mS cm^{-2} of conductivity and chemical oxygen demand (COD) between 17 and 50 mg L^{-1}. The rest of the effluent characterization is shown in Table SI-2 (see supplementary information).

2.2. Chemicals

Selected target microcontaminants were pentaclorophenol, terbutryn, chlorphenvinfos and diclofenac (from Sigma-Aldrich, analytical grade). Microcontaminants were previously dissolved in methanol in two stock solutions of 2.5 and 6.25 g L^{-1} (of each microcontaminant), aiming to add to the experiments the similar amount of dissolved organic carbon (DOC) coming from methanol, when working at low initial concentrations, between 100 and 200 μg L^{-1}, or higher, 500 μg L^{-1}.

Fe^{3+}:EDDS complex, in a concentration rate of 0.1:0.2 mM, was prepared dissolving iron (III) sulfate hydrate (~75% pure) from Panreac into acidified water (pH 2.8) in darkness conditions. After this, the desired amount of EDDS (from Sigma-Aldrich) was added stirring vigorously until the solution took a very intense yellow colour indicating the proper formation of the complex.

2.3. Analytical measurements

A LAQUAact PH110 (HORIBA) portable pHmeter was used to monitor pH. Electric conductivity was determined by a GLP 31 conductimeter from CRISON. DOC and carbonates were measured by a TOC-VCSN analyser (Shimadzu), after filtering the samples through 0.45 μm nylon filter from ASIMIO. COD was measured by a Cell Test Spectroquant® from Merck.

Anion and cation concentrations were measured by ion chromatography in a Metrohm 850 Professional IC after sample dilution (1:10 and 1:25, *v/v*) and filtration through a 0.45 μm nylon filter from ASIMIO. For anions, it was used a Metrosep A Supp 7 150/4.0 column thermoregulated at 45°C with 3.6 mM of sodium carbonate as eluent at 0.7 mL min^{-1}. For cations the column used was a Metrosep C6 150/4.0 with an eluent solution of 1.7 mM nitric acid and 1.7 mM dipicolinic acid at1.2 mL min^{-1}.

Free available chlorine was determined by the DPD Method 10069 from Hach, using DPD powder pillows and measuring absorbance at 530 nm. Iron concentration was measured following ISO 6332 and hydrogen peroxide following DIN 38409 H15, at 510 nm and 410 nm, respectively. The spectrophotometer used for those analyses was an Evolution 220 UV–Visible from Thermo Scientific.

Degradation of microcontaminants was monitored by a UPLC/UV Agilent Series 1200 system, equipped with a reverse phase column ZORBAX Eclipse XDB-C18 (4.6 × 50 mm, 1.8 μm particle size, Agilent Technologies). Initial conditions of the method were 90/10 (*v/v*) ultrapure water with formic acid 25 mM and acetonitrile, achieving in 14 min 100% acetonitrile at a flow rate of 1 mL min^{-1}. Inyection volume was 100 μL. Sample preparation before analysis consisted on a filtration step of 9 mL of the sample through a 0.22 μm hydrofobic polytetrafluoroethylene (PTFE) membrane filter from Millipore Millex. Then, the filter was flushed with 1 mL of acetonitrile in order to extract any absorbed compound. Analytical characteristics of the microcontaminants analyzed by UPLC/UV are shown in Table SI-3 (see supplementary information).

Fe^{3+}:EDDS concentration was determined by a HPLC Agilent 1100 Series with a reversed-phase column Luna C18 (150 × 3.00 mm, 5 μm particle size), using an isocratic method 95/5 (*v/v*) on buffer solution (2 mM tetrabutylammonium bisulfate – 15 mM sodium formiate) and methanol. Inyection volume was 20 μL with a flow rate of 0.5 mL min^{-1}. Maximun absortion of Fe^{3+}:EDDS occurs at 240 nm, and the limit of quantification was 0.005 mM.

Evaluation of microcontaminants contained in actual urban wastewater treatment plant secondary effluents was carried out by a liquid chromatography system (Agilent 1200 Series) coupled to a hybrid quadrupole-linear ion trap-mass spectrometer 5500 QTRAP® from Sciex Instruments equipped with an electrospray source (TurboIon Spray), operating in positive polarity. The analytical column was a Kinetex C18 column (150 × 4.6 mm, 2.6-μm particle size; Phenomenex) operated at a constant flow rate of 0.5 mL min^{-1} and using an injection volume of 10 μL. Eluent A was 0.1% formic acid in ultrapure water and eluent B was pure methanol. The analytical gradient was as follows: elution started with 20% B for 0.5 min, increased to 50% B within 3 min, and to 100% within 9.5 min, kept constant for 3.5 min and reduced to 20% B in 0.1 min. Total analysis run time was 13.1 min and the post-run equilibration time 6 min. The source settings were: ion spray voltage 5000 V; curtain gas 25 (arbitrary units); GS1 50 psi; GS2 40 psi; and 500 °C. N_2 served as nebulizer, curtain and collision gas. Compounds were analysed by multiple reaction monitoring. To increase the sensitivity of the analytical method, the Schedule MRM™ algorithm was applied with a retention time window of 40s per transition. The optimal MS/MS parameters for each compound are summarized in Table SI-4 (see supplementary information). Sciex Analyst version 1.6.2 software was used for data acquisition and processing. MultiQuant 3.0.1 software was used for quantification purposes.

2.4. Experimental Set-up

2.4.1. Preliminary Fe^{3+}:EDDS complex stability tests

Stability of Fe^{3+}:EDDS in each tested water matrix was evaluated. Also the possible interactions with the highest positive charge ions were studied, as well as the oxidant effect of hypochlorite to Fe^{3+}:EDDS. Experiments were carried out in 1 L borosilicate stirring flasks in the dark. Water matrices used during the tests were demineralized water, demineralized water with 50 mM of Na_2SO_4 and simulated nanofiltration retentate. For checking Mg^{2+} and Ca^{2+} effect, $MgSO_4$ and $CaSO_4$ were added in the concentration required to attain the same amount of divalent cations found in the simulated nanofiltration retentate, that is 247.6 mg L^{-1} and 724.8 mg L^{-1}, respectively. Finally, hypochlorite effect was checked by adding 10 and 20 mg L^{-1} (as NaClO) in demineralized water.

2.4.2. Nanofiltration pilot plant

Nanofiltration system (Fig. 1a and b) was composed by 400 L polypropylene feeding tank, 2.2 kW centrifugal pump (DP Pumps) with a frequency modulator and spiral-wound FILMTEC NF90-2540 membranes (2.6 m^2 of active area). Tests were carried out by adding the effluent to the feeding tank and passing the water through the membrane, recycling the retentate stream to the feeding tank and discarding the permeate stream. The system was operated in batch mode in order to reduce the total volume to be treated by subsequent electrooxidation processes. The feeding tank was periodically refilled to reduce 1 m^3 of urban wastewater treatment plant secondary effluent to 250 L that is a volume retention factor of 4. As nanofiltration pilot plant is controlled by a SCADA system, pressure, flow and conductivity of permeate and retentate streams were continuously monitored online.

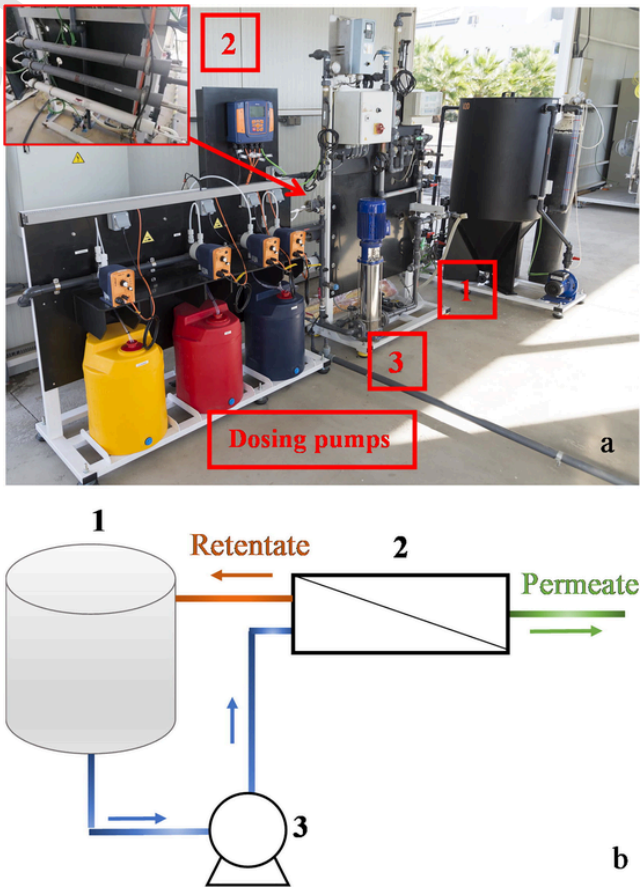

Fig. 1. (a) Nanofiltration pilot plant installed at Plataforma Solar de Almería. (b) Scheme of the pilot plant: (1) feeding tank, (2) nanofiltration membrane system, (3) centrifugal pump.

2.4.3. Electrooxidation pilot plant

Electrooxidation pilot plant consisted of an undivided electrochemical cell (Electro MP Cell from ElectroCell) conformed by a BDD film on a niobium mesh substrate as anode and a carbon-PTFE gas diffusion electrode as cathode, both with 0.010 m^2 geometrical area single-sides, separated by a 6 mm gap. Carbon-PTFE gas diffusion electrode cathode was fed by compressed air (ABAC air compressor, 1.5 kW) at 10 L min^{-1} and water flow rate in the cell was 300 L h^{-1}. When H_2O_2 electrogeneration was not necessary for AO and solar-assisted AO processes, carbon-PTEF cloth was removed using the support as counter cathode. Electrodes were connected to a Delta Electronika power supply (limited to 70 V and 22 A) that fed the cell fixing a constant current density (*j*) of 74 mA cm^{-2}, optimized by Salmerón et al. [33], in order to achieve the maximum H_2O_2 electrogeneration of 64.9 mg H_2O_2 min^{-1} in the first 5 min with 50 mM of Na_2SO_4 as supporting electrolyte.

Electrochemical cell was coupled to a compound parabolic collector (CPC) photo-reactor, consisting of 10 borosilicate glass tubes mounted on an aluminium platform tilted 37° (PSA, 37° N, 2.4° W) with a total illuminated area of 2 m^2 and 23 L of illuminated volume. Working volume was 30 L in dark tests (AO and EF) and 75 L for solar-assisted electrochemical assays (solar-assisted AO and SPEF). Scheme of the solar-assisted electrooxidation pilot plant is shown in Fig. 2.

Experiments were carried out by adding target wastewater (simulated nanofiltration retentate or actual retentate stream) to the rtank of the electrooxidation pilot plant. After that, microcontaminants from the stock solution were added, recirculating till their total homogenization and verifying their initial desired concentration. At that moment AO and solar assisted AO started, but in EF and SPEF assays, Fe^{3+}:EDDS was added after microcontaminants, homogenizing before starting the process.

Temperature was always maintained between 25 and 35°C through a cooling coil connected to a heat exchanger.

Solar global ultraviolet radiation (UV) was measured with a CUV 3 UV radiometer from KIPP & ZONEN, installed at Plataforma Solar de Almería and tilted 37° same as the CPC. Eq. (1) allows the combination of the data from several days' experiment and their comparison with other tests [34].

$$Q_{UV,n} = Q_{UVn-1} + \Delta t_n \bullet \overline{UV}_{G,n} \bullet A_i / V_t; \Delta t_n = t_n - t_{n-1} \quad (1)$$

where $Q_{UV,n}$ (kJ L^{-1}) is the accumulated UV energy per unit of volume, $\overline{UV}_{G,n}$ (W m^{-2}) is the average solar ultraviolet radiation ($\lambda < 400$ nm) measured between t_n and t_{n-1} being *n* the number of sample, A_i is the irradiated surface and V_t is the total volume.

3. Results and discussion

3.1. Testing Fe^{3+}:EDDS stability

EDDS is a structural isomer of ethylenediaminetetraacetic acid but more environmentally friendly, since it is not toxic and presents high biodegradability. EDDS is completely mineralized in a short time in the environment [35], whereas other similar complexing agents are only partially degraded [36,37]. In fact, this advantage has made EDDS one of the most studied complexing agent to keep iron in solution at neutral pH, so enhancing the production of $^{\bullet}OH$, and therefore the degradation of microcontaminants [38].

As determined by Klamerth et al. 2012 [39], Fe^{3+}:EDDS molar ratio of 1:2 is the optimal in terms of degradation and energy consumption. This ratio was successfully used by Miralles-Cuevas et al. 2014 [40] in a complex water matrix (real nanofiltration retentate with a volume retention factor of 4), for the degradation of a mix of microcontaminants in a concentration range of 47–63 μg L^{-1}, each and achieving 95% removal of the sum of microcontaminants in 86 min with a requirement of accumulated UV energy of 21.1 kJ L^{-1}. Fe^{3+}:EDDS behaviour during EF treatment by using 50 mM Na_2SO_4 solution as supporting electrolyte has been described elsewhere [41]. Nevertheless, to check the suitability of Fe^{3+}:EDDS for different electrochemical processes in a highly complex water, an EF assay was carried out with simulated nanofiltration retentate as water matrix at natural pH. Fe^{3+}:EDDS was completely degraded in 15 min despite iron continued in solution for 30 min (Fig. 3), which can be explained by the presence of oxidized species of Fe:EDDS [42].

To evaluate the possible interaction with the highest positive charge ions contained in simulated nanofiltration retentate, the stability of Fe^{3+}:EDDS was tested in the dark by using simulated nanofiltration retentate and demineralized water containing Na_2SO_4 (50 mM), $MgSO_4$ (247.6 mg L^{-1}) and $CaSO_4$ (724.8 mg L^{-1}). Fig. 3 shows, as expected, that the concentration of the complex remained constant in all cases.

As hypochlorite was going to be generated during electrochemical processes (taking into account the characterization of simulated nanofiltration retentate, as well as urban wastewater treatment plant secondary effluent), it was necessary to determine Fe^{3+}:EDDS degradation caused by this oxidant, demonstrating that with 10 and 20 mg L^{-1} of hypochlorite, Fe^{3+}:EDDS kept stable during at least one hour (data not shown).

After these preliminary tests, it was also determined that the use of this complex in electrochemical processes would be suitable for microcontaminant degradation with higher degradation rates. However, it must be stressed that, for the most recalcitrant compounds, the complex would have to be added continuously as it was degraded in 15 min, which would not be pertinent as a continuous addition of organic matter would scavenge microcontaminant degradation.

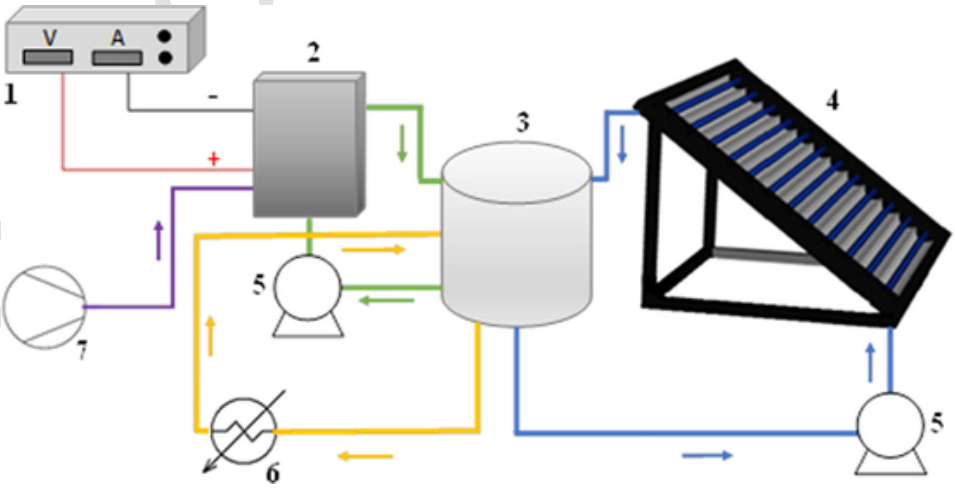

Fig. 2. Main components of the electrochemical pilot plant: (1) power supply, (2) ElectroCell with BDD anode and carbon-PTFE (gas diffusion electrode) cathode, (3) tank, (4) solar CPC photoreactor, (5) centrifugal pumps, (6) heat exchanger, (7) air compressor.

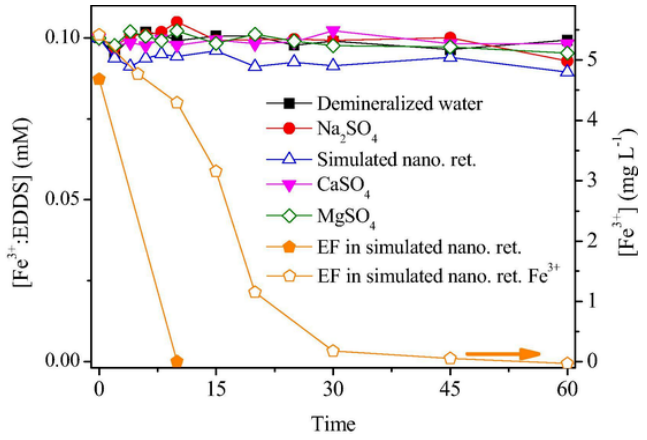

Fig. 3. Evolution of Fe^{3+}:EDDS in different water matrices and during EF processes in simulated nanofiltration retentate matrix. Evolution of dissolved iron (Fe^{3+}) during EF treatment is also plotted (against right Y axis, marked with an arrow).

3.2. Electrochemical oxidation of microcontaminants contained in simulated nanofiltration retentate

As a first approach, AO, EF and SPEF, were tested for the degradation of 200 μg L^{-1} of each selected microcontaminant (pentachlorophenol, terbutryn, chlorphenvinfos and diclofenac) in simulated nanofiltration retentate (Fig. 4a). AO assays were developed as reference, achieving the removal of 83% of the total amount of microcontaminants by applying 13.9 kWh m^{-3}. The organic content, coming from methanol of the microcontaminant stock solutions, simulating the organic carbon of a real urban wastewater treatment plant effluent (around 24 mg L^{-1}), was slightly mineralised (15% of DOC removal). In the case of EF treatment, 88% of the sum of microcontaminants was degraded with slightly higher energy consumption (15.6 kWh m^{-3}), showing similar trend as AO. The addition of Fe^{3+}:EDDS in the EF treatment implied a theoretical increase of 24 mg L^{-1} of organic carbon (52 mg L^{-1} of total initial DOC). So, despite the increasing in $^{\bullet}OH$ production, oxidant species were mainly consumed in the mineralization process of EDDS rather than in microcontaminant degradation, which was demonstrated by the increase in the mineralization percentage till 31%. Similar results were obtained by Huang et al. 2012 [38], in which 2,2-bis-(4-hydroxyphenyl)propane degradation by photo-Fenton was inhibited when the concentration of the complex increased from 0.2 to 0.4 mM evidencing the role of EDDS as a competitor of microcontaminants for $^{\bullet}OH$.

Moreover, in EF treatment, only 2.91 mg L^{-1} of iron remained dissolved after 15 min, being totally precipitated after 30 min. From the moment there was no iron in solution, the degradation process proceeded only through the anode action (mainly physisorbed $^{\bullet}OH$ and active chlorine species).

Since EF treatment did not achieve a substantial improvement in the degradation of microcontaminants compared with AO but entailed the addition of reagents that would imply an increase in operation costs, it was discarded as an alternative for the nanofiltration retentate treatment.

In SPEF process (EF combined with a CPC photoreactor), the volume of water to be treated was much higher (75 L) than in AO or EF (30 L), while electrodes surface remained constant. The production of oxidizing species was determined by the electroactive surface area and the current applied, being the same in both configurations. However, the relative concentration of oxidants depends on the electrode area/volume ratio so lower concentrations in SPEF were reached due to the higher working volume. For such reason, despite the initial concentration of microcontaminants was the same, in terms of mass the amount was much higher in SPEF than in AO or EF.

In SPEF, Fe^{3+}:EDDS was also required for maintaining iron in solution at neutral pH. Despite the increase in the mass of microcontaminants, it was shown an improvement in the degradation rate mostly at the beginning of the treatment, due to the oxidation of Fe^{2+} to Fe^{3+} that allowed photo-Fenton process occurred. Dissolved iron (5.5 mg L^{-1}) remained till 15 min of treatment, showing slow precipitation till 75 min, thus the degradation process went on for the generation of oxidizing species in the anode and for the solar promoted species. 14 kJ L^{-1} of accumulated UV energy were required for 88% elimination of the sum of microcontaminants.

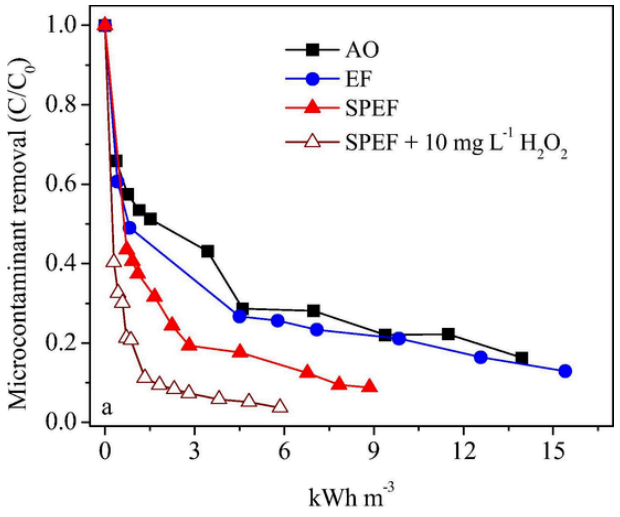

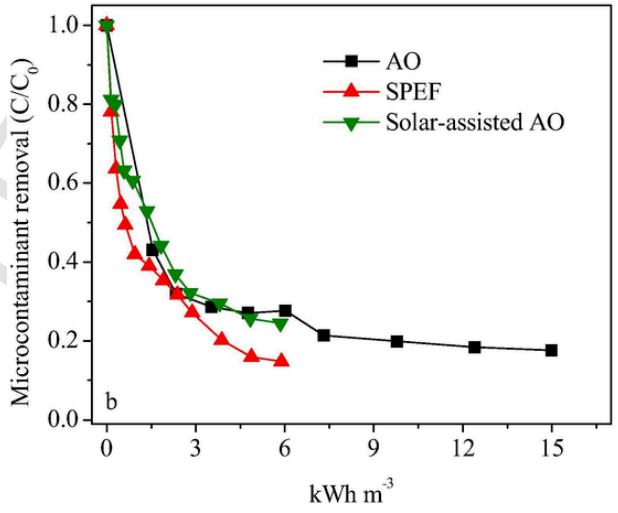

Fig. 4. Removal of the sum of microcontaminants (pentachlorophenol, terbutryn, chlorphenvinfos and diclofenac) in simulated nanofiltration retentate by using different electroxidation processes. (a) initial concentration of each microcontaminant 200 μg L^{-1} and (b) 500 μg L^{-1}, each .

Along SPEF process the generation of H_2O_2 (Reaction (7)) never exceeded an accumulated value of 2.3 mg L^{-1}, which supposed an important limitation in the process. In consequence, an additional SPEF test was carried out by adding 10 mg L^{-1} of H_2O_2 extra at the beginning of the test. In such a case, microcontaminant degradation rate increased greatly, verifying the limitation provoked by the lower ratio between electrode surface and total volume in SPEF compared to AO. Dissolved iron was totally precipitated after 30 min but at that time 80% of microcontaminant removal was achieved. At the end of the treatment 96% of microcontaminants were eliminated with lower electrical energy consumption (5.9 kWh m^{-3}) and an accumulated solar UV energy of 8.8 kJ L^{-1}.

Considering the fast removal obtained when the initial concentration of each microcontaminant was 200 μg L^{-1}, it was decided to increase it to 500 μg L^{-1} for a better monitoring of the operation parameters (Fig. 4b). In this case, AO achieved 70% of microcontaminant removal in 30 min consuming 2.3 kWh m^{-3} of energy (28 mg L^{-1} of free available chlorine and 11 mg L^{-1} of chlorates). From that point, degradation rate decreased and 82% of microcontami-

nant degradation was attained after consuming 15 kWh m^{-3} accompanied by an increase of free available chlorine till 71 mg L^{-1} and chlorates till 55 mg L^{-1}. When SPEF was applied, the removal rate increased significantly, attaining 85% microcontaminant removal with the requirement of 5.9 kWh m^{-3} of electric consumption and 10.5 kJ L^{-1} of Q_{UV} after 180 min of treatment. In this experiment, iron showed the same trend as in previous SPEF test (without adding extra amount of H_2O_2), remaining after 15 min in solution at a concentration of 4.8 mg L^{-1} and precipitating completely after 60 min. At that moment, the treatment went ahead by the action of other oxidant species (active chlorine species among them considering simulated nanofiltration retentate characterization) generated by the anode and assisted by solar energy, keeping free available chlorine stable between 22 and 31 mg L^{-1} until 120 min (chlorates concentration was 17 mg L^{-1}), when 80% of microcontaminant removal was reached.

From this point, free available chlorine started to increase till 71 mg L^{-1} at 180 min achieving 26 mg L^{-1} of chlorates. This means that the degradation promoted by active chlorine species stopped at 120 min and from that point instead of reacting with organics; they were accumulated in the solution as free available chlorine.

In view of the results obtained by SPEF, the excess of free available chlorine produced and how inefficiently it was used at the end of the treatment, it was considered to test solar-assisted AO (without the addition of iron nor the in-situ generation of H_2O_2) in order to evaluate the effect of solar energy on the electrogenerated species and the oxidants produced avoiding the addition of EDDS which competes with microcontaminants for $^{\bullet}OH$.

In solar-assisted AO, chlorides concentration (550–565 mg L^{-1} in simulated nanofiltration retentate) has a crucial role as precursors of active chlorine species. 76% of microcontaminants were degraded after an energy consumption of 5.9 kWh m^{-3} and an accumulated UV energy of Q_{UV} of 11.6 kJ L^{-1}. Free available chlorine showed similar behaviour as in SPEF, being constant (17 – 26 mg L^{-1}) till 150 min and increasing till 85 mg L^{-1} after 180 min of treatment. As well as free available chlorine, chlorates also showed same trend: 22 mg L^{-1} at 150 min and 26 mg L^{-1} at 180 min. Therefore, generated active chlorine species and $Cl^{\bullet}$ in this specific wastewater were not enough to completely degrade the sum of microcontaminants, evidencing the crucial role of $^{\bullet}OH$ in SPEF.

3.3. Actual nanofiltration retentate treatment by electrochemical oxidation processes

Several batches (1 m^3 each) of secondary effluent were taken from the urban wastewater treatment plant of El Ejido (Almería) and introduced in the nanofiltration system (till attaining a volume retention factor of 4). Permeate stream generated contained only some monovalent ions that passed across the membrane (DOC below 2 mg L^{-1} and carbonates below 25 mg L^{-1}), thus the conductivity kept under 100 μS cm^{-1} during the most of the nanofiltration process and below 200 μS cm^{-1} at the end due to the operation in batch mode. In such operation mode, retentate stream was recirculated into the feeding tank to reduce the total volume of final retentate and increase its conductivity for obtaining a better efficiency of electrochemical processes. Table 1 shows its main physicochemical characteristics.

Commonly, actual concentration of microcontaminants in urban wastewater treatment plant effluents is very low reaching, at most, tens of μg L^{-1} as found in Luo et al. 2014 [43]. For this reason, in actual nanofiltration retentate experiments, the spiked concentration of microcontaminants was 100 μg L^{-1} each (pentachlorophenol, terbutryn, chlorphenvinfos and diclofenac), trying to address a more realistic approach jointly with a direct analysis by UPLC/UV.

From the physicochemical characterization, it must be highlighted the presence of a high concentration of carbonates in the nanofiltration retentate, which are well known scavengers of hydroxyl radicals in Fenton and photo-Fenton processes [44]. Nevertheless, their influence in electro-oxidative processes has not been defined, yet. In order to investigate this matter, each electrochemical treatment was carried out with the natural hydrogen carbonate present in the retentate stream (>1000 mg L^{-1}), but also lowering it till 20 mg L^{-1} by adding acid and purging with air.

Table 1
Characterization of the retentate obtained in the nanofiltration pilot plant from urban wastewater treatment plant secondary effluent.

Parameter	Value	Parameter	Value
Conductivity (mS cm^{-1})	6.1–6.8	**SO_4^{-} (mg L^{-1})**	386–660
NTU	9–45	**Na^{+} (mg L^{-1})**	747–787
pH	8–8.6	**Ca^{2+} (mg L^{-1})**	259–273
DOC (mg L^{-1})	31–42	**NH_4^{+} (mg L^{-1})**	46–76
COD (mg L^{-1})	103–190	**Mg^{2+} (mg L^{-1})**	197–209
HCO_3^{-} (mg L^{-1})	1010–1316	**K^{+} (mg L^{-1})**	62–71
Cl^{-} (mg L^{-1})	1182–1960	**NO_3^{-} (mg L^{-1})**	25–27

Results from AO (Fig. 5) showed exactly the same trend of microcontaminant degradation in high and low hydrogen carbonate concentration, achieving 84% and 83%, respectively. About DOC elimination, it was attained 9% and 12% in the presence of high and low concentration of hydrogen carbonate, respectively, remaining at the end of the treatment 17 mg L^{-1} and 4 mg L^{-1} of free available chlorine, and 47 and 42 mg L^{-1} of chlorates. In both cases results are similar, and the slight difference found can be explained due to the recalcitrant character of the organic matter contained in the different water batches used, that despite achieved higher concentration of oxidizing species, they were not able to degrade the organic content. Therefore, in our study, carbonates had no substantial effect on AO or any scavenger effect on active chlorine species and $Cl^{\bullet}$.

This is consistent with what Xiong et al., [45] described in their study of propranolol degradation with UV-LED/chlorine system testing hydrogen carbonate concentrations till 840 mg L^{-1} (10 mM) without finding a remarkable difference in removal rates.

Regarding SPEF, retentate with high concentration of hydrogen carbonate showed 69% of microcontaminant degradation applying 5.1 kWh m^{-3} and requiring 14.2 kJ L^{-1} of accumulated UV energy. At lower concentration of hydrogen carbonate, with the same electrical consumption (5.2 kWh m^{-3}) and even lower Q_{UV} (10.8 kJ L^{-1}), higher microcontaminant removal was reached (75%) and thus it can be said that carbonates had a slight effect on SPEF. DOC degradation was 17% in both cases, and final free available chlorine was extremely low, 1.1 mg L^{-1} and 0.7 mg L^{-1} under both operation conditions, which means that most of the oxidant species were consumed by the organic load. Regarding chlorates, concentration reached 24 mg L^{-1} and 16 mg L^{-1} for

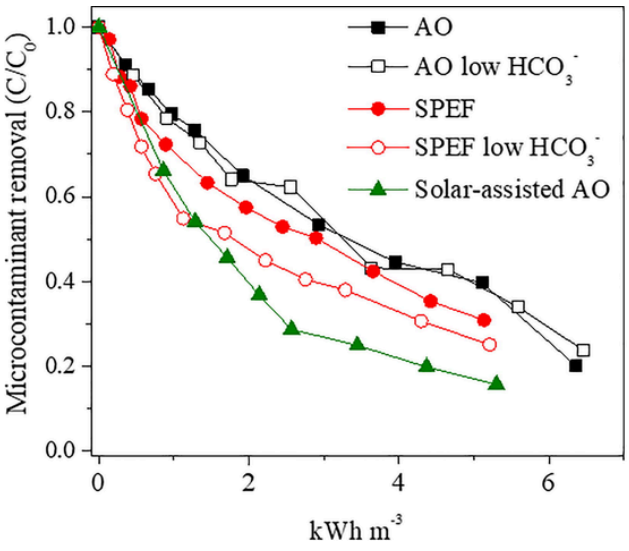

Fig. 5. Removal of the sum of microcontaminants (pentachlorophenol, terbutryn, chlorphenvinfos and diclofenac each one spiked at 100 μg L^{-1}) in actual nanofiltration retentate.

both high and low hydrogen carbonates content, respectively, showing a possible quencher effect in chlorates due to the presence of carbonates in the solution.

Inasmuch AO process was not affected by carbonates concentration, a solar-assisted AO test was developed with the retentate at natural (high) hydrogen carbonate concentration. With 5.3 kWh m^{-3} and 13.8 kJ L^{-1} of accumulated UV energy, 84% of microcontaminant removal was achieved, higher than in all previous experiments. Free available chlorine reached was 3.9 mg L^{-1} slightly higher than in SPEF with the same water matrix even with a lower DOC removal of 9%. Probably provoked by the higher recalcitrant character of organic matter contained in the actual water matrix used in AO and solar-assisted AO in regard with the easy mineralization of EDDS used in SPEF. Chlorates measured at the end of the process were 30 mg L^{-1}, in the same range of previous solar-assisted treatments (solar-assisted AO and SPEF).

In electrochemical treatments, chloride is the precursor of active chlorine species and $Cl^{\bullet}$, thus higher concentration of chloride pose higher electro-generation of active chlorine species. As described by Shu et al. [24], higher concentration of active chlorine species increased in solar processes and resulted in higher radicals generation (reactions (11) and (12)), enhancing microcontaminant degradation rates. Consequently, actual nanofiltration retentate with high concentration of chloride (See table 1), showed electro-generation of higher amount of oxidants, enough to degrade microcontaminants, avoiding the addition of any reagent and therefore, simplifying the process. In consequence, solar-assisted AO was selected as the best alternative for the treatment of nanofiltration retentates.

Finally, the effectiveness of solar-assisted AO was tested under complete actual conditions. A new batch of the urban wastewater treatment plant secondary effluent was introduced into the nanofiltration system, collecting the retentate stream (volume retention factor of 4) without reducing hydrogen carbonate concentration. Actual degradation of the microcontaminants contained in the retentate was monitored by using liquid chromatography coupled to a hybrid quadrupole-linear ion trap-mass spectrometry. A summary of the results is shown in Table 2. Detailed degradation of all microcontaminants contained in the actual effluent during electrochemical treatment, as well as their removal percentages, is shown in Table SI-5 (see supplementary information).

Table 2
Evolution of most relevant microcontaminants (>250 ng L^{-1}) detected by liquid chromatography coupled to a hybrid quadrupole-linear ion trap-mass spectrometry in the urban wastewater treatment plant secondary effluent, as well as their final removal percentage, nanofiltration retentate and their concentration after solar-assisted AO.

	Microcontaminants	El Ejido secondary effluent (ng L^{-1})	Nanofiltration Retentate (ng L^{-1})	After solar-assisted AO (ng L^{-1})	Removal (%) in solar-assisted AO
1	4FAA	7440	28,360	780	97
2	4AAA	3660	14,350	360	98
3	Gabapentin	3250	12,385	2730	78
4	Carbamazepine	1945	7070	3940	44
5	Iminostilbene	1500	5775	3410	41
6	4AA	1170	4580	ND	>99
7	Imidacloprid	1200	4525	2090	54
8	Sulpiride	1045	4060	13	>99
9	Venlafaxine	750	2930	ND	>99
10	Levofloxacin	490	1930	ND	>99
11	Cetirizine	435	1690	1030	39
12	Telmisartan	420	1590	1275	20
13	Irbesartan	400	1550	905	42
14	Diatrizoic acid	380	1460	690	53
15	OMCs < 250 ng L^{-1}	1960	7500	1730	77

*ND: Non detected.

Up to forty-four microcontaminants were detected in the secondary effluent of the urban wastewater treatment plant, highlighting the presence of 4FAA, 4AAA, (dipyrone metabolites) and gabapentin (antiepileptic) which were found in the highest concentrations, 7440, 3660 and 3250 ng L^{-1}, respectively. Eleven microcontaminants were detected at relevant concentrations between 300 and 2000 ng L^{-1} as carbamazepine, iminostilbene and others (see Table 2). The rest of microcontaminants were detected at lower concentrations (<250 ng L^{-1}), being mainly pharmaceuticals as naproxen, diazepam, propanolol or flecainide.

After nanofiltration pre-treatment, 99040 ng L^{-1} of total microcontaminants were found in the retentate stream. After 90 min of solar-assisted AO application to the retentate, with 2.7 kWh m^{-3} of electric consumption and a Q_{UV} of 4.2 kJ L^{-1}, fourteen microcontaminants were substantially degraded (>99%): 4AA, lincomicin, fenofibric acid, indomethacin, naproxen, propranolol, dimethoate, erythromycin, metronidazole, sulfathiazole, trimethoprim, levofloxacin, alfuzosin, domperidone, propafenone, memantine and trazodone. At that point, DOC removal was 9% and measured free available chlorine was only 2.6 mg L^{-1}, indicating the high oxidative power of the process.

At the end of the treatment, 80% of the total amount of microcontaminants detected in the nanofiltration retentate was eliminated (Fig. 6). Energy consumption at the end of the treatment was 5.5 kWh m^{-3} and the required accumulated UV energy was 11.5 kJ L^{-1}. Final DOC removal was similar to previous cases, 19%, and free available chlorine was 8.8 mg L^{-1}. This increase in free available chlorine, from 2.6 to 8.8 mg L^{-1} at the end of the process, means that active chlorine species were not able to efficiently react with the organic compounds still remaining in nanofiltration retentate, much more recalcitrant to oxidation than initial organics, after suffering several oxidation steps (but not mineralized). As it was observed in previous tests, chlorates are generated continuously regardless microcontaminant removal, so the kinetic constant of chlorates generation was calculated: 1.47 ± 0.02 (10^{-1} min^{-1}) (R^2 = 0.996).

Despite being among the pollutants with an important presence (>250 ng L^{-1}), it is remarkable the low removal of telmisartan (20%). Same applies to other compounds such as carbamazepine or iminostilbene, two tricyclic compounds that, despite being detected at higher concentrations than other microcontaminants (>1.5 μg L^{-1}), showed higher stability being only able to reach degradation rates lower that 50%.

4. Conclusions

It has been demonstrated that the combination of an electrochemical device with a solar CPC reactor entails an enhancement in microcontaminant removal percentages regarding pure electrooxidative processes, due to the generation of higher amount of oxidative species.

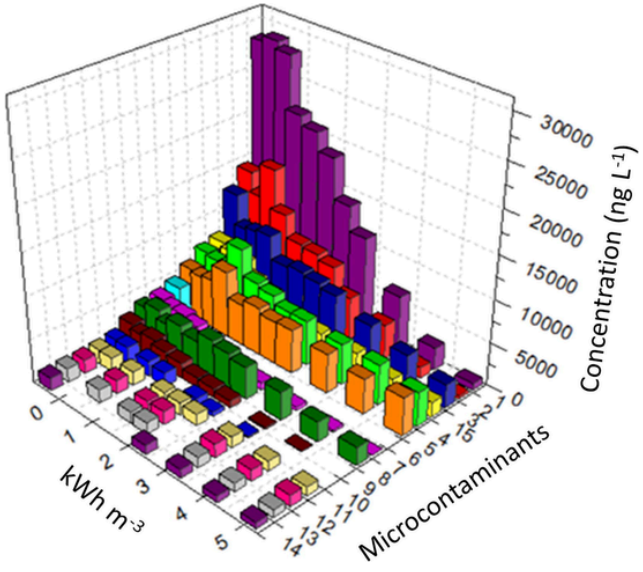

Fig. 6. Removal of microcontaminants contained in actual nanofiltration retentate from

EDDS has been a useful tool to keep iron in solution in solar-assisted processes but taking into consideration that it is only effective during the first part of the treatment due to its degradation by the electrochemical process itself.

If the effluent contains a high concentration of chloride, the use of Fe^{3+}:EDDS could be avoided as only with solar-assisted AO enough oxidant species can be generated for the complete degradation of microcontaminants.

Combined process, nanofiltration and solar-assisted electrooxidation, was successfully applied for the removal of microcontaminants of an actual urban wastewater treatment plant secondary effluent, reaching high degradation for most of them and 80% of elimination of the total amount. On the contrary, it is important to stress that this process is not effective for DOC removal. Such good performance on high elimination percentage of microcontaminants led to the possibility of obtaining high quality treated water (for instance, for reusing purposes), bearing witness on high sustainability of evaluated technologies.

Finally it important to mention that the measurement of high concentrations of chlorates at the end of the electrochemical treatments, makes necessary the performance of risk and health assessment studies before considering the reuse of treated wastewater for crops irrigation.

CRediT authorship contribution statement

I. Salmerón: Methodology, Investigation. **G. Rivas:** Data curation, Visualization. **I. Oller:** Conceptualization, Writing - review & editing. **A. Martínez-Piernas:** . **A. Agüera:** Supervision, Data curation. **S. Malato:** Project administration, Funding acquisition.

CRediT authorship contribution statement

I. Salmerón: Methodology, Investigation. **G. Rivas:** Data curation, Visualization. **I. Oller:** Conceptualization, Writing - review & editing. **A. Agüera:** Supervision, Data curation. **S. Malato:** Project administration, Funding acquisition.

Declaration of Competing Interest

The authors declare that they have no known competing financial interests or personal relationships that could have appeared to influence the work reported in this paper.

Acknowledgements

The authors wish to thank the Spanish Ministry of Science, Innovation and Universities (MCIU), AEI and FEDER for funding under the CalypSol Project (Reference: RTI2018-097997-B-C32).

Appendix A. Supplementary material

Supplementary data to this article can be found online at https://doi.org/10.1016/j.seppur.2020.117614.

References

[1] M Patel, R Kumar, K Kishor, T Mlsna, C U Pittman Jr., D Mohan, Pharmaceuticals of Emerging Concern in Aquatic Systems: Chemistry, Occurrence, Effects, and Removal Methods, Chem. Rev. 119 (2019) 3510–3673.
[2] K V Plakas, A J Karabelas, Removal of pesticides from water by NF and RO membranes — A review, Desalination 287 (2012) 255–265.
[3] C Fonseca Couto, L C Lange, M C Santos Amaral, A critical review on membrane separation processes applied to remove pharmaceutically active compounds from water and wastewater, J. Water Process Eng. 26 (2018) 156–175.
[4] R. Rienzie, S. Ramanayaka, N.M. Adassooriya, Nanotechnology applications for the removal of environmental contaminants from pharmaceuticals and personal care products, in: M. Prasad, M. Vithanage, A. Kapley (Eds.), Pharmaceuticals and Personal Care Products: Waste Management and Treatment Technology, 2019, pp. 279–296.
[5] J. Heo, S. Kim, N. Her, C.M. Park, M. Yu, Y. Yoon, Removal of contaminants of emerging concern by FO, RO, and UF membranes in water and wastewater, in: A. Hernandez-Maldonado, L. Blaney (Eds.), Contaminants of Emerging Concern in Water and Wastewater, 2020, pp. 139–176.
[6] R Gonzalez-Olmos, A Penadés, G Garcia, Electro-oxidation as efficient pretreatment to minimize the membrane fouling in water reuse processes, J. Membr. Sci. 552 (2018) 124–131.
[7] K Rajwade, A C Barrios, S Garcia-Segura, F Perreault, Pore wetting in membrane distillation treatment of municipal wastewater desalination brine and its mitigation by foam fractionation, Chemosphere 257 (2020) 127214.
[8] A Soriano, D Gorri, L T Biegler, A Urtiaga, An optimization model for the treatment of perfluorocarboxylic acids considering membrane preconcentration and BDD electrooxidation, Water Res. 164 (2019) 114954.
[9] G Perez, A R Fernandez-Alba, A M Urtiaga, I Ortiz, Electro-oxidation of reverse osmosis concentrates generated in tertiary water treatment, Water Res. 44 (2010) 2763–2772.
[10] D Rice, P Westerhoff, F Perreault, S Garcia-Segura, Electrochemical self-cleaning anodic surfaces for biofouling control during water treatment, Electrochem. Commun. 96 (2018) 83–87.
[11] M Panizza, Importance of electrode material in the electrochemical treatment of wastewater containing organic pollutants, in: C Comninellis, G Chen (Eds.), Electrochemistry for the Environment, Springer, 2010, pp. 25–54.
[12] Y He, H Lin, Z Guo, W Zhang, H Li, W Huang, Recent developments and advances in boron-doped diamond electrodes for electrochemical oxidation of organic pollutants, Sep. Purif. Technol. 212 (2019) 802–821.
[13] P V Nidheesh, G Divyapriya, N Oturan, C Trellu, M A Oturan, Environmental applications of boron-doped diamond electrodes: 1. Applications in water and wastewater treatment, ChemElectroChem 6 (2019) 2124–2142.
[14] E Mostafa, P Reinsberg, S Garcia-Segura, H Baltruschat, Chlorine species evolution during electrochlorination on boron-doped diamond anodes: In-situ electrogeneration of Cl_2, Cl_2O and ClO_2, Electrochim. Acta 281 (2018) 831–840.
[15] A Farhat, J Keller, S Tait, J Radjenovic, Oxidative capacitance of sulfate-based boron-doped diamond electrochemical system, Electrochem. Commun. 89 (2018) 14–18.
[16] M E H Bergmann, Drinking water disinfection by in-line electrolysis: Product and inorganic by-product formation, in: C Comninellis, G Chen (Eds.), Electrochemistry for the Environment, Springer, 2010, pp. 163–204.
[17] Y Meas, L A Godinez, E Bustos, Ozone Generation Using Boron-Doped Diamond Electrodes, in: E Brillas, C A Martínez-Huitle (Eds.), Synthetic Diamond Films: Preparation, Electrochemistry, Characterization, and Applications, Wiley Online Library, 2011, pp. 311–331.
[18] E Brillas, I Sirés, M A Oturan, Electro-Fenton process and related electrochemical technologies based on Fenton's reaction chemistry, Chem. Rev. 109 (2009) 6570–6631.
[19] E Brillas, A review on the photoelectro-Fenton process as efficient electrochemical advanced oxidation for wastewater remediation. Treatment with UV light, sunlight, and coupling with conventional and other photo-assisted advanced technologies, Chemosphere 250 (2020) 126198.
[20] P V Nidheesh, M Zhou, M A Oturan, An overview on the removal of synthetic dyes from water by electrochemical advanced oxidation processes, Chemosphere 197 (2018) 210–227.
[21] G Divyapriya, P V Nidheesh, Importance of Graphene in the Electro-Fenton Process, ACS omega 5 (2020) 4725–4732.
[22] B S Tawabini, K V Plakas, M Fraim, E Safi, T Oyehan, A J Karabelas, Assessing the efficiency of a pilot-scale GDE/BDD electrochemical system in removing phenol from high salinity waters, Chemosphere 239 (2020) 124714.
[23] L H Nowell, J Hoigné, Photolysis of aqueous chlorine at sunlight and ultraviolet wavelengths—II. Hydroxyl radical production, Water Res. 26 (1992) 599–605.
[24] Z Shu, C Li, M Belosevic, J R Bolton, M G El-Din, Application of a solar UV/chlorine advanced oxidation process to oil sands process-affected water remediation, Environ. Sci. Technol. 48 (2014) 9692–9701.
[25] W Huang, M Brigante, F Wu, C Mousty, K Hanna, G Mailhot, Assessment of the Fe(III)-EDDS complex in Fenton-like processes: from the radical formation to the degradation of bisphenol A, Environ. Sci. Technol. 47 (2013) 1952–1959.
[26] P. Soriano-Molina, J.L. García Sánchez, O.M. Alfano, L.O. Conte, S. Malato, J.A. Sánchez Pérez, Mechanistic modeling of solar photo-Fenton process with Fe3+-EDDS at neutral pH, 233 (2018) 234–242.
[27] P Soriano-Molina, P Plaza-Bolaños, A Lorenzo, A Agüera, J L García Sánchez, S Malato, J A Sánchez Pérez, Assessment of solar raceway pond reactors for removal of contaminants of emerging concern Appl Catal B-Environ., by photo-Fenton at circumneutral pH from very different municipal wastewater effluents, Chem. Eng. J. 366 (2019) 141–149.
[28] A Y Bagastyo, D J Batstone, I Kristiana, W Gernjak, C Joll, J Radjenovic, Electrochemical oxidation of reverse osmosis concentrate on boron-doped diamond anodes at circumneutral and acidic pH, Water Res. 46 (2012) 6104–6112.
[29] A Soriano, D Gorri, A Urtiaga, Efficient treatment of perfluorohexanoic acid by nanofiltration followed by electrochemical degradation of the NF concentrate, Water Res. 112 (2017) 147–156.
[30] S Garcia-Segura, A B Nienhauser, A S Fajardo, R Bansal, C L Coonrod, J D Fortner, M Marcos-Hernández, T Rogers, D Villagran, M S Wong, P Westerhoff, Disparities between experimental and environmental conditions: Research steps toward making electrochemical water treatment a reality, Curr. Opin. Electrochem. 22 (2020) 9–16.
[31] L Clarizia, D Russo, I Di Somma, R Marotta, R Andreozzi, Homogeneous photo-Fenton processes at near neutral pH: A review, Appl. Catal. B: Environ. 209 (2017) 358–371.
[32] S Miralles-Cuevas, I Oller, J A S Perez, S Malato, Removal of pharmaceuticals from MWTP effluent by nanofiltration and solar photo-Fenton using two different iron complexes at neutral pH, Water Res. 64 (2014) 23–31.
[33] I Salmerón, K V Plakas, I Sirés, I Oller, M I Maldonado, A J Karabelas, S Malato, Optimization of electrocatalytic H2O2 production at pilot plant scale for solar-assisted water treatment, Appl. Catal. B-Environ. 242 (2019) 327–336.

[34] S Malato, J Blanco, A Campos, J Caceres, C Guillard, J M Herrmann, A R Fernandez-Alba, Effect of operating parameters on the testing of new industrial titania catalysts at solar pilot plant scale, Appl. Catal. B-Environ. 42 (2003) 349–357.
[35] D Schowanek, T C J Feijtel, C M Perkins, F A Hartman, T W Federle, R J Larson, Biodegradation of [S, S],[R, R] and mixed stereoisomers of ethylene diamine disuccinic acid (EDDS), a transition metal chelator, Chemosphere 34 (1997) 2375–2391.
[36] E Cuervo Lumbaque, D Salmoria Araújo, T Moreira Klein, E R Lopes Tiburtius, J Argüello, C Sirtori, Solar photo-Fenton-like process at neutral pH: Fe(III)-EDDS complex formation and optimization of experimental conditions for degradation of pharmaceuticals, Catal. Today 328 (2019) 259–266.
[37] M Orama, H Hyvönen, H Saarinen, R Aksela, Complexation of [S, S] and mixed stereoisomers of N, N′-ethylenediaminedisuccinic acid (EDDS) with Fe(III), Cu(II), Zn(II) and Mn(II) ions in aqueous solution, J. Chem. Soc., Dalton Trans. (2002) 4644–4648.
[38] W Huang, M Brigante, F Wu, K Hanna, G Mailhot, Development of a new homogenous photo-Fenton process using Fe(III)-EDDS complexes, J. Photoch. Photobio. A. 239 (2012) 17–23.
[39] N Klamerth, S Malato, A Aguera, A Fernandez-Alba, G Mailhot, Treatment of municipal wastewater treatment plant effluents with modified photo-Fenton as a tertiary treatment for the degradation of micro pollutants and disinfection, Environ. Sci. Technol. 46 (2012) 2885–2892.
[40] S Miralles-Cuevas, F Audino, I Oller, R Sánchez-Moreno, J A S Pérez, S Malato, Pharmaceuticals removal from natural water by nanofiltration combined with advanced tertiary treatments (solar photo-Fenton, photo-Fenton-like Fe (III)–EDDS complex and ozonation), Sep. Purif. Technol. 122 (2014) 515–522.
[41] Z Ye, E Brillas, F Centellas, P L Cabot, I Sirés, Electro-Fenton process at mild pH using Fe(III)-EDDS as soluble catalyst and carbon felt as cathode, Appl Catal B-Environ. 257 (2019).
[42] P Soriano-Molina, J L García Sánchez, S Malato, L A Pérez-Estrada, J A Sánchez Pérez, Effect of volumetric rate of photon absorption on the kinetics of micropollutant removal by solar photo-Fenton with Fe3+-EDDS at neutral pH, Chem. Eng. J. 331 (2018) 84–92.
[43] Y Luo, W Guo, H H Ngo, L D Nghiem, F I Hai, J Zhang, S Liang, X C Wang, A review on the occurrence of micropollutants in the aquatic environment and their fate and removal during wastewater treatment, Sci. Total Environ. 473–474 (2014) 619–641.
[44] N Klamerth, N Miranda, S Malato, A Agüera, A R Fernández-Alba, M I Maldonado, J M Coronado, Degradation of emerging contaminants at low concentrations in MWTPs effluents with mild solar photo-Fenton and TiO_2, Catal. Today 144 (2009) 124–130.
[45] R Xiong, Z Lu, Q Tang, X Huang, H Ruan, W Jiang, Y Chen, Z Liu, J Kang, D Liu, UV-LED/chlorine degradation of propranolol in water: Degradation pathway and product toxicity, Chemosphere 248 (2020).

Supplementary Information

Table SI-1. Composition of simulated nanofiltration retentate

	Natural water composition (mg L^{-1})	Final ion concentration in simulated nanofiltration retentate (mg L^{-1})
HCO_3^-	813	813
Cl-	254	555
SO_4^{2-}	169	1465
Na^+	389	1050
Ca^{2+}	73	213
NH_4^+	0	18
Mg^{2+}	50	50
K^+	7.3	46
NO_3^-	11	73
$HPO4^{2-}$	0	14

Table SI-2. Characterization of El Ejido urban wastewater treatment plant effluent

	El Ejido urban wastewater treatment plant effluent
Conductivity (mS cm^{-1})	2.1 - 2.3
NTU	3.1 - 5.9
pH	7.4 - 7.7
DOC	11 - 12
COD	17 - 50
HCO_3^- (mg L^{-1})	264 - 440
Cl^- (mg L^{-1})	423 - 460
SO_4^- (mg L^{-1})	127 - 140
Na^+ (mg L^{-1})	254 - 264
Ca^{2+} (mg L^{-1})	96 - 105
NH_4^+ (mg L^{-1})	22 - 35
Mg^{2+} (mg L^{-1})	66 -67
K^+ (mg L^{-1})	23 - 25
NO_3^- (mg L^{-1})	12 - 31

Table SI-3. Retention time, limit of quantification (LOQ) and maximum absorption wavelength of studied microcontaminants under UPLC-UV analysis.3

OMCs	Retention time (min)	LOQ (μg L^{-1})	Maximum absorption (λ)
PCP	10.4	10	220 nm
TBT	7.7	10	230 nm
CFV	10.9	10	240 nm
DFC	9.6	10	285 nm

Table SI-4. Optimal LC-QqLIT-MS/MS conditions for microcontaminants multiresidue analysis.

Compound	Rt (min)	Precursor ion	Quantifier/ qualifyer	DP[a] (V)	EP[b] (V)	CE[c] (eV)	CXP[d] (V)
10,11 - Dihydrocarbamazepine	9.31	239.3	194.1	66	12	32	10
			180.2	150	10	47	11
4 -AA	5.3	204.2	56.2	45	5	30	2
			159.2	45	5	16	2
4 -AAA	6.62	246.2	228.1	46	5	18	2
			83.1	46	5	40	2
4 -DAA	5.1	232.2	113.2	48	5	17	2
			111.2	48	5	21	2
4 -FAA	6.54	232.2	214.2	60	5	18	2
			77	60	5	50	2
4 -MAA	4.75	218.2	56.1	35	5	30	2
			97.2	35	5	16	2
9-Acridinecarboxilic acid	11.63	224.2	196	63	12	36	11
			167.2	63	12	54	11
			180	63	12	42	10
Acetaminophen	5.8	152.1	110.1	40	5	20	2
			64.8	40	5	45	2
Acetamiprid	7.84	223	126	100	10	30	4
			128	50	13	25	7
Acetanilide	8	136	94	70	10	24	15
			77	70	11	40	10
Alfuzosin	7.17	390.3	235.1	50	12	40	12
			156.1	50	12	37	10
Amitriptyline	8.8	278.4	91.2	30	5	35	2
			233.1	30	5	22	2
Amoxicilin	4.91	366.1	114	70	12	30	19
			208	70	12	13	8

Compound	Rt (min)	Precursor ion	Quantifier/ qualifyer	DP[a] (V)	EP[b] (V)	CE[c] (eV)	CXP[d] (V)
			349.1	70	6	18	11
Antipyrine	7.41	189.2	77.1	48	5	51	2
			104.1	48	5	32	2
Atenolol	3.41	267.3	145.2	70	5	35	2
			190.2	70	5	27	2
Atrazine	9.93	216	174	100	13	25	10
			176	40	8	25	10
Azithromycin	7.07	749.5	83.1	50	11	110	20
			591.4	50	12	40	13
			573.3	50	8	47	14
Azoxystrobin	9.93	404.1	372.2	100	10	20	10
			329	56	10	42	6
Betamethasone	9.76	393.3	373.1	70	10	13	20
			355	70	11	18	20
			147	70	10	39	15
Buprofezin	11.69	306	201	20	11	17	5
			116	20	13	22	6
			106	20	13	40	6
C13 Caffeine	6.95	198.1	140.1	40	5	30	2
			112.2	40	5	35	2
C13 -Phenacetin	8.68	181.3	110.3	150	10	47	11
			139.3	150	10	47	11
Caffeine	6.95	195	138	20	4	27	4
			110	20	5	31	13
			123	20	5	45	5
Carbamazepine	9.38	237.2	194.3	80	5	25	2
			192.1	80	5	35	2
Carbendazim	6.15	192.3	160.1	100	10	27	4
			132.2	100	10	41	4
Cefalexin	6.43	348	158.1	60	12	13	8
			174.1	60	11	20	11
			106.1	150	10	47	11
Cefotaxime	6.76	456.1	324.1	40	5	15	3
			396.1	40	5	10	2
			241.3	40	5	20	2
Cetirizine	9.31	389.4	201	48	12	30	12
			166.2	48	12	55	8
Chlorfenvinphos	10.95	359.1	99	60	10	50	6
			155	100	8	18	10
Chlorpyriphos	12.19	352	97	55	10	55	7
			197.9	96	10	26	6
Chlortetracycline	7.37	479.2	444	100	9	31	10
			462	100	9	24	11
Ciprofloxacin	6.47	332.2	314.3	50	5	25	2

Compound	Rt (min)	Precursor ion	Quantifier/ qualifyer	DP[a] (V)	EP[b] (V)	CE[c] (eV)	CXP[d] (V)
			231.2	50	5	48	2
Citalopram	7.88	325.3	109.1	100	5	30	2
			262.1	100	5	25	2
Clarithromycin	8.87	748.4	158.4	45	5	35	2
			590.4	45	5	26	2
Clindamycin	7.88	425.2	126.1	80	11	35	7
			377.1	80	12	28	9
Clomipramine	9.05	315.2	86.1	40	5	27	2
			58.1	40	5	60	2
Clotrimazole	9.06	344.9	277.3	30	5	15	2
			165	30	5	43	2
Cotinine	3	177	80	45	5	36	2
			98	45	5	26	2
Cyclophosphamide	8.67	261.2	140	40	12	23	12
			233.2	40	8	30	8
			106	40	8	25	6
Cyprodinil	10.83	226	77	120	12	63	9
			93	120	12	80	9
D10-Carbamazepine	9.37	247.2	204.3	150	10	47	11
			202.1	150	10	47	11
Danofloxacin	6.48	358.2	340.2	100	8	31	12
			314.3	100	8	26	11
Dextromethorphan	8.1	272.4	215.1	150	10	47	11
			171.1	150	10	47	11
			173	150	10	47	11
Diatrizoic acid	5.03	632	361	80	9	35	8
			233.1	80	8	55	12
Diazepam	10.37	285.2	193.2	100	12	42	10
			154.2	100	12	36	10
Difloxacin	6.67	400.3	299	70	8	42	17
			356	70	8	30	20
Dimethoate	7.96	230	199.1	100	10	13	4
			125.1	100	10	28	4
			171	50	7	19	9
Dimethomorph	10.32	388	301	100	10	30	8
			165	100	10	45	8
			303	130	10	29	7
Diphenhydramine	8.01	256.4	167.2	40	12	21	9
			152	40	12	50	7
Diuron	10.04	233	72	60	7	50	12
			72	110	6	36	10
Domperidone	7.56	426.2	175	37	12	35	10
			147.1	37	11	55	7
Donepezil	7.51	380.4	91	65	12	63	9

Compound	Rt (min)	Precursor ion	Quantifier/ qualifyer	DP[a] (V)	EP[b] (V)	CE[c] (eV)	CXP[d] (V)
			151.1	65	14	40	8
Doxycycline	7.98	445.3	428.2	90	10	28	9
			410.2	90	10	34	10
			154.1	90	10	39	10
EDDP	7.96	278.6	234	30	11	42	14
			249.2	30	12	31	12
Enrofloxacin	6.48	360.3	245.2	80	10	37	10
			316.2	80	10	27	12
Eprosartan	8.01	425.2	135.1	79	11	47	9
			207.1	79	12	35	10
			163.2	79	10	44	5
Erithromicyn	8.45	734.6	158.3	58	5	40	2
			576.5	58	5	28	2
Famotidine	3.42	338	189.3	25	5	24	2
			259.4	25	5	15	2
Fenhexamid	10.51	302	97	80	14	30	12
			55	80	8	60	7
Fenofibrate	11.87	361.2	233.1	60	5	25	2
			139.1	60	5	35	2
Fenofibric acid	10.98	319.1	233.1	65	5	22	2
			139.1	65	5	42	2
Flecainide	7.84	415.2	301	48	12	49	7
			398.1	48	12	35	9
			98	48	12	36	15
Flumequine	9.38	262.3	244.08	50	5	21	14
			202.3	50	5	41	12
Fluoxetine	8.73	310.3	44.2	30	5	25	2
			148.2	30	5	10	2
Gabapentin	5.96	172.4	154.1	50	9	18	9
			137.2	50	9	22	7
Ifosfamide	8.49	261.1	91.9	60	5	33	2
			154.3	60	5	29	2
Imazalil	8.54	297	159	80	12	31	8
			255	80	12	25	7
Imazalil d6	8.54	302.1	159	60	10	32	4
			203	60	10	26	4
			255.1	60	10	26	4
Imidacloprid	7.45	256.1	175.1	100	10	27	4
			209.2	100	10	25	4
Iminostilbene	9.31	194	179	150	10	47	11
			167	150	10	47	11
			152	150	10	47	11
Indomethacin	10.91	358.2	139.1	50	5	25	2
			174.3	50	5	15	2

Compound	Rt (min)	Precursor ion	Quantifier/ qualifyer	DP[a] (V)	EP[b] (V)	CE[c] (eV)	CXP[d] (V)
Irbesartan	9.82	429.3	207	55	12	34	5
			195	55	12	32	14
Isoproturon	9.88	207	72	60	8	25	12
			165	60	8	20	10
Josamycin	8.77	828.6	174.2	54	12	46	13
			229.1	54	11	43	11
			600.2	54	11	37	14
Ketolorac	9.76	256.2	105.1	70	5	25	2
			178.1	70	5	34	2
Ketoprofen	10.03	255.2	105.1	47	5	33	2
			209.2	47	5	16	2
Labetalol	7.45	329.1	162.1	32	12	33	9
			90.9	32	12	67	8
			294.2	32	12	27	15
			311.2	32	12	21	7
Lansoprazole	9.29	370	252.2	45	5	15	2
			119.2	45	5	27	2
Levofloxacin	6.25	362.1	261.2	80	8	40	10
			318.2	80	8	26	15
Lidocaine	6.52	235	86	70	7	20	5
			58	70	8	50	4
Lincomycin	5.86	407.1	126.3	50	5	45	2
			359.3	50	5	23	2
Loratadine	10.7	383.1	337.3	50	5	29	2
			267.2	50	5	40	2
Mefanamic acid	11.68	242.2	224.2	36	5	34	2
			180.2	36	5	53	2
Memantine	8.1	180.3	163.1	28	12	22	10
			107.1	28	12	36	9
Mepivacaine	6.67	247.4	98.1	28	5	23	2
			70.1	28	5	53	2
Metalaxyl	9.76	280	220	85	12	20	12
			220	100	12	19	9
			192	70	12	25	9
Methadone	8.55	310.2	265.1	70	13	22	7
			105	70	11	40	20
			223	70	13	30	11
Methiocarb	10.33	226	169	44	14	13	9
			121	44	9	25	6
			107	44	9	51	5
Methotrexate	6.1	455.2	308	80	12	28	15
			175	90	12	55	15
			134	90	12	48	15
Metoclopramide	6.57	300	184	80	6	42	11

Compound	Rt (min)	Precursor ion	Quantifier/ qualifyer	DP[a] (V)	EP[b] (V)	CE[c] (eV)	CXP[d] (V)
			141	80	11	66	10
Metoprolol	6.9	268.2	116.2	30	5	25	2
			159.2	30	5	28	2
Metronidazol	5.63	172.1	128.1	35	5	20	2
			82.1	35	5	30	2
Mevastatin	11.4	391.3	185.2	55	5	25	2
			159.3	55	5	30	2
Myclobutanil	10.38	289.2	70.2	100	10	36	4
			125.1	100	10	44	4
Nadolol	6.15	310.2	254.4	45	5	30	2
			201.2	45	5	30	2
Nalidixic acid	9.25	233.2	187	45	10	35	12
			104	45	10	55	11
Naproxen	10.23	231.2	185.1	86	5	17	10
			170.1	86	5	35	10
N-desmethylcitalopram	7.85	311.3	109.1	66	12	31	7
			262.1	66	11	23	13
Nicotinamide	3.16	123.1	53.1	35	8	42	10
			80	35	12	28	8
			78	35	12	33	12
Nicotine	2.77	163.3	130	60	4	26	7
			132	60	10	20	7
			106	60	15	23	6
Nicotinic acid	3.34	124	80.1	76	6	29	13
			78.1	76	8	30	12
Nitrendipine	10.46	361	315	80	10	18	17
			329.1	80	10	15	15
			254.2	80	10	45	15
Norfloxacin	6.41	320	302.2	220	12	33	17
			233.1	220	12	33	5
O-desmethyltramadol	5.91	250.3	58.1	70	12	45	7
			232.2	70	13	17	11
O-desmethylvenlafaxine	6.76	264.1	57.9	190	9	50	6
			107	190	13	25	6
Oxcarbamazepine	8.68	253	180	73	10	44	11
			208.1	73	10	28	13
			235.9	150	10	47	11
Oxytetracycline	6.62	461.3	426.1	90	10	27	11
			443.1	90	10	19	11
Paraxanthine	6.19	181.2	124.2	50	5	25	2
			69.2	50	5	43	2
Paroxetin	8.46	330.3	192.2	70	5	25	2
			151.2	70	5	30	2

Compound	Rt (min)	Precursor ion	Quantifier/ qualifyer	DP[a] (V)	EP[b] (V)	CE[c] (eV)	CXP[d] (V)
Pentoxifylline	8.02	279	181	60	10	23	10
			138	60	10	35	10
Phenacetin	8.68	180.3	110.1	70	10	29	6
			138	70	10	22	9
			152	70	10	21	7
Pirimicarb	8.02	239	72.1	100	10	38	4
			182.1	100	10	23	4
Primidone	8.02	219.2	91.1	35	5	35	2
			162.3	35	5	16	2
Prochloraz	10.94	376.1	308	80	10	18	4
			266	80	10	23	4
Propafenone	8.47	342.4	116	69	8	32	7
			98.1	69	12	29	6
Propamocarb	4.97	189.1	101.9	29	10	25	4
			144.1	29	10	16	4
Propanolol	7.93	260	116.2	35	5	23	2
			183.2	35	5	23	2
Propyphenazone	9.43	231.3	189.2	55	5	22	2
			201.2	55	5	30	2
Pyrimethanil	10.13	200.1	107	246	12	33	6
			82.1	246	8	35	7
Quinmerac	8.37	222	204	47	10	25	12
			141	47	13	45	10
			206	46	10	24	6
Quinoxyfen	12.25	308	197	300	12	49	5
			162	300	12	61	8
Ranitidine	3.94	315.3	176.2	38	5	21	2
			130.1	38	5	30	2
Roxithromycin	8.91	837.5	158	140	8	43	15
			679.4	140	8	31	10
Salbutamol	3.42	240.3	148.2	44	5	26	2
			222.2	44	5	14	2
Sertraline	7.87	360.3	158.9	21	12	40	8
			275.1	21	12	18	6
Simazine	9.37	202.1	132	45	5	26	2
			124.2	45	5	23	2
Simvastatin	11.96	419.1	285.3	45	5	15	2
			199.1	45	5	15	2
Sotalol	3.4	273.3	255.2	45	6	14	2
			133.2	45	6	37	2
Sulfadiazine	5.68	251.2	92.1	40	5	35	2
			108.1	40	5	30	2
Sulfamethazine	6.8	279	186.2	42	5	20	2
			156.1	42	5	26	2

Compound	Rt (min)	Precursor ion	Quantifier/ qualifyer	DP[a] (V)	EP[b] (V)	CE[c] (eV)	CXP[d] (V)
Sulfamethizole	6.76	271.1	156.1	80	6	20	8
			92	80	6	37	10
			108.1	80	6	34	10
Sulfamethoxazole	7.21	254.2	156.1	47	5	21	2
			108.1	47	5	30	2
Sulfapyridine	6.06	250.1	156.1	47	5	21	2
			108.3	47	5	34	2
Sulfathiazole	5.87	256.2	156	45	5	18	2
			92.2	45	5	34	2
Sulpiride	3.66	342.3	112	47	11	34	15
			214.1	47	12	48	11
Tamoxifen	9.69	372	72	50	10	32	8
			70	50	8	75	10
			129	50	6	38	7
Tebuconazole	10.95	308	70	80	7	50	11
			125	80	10	50	6
			70	80	10	63	10
Telmisartan	9.14	515.5	497.3	40	12	47	11
			305.2	40	12	58	15
			276.2	40	12	60	7
Terbutaline	3.42	226.3	152.2	47	5	20	2
			107.1	47	5	40	2
Terbutryn	10.05	242	186	100	13	27	10
			68	100	12	60	4
Tetracycline	6.47	445.2	154.2	75	10	40	11
			410.2	75	10	27	9
Theophylline	6.45	181.1	124.2	50	8	24	19
			69.1	50	8	35	12
Thiabendazole	6.72	202	131.1	150	10	47	11
			175.1	150	10	47	11
Tramadol	6.85	264	246.1	15	8	15	3
			58	15	8	7	3
Tramadol N-oxide	7.04	280.4	135.1	70	13	32	11
			201.1	70	13	27	10
			58	70	14	47	15
			159	70	13	37	10
Trazodone	7.4	372.4	148.1	73	12	48	8
			176	73	12	35	10
Triamterene	6.66	254.6	238.1	29	12	39	12
			168.1	29	12	47	10
Trigonelline	2.65	138.2	78.2	45	8	33	12
			92.2	150	10	47	11
Trimethopim	5.95	291.3	230.2	45	5	28	2
			123.2	45	5	30	2

Compound	Rt (min)	Precursor ion	Quantifier/ qualifyer	DP[a] (V)	EP[b] (V)	CE[c] (eV)	CXP[d] (V)
Vancomycin	4.75	725.3	100.3	150	10	47	11
			144.3	150	10	47	11
Venlafaxine	7.71	278.4	58.1	50	5	45	2
			260.4	50	5	15	2
Verapamil	8.07	455.5	303.3	52	10	36	8
			260	52	12	41	14

[a]DP: Declustering Potential; [b]EP: Entrance Potential; [c]CE; Collision Energy; [d]CXP: Collision Cell Exit Potential

Table SI-5. Evolution of the removal of each OMC detected in the retentate during solar-assisted AO treatment

	Concentration (ng L^{-1})										
OMCs	**0 min**	**15 min**	**30 min**	**45 min**	**60 min**	**75 min**	**90 min**	**120 min**	**150 min**	**180 min**	**Removal (%)**
4AA	4579	173	101								>99
4AAA	14347		11136	8589	8346	7792	5041	4015	1287	362	98
4FAA	28357		21905	20859	18779	14167	11298	6491	2585	780	97
Carbamazepine	7068	6732		6532	6091		5159	4703	4651	3942	44
Citalopram	878		560	557	295	175	85				>99
Diatrizoic acid	1461	1382					1043	969	766	693	53
Pentoxifylline	842	726	541	564	464					442	48
Venlafaxine	2928	2127	1934	1747	1152	1042	806	195	50		>99
Gabapentin	12385		9450		7035	6741	6258	4918	3726	2727	78
Acetamiprid	471									438	7
Azoxistrobin	57	54		49			48	43	39	36	37
Imidacloprid	4525	4479	4116				3695	3227	2316	2087	54
Terbutryn	172									155	10
Azithromycin	537	414		234	182	108	56				>99
Lincomycin	705	421	0								>99
Cetirizine	1693	1624	1584		1510	1425	1312	1276	1147	1026	39
Sulpiride	4056	3805	3058	2182	1720	1173	846	396	256	13	>99
Telmisartan	1586		1562			1540		1533	1295	1274	20
N-desmethylcitalopram	479			391						350	27
Flecainide	403	341	257		209	189	162		107	96	76
Irbesartan	1554	1482		1334	1332	1313		1186	993	905	42
Iminostilbene	5775				5557	4953		4565		3406	41
Diazepam	25			25		24				22	15

OMCs	0 min	15 min	30 min	45 min	60 min	75 min	90 min	120 min	150 min	180 min	Removal (%)
Fenofibric acid	370	264	181	111	62	35					>99
Indomethacin	68	37									>99
Naproxen	928	811	775	705							>99
Propanolol	215	137									>99
Carbendazim	138		127	112	116	104	105	99	80	65	53
Dimethoate	127	118		100	77						>99
Diuron	70		67			65		59	57	47	33
Isoproturon	85	74	73	62	61	50	39	21			>99
Metalaxyl	18			17		17			15	15	16
Myclobutanil	41		41				39		39	37	11
Tebuconazole	34		33	33	33		30		28	27	20
Erithromycin	19	14	5	3							>99
Metronidazole	161	141		135	116	109	106	87			>99
Sulfathiazole	43										>99
Trimethoprim	272	185	94								>99
Levofloxacin	1929	1758		1557	918	879	451	168			>99
Alfuzosin	9	8	6	6							>99
Domperidone	34	33									>99
Propafenone	18	11									>99
Memantine	194	178	140	139	109	96	74	41			>99
Trazodone	85	51									>99

Target 3. Degradation of carbon-based cathodes in electro-Fenton treatment

Degradation of carbon-based cathodes in electro-Fenton treatment

I. Salmerón[a], I. Oller[a*], K.V. Plakas[b], S. Malato[a].

[a]*Plataforma Solar de Almería. Ctra Senés km 4, 04200 Tabernas (Almería), Spain.*

[b]*Chemical Process and Energy Resources Institute, Centre for Research and Technology – Hellas (CERTH), 6th Km Charilaou-Thermi Road, Thermi, Thessaloniki GR 57001, Greece*

E- mail: isabel.oller@psa.es (Isabel Oller)

Graphical Abstract

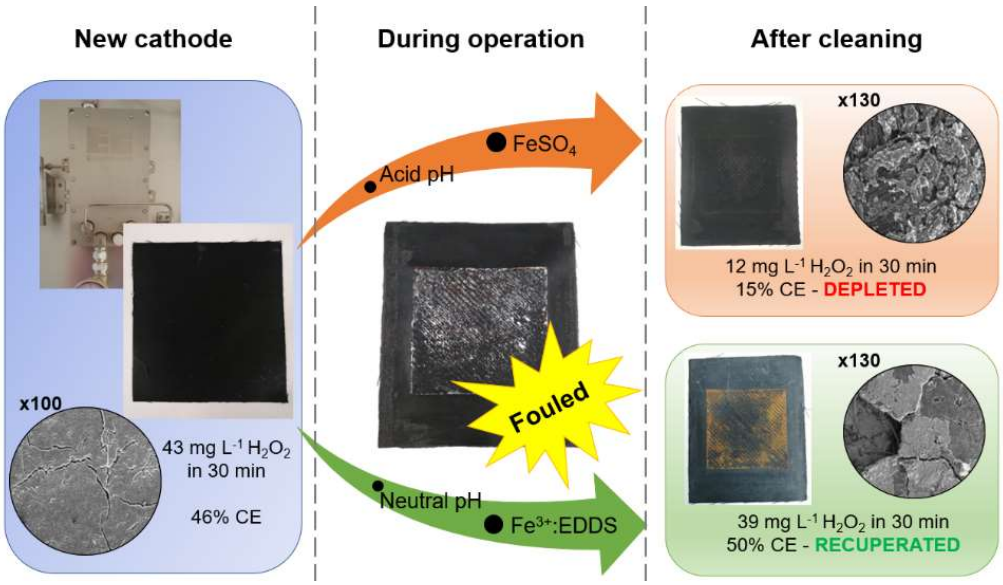

Abstract

This manuscript addresses the degradation of carbon-PTFE cathodes conforming a commercial plate-and-frame cell from ElectroCell with a Nb-BDD anode. The cell is arranged within an electrochemical pilot plant designed for treating wastewaters by electrochemical Fenton-like processes, thus an efficient electrocatalytic production of H_2O_2 is necessary to guarantee Fenton's reaction. Significant decrease on H_2O_2 electrogenerated occurred through pilot plant operation, avoiding the efficient performance of Fenton-like processes. Two cathodes were studied, first was operated at pH 3 and second at neutral pH by using EDDS as complexing agent to maintain iron in solution. Electrogenerated H_2O_2 decreased from 43 mg L^{-1} to 16 mg L^{-1} in the first cathode (after 50 h of operation) and from 49 mg L^{-1} to 24 mg L^{-1} in the second one (after 26 h of operation). Both were cleaned with 30% (v/v) solution of HCl/water during 24 hours, recovering H_2O_2 production only in the second cathode (able to generate 39 mg L^{-1}). Autopsy of the cathodes was tackled by scanning electron microscopy (SEM) and X-ray energy dispersive (EDX), evidencing a strong degradation of first cathode surface and iron oxide inlays in second one due to the decomposition of Fe^{3+}:EDDS and consequent iron precipitation at neutral pH.

Keywords: electrochemical water treatment, gas diffusion electrode, hydrogen peroxide electrogeneration, scaling, iron deposition, acid cleaning

1. Introduction

Electrochemical advanced oxidation processes (EAOPs) constitute a highly effective alternative for the treatment of complex and recalcitrant wastewaters [1, 2]. Such processes are based on the electrochemical production of hydroxyl radicals (•OH) and involve either the direct oxidation of pollutants on the surface of anodes (anodic oxidation, AO) or their indirect oxidation by electrogenerated reactive oxygen species (ROS) on the anode or the cathode surface, such as ozone, hydrogen peroxide (H_2O_2), sulphate radical ($SO_4^{\bullet-}$), chlorine species (e.g. Cl_2, ClO^-) and peroxosalts that interact with organics in the bulk, thus increasing the overall treatment efficiency [3, 4]. In order to increase the formation of •OH and therefore the oxidation power of the electrochemical remediation process, electro-Fenton (EF) technology has been developed. EF is based on the continuous H_2O_2 electrogeneration at a suitable cathode fed with O_2 or air (Eq. 1-2) and the presence or addition of an iron catalyst to generate •OH in the bulk from Fenton's reaction (Eq. 3).

$$O_2 + 2H^+ + 2e^- \rightarrow H_2O_2 \text{ (acid.)} \quad (1)$$

$$2H_2O + O_2 + 2e^- \rightarrow H_2O_2 + 2OH^- \text{ (alk.)} \quad (2)$$

$$H_2O_2 + Fe^{2+} \rightarrow Fe^{3+} + {}^{\bullet}OH + OH^- \quad (3)$$

In comparison to the planar 2-dimensional electrodes used as anodes (e.g. mixed metal oxides, graphite, boron-doped diamond thin films on titanium substrates), 3-dimensional carbonaceous electrodes of high specific surface area are preferred for enhancing the mass transfer of dissolved oxygen, thus favouring its electrochemical reduction to H_2O_2 at relatively low current densities [5].

Among the carbonaceous electrodes used in literature, such as carbon felt (CF), activated carbon fiber (ACF), reticulated vitreous carbon (RVC), carbon sponge and carbon nanotubes (NTs), the so called gas diffusion electrodes (GDEs) present a higher selectivity for H_2O_2 production, thanks to the direct supply of O_2 to the electrode surface that minimizes the extent of side reactions. In fact, GDEs have a catalytically active hydrophilic layer on one side of a carbon cloth matrix facing the solution and a PTFE impregnated hydrophobic layer on the other side, which is used for oxygen supply to the 3-phase interface. The porous structure and the coexistence of triple phase boundary from one hand, and the enhanced solubility and mass transport of O_2 in water from the other hand, allow a hydrogen peroxide electro-synthesis at rather low current densities and therefore a low energy consumption [6]. Like most carbon-based cathodes, GDEs present significant attributes such as high over-potential for H_2 evolution, high stability, conductivity, chemical resistance and non-toxicity [5]. However, GDEs, like most carbonaceous materials commonly suffer surface corrosion. Specifically, the electrochemical oxidation of carbon, referred to carbon corrosion, has a thermodynamical standard equilibrium potential as low as 0.21 V (Eq. 4). Therefore, corrosion can occur at high current densities [7] causing a collapse of the porous structure, which limits the mass transfer of reactants on the surface.

$$C + 2H_2O \rightarrow CO_2 + 4H^+ + 4e^- \quad (4)$$

Moreover, scaling issues due to the deposition of salts on the porous carbon surface (mostly calcium carbonate), and fouling caused by the accumulation of organic and/or polymeric films, can alter significantly the active surface of the electrode. Such effects can cause electrode passivation and can be detrimental to the H_2O_2 electrogeneration performance, leading to increased electric consumption and to additional maintenance costs. Although these phenomena have been

extensively investigated in the case of electro membrane separation processes (e.g. electrodialysis, capacitive deionization) [8, 9] and fuel cells [10], there are limited studies assessing such phenomena in EAOPs [11, 12] and especially in EF applications.

Since the long-term stability of electrodes is of great importance for the practical application of EF processes [13], the present study communicates the results of a systematic investigation on carbon-PTFE GDE cathodes performance deterioration that occurs during the treatment of actual wastewaters under different operating conditions by EF and solar photo-EF (SPEF) processes. Changes in current efficiency over the in-situ production of H_2O_2 were assessed as function of the changes observed in the active surface area of GDE electrodes. For this scope surface analysis of virgin and used GDEs were performed by scanning electron microscopy (SEM) and elemental composition by X-ray energy dispersive (EDX). The effect of electrodes acidic cleaning on the recovery of their H_2O_2 electrogeneration performance was also assessed and the respective results are presented herein.

2. Materials and methods

2.1 Reagents and analysis

As supporting electrolyte 50 mM Na_2SO_4 (from Sigma-Aldrich) dissolved in demineralized water was used. pH was adjusted with HSO_4 (from Merck) and measured with a portable pHmeter LAQUAact PH110 (HORIBA). Electric conductivity was monitored by a GLP 31 Conductimeter (CRISON).

Hydrogen peroxide was determined following DIN 38409 H15 by adding 0.5 mL of Titanium (IV) oxysulfate solution 1.9-2.1% (from Sigma-Aldrich) to 5 mL of sample. After mixing, samples were measured at 410 nm with an Evolution 220 UV-Visible spectrophotometer from Thermo Scientific.

The autopsy of the cathode surface was tackled to find out the phenomena responsible of H_2O_2 electrogeneration efficacy decrease. SEM images were obtained with a HITACHI S-3500N equipment working in high vacuum at 15 kV. Chemical composition of the electrode samples and their quantification were done with an EDX analyser Oxford INCAx-sight (Oxford Instruments).

Current efficiency (CE) is defined as the ratio between the electricity consumed to develop the reaction of interest and the total amount of electricity supplied to the cell, and it is calculated according to equation 5.

$$\% \, CE = \frac{n \, F \, [H_2O_2] \, Vt}{Q} \, x \, 100 \qquad (5)$$

where n represents the stoichiometric number of electrons transferred in the specific reaction under study (equal to 2; Eq. 1,2), F is the Faraday constant (96485 C mol^{-1}), $[H_2O_2]$ is the accumulated H_2O_2 in the solution (M), V_T the total volume of solution (L), and Q the charge consumed during the electrolysis (C).

2.2 Experimental setup

The electrochemical pilot plant consists of four commercial plate-and-frame cells of Electro MP-Cell type by ElectroCell (Denmark) but for this study only one of them was employed. The cell contained an anode made of boron-doped diamond thin film deposited on a niobium mesh (Nb-BDD) and an un-catalyzed carbon-PTFE GDE cathode with an effective area of 0.010 m^2. The system is connected to a Delta Electronika power supply SM 70-22. The cathode was fed by an ABAC air compressor (1.5 kW) and for pumping the solution from the tank to the cell a 0.75 kW PAN World magnetic drive pump was used. For both, air and wastewater, flow and pressure were regulated with a flowmeter and a back-

pressure gauge. The temperature was established in 25 ± 5 ºC, being regulated automatically by a heat exchanger connected to a cooling coil. A scheme of the whole system and pictures of the cell are shown in Figure 1.

Cathode surface was dissembled after carrying out two set of experiments consisting on the optimization and evaluation of the electrochemical system efficiency (EF and SPEF) for contaminant removal in a 50 mM Na_2SO_4 solution working at acid pH during 50 hours (first cathode analyzed), published by Salmerón et al. 2019 [14]. And a second set at neutral pH after 26 hours of operation (second cathode analyzed) by using EDDS as iron complexing agent to avoid its precipitation allowing a proper performance of Fenton-like reactions, addressed in Roccamante et al. 2019 [15].

It is important to highlight that after each test (normally around 4 hours of batch operation) the whole electrochemical plant was properly cleaned with a pH 3 acid solution of HCl in demineralized water.

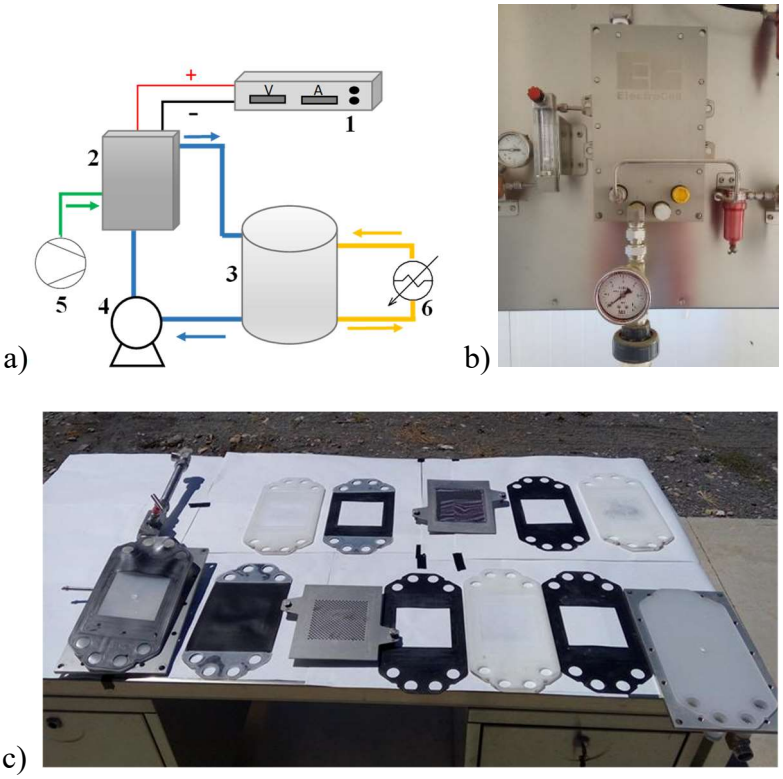

Figure 1. a) Flow diagram scheme of the electrochemical pilot plant used in this study. 1) power supply, 2) electrochemical cell 3) feeding tank, 4) centrifugal pump 5) air compressor and 6) heat exchanger; b) Electro MP-Cell installed in the pilot plant; c) Parts of the MP-Cell dissembled.

3. Results and discussion

3.1 Characterization of virgin carbon-PTFE GDE cathode

A new carbon-PTFE GDE cathode is shown in Figure 2. A more detailed cathode analysis by SEM showed a compact surface, with some cracks in the carbon black/PTFE coating at x100 of magnification (Fig. 2b) and a granulated texture when the magnification increased till x4500 (Fig. 2c). Moreover, the EDX microanalysis of the surface area (Fig. 2d) (~1.2 mm^2) revealed the composition of the coating with 59% in weight of carbon and the rest 41% of fluorine. According to the molecular weight

of PTFE ($(C_2F_4)n$) 13% in weight of carbon is part of the PTFE molecules and the rest of carbon, 46%, could be attributed to the active carbon black covering.

Regarding H_2O_2 electrogeneration, when the system works in batch mode, it is accumulated in the bulk solution reaching higher concentration at longer time but limited by several other "parasitic" reactions that decomposed H_2O_2. For this reason, H_2O_2 concentration usually achieve a plateau, as H_2O_2 produced is, at the same time, oxidized in the anode, reduced in the cathode and decomposed in the bulk solution [16]. In fact, the effect of these parasitic reactions under batch mode operation is usually shown as a decrease in CE over time.

According to these premises and in order to avoid the negative effects of long-term assays, test time for measuring accumulation of electrogenerated H_2O_2 was stablished in 30 min. It must be considered that the effect of those parasitic reactions is much less evident in EF and SPEF treatments than in AO with electrogenerated H_2O_2, since H_2O_2 generated is rapidly consumed in Fenton reaction lowering its accumulation. Specifically for this kind of cathode, the in-situ electrogeneration of H_2O_2 was previously studied, reaching 43 mg L^{-1} of accumulated H_2O_2 in 30 min with 46% of CE under optimum operation conditions: pH 3 and j 73.6 mA cm^{-2} [14].

a)

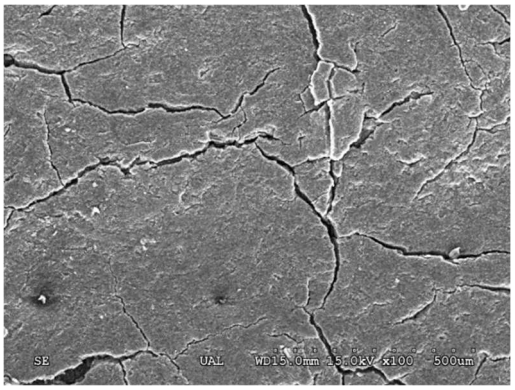

b)

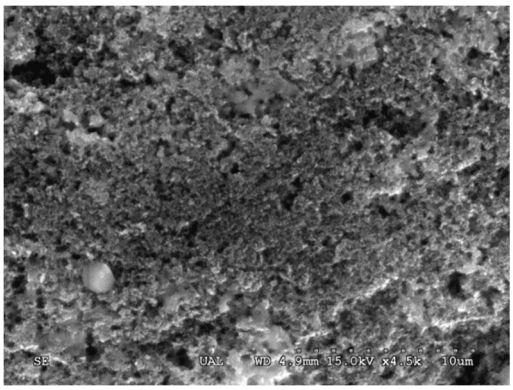

c)

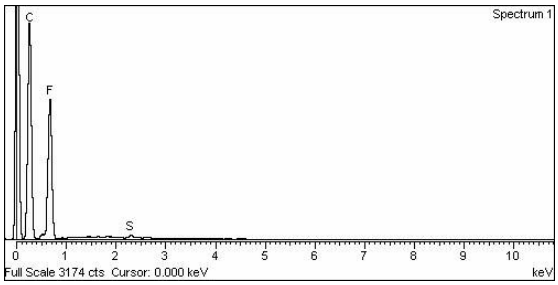

d)

Figure 2. Characterization of a virgin carbon-PTFE cathode: a) front side of carbon-cloth; b) detail obtained by SEM at x100 magnitude and c) x4500 magnitude; d) EDX microanalysis of the x100 SEM image.

3.2 Analysis of depleted carbon PTFE GDE cathodes after electrochemical assays

In all pilot runs, wastewater conductivity was different, so diverse current densities were applied maintaining the system voltage always below 25 V in order to avoid the corrosion of the BDD electrode employed in all tests as anode, and keep a reasonable CE [17]. Most relevant parameter in all Fenton and Fenton-like experiments was pH, using iron as catalyst when working at acidic pH while at natural pH, the use of Fe^{3+}:EDDS complex was required to keep iron in solution. After each experiment, electrochemical pilot plant was cleaned with demineralized water at pH 3 (HCl), maintaining recirculation for at least 15 min to ensure 2-3 cycles of the total volume, with the aim of dissolving and dragging precipitates that may have been generated along the experiments.

After several assays a decrease in the accumulated H_2O_2 concentration was shown, being even below the limit of detection (0.5 mg L^{-1}) in some cases (data not shown), which means that electrogenerated H_2O_2 was not enough to allow Fenton reaction successfully perform.

Aiming to know the phenomena that could cause the decrease in H_2O_2 electrogenerated, the cell was disassembled in order to inspect its pieces and the cathode surface.

Two carbon-PTFE GDE cathodes were analysed in this work: (a) after a set of EF and SPEF experiments carried out at pH 3; (b) after a series of EF and SPEF experimental runs at neutral pH by using Fe^{3+}:EDDS complex in which problems with iron precipitation were detected. In all cases, after disassembling the cell large deposits of salts in both the flow frame (Fig. 3a) and the cathode itself (Fig. 3b) were observed. These caused a significant reduction of the active surface and consequently decreased mass transfer of the electroactive species on the cathode. In addition, the ohmic resistance increased, reflected in an augment of the response voltage (data not shown here), entailing a lower CE.

a)  b) 

Figure 3. Deposits of salt and iron in a) the flow frame and b) the cathode surface.

The procedure followed for cathode cleaning was immersion of their pieces into 30% (v/v) HCl (37.5%)/water for 24 hours. After that, most of salt deposits were removed, thus the pieces were rinsed several times with demineralized water and reassembled in the cell to test if H_2O_2 electrogeneration capacity had been recovered.

3.2.1 Assessment of cathode performance after EF and SPEF assays at acidic pH

Figure 4 shows the performance of H_2O_2 electrogeneration by new, fouled and cleaned GDE electrode after the set of EF and SPEF experiments carried out at pH 3. Accumulated H_2O_2 concentration achieved with the new carbon-PTFE GDE cathode was 43 mg L^{-1} in 30 min and the CE was 46%. The deposition of salts on the cathode surface provoked a decrease in H_2O_2 electrogeneration to 16 mg L^{-1} of accumulated H_2O_2 after 30 min, with a respective CE down to 21%. After the cleaning procedure (Fig. 5a), a loss in the carbon-PTFE cover was evidenced by the naked eye, showing even lower accumulated H_2O_2 than before cleaning, 12 mg L^{-1}, with 15% CE. This result suggests that part of the carbon-PTFE coverage had been lost during cleaning, reducing significantly the reactive surface of the cathode and hence decreasing CE.

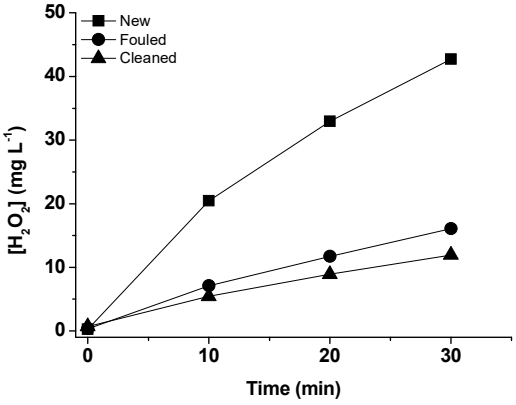

Figure 4. Concentration of accumulated H_2O_2 as function of electrolysis time for a new, fouled by salt depositions (after AO, EF and SPEF at acidic pH) and cleaned (37.5% HCl and water 30% (v/v)) GDE electrode. H_2O_2 electrogeneration was tested at pH 3 and *j* 73.6 mA cm^{-2}.

Considering the low H_2O_2 production of the cathode limiting EF and SPEF processes performance, cell was dissembled and an autopsy was done by means of SEM. A detailed view of the surface at x130 (Fig. 5b) showed that the cathode coverage was completely disaggregated, with many different layers and significant losses being observed, while several spots of carbon cloth substrate in direct contact with the air were identified. This loss of the cathode reactive surface justified the decrease in H_2O_2 production. In fact, x4500 image (Fig. 5c) showed a much spongier surface which had lost a large amount of the carbon cover compared with the new cathode at the same magnification. The strong degradation of the cathode surface was probably due to the acidic working pH (~3) maintained along all pilot runs (50 hours of operation) combined with the erosion caused by the water and air flow, stablished in 5 L min^{-1} and 1.7 bar, respectively for water and 10 L min^{-1} and 1.9 bar, respectively for air.

In this sense and trying to eliminate possible erosion effects, in the following experiments, efforts were made to operate with the minimum pressure values necessary to maintain same water and air flows, 0.5 and 0.7 bars.

Besides, XRD microanalysis was performed selecting specifically an area (~1.2 mm^2) of the surface which was not highly eroded (Fig. 5c and d), finding new signals of Na, S and O in a very low weight ratio: 0.5, 0.4 and 2%, proving that part of the salts from the working electrolyte (Na_2SO_4) remained embedded despite the cleaning.

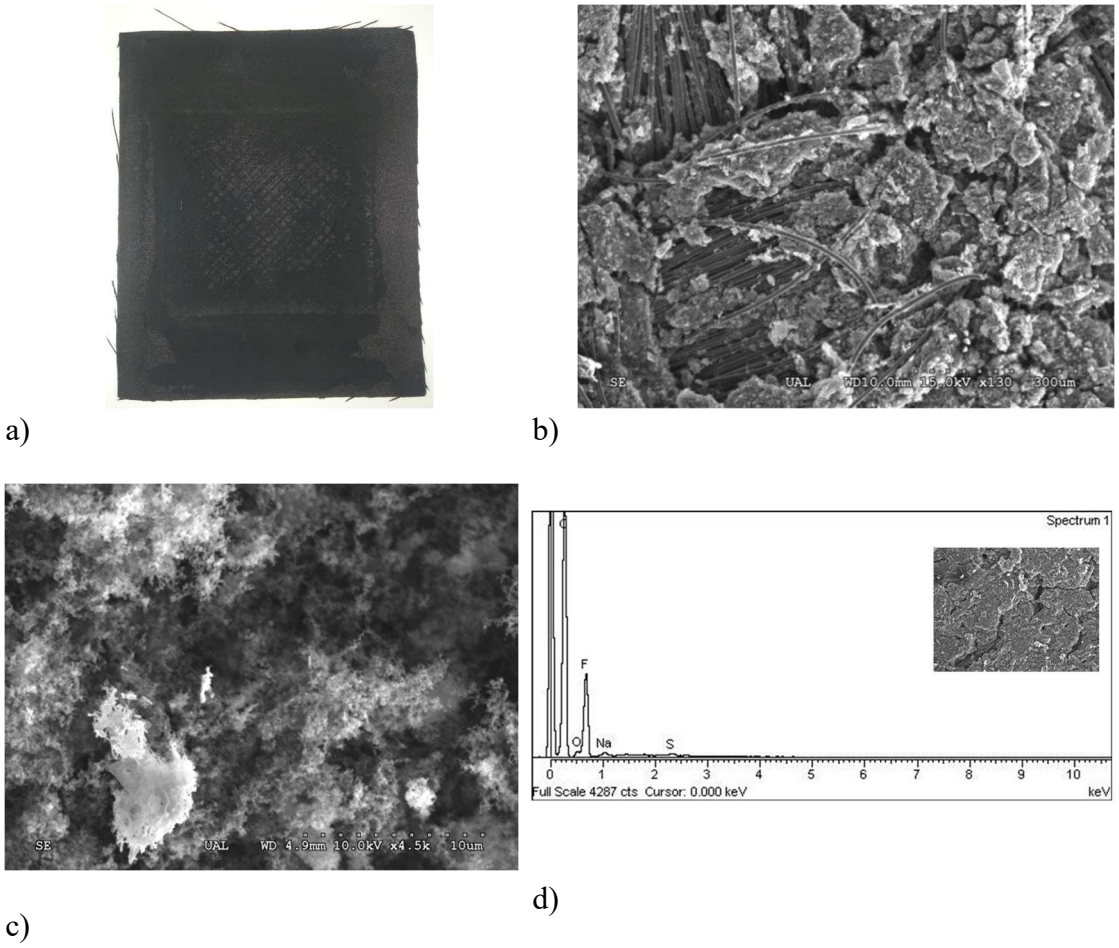

Figure 5. Images of the cathode surface after cleaning a) actual view, b) SEM image at x130, c) SEM image at x4500 and d) EDX elemental composition (inset: surface area studied by EDX).

3.2.2 Assessment of cathode performance after EF and SPEF assays at neutral pH

As stated before, water and air pressures were decreased to 0.5 and 0.7 bar respectively, in order to prevent abrasion on the cathode surface. In addition, a second set of EF and SPEF experiments (26 hours of operation) was carried out in 50 mM Na_2SO_4 at neutral pH by using Fe^{3+}:EDDS complex (0.1mM:0.2mM) to maintain iron in solution. In consequence, Fe^{3+}:EDDS decomposition could produce iron precipitates along assays.

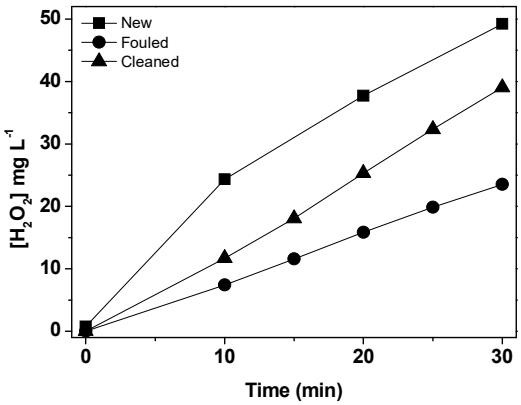

Figure 6. Concentration of accumulated H_2O_2 as function of electrolysis time for a new, fouled by salt depositions (after a set of AO, EF and SPEF runs at neutral pH), and cleaned (37.5% HCl and water 30% (v/v)) GDE electrode. H_2O_2 electrogeneration was tested at pH 3 and *j* 73.6 mA cm^{-2}.

A similar H_2O_2 electrogeneration performance was observed in the case of the new cathode, namely 49 mg L^{-1} of accumulated H_2O_2 in 30 min with a CE of 63%. Despite reducing the pressure, after several tests, carbon-PTFE cathode also lost its capability to electrogenerate H_2O_2, reaching 24 mg L^{-1} in 30 min (Fig. 6) (CE 30%). The same cleaning procedure already described was followed recovering a great part of the original cathode activity (39 mg L^{-1} of accumulated H_2O_2 with 50% CE).

Before cleaning, the cathode surface was fully covered by salt deposits of white and orange colour. Most of them were removed during cleaning, but some orange ones persisted on the carbon-PTFE surface (Fig. 7a). After cleaning, accumulated H_2O_2 production reached 79% of the new cathode performance.

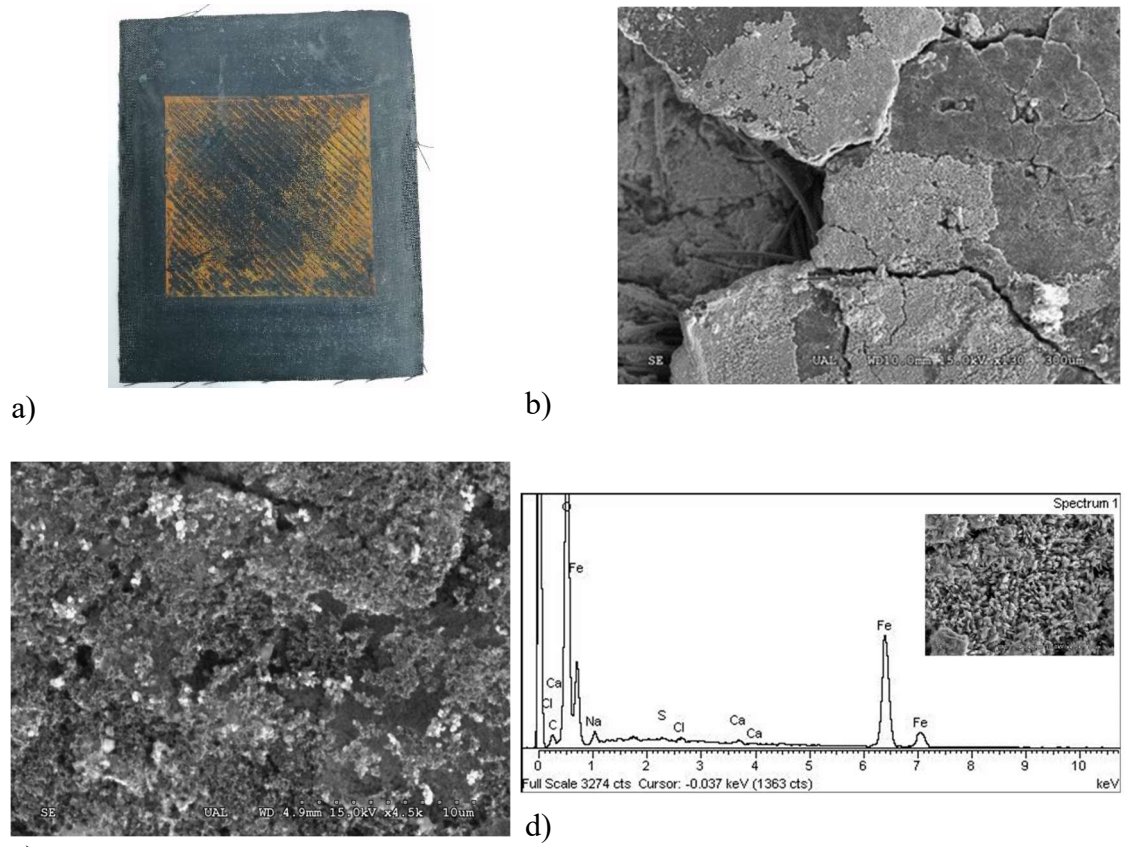

Figure 7. Images of the second GDE electrode after cleaning a) actual view, b) SEM image at x130, c) SEM image at x4500 and d) elemental composition by EDX (inset: point studied by microanalysis).

When analysing the cathode surface by SEM, some degraded parts were observed in which carbon-PTFE cover was lost (as it happened in the first cathode), but most of the surface was still covered by carbon-PTFE. It is worth mentioning the presence of areas with lighter colour and different texture (Fig. 7b). Thus, working at less pressure reduced erosion, which jointly with working at less extreme pH lengthened the operational life of the cathode. When enlarging the image up to x4500 (Fig. 7c) it was observed a similar surface to the new cathode (Fig. 2c) but slightly more eroded

and presenting some bright light white grains. On the contrary, a magnification of the lighter colour areas (inset of Fig. 7d) showed a new texture, which was probably crystals formed by iron from degraded Fe^{3+}:EDDS complex. To prove this assumption, a punctual microanalysis in that area was carried out (Fig. 7d) confirming that these deposits are iron oxides crystals: 54% Fe and that of 40% O_2.

4. Conclusions

Carbon-PTFE cathodes complement electro-oxidative systems generating simultaneously H_2O_2 with higher current efficiency to allow Fenton and Fenton-like processes increasing the oxidative power. However it is necessary to address their resistance and stability under the operation conditions proposed before their application at large scale, since the ability of electrogenerate H_2O_2 can be affected and so reducing the efficiency.

Durability and H_2O_2 electrogeneration capability of cathodes have been evaluated in this work, working at pilot plant scale. After operating at acid pH, it was observed a strong damage on the cathode surface losing the carbon cover, reducing their active surface and consequently, decreasing H_2O_2 production irreversibly. For this reason when scaling-up the system it must be considered cost associated to cathode replacement if working under such aggressive operation conditions.

On the other hand, when operating at neutral pH, despite decreasing H_2O_2 along the set of experiments, it was observed that loss of the carbon cover was not as high as at acidic pH, thus cathode capability was recovered after a proper acid cleaning, extending its useful life and reducing maintenance costs on commercial scale systems.

Once the effect of electrochemical processes under different pH conditions (key parameter on EF and SPEF treatments) on Carbon-PTFE cathodes have been studied, next step must include the effect of actual more complex water matrices. Investigation on durability and stability of materials in this kind of oxidation systems are crucial before tackling their scaling-up for certain applications.

Acknowledgements

The authors wish to thank the Spanish Ministry of Science, Innovation and Universities (MCIU), AEI and FEDER for funding this research under CalypSol Project (Reference: RTI2018-097997-B-C32).

References

[1] I. Sirés, E. Brillas, M.A. Oturan, M.A. Rodrigo, M. Panizza, Electrochemical advanced oxidation processes: today and tomorrow. A review, Environ. Sci. Pollut. R., 21 (2014) 8336-8367.

[2] K.V. Plakas, A.J. Karabelas, Electro-Fenton applications in the water industry, in: M. Zhou, M.A. Oturan, I. Sirés (Eds.) Electro-Fenton Process, Springer, 2017, pp. 343-378.

[3] B.S. Tawabini, K.V. Plakas, M. Fraim, E. Safi, T. Oyehan, A.J. Karabelas, Assessing the efficiency of a pilot-scale GDE/BDD electrochemical system in removing phenol from high salinity waters, Chemosphere, 239 (2020) 124714.

[4] S. Garcia-Segura, J.D. Ocon, M.N. Chong, Electrochemical oxidation remediation of real wastewater effluents—a review, Process Saf. Environ. Prot., 113 (2018) 48-67.

[5] E. Brillas, I. Sirés, M.A. Oturan, Electro-Fenton process and related electrochemical technologies based on Fenton's reaction

chemistry, Chem. Rev., 109 (2009) 6570-6631.

[6] X. Yu, M. Zhou, G. Ren, L. Ma, A novel dual gas diffusion electrodes system for efficient hydrogen peroxide generation used in electro-Fenton, Chem. Eng. J., 263 (2015) 92-100.

[7] M. Panizza, Importance of electrode material in the electrochemical treatment of wastewater containing organic pollutants, in: C. Comninellis, G. Chen (Eds.) Electrochemistry for the Environment, Springer, New York, 2010, pp. 25-54.

[8] X. Liu, S. Shanbhag, M.S. Mauter, Understanding and mitigating performance decline in electrochemical deionization, Curr. Opin. Chem. Eng., 25 (2019) 67-74.

[9] S. Al-Amshawee, M.Y.B.M. Yunus, A.A.M. Azoddein, D.G. Hassell, I.H. Dakhil, H.A. Hasan, Electrodialysis desalination for water and wastewater: A review, Chem. Eng. J., 380 (2020).

[10] P. Kanninen, B. Eriksson, F. Davodi, M.E.M. Buan, O. Sorsa, T. Kallio, R.W. Lindström, Carbon corrosion properties and performance of multi-walled carbon nanotube support with and without nitrogen-functionalization in fuel cell electrodes, Electrochim. Acta, 332 (2020) 135384.

[11] R.E. Wilson, I. Stoianov, D. O'Hare, Biofouling and in situ electrochemical cleaning of a boron-doped diamond free chlorine sensor, Electrochem. Commun., 71 (2016) 79-83.

[12] D. Rice, P. Westerhoff, F. Perreault, S. Garcia-Segura, Electrochemical self-cleaning anodic surfaces for biofouling control during water treatment, Electrochem. Commun., 96 (2018) 83-87.

[13] W. Zhou, X. Meng, J. Gao, A.N. Alshawabkeh, Hydrogen peroxide generation from O2 electroreduction for environmental remediation: A state-of-the-art review, Chemosphere, 225 (2019) 588-607.

[14] I. Salmerón, K.V. Plakas, I. Sirés, I. Oller, M.I. Maldonado, A.J. Karabelas, S. Malato, Optimization of electrocatalytic H2O2 production at pilot plant scale for solar-assisted water treatment, Appl. Catal. B-Environ., 242 (2019) 327-336.

[15] M. Roccamante, I. Salmerón, A. Ruiz, I. Oller, S. Malato, New approaches to solar Advanced Oxidation Processes for elimination of priority substances based on electrooxidation and ozonation at pilot plant scale, Catal. Today, (2019).

[16] G.R. Agladze, G.S. Tsurtsumia, B.I. Jung, J.S. Kim, G. Gorelishvili, Comparative study of hydrogen peroxide electro-generation on gas-diffusion electrodes in undivided and membrane cells, J. Appl. Electrochem., 37 (2007) 375-383.

[17] M. Panizza, G. Cerisola, Direct and mediated anodic oxidation of organic pollutants, Chem. Rev., 109, 12 (2009) 6541–6569.

Target 4. Electrochemically Assisted Photocatalysis for the Simultaneous Degradation of Organic Micro-Contaminants and Inactivation of Microorganisms in Water

Electrochemically Assisted Photocatalysis for the Simultaneous Degradation of Organic Micro-Contaminants and Inactivation of Microorganisms in Water

I. Salmerón[a], P. K. Sharma[b], M.I. Polo-López[a], A. Tolosana[b], I. Oller[a], J.A. Byrne[b], P. Fernández-Ibañez[b*]

[a]*Plataforma Solar de Almería-CIEMAT. Ctra Senés km 4, 04200 Tabernas (Almería), Spain.*

[b]*Nanotechnology and Integrated BioEngineering Centre, School of Engineering, Ulster University, Northern Ireland, BT37 0QB, United Kingdom*

Email: p.fernandez@ulster.ac.uk (Pilar Fernandez)

Graphical abstract

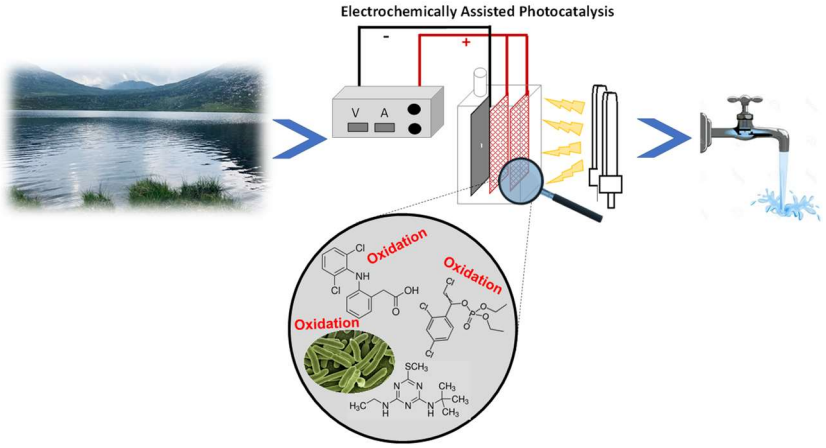

Abstract

This study presents the assessment of the performance of a photoelectrochemical reactor for the simultaneous degradation of organic microcontaminants (OMCs) and inactivation of bacteria in real surface water. Target OMCs were terbutryn, clorfenvinphos and diclofenac (500 µg L-1 each), and *E. coli* K12 (10^6 CFU mL^{-1}) was used as the model microorganism. The reactor utilised a photoanode consisting of two Ti mesh electrodes anodised to give aligned self-assembled TiO_2 nanotubes on the surface. Two cathode materials were investigated i.e. Pt and carbon felt. Higher *E. coli* inactivation rates were observed with electrochemically assisted photocatalysis (EAP) with a 2-Log Reduction Value (LRV) for Pt CE and 2.7-LRV in 2h for carbon felt cathode, as compared to only a 0.8 LRV for photocatalysis (open circuit). For the simultaneous degradation of OMCs and inactivation of bacteria a 4.5-LRV was achieved in 90 min with applied potential and a carbon felt cathode. Similar degradation kinetics were observed for the OMC for both electrochemically assisted photocatalysis and photocatalysis (open circuit) with ca 70% of the removal of the total OMCs in 60 min. Hydroxyl radical, H_2O_2 and chlorine generation were also evaluated to elucidate the mechanisms of degradation and disinfection. This work suggests that electrochemically assisted photocatalysis is more efficient than photocatalysis alone for the combined removal of OMCs and disinfection of water.

Keywords: Carbon-felt cathode, *Escherichia coli*, organic microcontaminants, photoelectrocatalysis, TiO_2 nanotubes photoanode, water purification.

1. Introduction

The increase of the pharmaceutical and agricultural industry during the last decades has led to the appearance of new organic substances into the environment. These compounds are commonly present at very low concentrations, from ng L^{-1} to µg L^{-1}, however they are highly toxic or non-biodegradable and their effects into the ecosystems and humans are still unknown. Their recalcitrant character makes them unable to be removed by biological treatments thus in wastewater treatment plants (WWTP) without a proper tertiary treatment they are directly discharged into water bodies. Furthermore, wastewater will contain pathogenic microorganisms which should be inactivated before discharge to certain catchments or before reuse for irrigation. In this context Advanced Oxidation Processes, able to generate a highly oxidative species, appear as a useful tool for the simultaneous removal of organic microcontaminants (OMCs) and bacteria.

Titanium dioxide (TiO_2) is a semiconductor photocatalyst widely investigated for the degradation of pollutants and inactivation of microorganisms.; however, TiO_2 photocatalysis requires UV excitation, and typically displays low quantum efficiencies due to fast charge carrier recombination. Where the TiO_2 is immobilised on an electrically conducting support, the application of an external electrical bias improves the separation of the photogenerated charge carriers, and thus improves the overall efficiency [1]. This process is normally referred to as electrochemically assisted photocatalysis (EAP), photoelectrocatalysis or sometimes, photoelectrolysis. The immobilization or formation of the catalyst on a support can decrease the effective surface area available for reaction, and may result in mass transfer limitations in the reactor [2, 3]. However, in EAP, mass transport might be improved due to the electromigration of negatively charged bacteria to a positively biased photoanode [2].

With EAP, oxidation of water at the semiconductor electrode (photoanode) gives hydroxyl radicals and reduction of molecular oxygen at the cathode can generate superoxide radical anion, hydrogen peroxide, and hydroxyl radicals. In natural water matrices containing dissolved ions, the EAP leads to the generation of other species including active chlorine species (ACS), HClO (E^0= 1.49 V/SHE) and ClO^- (E^0=0.89 V/SHE) [4], which are widely recognized as key oxidants in electrolytic water treatment. In a photoelectrochemical cell (PEC), the sites for oxidation and reduction are spatially separated avoiding surface recombination reactions, and photogenerated charge carriers are separated under the influence of the electric field, decreasing the rate of bulk recombination.

Generally, Pt has been used as counter electrode because its good chemical resistance to corrosion even in strongly aggressive media [5] and low over-potential for reduction reactions such as H_2 evolution. However, carbon-based electrodes have been extensively studied as cathodes [6, 7] due to their selective reduction of molecular oxygen to hydrogen peroxide [5]. The use of carbon cathodes is widespread in other electro-oxidative processes for the in situ generation of Fenton reagent, such as electro-Fenton [7] or solar photoelectro-Fenton. Most published research does not specifically consider the nature of the counter electrode in EAP, however, Xie and Li [8] reported a significant increase in the degradation of orange-G dye from 3.4% with a Pt cathode to 25.1% using reticulated vitreous carbon (RVC).

Previous research has reported that EAP using titanium dioxide nanotube (TiO_2-NTs) electrodes can achieve high inactivation rates for bacteria [9, 10], even in seconds [11] depending on the reactor configuration,

electrical potential applied, and the electrolyte solution. For degradation of organic micropollutants, TiO_2-NTs PEC have been applied for contaminants removal such as diclofenac [12], pentachlorophenol [13], or even aromatic amines [14]. However, the use of these systems for real waters with the aim of simultaneous disinfection and elimination of OMCs, in a realistic range of μg L^{-1}, has not been reported.

The goal of this study is to compare electrochemically assisted photocatalysis using a PEC reactor with a TiO_2-NT photoanode with either a carbon felt or Pt cathode for the simultaneous degradation of OMCs and inactivation of bacteria. In this work terbutryn (TBT), chlorfenvinphos (CVP), and diclofenac (DFC), were selected as OMCs and *E. coli* K12 (at 10^6 CFU mL^{-1}) was used as model microorganism. Natural (non-autoclaved or filtered) surface water was used for all experiments.

2. Materials and methods

2.1 Water matrix characterization

The water matrix used in this study was surface water. It was collected from a natural stream in Whiteabbey (Newtownabbey, UK). The characterization of this water matrix was done using a pH meter (multi720, WTW, Germany), conductivity meter (GLP31, CRISON, Spain), and turbidimeter (Model 2100N, Hach, USA). Ionic composition was measured using an ion chromatograph (IC) (Model 850, Metrohm, Switzerland). Dissolved organic carbon (DOC) was measured with a TOC analyser (Shimadzu TOC 5000A, Japan). Main characteristics of the water are pH 7.35, electric conductivity of 697 μS cm^{-1}, 0.1 NTU of turbidity, 6.9 mg L^{-1} of DOC and 18.4 mg L^{-1} of chloride. The detailed characterization is shown in Table SI-1.

2.2 Bacterial enumeration and quantification

E. coli K12 was obtained from the Spanish Culture Collection (CECT 4624). Fresh liquid cultures were prepared in Tryptone Soya Broth CM0129 (OXOID) and incubated during 20 h at 37 °C with rotary shaking, in order to achieve the stationary phase of 10^9 CFU mL^{-1}. Bacterial suspensions were diluted in the reactor to reach an initial concentration of 10^6 CFU mL^{-1}. The bacteria stock solution added to the water sample a DOC concentration of 6.7 mg L^{-1}. All samples were enumerated using the standard plate counting method with Tryptone Soya Agar CM0131 (OXOID). Six 20 μL drops of each dilution were plated. Colonies were counted after incubation at 37 °C for 24 h. The limit of detection (DL) was 9 CFU mL^{-1}.

For hole-acceptor experiments bacterial suspensions were harvested by centrifugation at 3000 rpm for 10 min. Then, the pellet was re-suspended in Phosphate Buffer Saline (PBS) solution and diluted directly into the sample to reach the initial concentration of 10^6 CFU mL^{-1}. Water samples taken during the experiments were enumerated using the standard plate counting method with ChromoCult®Coliform Agar (Merck KGaA, Darmstadt, Germany). 10-fold dilutions of water samples were done in PBS, and volumes ranged between 50-500 μL were spread onto Petri-dishes surface. Colonies were counted after an incubation period of 24 h at 37 ºC. Detection limit of this procedure was 2 CFU mL^{-1}.

2.3 Organic Microcontaminant Analysis

TBT, CVP, and DFC were used as a representative mixture of OMCs since they cover a wide spectrum of commonly found chemical anthropogenic contamination in surface waters (herbicide, pesticide and drugs respectively). The OMCs used were

analytical grade, purchased from Sigma-Aldrich. Stock solutions containing the three OMCs at 2.5 g L^{-1}/OMCs were prepared in methanol (organic matrix to dissolve the OMCs) and stored at 4ºC. stock solution (38 µL) was diluted in the sample to reach an initial concentration of 500 µg L^{-1}/OMCs. The dilution of OMCs added 60 mg L^{-1} of extra DOC concentration to the water matrix. The OMC concentration was monitored by high performance liquid chromatography using a HPLC/UV Agilent Technologies Series 1100, equipped with an analytical column Luna C18 (4.6 mm x 150 mm, 3µm) from Phenomenex. Injection volume was 100µL. The three OMCs were simultaneously detected using a gradient method, from 90/10 (v/v) of formic acid (25 mM)/acetonitrile (ACN) to 100% ACN after 14 min with a flow rate 1 mL min^{-1}.

For HPLC measurements, samples were prepared mixing 900 µL of sample and 100 µL of ACN that were filtered through a Millipore Millex-GN 0.20 µm nylon membrane filter. Then, the solution was transferred into HPLC vials, put in the HPLC and results analysed. Quantification of each OMC was done according to a standard curve previously prepared in the range of 10 to 1000 µg L^{-1}. Retention time, limit of quantification (LOQ), limit of detection (LOD), and maximum absorption for each OMCs are shown in Table SI-2.

2.4 Electrode preparation and characterization

The TiO_2-NT photoanodes were fabricated by electrochemical anodization of titanium mesh (Sigma-Aldrich) using the method described elsewhere [15]. Briefly, titanium mesh (75 x 95 mm^2) were sonicated and washed in 5% Decon90 detergent, distilled water and ethanol, sequentially. Electrochemical cell for anodization consisted of Pt coated Ti mesh cathode and titanium mesh as anode on each side of cathode, in a polypropylene beaker. The anodization process was repeated on the opposite side of the Ti mesh to have uniform nanotubes growth on both sides of the Ti mesh. The electrolyte solution was prepared by mixing NH_4F (0.3 wt%) in distilled water (3.0 vol%) and ethylene glycol (97 vol%). The anodization was performed at 30 V for 3 h using a PLH120 Power Supply. After anodization, the foils were rinsed multiple times in distilled water and then annealed at 500°C in air for 20 h (ramp 2°C min^{-1} up and 1°C min^{-1} down) in a Lenton AWF 12/5 Chamber Furnace.
The growth, coverage and dimensions of the TiO_2-NTs were examined using scanning electron microscopy (SEM) at 10 kV (Hitachi SU5000 FESEM). Energy dispersive X-ray analysis (EDX) was performed using Oxford Instruments EDX coupled with FESEM system.

2.5 Photoelectrochemical cell configuration

The total volume of the PEC reactor was 190 mL, which was irradiated through a quartz window (Figure 1a). TiO_2-NTs and platinized Ti mesh (Ti-Pt) mesh (Sigma-Aldrich) or carbon felt (Sigracet GDL 28 BC from Ion Power) were used as photoanode and cathodes for the different experiments, respectively. Electrode dimensions were 7.5 cm x 9.5 cm, with a total surface area of 71.25 cm^2 each. The electrodes were assembled following an anode-anode-cathode configuration in order to maximise the absorption of irradiated photons. The nanotubes were grown on Ti mesh that allowed 50% of the light to pass through its faces (experimentally determined). The misaligned mesh electrodes combination allowed only 25% of the light to pass through, so at least 75% of the direct photons interacted with the photoanodes. The reactor was operated in batch mode and electrodes were biased with a PLH120 Power Supply.

An air-blower was connected to the reactor with a flow rate of 0.36 mL min^{-1} to avoid the depletion of dissolved oxygen during the

photocatalytic process and simultaneously kept the solution stirred. Two 9W UVA black light lamps were placed in front of the Ti-mesh side of the PEC (Phillips, Actinic BL PL-S 9W/10/2P; 370 nm-peak wavelength). The irradiation profile of the lamps (Fig SI-1) was determined by the use of a GEMINI 180 scanning monocromator from HORIBA, measuring at different distances of the source aiming to achieve an incident irradiance of 50 W m^{-2} in the UVA, equivalent to high intensity solar UV with Air Mass of 1.5 (ASTM E-490-00). A scheme of the complete system is shown in Figure 1b.

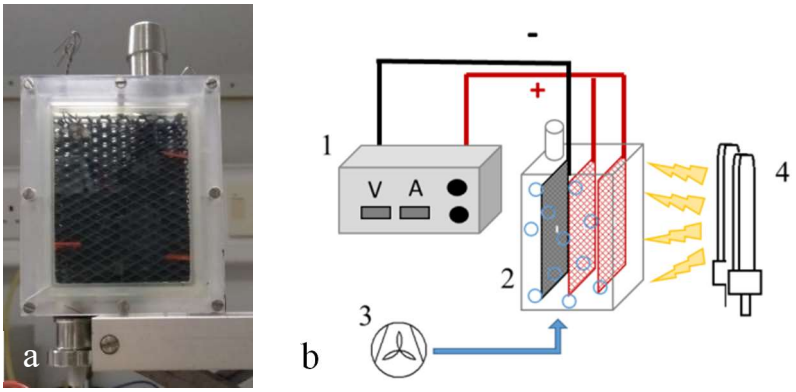

Figure 1. a) photograph of PEC reactor b) Experimental setup: (1) power supply (2) PEC cell (cathode in black, anodes in red), (3) air-blower, (4) UVA lamps.

2.6 Photoelectrochemical experiments

The reactor operational potential was determined according to the minimum potential at which maximum photocurrent (plateau) is reached (see section 3.3). For this purpose, several potentials were applied to the cell, increasing the interval by 0.1 V each time, measuring the current response in dark conditions and under irradiation for each applied potential. The photocurrent is calculated thought the difference between the current response under radiation and in dark. Current densities and applied potentials were measured using LAP MAS830B multimeter.

For OMCs and bacterial removal experiments the reactor was filled with surface water in natural conditions (without any pre-treatment or addition of reagents), at pH 7.4 and air sparged. After a few minutes the target contaminant was added, whether it was the microorganism, the OMCs, or both, leaving to equilibrate for 10 min. An initial sample t=0 was taken and the reactor was biased and exposed to irradiation. The samples were taken at 5 min interval till 20 min, every 15 min till 60 min and then every 30 min until the end of the. Before and after carrying out each experiment, the reactor was washed with a solution of 10 mg L^{-1} hydrogen peroxide and was rinsed three times with distilled water.

2.7 ROS determination

Several oxidative agents generated during PEC operation were detected by spectrophotometric methods. A JENWAY 6300 UV-VIS spectrophotometer was used with glass cuvettes of 1 cm path length.

i) Hydroxyl radicals generated were measured by spectrophotometry following procedure described elsewhere [16, 17]. Briefly, it consists of detecting the bleaching of a solution with 17 µM P-nitrosodimethylaniline (RNO) (Sigma-Aldrich) by measuring light absorbance at 440 nm. Quantification was made in the range from 1 to 20 µM. It has to be considered that the presence of other oxidant could generate interferences in this method.

ii) Free chlorine (FC) was determined following N,N-diethyl-p-phenylenediamine (DPD) method 10069 from HACH. It consists on the addition of DPD powder pillows from HACH to the sample, mixing for 30 seconds and measuring at 530 nm.

iii) Hydrogen peroxide concentration was determined by direct reaction with titanium (IV) oxysulfate. For that, 2 mL of 280 mM solution of $TiOSO_4$ (Sigma-Aldrich) were mixed with 2 mL of sample [17]. The yellow complex formed from the reaction of titanium IV oxysulfate with H_2O_2 is measured at 410 nm. Absorbance was read after 5 min equilibration time against a standard curve in the H_2O_2 concentration range 1 - 60 mg L^{-1}.

3. Results and discussion

3.1 Anodised TiO_2-NTs characterisation

Figure 2a shows SEM images of the nanotubes fabricated by the electrochemical anodisation of Ti mesh. There was a reasonable uniform coverage of the mesh with TiO_2-NT with an average outer diameter of 95.2 nm, inner diameter of 73.6 nm diameter, tube wall thickness of 21.6 nm and average length of 1.05 μm.

The SEM-EDX measurements of the annealed nanotubes show the peaks corresponding to Ti and O elements, indicating the formation of the TiO_2 nanotubes (data not shown). The XRD analysis of the samples was performed on annealed nanotubes, (Figure 2b). As shown in the figure, the major peaks correspond to anatase planes A(101) and A(004). Other peaks corresponding to A(200), rutile R(110) and titanium metal were obtained. The titanium metal peaks are coming from the Ti substrate used for the nanotubes growth. Presence of significantly less intense rutile peaks indicates that the nanotubes are mostly anatase with very little contribution from rutile phase.

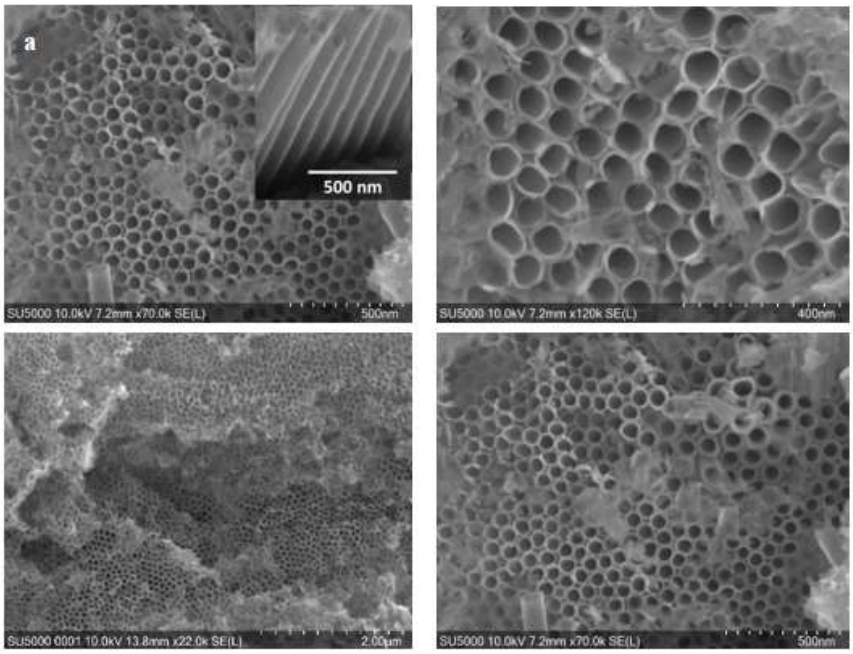

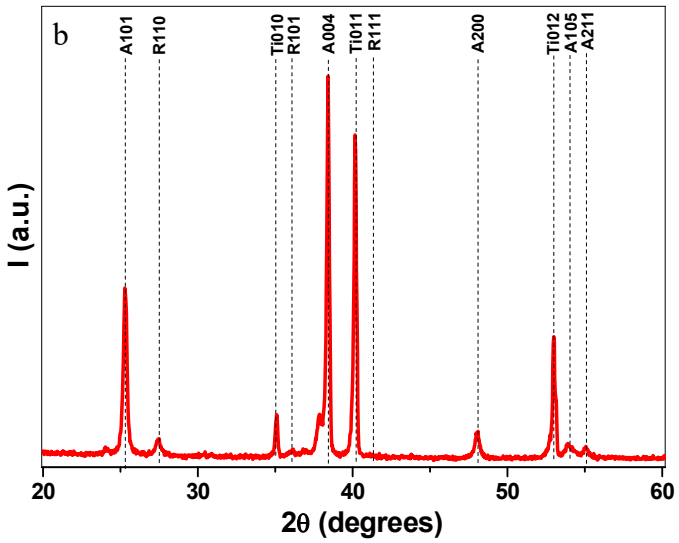

Figure 2. Characterization of TiO_2-NTs prepared by electrochemical anodization of Ti mesh: a) SEM images with inset(a) view of cross-section of the nanotubes and b) XRD analysis.

3.2 Assessment of boundary effects on PEC cell: dark and photocatalytic (PC) tests

To discriminate the influence of any possible parameter on the water disinfection and decontamination performance of PEC a series of different tests were carried out. Firstly, the viability of *E. coli* in the presence of OMCs were assessed in the dark. Results obtained demonstrated that the initial concentration of bacteria (10^6 CFU mL^{-1}) remained constant for 3 h (Fig. SI-2). This result discarded therefore any toxic effect over bacterial viability due to the presence of 500 µg L^{-1} of each contaminant (including the 158 mg L^{-1} -approximately 5 mM- of methanol added from the OMCs stock solution).

The photocatalytic activity of TiO_2-NT to inactivate *E. coli* and remove OMCs from water was also investigated using the same PEC without applying the electrical bias (open circuit = photocatalysis). Figure 4a shows a very small decay of *E. coli* concentration in 2 h of photocatalytic (PC) treatment, attaining only 0.8-Log Reduction Value (LRV) after 2 h of PC. This low efficiency is not surprising in an immobilized catalyst configuration. It is very well known that its photocatalytic disinfection efficiency is lower compared with similar load of catalyst in slurry, especially if the catalyst is disposed as a flat plate as mode of immobilisation. This is due to the reduced catalytic surface area available ROS generation, and mass transport limitations from bulk solution to the electrode surface.

Prior to any OMCs degradation test, controls were performed to determine dark adsorption of the OMCs on the electrodes. For that, OMCs were added to the reactor leaving in dark during 1h, being the decay negligible. The removal of the ∑OMCs by PC during 60 min of treatment was studied (Figure 4b). The mixture of OMCs illustrated a representative mixture of different anthropogenic contaminants that could be found in surface waters, therefore the ∑OMCs was monitored during the experiment which permitted the comparison with different operating conditions. A linear decrease was observed in this case, reaching ca. 70% of degradation of the mixture, with a zero order rate constant k =1.07 ± 0.08 (10^{-2} min^{-1}). Nevertheless, the removal was not similar for each OMC, a degradation of 57%, 60% and 87% of TBT, CVP and DCF, respectively were attained (Fig SI-3). After

60 min of PC treatment, OMCs concentrations were below their limit of quantification (see Table SI-2). TBT and CVP presented similar behaviour, with a slower degradation rates that shows its greater recalcitrant character when compared to DCF, which almost eliminated. The removal of ∑OMCs achieved (ca. 70%) without system optimisation was near to that established as target by Switzerland regulations for WWTP effluents (80% of ∑OMCs removal), being a reference for the rest of countries since it is the first water regulation addressing OMCs concern [18] in Europe. DOC effect was also followed in other study [19] determining that in a concentration higher than 10 mg L^{-1} produces a decrease in the degradation rates of DFC due to competition for active sites and ROS. In the present study, with at least 60 mg L^{-1} of DOC, a marked reduction in the degradation efficiency of the PEC for both, organics and bacteria, was expected. In fact, this study is focused on a real water matrix scenario, where naturally present ions interfere and the total organic matter acts as background organic matter.

3.3 Photoelectrocatalysis with cathode of Pt

The optimal current density (calculate photocurrent) for the Pt cathode PEC (PEC-Pt) was established by measuring current response in the dark and under UVA irradiation with applied cell potential between 0.0 V to 1.5 V, using surface water as electrolyte. Figure 3 shows that the photocurrent rises significantly till 0.5 V, from which the increase was moderated reaching a plateau after the application of 1.0 V. Therefore, 1.0 V was selected as the operating potential for EAP tests, corresponding to a photocurrent response of 3 mA (estimated current density of 21 µA cm^{-2}).

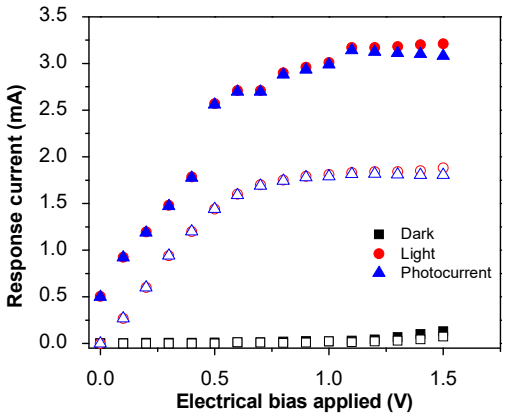

Figure 3. Response current densities in dark and under radiation, and the calculated photocurrent, obtained by the application of a serial of potentials from 0 to 1.5 V using a Pt cathode (full symbol) and C-felt cathode (open symbol).

As this is an electrochemical process, the PEC efficiency is clearly influenced by the concentration of salts in the water to be treated, not only due to the impedance presented for the electrical current, but also from the specific ionic content. It has been demonstrated that the ionic species dissolved in the water determine the oxidant species generated during the electrochemical treatment [20, 21] since ACS are produced from chlorides oxidation and sulphate radicals (E^0 = 2.5 – 3.1 V) from sulphates, adding their oxidative effect to that of the hydroxyl radicals.

The content of salts from the actual stream under study (see Table SI-1) was far from the majority of studies previously published, in which highly concentrated solutions of Na_2SO_4, NaCl or $NaNO_3$, etc., are used as electrolytes, thus the behaviour of our system was very different. The matrix effect is also remarked by Moles, Valero, Escuadra, Mosteo, Gomez and Ormad [22] where it was clear the difference between a NaCl solution and a real effluent as water matrix, since disinfection with saline solution achieved 7-LRV while in the wastewater effluent was reached ca. 1-LRV,

evidencing the influence of the water composition in the disinfection process by PEC.

Despite the low salinity of the surface water (697 µS cm^{-1} vs 8.8 mS cm^{-1} of a 50 mM Na_2SO_4 supporting electrolyte solution), the PEC-Pt system gave a 2-LRV in 120 min of treatment as is shown in Figure 4a. In comparison with PC alone, a similar pattern of bacteria inactivation was obtained with PEC-Pt, but with a slight increase on the bacterial reduction at the end of the treatment. This enhancement can be attributed to the enhanced charge carrier separation.

The application of an electrical bias has been reported to give also an enhancement in the degradation of OMCs as compared to PC [12, 23]. In this work no real difference was observed in the rate of OMC degradation with EAP (k =1.15 ± 0.12 (10^{-2} min^{-1})) as compared to PC (k =1.07 ± 0.08 (10^{-2} min^{-1})) (Fig. 4b). This behaviour remarked the influence of the high amount of organic matter provided by the stock solution, that competed with OMCs for oxidizing radicals.

The direct comparison with previous work on the EAP degradation of OMCs is not realistic due differences in experimental parameters (mainly a high OMCs concentration in the range of several mg L^{-1}). However Mazierski, Borzyszkowska, Wilczewska, Bialk-Bielinska, Zaleska-Medynska, Siedlecka and Pieczynska [24] studied the removal of 0.385 mM (50 mg L^{-1}) of 5-fluorouracil in a 42 mM Na_2SO_4 solution with a TiO_2-NT photoanode, using in a solar simulator with a Xenon lamp applying an UV-A irradiation of 4.5 mW cm^{-2} (45 W m^{-2}). When applied a potential of 1 V, more than 60 min were needed to remove the 80% of the initial concentration of 5-fluorouracil, approximately the same time as was needed to our system to remove the same percentage starting from a lower concentration of pollutant. In other cases, as Cheng, Cheng, Deng, Wang and Liu [12], the treatment time is much longer, since using a TiO_2-NT anode (4 cm^2) and a 35W Xenon lamp, needed more than 5 h to remove the 80% of 5 mg L^{-1} of DCF in a 0.1M solution of Na_2SO_4 applying 0.4 V.

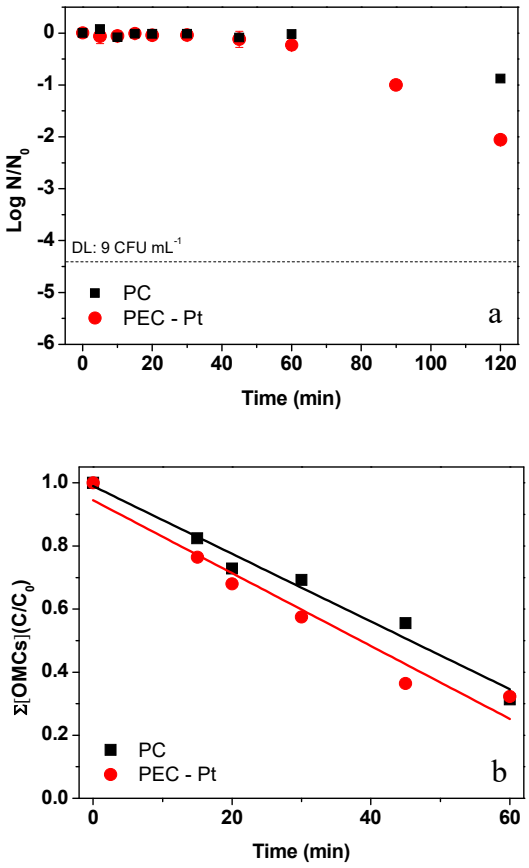

Figure 4. a) E. coli inactivation and b) ΣOMCs concentration during photocatalysis (PC), EAP with Pt cathode (PEC-Pt) in surface water.

3.4 Photoelectrocatalysis with cathode of C-felt

The working potential for PEC with C-felt cathode (PEC-C felt) was determined by monitoring the photocurrent response with the cell potential increasing from 0.0 V to 1.5 V and observing the maximum photocurrent value (Fig. 3). The photocurrent behaviour was similar to PEC-Pt, reaching the maximum at 1V, but with a lower current density value, 1.8 mA (12.5 µAcm^{-2}) due to

the higher resistance of the carbon felt as compared to Ti-Pt mesh.

Figure 5a shows the *E. coli* inactivation profile obtained by PEC-C felt. Although a lower photocurrent was observed, there was a greater LRV of 2.7 achieved. It has been reported previously that the rate of disinfection is not directly proportional to the photocurrent in EAP [9]. The improvement in the rate of disinfection may be attributed to the selective production of hydrogen peroxide (H_2O_2) at the carbon cathode.

It is well known that H_2O_2 is a disinfectant that even at low concentrations it can enhance the rate of photo-inactivation of microorganisms [25]. This phenomenon is explained by the diffusion of H_2O_2 across the cell membrane as it is a non-charged molecule. Once inside the cell, the equilibrium of ROS changes, releasing the iron naturally occurring in cells that reacts with H_2O_2 to produce internal $^{\bullet}OH$ which accumulation and reaction with internal structures (DNA, proteins, enzymes, etc) finally determines the cell death [26]. In fact, the use of a carbon cathode for in situ generation of H_2O_2 as an enhancement for solar disinfection (SODIS) process was investigated by Jin, Shi, Chen, Chen, Chen, Zheng, Liu and Ding [27] that reach approximately 6-LRV on *E. coli K12* concentration in 180 min while 3-LRV was attained by only SODIS and electrolysis 1-LRV.

For the PEC-C felt system it is possible to calculate the theoretical maximum amount of H_2O_2 electrogenerated that could be obtained in the system. Knowing the electrical charge (Q), with the Faraday constant (F, 96485 Q mol^{-1}), the e^- moles (n_e) can be calculated based on equation 1. The maximum accumulated H_2O_2 that could be generated in our experimental system, assuming that all e^- are employed in its production, was 15 mg L^{-1} after 120 min. However, as it was consumed as being generated, we were not able to detect the level of H_2O_2 using the titanium oxysulphate method as the limit of quanitifation was only 1 ppm.

$$Q = n_e \cdot F \qquad \text{(Eq. 1)}$$

In addition, FC is generated simultaneously due to chlorine oxidation, being able to react with the electrogenerated H_2O_2 (reaction 1). In fact the use of H_2O_2 as quencher for FC in drinking water is commonly used [28]. Thus apart from H_2O_2 internal diffusion across cell membranes, H_2O_2 could generate O_2 through reaction 1, so producing ROS according to reactions 2-5, explaining the subsequently enhance of bacteria inactivation.

$$HOCl + H_2O_2 \rightarrow O_2 + H_2O + HCl \qquad \text{(R.1)}$$

$$e_{CB}^- + O_2 \rightarrow O_2^{\bullet -} \qquad \text{(R.2)}$$

$$O_2^{\bullet -} + H^+ \rightarrow HO_2^{\bullet} \qquad \text{(R.3)}$$

$$2HO_2^{\bullet} \rightarrow H_2O_2 + O_2 \qquad \text{(R.4)}$$

$$H_2O_2 + O_2^{\bullet -} \rightarrow {}^{\bullet}OH + OH^- + O_2 \qquad \text{(R.5)}$$

There was no improvement in the degradation rate of the OMCs using the carbon cathode (Figure 5b). The degradation of the sum of OMCs was similar to that observed with the Pt cathode, with k =1.17 ± 0.05 (10^{-2} min^{-1}). The % degradation achieved for the individual OMCs was 63% of TBT, 57% of CVP and >90% of DCF in 60 min (Figure SI-3).

In other studies it was demonstrated that H_2O_2 itself is not able to remove OMCs, as in Michael, Michael-Kordatou, Nahim-Granados, Polo-López, Rocha, Martínez-Piernas, Fernández-Ibáñez, Agüera, Manaia and Fatta-Kassinos [29] where the combination of sunlight and H_2O_2, in a concentration of 30 mg L^{-1}, after 5 h of treatment only achieved the removal of the 46% of sulfamethoxazole in an urban wastewater with 15 mg L^{-1} of DOC.

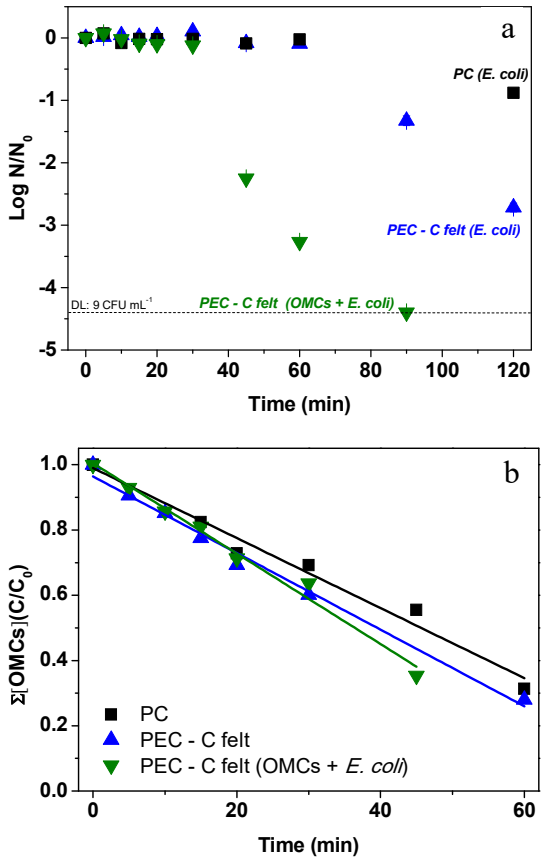

Figure 5. a) *E. coli* inactivation and b) OMCs degradation profiles obtained by photocatalysis (PC), photoelectrocatalysis with carbon felt cathode (PEC-C felt) in surface water.

Moreover, in Jiménez-Tototzintle, Oller, Hernández-Ramírez, Malato and Maldonado [30], it was studied the effects of H_2O_2 addition to a TiO_2 supported catalyst for the removal of imazalil, thiabendazole and acetamiprid (200 µg L^{-1} each) in a wastewater treatment plant effluent with 25.2 mg L^{-1} of DOC, being required 500 mg L^{-1} of H_2O_2 to achieve a remarkable improvement, evidencing its low efficiency to remove OMCs even acting as electron acceptor. Therefore in our system, where peroxide production is very low, no improvement is expected. Moreover if it reacts with FC generating producing finally ROS, consequently the amount generated will be also very low and, even if they improves the inactivation of bacteria, they will probably not be enough to mineralize the OMCs.

The simultaneous removal of OMCs and *E. coli* was also investigated aiming to evaluate any possible competition effect between both targets during the PEC-C felt treatment. Results are shown in Figure 5a and b for *E. coli* and OMCs, respectively.

The PEC-C felt system for the simultaneous treatment improved the rate of *E. coli* inactivation as compared to the disinfection results in the absence of OMCs. The detection limit was reached in 90 min of treatment (approximately 4.5-LRV). The enhancement in bacterial inactivation could be cause due to the methanol added from the OMCs stock solution. On the one hand the oxidation of methanol generates formaldehyde (HCHO) [31] which is bactericidal even at low concentrations (LC_{50} for *E. coli* = 1 mg L^{-1} or 33 µM) [32, 33]. On the other hand, methanol is a hole scavenger that increases the photocurrent and may led to the generation of more H_2O_2 at the cathode. The action of hole scavengers is described in detail in section 3.6. Regarding ∑OMCs a slight enhancement is observed with a rate constant of k =1.38 ± 0.07 (10^{-2} min^{-1}).

3.5 Oxidant species generated during PEC

The generation oxidant species was monitored during PC (as reference) and for EAP with the carbon electrode. Figure 6a shows the results of of RNO bleaching measured •OH when using PEC-C felt system in comparison with PC. It should be considered that in waters containing chlorides, ACS are produced which are able to bleach RNO by themselves, being an interference for •OH determination [16]. For that reason the RNO bleaching was considered as a parameter to evaluate the oxidative power of the electrochemical system.Specifically, after 30 min of EAP with the carbon cathode, 66% of the RNO

was removed while 27% with PC. These results support the benefits of EAP for the inactivation and degradation of *E. coli* and OMCs (Fig. 5a and 5b, respectively) in comparison with PC in water. The application of an external electrical bias serves to separate the charge carriers and therefore should increase oxidant species production at the photoanode.

H_2O_2 quantification was not feasible as the detected amount was but below the quantification limit (1 mg L^{-1}). As described in section 3.4, electrogenerated H_2O_2 rapidly reacts with FC thus avoid its proper quantification.

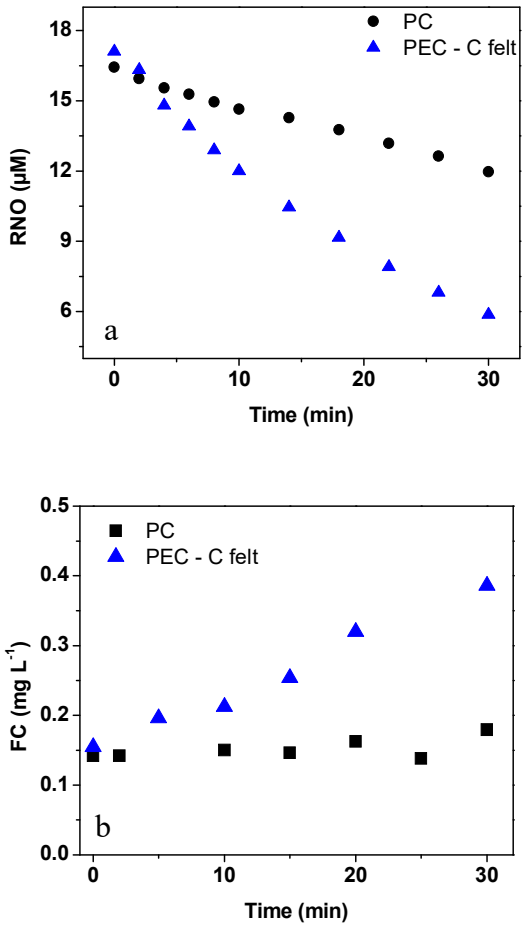

Figure 6. Generation of a) RNO bleaching and b) FC during PC and EAP in a PEC-C felt cathode.

The generation of FC measured with the PEC-C felt and PC is shown in Figure 6b. It is observed that values of FC detected was higher in the case of EAP than in PC. FC is formed by the oxidation of chloride present in the surface water (18.4 mg L^{-1}). With EAP, the separation of charge carriers means the holes are longer lived and more likely to react with chloride. Moreover, according to reaction 1, part of the FC produced is quenched by the electrogenerated H_2O_2, so the measurement represents residual FC in the solution. The concentration of FC detected during PEC-C felt treatment was very low (< 0.5 mg L^{-1}) in 30 min of treatment. This is below the recommended free chlorine level for residual disinfection of water [34] .

3.6 Influence of hole acceptors in PEC disinfection

In this study, the bacteria inactivation by PEC-C felt cathode was tested in the presence of 5 mM of methanol and acetate as hole-acceptors (Fig. 7), as this was the concentration of methanol added with the stock solution of OMCs. In EAP processes with TiO_2 photoanodes, hole-acceptors such as methanol and acetate, generate an increase in the photocurrent studied in detail by Byrne, Eggins, Linquette-Mailley and Dunlop [35]. The one electron oxidation of methanol generates a radical which injects a second electron to the conduction band, giving rise to photocurrent doubling. However, acetate is not a current doubling agent. For that reason, in our study the average of photocurrent with methanol was a 38% higher than without hole scavengers while for acetate was a 20% higher.

Regarding disinfection, the inactivation rates obtained in the presence of hole acceptors are much higher (Fig. 7). For methanol, this enhancement was previously explained due to the formation of formaldehyde which is highly toxic for microorganism and the generation of ROS derived from oxygen reduction reactions (reactions 2-5) while for acetate, the improvement have to be caused mainly for the ROS.

That way, extracellular ROS and intracellular •OH can inactivate bacteria through DNA/RNA damage, membrane rupture, interruption of respiratory pathways or increased ion permeability [36]. Previous studies pointed out the sensitivity of *E. coli* to H_2O_2 [37] and the effective inactivation in the presence of superoxide radicals ($O_2^{\bullet-}$) [38]. Therefore, using a hole scavenger and carbon felt as a cathode simultaneously could lead to a lower electron-hole recombination rate, allowing increasing the number of photoinduced electrons that are able to reduce oxygen and produce higher concentrations of ROS, such as H_2O_2 and $O_2^{\bullet-}$.

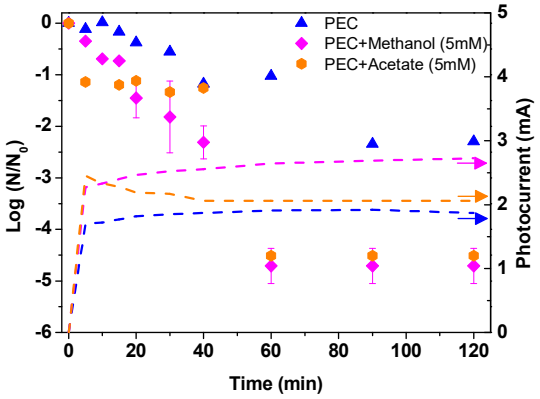

Figure 7. *E. coli* inactivation profile for PEC with C-felt cathode with methanol and acetate as hole acceptors.

4. Conclusions

PEC systems based on TiO_2-NTs has been evaluated as an alternative for the treatment of real surface water, in which salt concentration is substantially lower than in the solutions used as supporting electrolytes, eg., Na_2SO_4 that is commonly used in concentrations of 50 mM or higher. This research has confirmed the suitability of using C-felt cathode for a PEC cell as promising alternative to Pt. Carbon-based electrodes at the same current, without additional energy cost, are able to simultaneously produce H_2O_2, improving current efficiency of the system. The simultaneous removal of OMCs and *E. Coli* has been successfully proven in the PEC - C felt system for surface water depuration being the first step for the application of this system in conditions closer to reality. The presence of a significant amount of background organic matter (60 mg L^{-1}) had a critical effect on the efficiency since it caused a scavenger effect for the oxidant radicals. Despite this, 70% degradation of the OMCs was reached. The study of oxidizing species confirmed that the generation of H_2O_2 and FC represents a great improvement for disinfection purposes, despite they do not significantly affect the removal of OMCs. Nevertheless, it is important to highlight that further research must be tackled to better distinguish and define the inactivation mechanism when PEC-C felt system is applied.

Acknowledgements

This research has received funding from the European Union's Horizon 2020 via the Marie Curie Action under the grant agreement number 734560 (ALICE), and the research and innovation program under the grant agreement number 820718 , which is jointly funded by the European Commission and the Department of Science and Technology of India (PANIWATER).

Declarations of interest: none

References

[1] J.A. Byrne, A. Davidson, P.S.M. Dunlop, B.R. Eggins, Water treatment using nano-crystalline TiO_2 electrodes, J. Photoch. Photobio. A., 148 (2002) 365-374.

[2] C. Pablos, J. Marugán, C. Adán, M. Osuna, R. van Grieken, Performance of TiO_2 photoanodes toward oxidation of methanol and E. coli inactivation in water in a scaled-up photoelectrocatalytic reactor, Electrochim. Acta, 258 (2017) 599-606.

[3] W.H. Leng, W.C. Zhu, J. Ni, Z. Zhang, J.Q. Zhang, C.N. Cao, Photoelectrocatalytic

destruction of organics using TiO_2 as photoanode with simultaneous production of H_2O_2 at the cathode, Appl. Catal. A-Gen, 300 (2006) 24-35.

[4] F.C. Moreira, R.A.R. Boaventura, E. Brillas, V.J.P. Vilar, Electrochemical advanced oxidation processes: a review on their application to synthetic and real wastewaters, Applied Catalysis B: Environmental, 202 (2017) 217-261.

[5] M. Panizza, Importance of electrode material in the electrochemical treatment of wastewater containing organic pollutants, in: C. Comninellis, G. Chen (Eds.) Electrochemistry for the Environment, Springer, New York, 2010, pp. 25-54.

[6] S. Cotillas, J. Llanos, M.A. Rodrigo, P. Canizares, Use of carbon felt cathodes for the electrochemical reclamation of urban treated wastewaters, Appl. Catal. B-Environ., 162 (2015) 252-259.

[7] T.X.H. Le, M. Bechelany, M. Cretin, Carbon felt based-electrodes for energy and environmental applications: a review, Carbon, 122 (2017) 564-591.

[8] Y.B. Xie, X.Z. Li, Interactive oxidation of photoelectrocatalysis and electro-Fenton for azo dye degradation using TiO_2–Ti mesh and reticulated vitreous carbon electrodes, Mater. Chem. Phys., 95 (2006) 39-50.

[9] C. Pablos, J. Marugán, R. van Grieken, P. Dunlop, J. Hamilton, D. Dionysiou, J. Byrne, Electrochemical enhancement of photocatalytic disinfection on aligned TiO_2 and nitrogen doped TiO_2 nanotubes, Molecules, 22 (2017) 704.

[10] N. Baram, D. Starosvetsky, J. Starosvetsky, M. Epshtein, R. Armon, Y. Ein-Eli, Enhanced inactivation of E. coli bacteria using immobilized porous TiO_2 photoelectrocatalysis, Electrochim. Acta, 54 (2009) 3381-3386.

[11] X. Liu, Y. Han, G. Li, H. Zhang, H. Zhao, Instant inactivation and rapid decomposition of Escherichia coli using a high efficiency TiO_2 nanotube array photoelectrode, RSC Adv., 3 (2013) 20824-20828.

[12] X. Cheng, Q. Cheng, X. Deng, P. Wang, H. Liu, A facile and novel strategy to synthesize reduced TiO_2 nanotubes photoelectrode for photoelectrocatalytic degradation of diclofenac, Chemosphere, 144 (2016) 888-894.

[13] X. Quan, X. Ruan, H. Zhao, S. Chen, Y. Zhao, Photoelectrocatalytic degradation of pentachlorophenol in aqueous solution using a TiO_2 nanotube film electrode, Environ. Pollut., 147 (2007) 409-414.

[14] J.C. Cardoso, T.M. Lizier, M.V.B. Zanoni, Highly ordered TiO_2 nanotube arrays and photoelectrocatalytic oxidation of aromatic amine, Appl. Catal. B-Environ., 99 (2010) 96-102.

[15] Y. Shin, S. Lee, Self-Organized Regular Arrays of Anodic TiO_2 Nanotubes, Nano Lett., 8 (2008) 3171-3173.

[16] J. Muff, L.R. Bennedsen, E.G. Søgaard, Study of electrochemical bleaching of p-nitrosodimethylaniline and its role as hydroxyl radical probe compound, J. Appl. Electrochem., 41 (2011) 599-607.

[17] B.R. Cruz-Ortiz, J.W.J. Hamilton, C. Pablos, L. Díaz-Jiménez, D.A. Cortés-Hernández, P.K. Sharma, M. Castro-Alférez, P. Fernández-Ibañez, P.S.M. Dunlop, J.A. Byrne, Mechanism of photocatalytic disinfection using titania-

graphene composites under UV and visible irradiation, Chem. Eng. J., 316 (2017) 179-186.

[18] M. Bourgin, B. Beck, M. Boehler, E. Borowska, J. Fleiner, E. Salhi, R. Teichler, U. von Gunten, H. Siegrist, C.S. McArdell, Evaluation of a full-scale wastewater treatment plant upgraded with ozonation and biological post-treatments: Abatement of micropollutants, formation of transformation products and oxidation by-products, Water Res., 129 (2018) 486-498.

[19] L. Gao, B. Zhou, F. Wang, R. Yuan, H. Chen, X. Han, Effect of dissolved organic matters and inorganic ions on TiO2 photocatalysis of diclofenac: mechanistic study and degradation pathways, Environ. Sci. Pollut. Res., 27 (2020) 2044-2053.

[20] A. Farhat, J. Keller, S. Tait, J. Radjenovic, Assessment of the impact of chloride on the formation of chlorinated by-products in the presence and absence of electrochemically activated sulfate, Chem. Eng. J., 330 (2017) 1265-1271.

[21] A. Farhat, J. Keller, S. Tait, J. Radjenovic, Oxidative capacitance of sulfate-based boron-doped diamond electrochemical system, Electrochem. Commun., 89 (2018) 14-18.

[22] S. Moles, P. Valero, S. Escuadra, R. Mosteo, J. Gomez, M.P. Ormad, Performance comparison of commercial TiO2: separation and reuse for bacterial photo-inactivation and emerging pollutants photo-degradation, Environ. Sci. Pollut. Res., (2020).

[23] X. Nie, J. Chen, G. Li, H. Shi, H. Zhao, P.-K. Wong, T. An, Synthesis and characterization of TiO_2 nanotube photoanode and its application in photoelectrocatalytic degradation of model environmental pharmaceuticals, J. Chem. Technol. Biot., 88 (2013) 1488-1497.

[24] P. Mazierski, A.F. Borzyszkowska, P. Wilczewska, A. Bialk-Bielinska, A. Zaleska-Medynska, E.M. Siedlecka, A. Pieczynska, Removal of 5-fluorouracil by solar-driven photoelectrocatalytic oxidation using Ti/TiO_2(NT) photoelectrodes, Water Res., 157 (2019) 610-620.

[25] M.I. Polo-López, I. García-Fernández, I. Oller, P. Fernández-Ibáñez, Solar disinfection of fungal spores in water aided by low concentrations of hydrogen peroxide, Photoch. Photobio. Sci., 10 (2011) 381-388.

[26] S. Giannakis, M.I. Polo López, D. Spuhler, J.A. Sánchez Pérez, P. Fernández Ibáñez, C. Pulgarin, Solar disinfection is an augmentable, in situ -generated photo-Fenton reaction—Part 1: A review of the mechanisms and the fundamental aspects of the process, Appl. Catal. B-Environ, 199 (2016) 199-223.

[27] Y. Jin, Y. Shi, Z. Chen, R. Chen, X. Chen, X. Zheng, Y. Liu, R. Ding, Enhancement of solar water disinfection using H2O2 generated in situ by electrochemical reduction, Appl. Catal. B-Environ., 267 (2020).

[28] L.K. Wang, Y.T. Hung, N.K. Shammas, Handbook of Environmental Engineering: Advanced Physicochemical Treatment Processes, Humana Press, 2006.

[29] S.G. Michael, I. Michael-Kordatou, S. Nahim-Granados, M.I. Polo-López, J. Rocha, A.B. Martínez-Piernas, P. Fernández-Ibáñez, A. Agüera, C.M. Manaia, D. Fatta-Kassinos, Investigating the impact of UV-C/H_2O_2 and sunlight/H_2O_2 on the removal of antibiotics, antibiotic resistance

determinants and toxicity present in urban wastewater, Chem. Eng. J., 388 (2020).

[30] M. Jiménez-Tototzintle, I. Oller, A. Hernández-Ramírez, S. Malato, M.I. Maldonado, Remediation of agro-food industry effluents by biotreatment combined with supported $TiO_2/H2O_2$ solar photocatalysis, Chem. Eng. J., 273 (2015) 205-213.

[31] C. Pablos, J. Marugán, R. van Grieken, C. Adán, A. Riquelme, J. Palma, Correlation between photoelectrochemical behaviour and photoelectrocatalytic activity and scaling-up of P25-TiO_2 electrodes, Electrochim. Acta, 130 (2014) 261-270.

[32] E. Bae, J.W. Lee, B.H. Hwang, J. Yeo, J. Yoon, H.J. Cha, W. Choi, Photocatalytic bacterial inactivation by polyoxometalates, Chemosphere, 72 (2008) 174-181.

[33] K. Verschueren, Handbook of environmental data on organic chemicals: Vol. 1, John Wiley and Sons, Inc, 2001.

[34] W.H.O. WHO, Guidelines for drinking-water quality. Fourth edition incorporating the first adenddum, (2017).

[35] J.A. Byrne, B.R. Eggins, S. Linquette-Mailley, P.S.M. Dunlop, The effect of hole acceptors on the photocurrent response of particulate TiO_2 anodes, Analyst, 123 (1998) 2007-2012.

[36] H. Sun, G. Li, T. An, H. Zhao, P.K. Wong, Unveiling the photoelectrocatalytic inactivation mechanism of Escherichia coli: Convincing evidence from responses of parent and anti-oxidation single gene knockout mutants, Water Res., 88 (2016) 135-143.

[37] L.A. Morais, C. Adán, A.S. Araujo, A.P.M.A. Guedes, J. Marugán, Photocatalytic Activity of Suspended and Immobilized Niobium Oxide for Methanol Oxidation and Escherichia coli Inactivation, J. Adv. Oxid. Technol., 19 (2016) 256-265.

[38] R. Gupta, J.M. Modak, G. Madras, Behavioral analysis of simultaneous photo-electro-catalytic degradation of antibiotic resistant E. coli and antibiotic via ZnO/CuI: a kinetic and mechanistic study, Nanoscale Advances, 1 (2019) 3992-4008.

Supplementary information

Table SI-1. Physic-chemical characterization of surface water used in this study.

Sodium	14.9 mg L^{-1}
Ammonium	0.2 mg L^{-1}
Magnesium	13.5 mg L^{-1}
Calcium	50.5 mg L^{-1}
Potassium	1.2 mg L^{-1}
Chloride	18.4 mg L^{-1}
Nitrite	0.1 mg L^{-1}
Nitrate	2.8 mg L^{-1}
Phosphate	1.3 mg L^{-1}
Sulphate	110.9 mg L^{-1}
pH	7.4
Conductivity	697 µS cm^{-1}
Turbidity	0.1 NTU
DOC	6.9 mg L^{-1}

Table SI-2. Retention time, LOD, LOQ and maximum absorption of each OMC used in this study.

OMCs	**Retention time (min)**	**LOQ (µg L^{-1})**	**LOD (µg L^{-1})**	**Maximum absorption (λ)**
TBT	10.6	130	10	230 nm
CVP	13.5	170	40	240 nm
DFC	12.7	40	40	285 nm

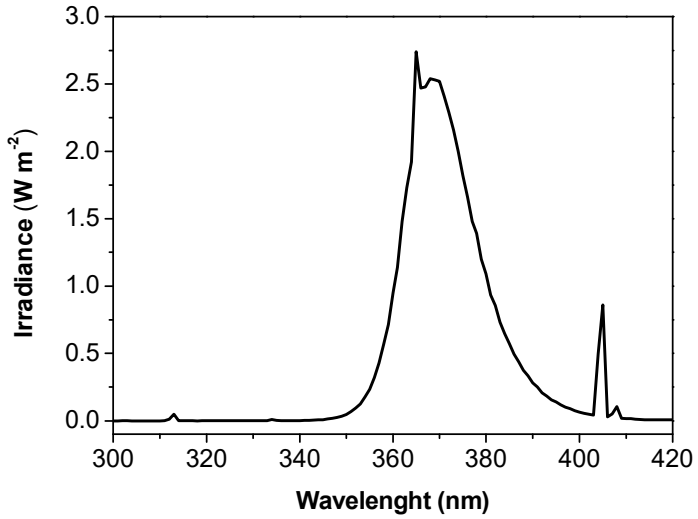

Figure SI-1. Irradiation profile of the 9W UVA blacklight lamps used to illuminate the TiO_2-NTs photoanodes.

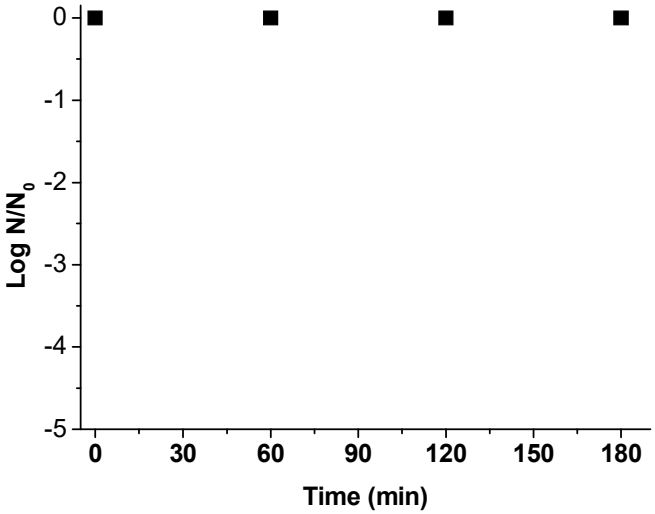

Figure SI-2. Profile of *E. coli* concentration detected along 3 h in the presence of 500 μgL^{-1} of each OMC in the dark.

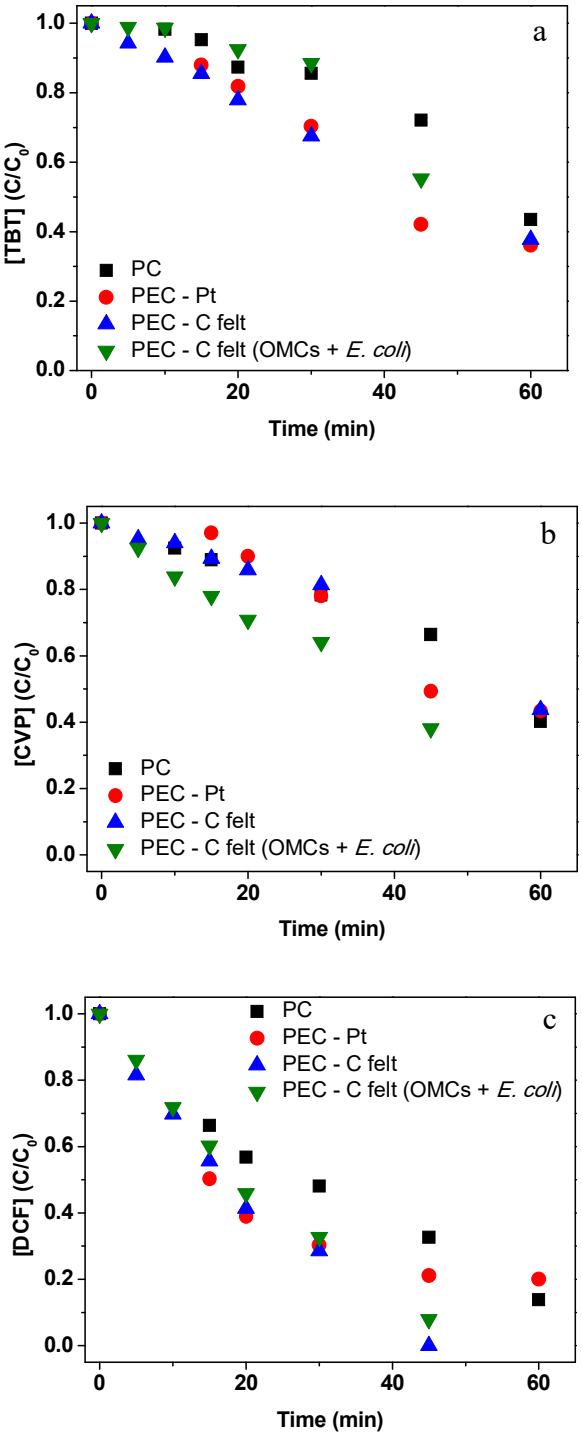

Figure SI-3. Degradation profile of each OMCs during the development of the different tests, a) TBT, b) CVP and c) DCF

Submited to: Process Safety and Environmental Protection

Submision status: Mayor Revisions

Submissions Needing Revision for Author Pilar Fernandez-Ibanez

Click 'File Inventory' to download the source files for the manuscript. Click 'Revise Submission' to submit a revision of the manuscript. If you Decline To Revise the manuscript, it will be moved to the Declined Revisions folder.

IMPORTANT: If your revised files are not ready to be submitted, do not click the 'Revise Submission' link.

Page: 1 of 1 (1 total submissions) Display 10 results per page.

Action	Manuscript Number	Title	Initial Date Submitted	Date Revision Due	Status Date	Current Status	View Decision
Action Links	PSEP-D-20-00435	Electrochemically Assisted Photocatalysis for the Simultaneous Degradation of Organic Micro-Contaminants and Inactivation of Microorganisms in Water	Jul 08, 2020	Sep 04, 2020	Aug 05, 2020	Revise	Major Revision

Page: 1 of 1 (1 total submissions) Display 10 results per page.

Target 5. Electro-oxidation process assisted by solar energy for the treatment of wastewater with high salinity

Science of the Total Environment 705 (2020) 135831

Contents lists available at ScienceDirect

Science of the Total Environment

journal homepage: www.elsevier.com/locate/scitotenv

Electro-oxidation process assisted by solar energy for the treatment of wastewater with high salinity

I. Salmerón, I. Oller *, S. Malato

Plataforma Solar de Almería-CIEMAT, Carretera de Senés Km 4, 04200 Tabernas, Almería, Spain
CIESOL, Joint Centre of the University of Almería-CIEMAT, 04120 Almería, Spain

HIGHLIGHTS

- Solar-assisted electro-oxidative treatment enhanced wastewater biodegradability.
- Solar light promotes the formation of chlorine radicals from electrogenerated chlorine species.
- Combination of solar and electrochemical processes achieved substantial organic removal.
- Electro-oxidation is effective for removal of nitrogenated compounds.

GRAPHICAL ABSTRACT

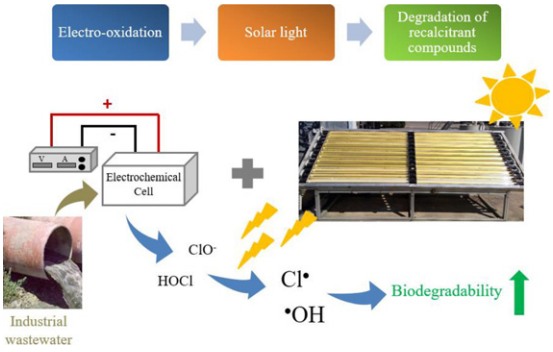

ARTICLE INFO

Article history:
Received 23 October 2019
Received in revised form 27 November 2019
Accepted 27 November 2019
Available online 4 December 2019

Editor: Paola Verlicchi

Keywords:
Chlorine radical
Electro-oxidation
Nitrogen removal
Photochemistry
Water chemistry

ABSTRACT

Industrial wastewaters characterized by its high content in organics and conductivity entails a challenge for conventional treatments due to its low biodegradability. Electro-oxidative processes have been successfully applied for the treatment of this kind of wastewaters achieving high organics and ammonia removal. The degradation process is executed mainly by electrochemically generated active chlorine species, as HClO and ClO^- with $E^0 = 1.49$ V; and $E^0 = 0.89$ V, respectively. Under solar radiation, specifically at 313 nm, the formation of Cl• ($E^0 = 2.4$ V) from ClO^- is promoted, improving the oxidizing capacity of the process. In this work the combination of an electrochemical device with a solar photo-reactor has been evaluated aiming to increase the degradation rate per kWh^{-1}. Two different complex industrial wastewaters were tested, achieving higher organics degradation when electrochemical treatment was assisted by solar light. Toxicity reduction was also assessed and biodegradability enhanced and allowing its ulterior lower-cost biological treatment.

1. Introduction

Wastewater with high content of organic matter and salts suppose a challenge to conventional depuration processes. Such complex wastewaters are normally toxic and/or contain bio-recalcitrant unknown contaminants. A good representative example is landfill leachate, which composition is complex and depends on several factors such as age, precipitation, seasonal weather variations, waste type and surrounding population (Kjeldsen et al., 2002). In general, its principal characteristics are high organic load and the presence of molecules with high molecular weight, as well as ammonia, heavy metals and

* Corresponding author.
E-mail address: isabel.oller@psa.es (I. Oller).

https://doi.org/10.1016/j.scitotenv.2019.135831
0048-9697/

chlorinated organic and inorganic salts (Renou et al., 2008; Wiszniowski et al., 2006), all granting them a highly toxic character, hampering a conventional treatment based on bioprocesses.

According to its age, landfill leachates are classified into two categories. Young leachates, a few years old, in which organic matter content is normally higher than 18 g L^{-1} of Chemical Oxygen Demand (COD) and ammonium between 10 and 800 mg L^{-1}. Despite this, the BOD_5/COD (BOD_5, Biological Oxygen Demand in five days) ratio is generally higher than 0.6 evidencing the presence of biodegradable substances. Old leachates, with more than five years old, present a lower concentration of organics. With COD range usually between 100–500 mg L^{-1} and 20–40 mg L^{-1} of ammonium, but BOD_5/COD ratio normally lower than 0.3, evidencing that high biodegradable substances have been already degraded (Deng and Englehardt, 2007).

Given that conventional biological processes are very often unfeasible, especially for old leachates, alternative treatments based on Advanced Oxidation Processes (AOPs) have been widely studied and described in the literature reaching high COD degradation rates (Deng, 2009; Li et al., 2010; Primo et al., 2008; Wang et al., 2003) and/or increasing their biodegradability (de Morais and Zamora, 2005). Most efficient AOPs reported are photo-Fenton (Reactions 1 and 2) or ozonation processes attaining high mineralization rates but obtaining high concentration of ammonium at the end of the treatments due to the mineralization of the nitrogen included in the structure of organic contaminants.

$$Fe^{2+} + H_2O_2 \rightarrow Fe^{3+} + {}^{\cdot}OH + OH^- \quad (R.1)$$

$$Fe^{3+} + H_2O + h\nu \rightarrow Fe^{2+} + {}^{\cdot}OH + H^+ \quad (R.2)$$

In consequence, the effluent generated normally contains a very high concentration of ammonium unbalanced with the organic carbon available for a subsequent biological treatment. Therefore, alternative AOPs, showing a stronger oxidation effect based on other mechanisms apart from the hydroxyl radicals generation are required to obtain higher quality effluents.

Within the powerful advanced oxidation technologies, indirect electro-oxidation processes represent an effective alternative for the destruction of substances with high molecular weight and, specifically the elimination of COD as well as ammonium oxidation, considering it as an interesting technology specifically for the treatment of wastewaters with high conductivity (Bashir et al., 2013; Chiang et al., 1995; Turro et al., 2011)

Within these processes, organic load is degraded by strong oxidants as active chlorine species (ACS). ACS are generated from chloride present in water by an electron transfer to the anode (Reaction 3), which reacts with water producing hypochlorous acid (Martinez-Huitle and Brillas, 2009) (Reaction 4). According to the speciation of chlorine in water, equilibrium between hypochlorous acid and hypochlorite ion depends on the concentration and pH of the solution (pK_a 7.55) (Sirés et al., 2014), following Reaction 5. Besides these active species, the chloride radical is generated by the direct oxidation at the anode (Reaction 6).

$$2Cl^- \rightarrow Cl_{2(aq)} + 2e^- \quad (R.3)$$

$$Cl_{2(aq)} + H_2O \rightarrow HClO + Cl^- + H^+ \quad (R.4)$$

$$HClO \leftrightarrow ClO^- + H^+ \quad (R.5)$$

$$Cl^- \rightarrow Cl^{\cdot} + e^- \quad (R.6)$$

These species have a redox potential sufficiently high to be able to efficiently degrade organics, $Cl_{2(aq)}$ $E^0 = 1.36$ V; HClO $E^0 = 1.49$ V; ClO^- $E^0 = 0.89$ V and Cl• $E^0 = 2.4$ V (Armstrong et al., 2015).

Sunlight exposure of chlorine species could result in the chlorine and hydroxyl radicals' generation (see Table 1, $\lambda > 300$ nm). Although these radicals could be consumed by some scavengers present in solution, such as carbonate species and dissolved organic matter, a portion of them could react with the contaminants (Nowell and Hoigné, 1992) increasing the efficiency of the treatment.

This work studies the application of an electrolytic device based in ACS generation at pilot plant scale for the treatment of landfill leachate. Experiments include the assessment of some operational parameters' effect on the target wastewater remediation, such as the integration with a solar photo-reactor based on Compound Parabolic Collectors (CPC) aiming an increase of treatment efficiency accompanied of a reduction of related operating costs. Therefore, the main objective has been the evaluation of the efficiency of this combined system for the depuration of two landfill leachates, characterized by 2–3.2 g L^{-1} of dissolved organic carbon (DOC), a high conductivity between 25 and 70 mS cm^{-1} and till 4 g L^{-1} of chloride. Toxicity and biodegradability analyses have been also carried out along the studied processes. The final main objective was not to achieve complete mineralization but to increase biodegradability of the effluent.

2. Experimental section

2.1. Wastewater characterization

Two different landfill leachates were studied (see Table 2). Although both are categorized as young leachates for its content of organics, there was evidence of maturity in leachate 1, with a lower COD value and higher toxicity. Both leachates were classified as non-biodegradable. It is important also to highlight the difference in turbidity between leachates, 35 NTU compared to 200–300 NTU.

2.2. Analysis

COD measurements were done by a COD Cell Test Spectroquant® by Merck. DOC and total nitrogen (TN) were monitored by using a Shimadzu TOC-VCSN analyzer after filtering the samples through 0.22 μm nylon filter from ASIMIO. Ions concentration was determined by ion chromatography (IC) by a Metrohm 850 Professional IC after sample filtration with the same filters. For anions determination, it was used a Metrosep A Supp 7150/4.0 column thermoregulated at 45 °C with 3.6 mM of sodium carbonate as eluent in a flow of 0.7 mL min^{-1}. For cations the column was a Metrosep C6 150/4.0 with a solution 1.7 mM nitric acid - 1.7 mM dipicolinic acid in a flow of 1.2 mL min^{-1}.

A CRISON 25 pH meter was used for measuring the pH continuously, which was always maintained above 3.5 through sodium hydroxide (J.T. Baker) addition to avoid the formation of toxic gaseous Cl_2. Conductivity was determined with a GLP 31 Conductimeter (from CRISON).

Iron concentration was measured spectrophotometrically by using 1,10-phenanthroline following ISO 6332. In the experiments done with the addition of hydrogen peroxide (30% in water from Chem-

Table 1
Reactions and quantum yield of photo-transformation of chlorine species at different wavelengths.
Modified from Nowell and Hoigné (1992).

	Φ(λ)		
	λ: 365 nm	313 nm	254 nm[a]
Gaseous phase			
$HOCl \rightarrow {}^{\bullet}OH + Cl^{\bullet}$		1[b]	
Aqueous phase			
$ClO^- \rightarrow Cl^{\bullet} + O^- + O\ (^3P)$	0.28	0.075	0.074
$ClO^- \rightarrow Cl^{\bullet} + O^- \rightarrow {}^{\bullet}OH$	0.08	0.127	0.278
$ClO^- \rightarrow Cl^{\bullet} + O\ (^1D)$		0.020	0.133

[a] Reactions at 254 nm are not possible under sunlight.
[b] At aprox 310 nm.

Table 2
Characterization of the landfill leachates studied.

	Leachate 1	Leachate 2
pH	7–8	7–8
Conductivity (mS cm^{-1})	50–70	25–35
Turbidity (NTU)	35	200–300
Cl^- (g L^{-1})	6.4–8.2	4.5–5.2
COD (g L^{-1})	8.1–8.4	8.8–11
DOC (g L^{-1})	2–2.5	2–3.2
TN (g L^{-1})	6–6.5	3.9–4.7
Iron (mg L^{-1})	70–115	38–44
Toxicity (activated sludge inhibition)	53%	0%
Total Solids (g L^{-1})	1.7	<Detection limit

Lab), its concentration was determined following DIN 38409 H15. Both iron and hydrogen peroxide were measured in a Unicam Uv/Vis UV2 spectrophotometer, at 510 nm and 410 nm, respectively.

Toxicity and biodegradability along the electro-oxidation treatment were analyzed with a SURCIS BM-Advanced Respirometer. This equipment allows studying the stimulation or inhibition rate in activated sludge coming from a municipal wastewater treatment plant (MWWTP) by direct contact with the sample. Toxicity analyses were performed by feeding 1 L of activated sludge with sodium acetate (0.5 g per gram of volatile solids) and, when the Oxygen Uptake Rate (OUR) was stable, putting in contact with 30 mL of the sample. The change in this parameter gives the percentage of inhibition related to the OUR of the activated sludge. Biodegradability of the samples was measured by adding 100 mL of sample to 900 mL of activated sludge. The system gives the biodegradable COD (CODb) which must be compared with the total COD of the sample. According to the protocol of the respirometer, when the ratio CODb/COD is higher than 0.2 the sample is considered slightly biodegradable and so a biological reactor could be adapted.

2.3. Experimental set-up

The electro-oxidative process was carried out by using a monopolar electrolyzer with a dimensionally stable electrode formed by five anodes with a total surface of 0.324 m^2 and fed by a power supply able to reach 110 A and 25 V maximum in direct current (DC). Considering the manufacturer's specifications for this type of water, a fixed current density was established in 25 mA cm^{-2}. Reactor configuration consists of an open tank that contains the submerged electrode generating in-situ the oxidants for the degradation of recalcitrant compounds. The reactor treats up to 15 L per batch.

The electrochemical device was connected to a solar photo-reactor based on CPC with a total illuminated area of 3.08 m^2 and an illuminated volume of 22 L formed by 24 borosilicate glass tubes (150 cm length × 3.2 cm diameter) mounted on a platform tilted 37°. The total volume of the whole combined system was 38 L (Fig. 1).

Electro-oxidation experiments, with only the electrolyzer or combining with the CPC reactor, were developed by adding the wastewater to the open tank; homogenize the total volume by recirculation and running the electrolyzer. Samples were taken every 2 h of treatment. Sodium hydroxide was added if pH dropped under 3.5 in order to avoid the formation of toxic gaseous Cl_2.

In the experiments with hydrogen peroxide, after solution homogenization, 600 mg L^{-1} of hydrogen peroxide were added. Afterwards, the electrolyzer started to operate. Periodically hydrogen peroxide was added trying to maintain a stable concentration of 600 mg L^{-1} throughout the experiment. As in the previous case, samples were taken every 2 h of treatment.

Photo-Fenton tests for comparison purposes were carried out by using the CPC photo-reactor alone. The operating conditions were pH 3 and an initial concentration of hydrogen peroxide of 1000 mg L^{-1}. The addition of iron was not necessary due to the high

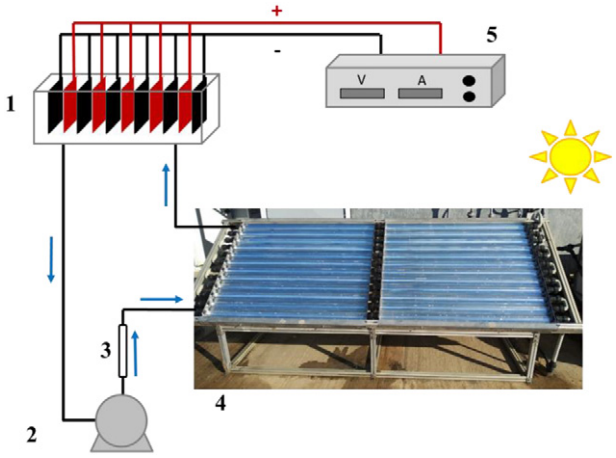

Fig. 1. Pilot plant scheme: (1) electrolyzer, (2) pump, (3) rotameter, (4) CPC, (5) power supply.

concentration present in the leachates. After 15 min of Fenton reaction (in dark), the CPC was uncovered starting the photo-Fenton process. Samples were taken every 15 min during the first hour and then every 30 min till reach 10 h of treatment. New additions of hydrogen peroxide were done with the aim of maintaining a concentration of above 500 mg L^{-1} during the whole test.

The comparison between the different processes studied has been carried out by using Eq. (1), based on the relation between the degradation of DOC regarding to the energy required to reach it.

$$r_e = \Delta DOC/e \quad (1)$$

r_e (g DOC kWh^{-1}) is the degradation rate, ΔDOC is the degradation of DOC (g DOC m^{-3}) along the treatment and e is the electrical energy applied per volume treated (kWh m^{-3}). As well as for DOC, r_e can be applied to compare efficiencies according to other parameters, such as TN.

Solar radiation collected in the CPC (Q_{uv}), is considered separately since it comes from a different energy source and so it is not included in Eq. (1). For avoiding confusions, the units for solar collected energy were kJ L^{-1} instead of kWh m^{-3} which corresponds to electrical consumption.

Solar ultraviolet radiation (UV) was measured by a global UV radiometer KIPP&ZONEN, model CUV 3 installed at Plataforma Solar de Almería (Spain) and tilted of 37° according to the local latitude, as the CPC. Eq. (2), allows the combination of the data from several days of experiments and their comparison with other tests (Malato et al., 2003).

$$Q_{UV,n} = Q_{UVn-1} + \Delta t_n \cdot \overline{UV}_{G,n} \cdot A_i/V_t ; \Delta t_n = t_n - t_{n-1} \quad (2)$$

where $Q_{UV,n}$ (kJ L^{-1}) is the accumulated UV energy per unit of volume, $\overline{UV}_{G,n}$ (W m^{-2}) is the average solar ultraviolet radiation ($\lambda < 400$ nm) measured between t_n and t_{n-1} being n the number of sample, A_i (3.08 m^2) is the irradiated surface and V_t is the total volume.

3. Results and discussion

3.1. Preliminary solar photo-Fenton tests

As first approach to the treatment of the target wastewater, solar photo-Fenton test at pH 3, was carried out in order to compare with the results obtained when applying electro-oxidation alone or combined with the solar CPC photo-reactor.

Leachate 1 showed a strong dark color that hindered the transmission of photons inside the reactor tubes so, for oxidation studies it was diluted 1:1 with demineralized water in order to enhance the treatment itself. Moreover, due to the high organic load and the complexity of the

water, during the first stages of the treatment a large amount of foam was generated retaining DOC and TN, which, in turn, was re-dissolved in the water bulk during the treatment, causing oscillations in the parameters monitored (Fig. 2). TN was not degraded during the experiment and DOC started to decrease only after 75 kJ L^{-1} of accumulated UV energy, approximately. Finally, after 10 h of treatment, with a Q_{uv} of 142.2 kJ L^{-1} and a H_2O_2 consumption of 3.3 g L^{-1}, almost 30% of mineralization (DOC abatement) was reached though TN did not change.

Since the organic load of leachate 2 was higher than 1, despite diluting it, the huge foam production made unfeasible the monitoring of DOC along the treatment. TN did not change during the treatment of leachate 2 by solar photo-Fenton at pH 3 (data not shown).

3.2. Electro-oxidative treatments

Electrochemical advanced oxidation processes (EAOPs) tested for the treatment of landfill leachates (without any dilution) were the electrolyzer alone, electrolyzer combined with solar treatment, and the electrolyzer with the addition of hydrogen peroxide (Fenton process using Fe content of leachate, see Table 2). The results obtained in each one of these processes, are summarized in Table 3, including those obtained with solar photo-Fenton treatment of leachate 1 (shown above).

Main difference between both leachates is their conductivity and TN (see Table 2). Electrical consumption when the electrolyzer was applied alone was higher in the treatment of leachate 1, as well as when combining with solar CPC. Even when solar energy assisting the electrolytic process, higher accumulated UV energy was required for leachate 1. These results confirm that the organic matter contained in younger leachate (leachate 2) was easier to degrade than the recalcitrant organics contained in the more mature leachate (leachate 1).

According to DOC elimination rate (g DOC h^{-1}), it can be observed, for both leachates, that the combination with the CPC photo-reactor did not implied an acceleration in DOC abatement. Regarding TN removal rate (g TN h^{-1}), for leachate 1 there was no enhancement when using the combined system, however leachate 2 showed an increase of 1.5 g TN h^{-1} in its elimination.

When considering organics degradation rate as a function of the electrical energy applied, r_e, instead of treatment time, solar-assisted electrolytic processes entailed a clear improvement increasing the DOC and TN removal per applied kWh, evidencing that the application of solar radiation favors the formation of chlorine radicals, which provoked extra DOC and TN removal lower electrical consumption.

The potential benefits of hydrogen peroxide addition (Fenton process combined with electrolytic process) were studied by maintaining a hydrogen peroxide concentration of 600 mg L^{-1} throughout the entire electrolytic process (Test C_1). Total amount of hydrogen peroxide consumed was 7.32 g L^{-1}. Despite adding a large amount of hydrogen peroxide, no remarkable improvement was obtained regarding any key parameter. This effect would be provoked by the fact that hydrogen peroxide was also oxidized in the anode generating hydroperoxyl radicals of lower oxidation potential, $E^0 = 1.06$ V (Buettner, 1993), following Reaction 7 but in turn it could be also consumed in the own anode by Reaction 8.

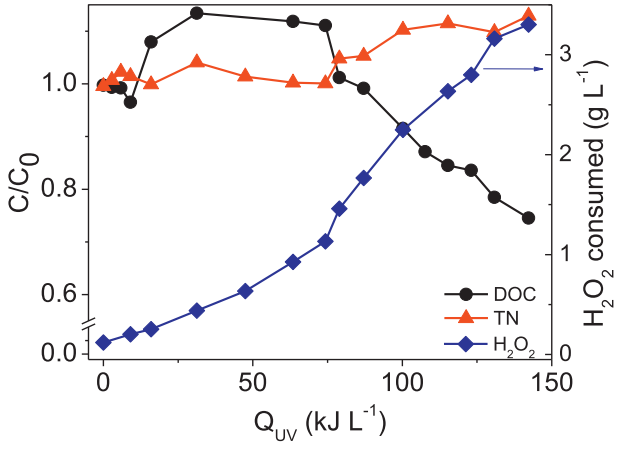

Fig. 2. Evolution of DOC, TN and hydrogen peroxide consumption along the solar photo-Fenton treatment.

Table 3
Summary of the results obtained in solar photo-Fenton, electrolytic treatment, electrolytic combined with solar treatment and electrolytic treatment with H_2O_2 applied to leachate 1 and 2.

	P-F_1	A_1	B_1	C_1	A_2	B_2
e (kWh m^{-3})	–	357	96.3	278	244	54.0
Q_{UV} (kJ L^{-1})	142	–	232	–	–	126
DOC removal (g DOC h^{-1})	0.8	0.6	0.6	0.5	1.6	1.9
TN removal (g TN h^{-1})	0	4.0	3.0	3.8	4.9	6.4
r_e DOC (g DOC kWh^{-1})	–	1.3	3.5	1.2	5.5	13.4
r_e TN (g TN kWh^{-1})	–	9.2	18.0	9.1	16.7	45.2
H_2O_2 consumption (g L^{-1})	3.3	–	–	7.3	–	–

(P-F) solar photo-Fenton; (A) electrolyzer; (B) electrolyzer + solar CPC; (C) electrolyzer + H_2O_2 (1) leachate 1 (2) leachate 2.

$$H_2O_2 \rightarrow HO_2^{\cdot} + H^+ + e^- \quad (R.7)$$

$$HO_2^{\cdot} \rightarrow O_{2(g)} + H^+ + e^- \quad (R.8)$$

In view of the low efficient results obtained in C_1, it was decided not to test leachate 2 with the addition of hydrogen peroxide to the electrolytic process.

DOC and TN evolution along the studied processes are plotted in Fig. 3a and b, respectively. All cases showed a moderate DOC removal, being close to 50% for the best case. Higher and faster DOC removal were observed for leachate 2 (younger one) when applying both processes and with lower energy consumption when combining with the solar CPC. Conversely, TN removal showed the same behavior as DOC but reaching upper degradation (almost 100% in A_2 test). It is important to stress that one of the main advantages of applying an electrochemical system is the capacity of TN elimination compared with other processes based on the generation of hydroxyl radicals (such as photo-Fenton treatment) (Bejan et al., 2013). Elimination of TN is based on the reaction of generated ACS with ammonia that produced gaseous N_2 and chloride (Reaction 9).

$$2NH_4^+ + 3HClO \rightarrow N_2 + 3H_2O + 5H^+ + 3Cl^- \quad (R.9)$$

3.3. Chloride monitoring

From chloride present in leachates, ACS were generated having a crucial role in the degradation process. Fig. 4 shows the evolution of chloride, which in all cases decreased due to its continuous oxidation on the anode forming ACS. Part of them was not combined with organic matter, known as free available chlorine (FAC), and other part reacted with organics, and for instance, in the presence of nitrogenous species, chloramines could be produced provoking toxicity into the solution if they are not completely removed during the treatment.

In A_1 and C_1 tests the generation of oxidizing species was low, evidenced by the decrease of chlorides (Fig. 4), affecting the DOC degradation rate, being r_e = 1.3 and 1.2 g DOC kWh^{-1} for A_1 and C_1, respectively. B_1 treatment, that combined electrooxidation with solar CPC reactor, increased DOC degradation rate till $r_e = 3.5$ g DOC kWh^{-1}.

A_2 and B_2 treatments showed similar trends of chloride along the process, but B_2 showed higher DOC removal rate, being $r_e = 5.5$ and 13.4 g DOC kWh^{-1} for A_2 and B_2, respectively. The higher degradation rates achieved in solar assisted treatments and similar chloride behavior confirmed the generation of oxidizing chlorine radicals from ClO^- (see

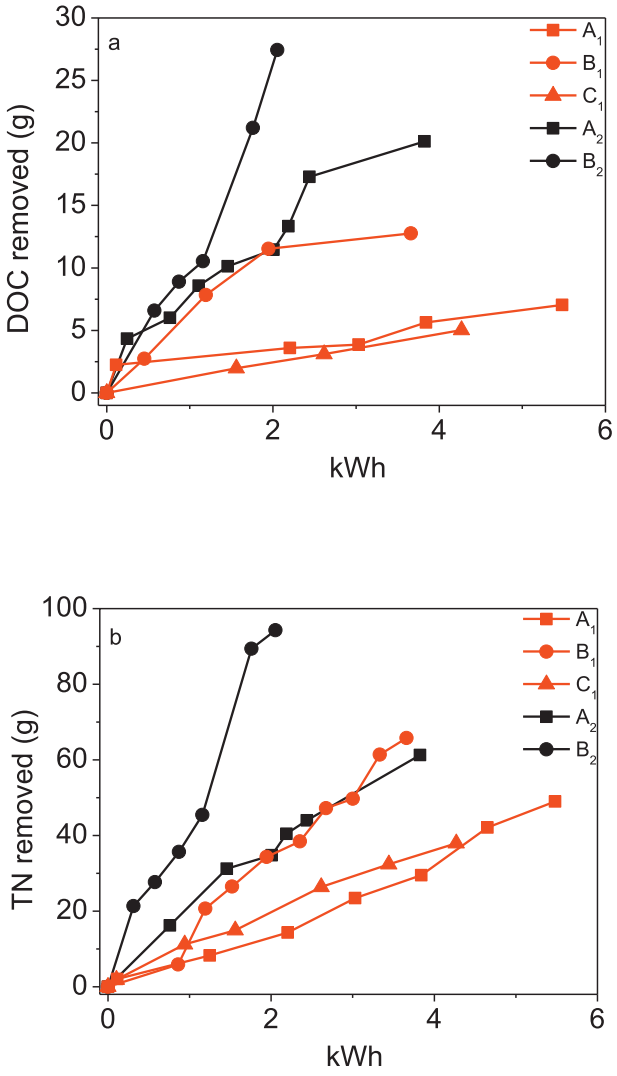

Fig. 3. (a) DOC and (b) TN evolution during the tested oxidation processes as function of the energy required: (A) electrolyzer; (B) electrolyzer + solar CPC; (C) electrolyzer + H_2O_2. (1) Leachate 1 and (2) leachate 2.

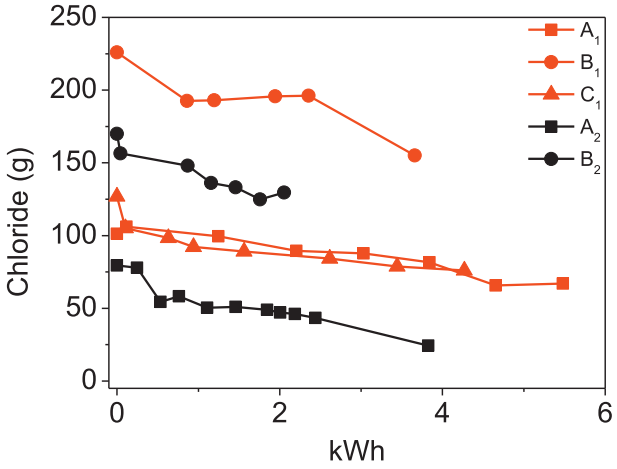

Fig. 4. Chloride evolution during the applied oxidation processes as function of the energy required: (A) electrolyzer; (B) electrolyzer + solar CPC; (C) electrolyzer + H_2O_2. (1) Leachate 1 and (2) leachate 2.

Table 1), so reducing the electric energy consumption in the electrolyzer, and, in consequence, also reducing the possible presence of chloramines.

3.4. Toxicity and biodegradability analysis

Evaluating the possibility of a subsequent application of a biological treatment after the electrochemical process in order to attain complete depuration of the target wastewater, both toxicity and biodegradability of partially treated leachates were monitored by means of respirometry assays using conventional activated sludge from a municipal wastewater treatment plant.

Toxicity tests showed absence of inhibition for raw leachate 2 but 53% of inhibition for leachate 1 (see Table 2). The treatment with electrolytic system combined or not with solar energy did not affect this parameter significantly for leachate 2. Nevertheless, positive effect was observed for leachate 1, in which the electrooxidation alone reduced inhibition till 6%, and when combined with CPC or with addition of hydrogen peroxide, toxicity was completely eliminated.

With respect to biodegradability results, for all the treatments tested the relation between COD_b and COD finally attained values higher than 0.2, being exceptionally high in the case of B_2 test, in which a ratio of 0.75 was reached. Therefore, it was demonstrated that the tested electro-oxidative processes increased the biocompatibility of leachates, permitting a subsequent conventional aerobic biological system to achieve the complete treatment of the studied wastewater.

4. Conclusions

Solar photo-Fenton process has been demonstrated not to be suitable for the treatment of the landfill leachates under study, so Electrochemical Advanced Oxidation Processes has been tested with successful results as alternative for high salinity, high organic loaded and biorecalcitrant wastewaters, achieving both DOC and TN removal without the addition of any reagent.

Combination of electrolytic treatment with solar energy showed lower electrical consumption per volume of treated leachate compared with electrolytic treatment alone achieving biodegradability of the leachate with highest organic contents (leachate 2) with an electric consumption of 54 kWh m^{-3} and a Q_{UV} of 126 kJ L^{-1} without the addition of any reagent. Generation of chlorine radicals from ACS present in water by solar radiation was corroborated, due to the increment in organics removal.

Toxicity and biodegradability were also improved by the combined oxidation processes, preventing, at least partially, the generation of chloramines making feasible the option of a subsequent biological treatment.

Declaration of competing interest

The authors declare that they have no known competing financial interests or personal relationships that could have appeared to influence the work reported in this paper.

Acknowledgements

The authors wish to thank the Spanish Ministerio de Ciencia, Innovación y Universidades for funding under the CalypSol Project (RTI2018-097997-B-C32).

References

Armstrong, D.A., Huie, R.E., Koppenol, W.H., Lymar, S.V., Merényi, G., Neta, P., Ruscic, B., Stanbury, D.M., Steenken, S., Wardman, P., 2015. Standard electrode potentials involving radicals in aqueous solution: inorganic radicals (IUPAC technical report). Pure Appl. Chem. 87, 1139–1150.

Bashir, M.J.K., Aziz, H.A., Aziz, S.Q., Abu Amr, S.S., 2013. An overview of electro-oxidation processes performance in stabilized landfill leachate treatment. Desalin. Water Treat. 51, 2170–2184.
Bejan, D., Graham, T., Bunce, N.J., 2013. Chemical methods for the remediation of ammonia in poultry rearing facilities: a review. Biosyst. Eng. 115, 230–243.
Buettner, G.R., 1993. The pecking order of free radicals and antioxidants: lipid peroxidation, α-tocopherol, and ascorbate. Arch. Biochem. Biophys. 300, 535–543.
Chiang, L.-C., Chang, J.-E., Wen, T.-C., 1995. Indirect oxidation effect in electrochemical oxidation treatment of landfill leachate. Water Res. 29, 671–678.
de Morais, J.L., Zamora, P.P., 2005. Use of advanced oxidation processes to improve the biodegradability of mature landfill leachates. J. Hazard. Mater. 123, 181–186.
Deng, Y., 2009. Advanced oxidation processes (AOPs) for reduction of organic pollutants in landfill leachate: a review. Int. J. Environ. Waste Manag. 4, 366–384.
Deng, Y., Englehardt, J.D., 2007. Electrochemical oxidation for landfill leachate treatment. Waste Manag. 27, 380–388.
Kjeldsen, P., Barlaz, M.A., Rooker, A.P., Baun, A., Ledin, A., Christensen, T.H., 2002. Present and long-term composition of MSW landfill leachate: a review. Crit. Rev. Environ. Sci. Technol. 32, 297–336.
Li, W., Zhou, Q., Hua, T., 2010. Removal of organic matter from landfill leachate by advanced oxidation processes: a review. Int. J. Chem Eng. 2010, 1–10.
Malato, S., Blanco, J., Campos, A., Caceres, J., Guillard, C., Herrmann, J.M., Fernandez-Alba, A.R., 2003. Effect of operating parameters on the testing of new industrial titania catalysts at solar pilot plant scale. Appl. Catal. B Environ. 42, 349–357.
Martinez-Huitle, C.A., Brillas, E., 2009. Decontamination of wastewaters containing synthetic organic dyes by electrochemical methods: a general review. Appl. Catal. B Environ. 87, 105–145.
Nowell, L.H., Hoigné, J., 1992. Photolysis of aqueous chlorine at sunlight and ultraviolet wavelengths—II. Hydroxyl radical production. Water Res. 26, 599–605.
Primo, O., Rivero, M.J., Ortiz, I., 2008. Photo-Fenton process as an efficient alternative to the treatment of landfill leachates. J. Hazard. Mater. 153, 834–842.
Renou, S., Givaudan, J.G., Poulain, S., Dirassouyan, F., Moulin, P., 2008. Landfill leachate treatment: review and opportunity. J. Hazard. Mater. 150, 468–493.
Sirés, I., Brillas, E., Oturan, M.A., Rodrigo, M.A., Panizza, M., 2014. Electrochemical advanced oxidation processes: today and tomorrow. A review. Environ. Sci. Pollut. Res. 21, 8336–8367.
Turro, E., Giannis, A., Cossu, R., Gidarakos, E., Mantzavinos, D., Katsaounis, A., 2011. Electrochemical oxidation of stabilized landfill leachate on DSA electrodes. J. Hazard. Mater. 190, 460–465.
Wang, F., Smith, D.W., El-Din, M.G., 2003. Application of advanced oxidation methods for landfill leachate treatment - a review. J. Environ. Eng. Sci. 2, 413–427.
Wiszniowski, J., Robert, D., Surmacz-Gorska, J., Miksch, K., Weber, J.V., 2006. Landfill leachate treatment methods: a review. Environ. Chem. Lett. 4, 51–61.

Chapter V. Conclusions/Conclusiones

Conclusions

Specific conclusions

Target 1. Optimization of electrocatalytic H_2O_2 production at pilot plant scale for solar-assisted water treatment

The study of the influence of input and output variables on the response parameters (such as electrogeneration of H_2O_2) through a central composite experimental design, allowed to define the optimal values for each operation variable as well as to obtain a mathematical model. This previous step allowed the operation of the electrocatalytic pilot plant at its maximum performance. System optimization becomes even more relevant when the process is intended to be scaled up, due to the high costs that an inadequate operation can entail.

This work confirms that the combined use of Nb-BDD anode and carbon-PTFE GDE cathode leads to a more efficient use of the applied current in relation to direct anodic oxidation. The high electrogeneration of H_2O_2 reached after optimization of the main parameters, 64 mg of H_2O_2 min^{-1} in 5 min with 89% of current efficiency when operating at pH 3 and applying 73 mA cm^{-2}, allows the development of Fenton-like reactions and electro-oxidative ones simultaneously.

Electro-Fenton processes increased the oxidative power of the system. Hydroxyl radicals, generated directly in solution by the Fenton reaction, extend the presence of oxidants to the entire solution and not exclusively to the surrounding areas of the electrode surface, so reference compound removal rate was increased.

It has been demonstrated that solar photoelectro-Fenton process achieved a significant increase in the removal rate of the pesticide mixture (50% of each in 5 min) compared to that reached by anodic oxidation and electro-Fenton, both developed in dark. Thus, the feasibility of the electrochemical process combined with solar energy at pilot plant scale has been confirmed, being this a first step in the progress towards industrial scale operation.

Target 2. Nanofiltration retentate treatment from urban wastewater secondary effluent by solar electrochemical oxidation processes

It has been demonstrated the high efficiency of different electro-oxidative treatments for the elimination of organic microcontaminants present in complex, simulated and real wastewater, at pilot plant scale and working at pH values close to neutrality. EDDS has been successfully used as complexing agent in solar photoelectro-Fenton processes

keeping iron in solution during the first minutes of treatment (~30 min), when the highest percentage of the sum of microcontaminant degradation is reached. However, as an objective for a future work, it must be convenient to check the efficiency of the operation in continuous mode with automatic addition of Fe^{3+}:EDDS, ensuring its availability for Fenton-like reactions throughout the entire treatment.

In addition, it has been also demonstrated the suitability of nanofiltration concentrate streams for the application of electrochemical processes mainly due to their high salinity. It has been observed that the ionic content of target wastewater is essential for the selection of the electro-oxidative process to be applied (anodic oxidation assisted by solar energy or not, electro-Fenton and solar photoelectro-Fenton), not only in terms of energy consumption due to its salinity, but also as precursors of the oxidant species that can be electro-generated (ClO^-, $S_2O_8^{2-}$, $C_2O_6^{2-}$, $P_2O_8^{4-}$, etc.) and these in turn photoactivated ($Cl^{\bullet}$ o $SO4^{-\bullet}$) playing a crucial role in the performance of the process.

Solar-assisted anodic oxidation has been successfully applied for the first time at pilot plant scale for the treatment of an actual nanofiltration membrane retentate with high chloride concentration, reaching 80% degradation of the organic microcontaminants contained in the effluent (5.5 kWh m^{-3} and Quv 11.5 kJ L^{-1}), thus facilitating the operation of the system in comparison to solar photoelectro-Fenton process and reducing the operation cost by avoiding the addition of Fe^{3+}:EDDS required for working at neutral pH.

Target 3. Degradation of carbon-based cathodes in electro-Fenton treatment

This PhD Thesis has addressed the evaluation of carbon-PTFE cathodes status, that are part of the commercial electrochemical cells of the solar photoelectro-Fenton pilot plant installed at PSA, after a series of electrochemical tests under different working conditions. This study allowed to determine the durability and stability of these cathodes, as well as to assess the cleaning procedure for the recovery of their activity (electrogeneration of H_2O_2).

It has been observed that, after 50 hours of pilot plant operation at acid pH, the concentration of electrogenerated H_2O_2 in aqueous solution (with 50 mM Na_2SO_4) was significantly reduced (63%), checking through SEM a severe loss of the carbon-PTFE coating and so confirming its depletion due to the highly aggressive working conditions. These results suggest that the use of this type of carbon-based cathodes on an industrial scale under extreme operating conditions in terms of pH, would mean an increase in the operation costs due to the requirement of continuous replacement when operated for long periods of time.

The operation of carbon-PTFE cathode at natural pH (aqueous solution with 50 mM Na_2SO_4), showed also a decrease of the electrogenerated H_2O_2 after 26 h of operation (51% reduction). However, the analysis by SEM and EDX showed that the loss of active surface was much lower than operating at acid pH, and a greater recovery of the cathode activity was achieved after the cleaning procedure (20% less H_2O_2 generation compared to the new cathode). This confirms the suitability of this electrode for the development of electrochemical processes at pH close to neutrality since it can be regenerated only by an acid cleaning and so reducing operation costs.

Target 4. Electrochemically Assisted Photocatalysis for the Simultaneous Degradation of Organic Micro-Contaminants and Inactivation of Microorganisms in Water

As part of the PhD stay at the Nanotechnology and Integrated BioEngineering Centre (NIBEC) in the University of Ulster (UK), a laboratory-scale photoelectrocatalytic system consisting of titanium dioxide nanotubes as photoanodes has been developed and evaluated, being produced and characterized at NIBEC. The effectiveness of this system has been studied, for the first time, with actual wastewater and for the simultaneous elimination of microcontaminants and pathogens.

The use of a carbón felt cathode was addressed in order to evaluate the improvement of the process reached by means of H_2O_2 electrogeneration. Although this improvement is not reflected in organic microcontaminant degradation (70% of the total), which maintained similar values to the merely photocatalytic process, it was achieved an increase on *E. coli* inactivation rate (2.7-log reduction) compared to the photocatalytic process (2-log reduction) and even compared to the application of photoelectrocatalysis with a platinum cathode (1-log reduction).

The analysis of the generated oxidizing species showed higher oxidizing power of the photoelectrocatalytic system with carbon felt cathode in comparison with only photocatalysis. With this study, it is confirmed the improvement of the use of carbon cathodes versus cathodes without contribution to the oxidative process during wastewater treatment.

Target 5. Electro-oxidation process assisted by solar energy for the treatment of wastewater with high salinity

The high organic and biorecalcitrant content of many industrial wastewaters impedes their treatment by using conventional biological processes. An example of this kind of complex wastewater is landfill leachate. This PhD has addressed the application of a commercial treatment based in DSA electrodes at pilot plant scale as a previous step to

a lower cost biological treatment by achieving toxicity reduction and biodegradability increase of studied leachates.

The combination of the electrochemical DSA system with a solar CPC photoreactor for the generation of species with higher oxidation potential (mainly $Cl^{\bullet}$), from those previously electrogenerated, reduced the electrical energy needed to improve leachates biodegradability. In this sense, the combination with a conventional biological post-treatment would be feasible with the consequent reduction in operation costs regarding the stand-alone electrochemical treatment. Specifically, two batches of leachates were studied: biodegradability improvement of the first one required an electricity consumption of 96.3 kWh m^{-3} and a Q_{uv} of 232 kJ L^{-1} for the combined treatment against 357 kWh m^{-3} for the electrochemical alone; while for the second leachate, 54 kWh m^{-3} and Q_{uv} 126 kJ L^{-1} were required for the combined treatment against 244 kWh m^{-3} for the electrochemical alone.

General conclusions

The extensive study carried out under this PhD Thesis corroborates the suitability of electrochemical processes as an effective tool for the treatment of industrial wastewater and as tertiary treatment of urban effluents at pilot scale. Their highly oxidative power and ease of both operation and maintenance make them a very promising technology with potential application at industrial scale.

The special relevance of the anode material electrochemical systems is widely recognized in the literature since it determines the electrogenerated oxidizing species. However and despite that the cathode material also determines the development of the process, it has been much less studied. Through the studies developed in this PhD Thesis, it has been demonstrated that the use of carbon cathodes able to electrogenerate H_2O_2 implies an improvement in the elimination of both microcontaminants and microorganisms, and also confers versatility to the system allowing the development of Fenton-like processes such as electro-Fenton and solar photoelectro-Fenton.

The combination of solar energy and electrochemical processes for the treatment of complex wastewaters with high ionic charge means an increase in the oxidation potential of the process, requiring a lower amount of electrical energy to achieve the established degradation target.

It is important to point out that, for the first time, it has been observed a clear advantage in the application of anodic oxidation, assisted or not by solar energy, compared to systems based on electrogeneration of H_2O_2 for the elimination of organic micropollutants contained in actual wastewater at neutral pH. The use of complexing agents to keep iron in solution means an input of extra organic charge to the system, thus the overall performance of electro-Fenton and solar photoelectro-Fenton processes is reduced against anodic oxidation. In addition, it is necessary to consider the low stability of iron complexes that limit the efficiency of the process to the first minutes of the treatment. In general, there has been observed two limiting factors to the electrochemical oxidation of microcontaminants, the low electrogeneration of H_2O_2 and direct competition for oxidizing species of additional organic carbon coming from the complexing agent.

Finally, it must be stressed that in any electrochemical system it is necessary to evaluate the generation of chlorates, perchlorates and chloramines from the active species of chlorine present in the reaction bulk, which makes necessary toxicity analysis after the electro-oxidative treatment, as well as an associated risks assessment depending on the subsequent use of the regenerated water.

Conclusiones

Conclusiones específicas

Objetivo 1. Optimización de la producción electrocatalítica de H_2O_2 a escala planta piloto para el tratamiento de agua asistido por energía solar

El estudio de la influencia de las variables de entrada y salida sobre los parámetros de respuesta (como la electro-generación de H_2O_2) mediante un diseño experimental central compuesto, ha facilitado la obtención de los valores óptimos para cada variable de operación así como la obtención de un modelo matemático. Este paso previo ha permitido la operación de la planta piloto al máximo rendimiento. Las tareas de optimización adquieren aún mayor relevancia cuando se escala el proceso, debido a los elevados costes que puede entrañar un funcionamiento inadecuado.

Este trabajo confirma que el uso combinado del ánodo de Nb-BDD y del cátodo GDE de carbono-PTFE conduce a un uso más eficiente de la corriente aplicada en relación con la oxidación anódica directa. La alta electro-generación de H_2O_2 alcanzada tras la optimización de los parámetros principales, 64 mg de H_2O_2 min^{-1} en 5 min con el 89% de eficiencia de la corriente al operar a pH 3 y aplicando 73 mA cm^{-2}, permite el desarrollo de reacciones tipo Fenton de forma simultánea a las propiamente electro-oxidativas.

Los procesos de electro-Fenton aumentaron la capacidad oxidante del sistema. Los radicales hidroxilo, generados directamente en solución mediante la reacción Fenton, extienden la presencia de oxidantes a toda la solución y no exclusivamente en las áreas adyacentes a la superficie del electrodo, por lo que la tasa de eliminación de los contaminantes de referencia fue incrementada.

Se ha demostrado que el proceso foto electro-Fenton solar logra un aumento significativo en el porcentaje de eliminación de una mezcla de plaguicidas (50% de cada uno en 5 min) en comparación con el logrado mediante oxidación anódica y electro-Fenton, ambos desarrollados en la oscuridad. Así pues, se ha confirmado la viabilidad del proceso electroquímico combinado con energía solar a escala planta piloto, lo que supone un primer paso en los avances hacia la operación a escala industrial.

Objetivo 2. Tratamiento de concentrados de nanofiltración de efluente secundario de aguas residuales urbanas mediante procesos de oxidación electroquímica solar.

Se ha demostrado la elevada eficacia de diferentes tratamientos electro-oxidativos para la eliminación de microcontaminantes orgánicos presentes en aguas residuales complejas, simuladas y reales, a escala planta piloto y trabajando a valores de pH cercanos a la neutralidad. El agente complejante EDDS ha sido utilizado con éxito en los procesos electro foto-Fenton solar permitiendo mantener el hierro en disolución en los primeros minutos del tratamiento (~30 min), cuando es alcanzado el mayor porcentaje de degradación de la suma de microcontaminantes. Sin embargo, como objetivo para trabajos futuros, es conveniente probar la eficiencia de la operación en modo continuo con la subsecuente adición automática de Fe^{3+}:EDDS, asegurando su disponibilidad para reacciones Fenton a lo largo del tratamiento completo.

Además, se ha demostrado que las corrientes de concentrado de sistemas de membrana resultan muy adecuadas para la aplicación de procesos electroquímicos debido, principalmente, a su alta salinidad. Se ha observado que el contenido iónico del agua a tratar es esencial para la selección del proceso electro-oxidativo a aplicar (oxidación anódica asistida o no por energía solar, electro-Fenton y foto electro-Fenton solar), no sólo en términos de consumo de energía debido a cuestiones de salinidad, sino también como precursores de las especies oxidantes que pueden ser electro-generadas (ClO^-, $S_2O_8^{2-}$, $C_2O_6^{2-}$, $P_2O_8^{4-}$, etc.) y éstas a su vez fotoactivadas ($Cl^\bullet$ o $SO4^{-\bullet}$) jugando un papel crucial en el rendimiento del proceso.

La oxidación anódica asistida por energía solar se ha aplicado con éxito por primera vez a escala planta piloto para la depuración de una corriente real de concentrado de membrana de nanofiltración con alta concentración de cloruros, alcanzando un porcentaje de degradación del 80% de los microcontaminantes orgánicos contenidos en el efluente (5.5 kWh m^{-3} y Quv 11.5 kJ L^{-1}) facilitando así la operación del sistema frente al proceso de foto electro-Fenton solar y reduciendo el coste de operación al evitar la adición de Fe^{3+}:EDDS como reactivo necesario para trabajar a pH neutro.

Objetivo 3. Degradación de cátodos de carbono en el tratamiento electro-Fenton.

En este estudio se ha llevado a cabo la evaluación del estado de los cátodos de carbono-PTFE que constituyen las celdas electroquímicas comerciales de la planta piloto de foto electro-Fenton solar, instalada en la PSA, tras unas series de ensayos electroquímicos en condiciones de trabajo diversas. Este trabajo ha permitido determinar la durabilidad

y estabilidad de dichos cátodos, al igual que la idoneidad del procedimiento de limpieza en la recuperación de su actividad (electro-generación de H_2O_2).

Se observó que, tras 50 h de operación de la planta piloto a pH ácido, la concentración de H_2O_2 electro-generado en la solución acuosa (50 mM Na_2SO_4) se redujo significativamente (63%), comprobando mediante SEM una severa pérdida del recubrimiento de carbono-PTFE y confirmando su agotamiento debido a las condiciones tan agresivas de trabajo. Estos resultados hacen prever que la utilización de este tipo de cátodos a escala industrial bajo condiciones de operación extremas en cuanto al pH, supondría un claro incremento en los costes de operación debido a la necesidad de reemplazarlos de forma continuada si se opera durante periodos prolongados.

La operación del cátodo de carbono-PTFE a pH natural (en 50 mM Na_2SO_4), mostró de nuevo una disminución del H_2O_2 electro-generado tras 26 h de operación (51% de reducción). Sin embargo, el análisis mediante SEM y EDX mostraron que la pérdida de superficie activa fue mucho menor que operando a pH ácido, observándose, as su vez, una mayor recuperación de la actividad del cátodo tras el procedimiento de limpieza (20% menos de generación de H_2O_2 en comparación con el cátodo nuevo). De esta forma se confirma la idoneidad de este electrodo para el desarrollo de procesos electroquímicos a pH cercanos a la neutralidad ya que pueden ser regenerados únicamente mediante una limpieza ácida, disminuyendo los costes de operación.

Objetivo 4. Degradación de microcontaminantes e inactivación simultánea de microorganismos en agua mediante foto electro-catálisis.

En el marco de la estancia pre-doctoral en el Centro de Nanotecnología y Bioingeniería Integrada (NIBEC) de la Universidad de Ulster (Reino Unido), se ha desarrollado y evaluado un sistema foto electro-catalítico a escala de laboratorio formado por foto-ánodos de nanotubos de dióxido de titanio producidos y caracterizados específicamente en NIBEC. La efectividad de dicho sistema se ha estudiado, por primera vez, con agua real y para la eliminación simultánea de microcontaminantes y patógenos.

Se abordó el uso de un cátodo de fieltro de carbono con el fin de evaluar la mejorar del proceso mediante la electro-generación de H_2O_2. Pese a que dicha mejora no se ve reflejada en la degradación de los microcontaminantes orgánicos (70% del total), que se mantiene en valores similares al proceso meramente foto-catalítico, mediante el uso del cátodo de fieltro de carbono se logra un incremento en la velocidad de inactivación de *E. coli* (reducción de 2.7 log) respecto al proceso foto-catalítico (reducción de 2 log) e incluso frente a la aplicación de foto electro-catálisis con cátodo de platino (reducción de 1 log).

El análisis de las especies oxidantes generadas evidencia el alto poder oxidante del sistema foto electro-catalítico con cátodo de fieltro de carbono con respecto a la fotocatálisis. Con este estudio se confirma la mejora que supone el uso de cátodos de carbono con respecto a cátodos sin contribución al proceso oxidativo en la depuración de aguas.

Objetivo 5. Procesos electro-oxidativos asistidos por energía solar para el tratamiento de aguas residuales con alta salinidad.

El alto contenido orgánico y biorecalcitrante de muchas de las aguas residuales industriales dificulta su depuración mediante tratamientos biológicos convencionales. Un ejemplo de este tipo de aguas complejas son los lixiviados de vertedero. Este trabajo estudia la aplicación de un tratamiento comercial con electrodos DSA a escala planta piloto como paso previo a un tratamiento biológico de menor coste, logrando reducir la toxicidad e incrementar la biodegradabilidad de los lixiviados objeto de estudio.

La combinación del sistema electroquímico con un foto-reactor solar tipo CPC para la generación de especies con mayor potencial de oxidación (principalmente $Cl^{\bullet}$), a partir de las previamente electro-generadas, logra disminuir la energía eléctrica necesaria para lograr mejorar la biodegradabilidad de los lixiviados. De esta manera se puede garantizar su posible combinación con un post-tratamiento biológico convencional con la consiguiente reducción en los costes de operación respecto a la aplicación del tratamiento puramente electroquímico. Concretamente se estudiaron dos lotes de lixiviados, para mejorar la biodegradabilidad del primero se necesitó un consumo eléctrico de 96.3 kWh m^{-3} y un Quv 232 kJ L^{-1} en el tratamiento combinado frente a 357 kWh m^{-3} en el electroquímico; mientras que para el segundo, se requirió 54 kWh m^{-3} y Quv 126 kJ L^{-1} en el tratamiento combinado frente a 244 kWh m^{-3} en el electroquímico.

Conclusiones generales

El amplio estudio llevado a cabo en esta Tesis Doctoral corrobora la idoneidad de los procesos electroquímicos como alternativa eficaz para la depuración de aguas residuales industriales y tratamiento terciario en efluentes urbanos a escala planta piloto. Su alto poder oxidante y facilidad de operación y mantenimiento los convierte en una tecnología muy prometedora con potencial aplicación a escala industrial.

La especial relevancia del material que conforma el ánodo en sistemas electroquímicos es ampliamente reconocida en la literatura ya que determina las especies oxidantes electro-generadas. Sin embargo, y a pesar de que el material que constituye el cátodo también determina el desarrollo del proceso, ha sido mucho menos estudiado. Tal y

como se ha demostrado en los estudios desarrollados en esta Tesis Doctoral, el uso de cátodos de carbono capaces de electro-generar H_2O_2 implican una mejora en la capacidad de eliminación de microcontaminantes y de inactivar microorganismos y además confieren versatilidad al sistema permitiendo el desarrollo de procesos tipo electro-Fenton y foto electro-Fenton solar.

La combinación de energía solar y procesos electroquímicos para el tratamiento de aguas residuales complejas y con gran carga iónica supone un incremento de la capacidad de oxidación del proceso, necesitando una menor cantidad de energía eléctrica para alcanzar el objetivo de degradación establecido.

Por otro lado, es importante destacar que se ha observado, por primera vez, una clara ventaja en la aplicación de oxidación anódica asistida o no por energía solar frente a sistemas basados en electro-generación de H_2O_2, para la eliminación de microcontaminantes orgánicos contenidos en aguas residuales reales a pH neutro. La necesidad de emplear agentes complejantes que aportan carga orgánica al sistema para mantener el hierro en disolución en procesos de electro-Fenton y foto-electro-Fenton solar, reducen el rendimiento global del proceso frente al uso de oxidación anódica. Además, es necesario tener en cuenta la baja estabilidad de los complejos de hierro que limitan la eficacia del proceso a los primeros minutos del tratamiento. En general, se observa la existencia de dos factores limitantes a la oxidación electroquímica de microcontaminantes, por un lado la baja generación de H_2O_2 así como la competencia directa por especies oxidantes del carbono orgánico adicional procedente del agente complejante.

Finalmente, en toda aplicación electroquímica es necesario tener en cuenta la generación de cloratos, percloratos y cloraminas a partir de las especies activas del cloro presentes en el seno de la reacción, lo que hace necesario un análisis de toxicidad tras el tratamiento electro-oxidativo, así como de riesgos asociados dependiendo del posterior uso que se pretenda dar al agua depurada.

List of abbreviations

ACS - Active chlorine species

AEM - Anion exchange membrane

AOPs - Advanced Oxidation Processes

BDD - Boron doped diamond

BOD_5 - Biological oxygen demand

CCD - Central Composite Design

CDI – Capacitive deionization

CE - Current efficiency

CEM - Cation exchange membrane

CFC - Chlorofluorocarbon

CFU - Colony-Forming unit

COD - Chemical oxygen demand

CODb -Biodegradable COD

CODu - COD removal rate

CPC - Compound parabolic collector

DAD - Diodo array detector

DBPs - Disinfection byproducts

DC - Direct current

DDT - Dichloro-diphenyl-trichloroethane

DO - Dissolved oxygen

DPD - N, N-diethyl-p-phenylenediamine (DPD)

DSA - Dimensionally stable anodes

EAOP - Electrochemical Advanced Oxidation Process

EC - Electrocoagulation

ED - Electrodialysis

EDDS - Ethylenediamine-N,N'-disuccinic acid (EDDS)

EDX - Energy dispersive X-ray

EF - Electro-Fenton

EPA - Environmental Protection Agency of the United States of America

ESI - Electrospray ionization

EU - European Union

FAC - Free available chlorine

FCD - Face Centered Design

GDE - Gas difussion electrode

HBCD - Hexabromocyclodecane

HPLC - High Performance Liquid Chromatography

IC - Ionic chromatograph

ISO - International Organization for Standardization

LC-QqLIT-MS/MS – Liquid Chromatography-Quadrupole Linear Ion Trap-Tandem Mass Spectrometry

LFS - Liquid phase principle, flowing gas, static liquid

LOQ: Limit of quantification

LSS - Liquid phase principle, static gas, static liquid

M - Metal anode

MCDI – Membrane capacitive deionization

MF - Microfiltration

Nb-BDD - Niobium-supported boron doped diamond anode

NDIR - Non-dispersive infra-red

NF - Nanofiltration

NTU - Nephelometric turbidity units

OMCs - Organic microcontaminants

OUR - Oxygen uptake rate

PBS - Phosphate buffer saline

PE - Population equivalent

PEF - Photo electro-Fenton

PSA - Plataforma Solar de Almería

PTFE - Polytetrafluoroethylene

QqLIT-MS/MS - Hybrid quadrupole/linear ion trap tandem mass analyzer

RNO - *p*-nitrosodimethylaniline

RO - Reverse osmosis

Rs - Dynamic respiration rate

RSM - Response Surface Methodology

SEM - Scanning Electron Microscopy

SNR - Simulated nanofiltration retentate

SPEF - Solar photo electro-Fenton

THMs - Trihalomethanes

TiO_2-NT - Titanium dioxide nanotubes

UF - Ultrafiltration

UN - United Nations

UPLC - Ultra-Performance Liquid Chromatography

UWWTD - Urban Waste Water Treatment Directive

UWWTP - Urban wastewater treatment plant

VRF - Volume retention factor

WEFE Nexus - Water Energy Food and Ecosystem Nexus

WFD - Water Framework Directive